



Generalized Vehicle Dynamics

Daniel E. Williams

Generalized Vehicle Dynamics

Generalized Vehicle Dynamics

BY DANIEL E. WILLIAMS, PhD, PE



Warrendale, Pennsylvania, USA



400 Commonwealth Drive
Warrendale, PA 15096-0001 USA
E-mail: CustomerService@sae.org
Phone: 877-606-7323 (inside USA and Canada)
724-776-4970 (outside USA)
FAX: 724-776-0790

Copyright © 2022 SAE International. All rights reserved.

No part of this publication may be reproduced, stored in a retrieval system, or transmitted, in any form or by any means, electronic, mechanical, photocopying, recording, or otherwise, without the prior written permission of SAE International. For permission and licensing requests, contact SAE Permissions, 400 Commonwealth Drive, Warrendale, PA 15096-0001 USA; e-mail: copyright@sae.org; phone: 724-772-4028.

Library of Congress Catalog Number 2022933564

<http://dx.doi.org/10.4271/9781468601411>

Information contained in this work has been obtained by SAE International from sources believed to be reliable. However, neither SAE International nor its authors guarantee the accuracy or completeness of any information published herein and neither SAE International nor its authors shall be responsible for any errors, omissions, or damages arising out of use of this information. This work is published with the understanding that SAE International and its authors are supplying information but are not attempting to render engineering or other professional services. If such services are required, the assistance of an appropriate professional should be sought.

ISBN-Print 978-1-4686-0140-4

ISBN-PDF 978-1-4686-0141-1

ISBN-ePub 978-1-4686-0444-3

To purchase bulk quantities, please contact: SAE Customer Service

E-mail: CustomerService@sae.org

Phone: 877-606-7323 (inside USA and Canada)

724-776-4970 (outside USA)

Fax: 724-776-0790

Chief Growth Officer

Frank Menchaca

Publisher

Sherry Dickinson Nigam

Development Editor

Publishers Solutions, LCC
Albany, NY

Director of Content

Management

Kelli Zilko

Production and

Manufacturing Associate

Erin Mendicino

Visit the SAE International Bookstore at books.sae.org

To Grant, Elizabeth, Grace, and Sophia

The greatest contribution is the ones you leave behind.

—Alan Jackson, Small Town Southern Man

Contents

Foreword	xiii
Acknowledgments	xv

SECTION ONE

CHAPTER 1

Introduction

1.1 Overview	1
1.2 Historical Perspective	2
1.3 Structure of the Text	6

CHAPTER 2

Simple Suspension as a Linear Dynamic System

2.1 Introduction	11
2.2 The Simply Suspended Mass and Linear Systems Theory	12
2.3 A Suspended Mass with Damping	18
2.4 Basic Frequency Responses	22
2.5 State Space and Block Diagram Algebra	28
2.6 State Space Realization	33
2.7 First-Order Matrix Differential Equations	35
2.8 Summary	37

CHAPTER 3

The Quarter-Car Model

3.1 Introduction	39
3.2 Representing Reality with the Quarter-Car Model	40

viii Generalized Vehicle Dynamics

3.3 Two Fundamental Frequencies of Interest	46
3.4 The Conventional Quarter-Car Model	48
3.5 Stochastic Road Input and Human Sensitivity to Vibration	55
3.6 Nonlinear Damping	61
3.7 Summary	62

CHAPTER 4**The Pitch Plane Model**

4.1 Introduction	65
4.2 Basic Pitch-Plane Model	66
4.3 Pitch Plane-Free Response	69
4.4 Road Inputs to the Pitch-Plane Model	72
4.5 Pitch-Plane Ride Quality and the Olley Ride Criteria	76
4.6 Pitch-Plane Model with Damping	78
4.7 Generalized Pitch-Plane Model and Olley Solution	81
4.8 Three-Axle Vehicle Example	88
4.9 Summary	92

CHAPTER 5**The Roll-Plane Model**

5.1 Introduction	95
5.2 Simple Two-Axle Roll-Plane Model	96
5.3 The Roll Mode for a Single Axle	100
5.4 The Roll-Plane Model with Stabilizer Bar	103
5.5 Single-Wheel Inputs	109
5.6 Passenger Car Roll	111
5.7 Generalized Roll-Plane Model	113
5.8 Roll and Handling	113
5.9 Summary	114

CHAPTER 6

Active Suspension to Optimize Ride

6.1 Introduction	117
6.2 Inertial Damping	119
6.3 Lotus Modal Control	126
6.4 Modal Inertial Damping	127
6.5 Sprung Mass Acceleration Feedforward	131
6.6 Quarter-Car Optimal Control	132
6.7 Full Vehicle Optimal Control	139
6.8 Modal Inertial Damping and Handling	142
6.9 Summary	144

SECTION TWO**CHAPTER 7**

Handling Basics

7.1 Introduction	149
7.2 Ackermann Steering	150
7.3 Steering Efforts	157
7.4 Slip Angles	165
7.5 Tire Forces	168
7.6 The Conventional Bicycle Model	170
7.7 Summary	175

CHAPTER 8

Reference Frames

8.1 Introduction	179
8.2 Reference Frames in General	180
8.3 Velocity of a Point Translating in a Rotating Reference Frame	182
8.4 Velocity and Acceleration of a Point in a Translating and Rotating Reference Frame	183

x Generalized Vehicle Dynamics

8.5 External Forces and Inertia	185
8.6 The Vehicle as a Rigid Body	189
8.7 Summary	192

CHAPTER 9**New Conventions**

9.1 Introduction	195
9.2 State-of-the-Art Conventions	196
9.3 New Axle Location Convention	200
9.4 New Attack Angle Convention	200
9.5 Summary	204

CHAPTER 10**Two-Axle Yaw-Plane Model**

10.1 Introduction	207
10.2 The Two-Axle Vehicle Model	208
10.3 Drift Angle and Yaw Rate Transfer Functions	215
10.4 Ideal Two-Axle Model	218
10.5 Steady-State Analysis	222
10.6 Pole Locations	226
10.7 Summary	230

CHAPTER 11**Rear Axle Steering and Lanekeeping**

11.1 Introduction	233
11.2 Vehicle Model with Rear Axle Steering	236
11.3 Determination of Rear Axle Steer Control	241
11.4 Open-Loop Response of Ideal Vehicle	246
11.5 Specified Preview	247
11.6 Determination of Rear Axle Control of Ideal Vehicle	249
11.7 Numerical Results	250

11.8 Theoretical Interpretation of Practical Systems	254
11.9 Summary	255

CHAPTER 12**Two-Axle Vehicles that Roll**

12.1 Introduction	259
12.2 Roll Axis Definitions	260
12.3 Acceleration Equations	262
12.4 External Roll Forces on Sprung Mass	265
12.5 Camber Effects	267
12.6 Roll Steer Effects	269
12.7 Differential Equations of Motion with Roll	271
12.8 Roll Steer Compensation	275
12.9 Including Steering Compliance in Understeer	277
12.10 Inclusion of Nonlinear Tires	278
12.11 Summary	278

CHAPTER 13**Three-Axle Vehicle Dynamics**

13.1 Introduction	281
13.2 Peculiarities of the Three-Axle Vehicle	282
13.3 The Three-Axle Model	287
13.4 Third Axle Steering	294
13.5 Trajectory Tracking	299
13.6 Summary	301

CHAPTER 14**Generalized Multiaxle Vehicle Dynamics**

14.1 Introduction	303
14.2 General Model	304
14.3 An Arbitrarily Steered Axle	310

14.4 All Arbitrary Axles Steered Proportionally	312
14.5 The Multiaxle Vehicle with Roll	314
14.6 Summary	319

CHAPTER 15**Automated Vehicle Architecture from
Vehicle Dynamics**

15.1 Introduction	321
15.2 Properties of a Typical Three-Axle Commercial Vehicle	323
15.3 Control of Rear Axle	325
15.4 Rear Axle Control for Yaw Rate Equivalence	327
15.5 Vehicle Results	331
15.6 Proposed Three-Axle Vehicle	335
15.7 Summary	337
Afterword	341
Index	343
About the Author	351

Foreword

It has been said that the first automobile race was probably held the day the second automobile was finished. Some rudimentary thinking about the idea of “vehicle dynamics” surely must have followed at the victory ceremony! In the intervening decades, there have been a large number of seminal publications and books that have amplified, enlarged and developed ever more sophisticated concepts on the subject. As new concepts were introduced, a general approach based on statics and dynamics evolved and became near-standard.

This new book by Dr. Williams examines the concept of vehicle dynamics from a different viewpoint, and contains a number of important and hitherto unappreciated elements. Vehicle dynamics is, ultimately, applied control theory. Control theory is a well-developed field but its application has been largely, though not completely, ignored by practicing vehicle dynamicists. When viewed through the lens of control, there is much to be learned, and many new insights to be gained, particularly when we consider the potential for autonomous, i.e., self-driving vehicles. The control theory approach is fundamental and is carried throughout this book.

Essentially all real-world driving experiences involve transient vehicle behavior. Nevertheless, most previous books and research papers have concentrated on steady-state, and often limit-performance steady-state, vehicle behavior. The most sophisticated of these used to analyze cornering behavior is the Milliken Moment Method. This is undoubtedly because, until sufficient advances in computing capability were made, the relevant transient equations were too formidable and too nonlinear to permit closed-form solutions. While this book contains some sections that emphasize steady-state concepts, most of the equations contained allow analysis of transient behavior. The importance of transient behavior analysis, particularly during vehicle development, cannot be overemphasized. As research, design and ultimately production of autonomous vehicles approaches practicality, the concepts of control theory can and will become ever more important.

At its core, systems and control emphasizes three basic behaviors of any dynamic system: stability, satisfactory steady-state performance and satisfactory

transient performance. Hundreds of scientific studies and publications have shown that citizen drivers seldom use the full dynamic potential of their vehicles during driving maneuvers on purpose. Emergencies often entail the driver venturing into unknown waters and employing control strategies that may be, and often are, either only partially successful or even completely inappropriate. With a control-theoretic approach, it is directly possible to include human performance. The early transfer-function models of human control behavior have grown into a sophisticated area of independent research. Such models blend seamlessly into the control-theoretic vehicle dynamics environment developed by Dr. Williams.

Dr. Williams' book generalizes a number of concepts to vehicles with more than two axles, a step forward and one that is unique. While passenger cars are unlikely to ever have more than two axles, utility, work and other vehicles used not for transportation but for task accomplishment certainly have multiple axles. The book is a valuable contribution to this area all by itself.

I greatly enjoyed the time I spent with the author when he was a student. I feel certain that readers of this book will enjoy the rewarding time spent studying it as well.

Prof. Dan Metz, PhD
Fellow, SAE

Acknowledgments

If I were giving a young man advice as to how he might succeed in life, I would say to him, pick out a good father and mother, and begin life in Ohio.

—Wilbur Wright

Most fundamentally, I am a farm boy with a PhD in control theory. The first element of this duality was made possible through my parents, Eugene and Nancy Williams. The epicenter of fortunate birth had moved two states west since Wilbur Wright was born. There was plenty of hard work on the farm, and as I look back I am thankful for every bit of it. But there were also plenty of vehicles to drive. Before I could sit on the bench seat and reach the pedals of my Dad's pickup truck, I drove it standing up from one side of an 80-acre field to the other as my Dad walked it. I got the truck up to 70 mph when there was a stand of timber between me and Dad so that he couldn't see me. It didn't occur to me that Dad could no doubt hear the whine of the engine, but he didn't say anything. I think he somehow approved. He provided a succession of minibikes, go-carts, motorcycles, cars, and even a 1968 Dodge grain truck chassis that I endlessly drove through the gears on a dirt lane, not to mention the tractors and grain trucks for regular farm work. Never has a boy had a better childhood than my Mom and Dad gave me. There are two things that every farm boy obtains: a sense of practicality and a sense of urgency. The farm is not the only place these senses are obtained; just as planting happens in the spring and harvest in the fall, race day is Sunday whether you are ready or not. In this important respect, demanding both practicality and urgency, racing and farming are similar, and somewhat unique. As my first job after college was associated with racing, I did not realize how unique yet complementary these two "fields" were until later in my career.

The flip side of that duality was an excellent formal education in vehicle dynamics and control theory. My high school physics teacher, John Pearson, planted the seed. Dr. Dan Metz, my MS thesis advisor at the University of

Illinois, was perhaps the most significant influence on my professional career. He imparted a love of vehicle dynamics and chassis control systems, and in supervising my thesis taught me how to solve complex problems. Specifically, he taught me that all things are not equally important. It is worth contemplating what aspects of a problem are important, spending more time on getting the important things right. Dr. Metz taught vehicle dynamics with a control theory perspective, and incorporated the roll mode dynamics first developed by JR Ellis. I talked over the phone briefly with Prof. Ellis to get a copy of the self-published edition of his out of print classic book. This book is largely an extension of Metz and Ellis' work. After starting my career in Florida, I was lucky to attend the Florida Institute of Technology, where my part-time PhD in controls was supervised by Dr. Wassim Haddad, a uniquely brilliant and hardworking researcher. At the time, owing to interesting control systems work occurring at Harris, Florida Tech had a great assembly of controls professors, including Dr. Fred Ham. I was lucky to grow up on a farm close to the University of Illinois, and I was lucky to have found my first job close to Florida Tech where I could attend classes at night.

My good fortune continued. This farm boy with a PhD in controls crossed paths with giants in the vehicle dynamics field. My first job was with a joint venture between Moog, Inc. and Lotus to develop active suspension. I quickly met Peter Wright of Lotus and David Williams of Cranfield Institute of Technology, both brilliant inventors of the Lotus active suspension system that was then running on the Lotus F1 car driven by Ayrton Senna. Shortly after starting I met Bill Milliken, who previously brokered the deal between Moog and Lotus. I had heard much about Bill through Prof. Metz who worked with him at Cornell, but was not prepared for what a truly nice guy he was. Not long after meeting Bill I met his son Doug, who has remained a valued colleague for many years, and along with Dan Metz helpfully reviewed my SAE Buckendale Lecture that was the backbone of the handling portion of this work. After TRW purchased the JV and I moved to Lafayette, I met Tom Gillespie, author of perhaps the most significant vehicle dynamics book of our time, and another true gentlemen who thankfully made plenty of time for a young engineer. Later my path crossed Dr. Don Margolis at a vehicle dynamics conference. Don invited me to UC Davis to present a Hyundai Lecture on Vehicle Dynamics, where I met his colleague Dr. Dean Karnopp. Don and Dean developed an alternate, and as we shall see, complementary active control strategy. Between Don and Dean, Peter Wright and Dave Williams, I had the extreme good fortune to know the truly influential pioneers of active suspension. The reader will find that this work directly benefited from these "giants."

All of this professional networking was made possible through my job. Starting with Moog and Lotus, and then for many years with TRW after they purchased Moog/Lotus, and finally with ZF after they purchased TRW, my

ideas and experiences have been generally shaped by too many colleagues and supportive managers to mention. Collectively these have been excellent companies to work for, with the good times far outnumbering the bad. A few colleagues at work must be mentioned because of their specific impactful collaboration leading directly to the ideas presented in this work: Kevin McLaughlin, Ken Sherwin, and Abe Ghaphery. Another, Dr. Amine Nhila, deserves special mention. Amine coauthored many papers, and reviewed other work. Most significantly, he was the primary author of the original publication of some of the materials presented in [Chapter 15](#).

When Isaac Newton was at Cambridge the university was shut down during the black plague. Newton went back to the family farm and invented Calculus. During Covid my weak imitation is this book. The start of the work was my 2012 SAE Buckendale Lecture, followed by my Purdue lectures and the 2016 ASME Milliken Lecture. During Covid I merged these sources with previously published papers. Thanks to the SAE staff, Sherry Nigam, Linda DeMasi, and Bruce Sherwin, the work developed. Their patience with a rookie author is much appreciated. Dan Metz, Greg Shaver, and Tim Drotar reviewed the work. It is possible mistakes reside in the work, but there are fewer errors thanks to these reviewers. Those errors that remain are attributable solely to the author.

Whether it is growing up on a farm, getting a great theoretical education, rubbing shoulders with giants of the field, or working with great people for the same company for 34 years (more or less, I never left, although the name on the door occasionally changed), I think my career is proof of the old adage—it is better to be lucky than good.

Introduction

If I have seen further it is by standing on the shoulders of giants.

—Isaac Newton

1.1 Overview

Vehicle dynamics is a mature field when applied to two-axle vehicles. Passenger cars are responsible for most vehicle miles traveled, and their generally consistent architecture justifies the analytical attention they have historically received. There are excellent vehicle dynamics books available; the reader deserves to know what makes this book particularly valuable. First, this book uses new and nonstandard conventions that allow wider applicability to complex vehicles. These conventions allow the development of the most general vehicle handling model to date. Second, this book is written from the standpoint of the vehicle as a dynamic system to control. The development and presentation of vehicle dynamics will be in familiar terms to control theorists. These terms include treating the dynamics as a system that converts inputs to outputs. Finally, the book is written from a perspective of an industry professional with more than 30 years of experience in chassis control systems, from concept to launch. It has been said that electrical engineers control equations, and mechanical engineers control “stuff.” Vehicles are the most satisfying “stuff” to control. A capstone chapter concluding the ride section draws on the author’s experience in developing and quantifying the performance of an actively suspended vehicle, and similarly the handling section is concluded by with an innovative use of vehicle dynamics to develop a redundant steering concept for automated vehicles that allow improved vehicle functionality as well as providing steering redundancy.

This work is intended for readers from at least two categories. First, are those generally familiar with the well-developed body of vehicle dynamics knowledge. This body of knowledge was generated, with good reason, largely for passenger cars and then extended to other vehicles. This work will present vehicle dynamic models, recast with changes in long-held vehicle dynamics conventions, which allow generalized vehicle dynamic models that are more applicable to complex vehicles. Second, are those coming from a general background in control theory and dynamic systems and want to see how the general techniques they have learned can apply to the dynamics of ground vehicles. A practitioner with a background in control systems and artificial intelligence would find this study helpful when working on autonomous vehicles. To the extent the reader has both knowledge of control systems and vehicle dynamics, the convention changes leading to new vehicle dynamic models will be appreciated as more intuitive.

1.2 Historical Perspective

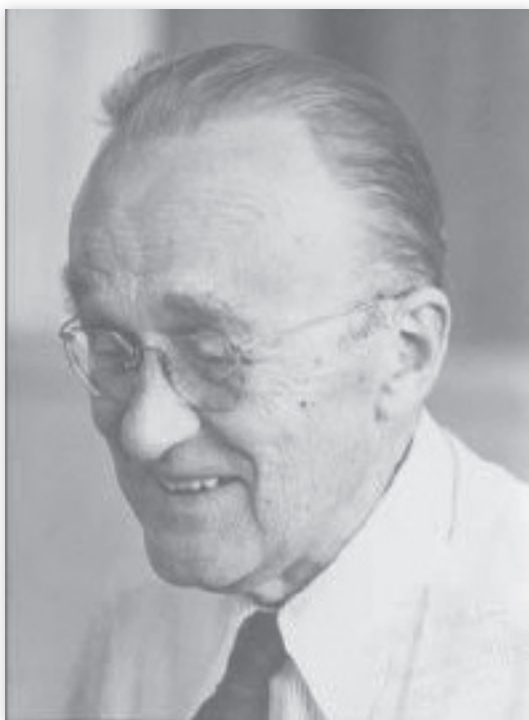
Maurice Olley was the first to consider the concepts explored in this work. Olley was born in 1889 and started his career with Rolls-Royce prior to World War I ([Figure 1.1](#)). While at Rolls-Royce, Olley made transitions from aircraft to automotive work, and from Europe to the United States. In 1930, Olley joined General Motors, where he continued for nearly 30 years. Upon his retirement from General Motors, in the early 1960s, Olley produced a series of monographs intended to convey his pioneering experience. This work is published and very helpfully annotated by Bill and Doug Milliken.

Olley claims that the published literature on automotive handling prior to the 1930s was “valueless because it was done with no knowledge of actual tire characteristics.” He thought that “primary” vehicle-handling fundamentals were determined by the difference between the direction the tires are pointing and the direction they are moving. Other factors that affected the handling of a vehicle without changing these angles (e.g., roll and suspension effects) were considered secondary and could be expressed as equivalent changes in tire angle [1].

Because of Maurice Olley’s appreciation for the fundamental importance of this angular difference between tire orientation and motion, he suggested combining the action of opposite tires on a given axle as they experience similar attack angles, giving rise to the celebrated “bicycle” model used in this work. Olley was an early proponent of steady-state vehicle testing on a skid pad to sort out the forces created by the generation of these angles. By 1940, Olley became interested in dynamic vehicle analysis to describe behavior that could

FIGURE 1.1 Maurice Olley.

Reprinted with permission from © General Motors LLC.



not be fully explained by steady-state characterization. Just as Olley considered handling yaw-plane phenomena, he considered ride in the pitch plane as an interaction of vertical and pitching motion. He suggested ride criteria that bear his name today.

Bill Milliken would be notable in this review if his only contribution was editing Olley's monographs, but in fact his contributions were far greater. Bill was born 22 years after Olley but took a similar career path from the aircraft to automotive industry ([Figure 1.2](#)). At the dawn of the 20th century, George Bryan produced differential equations describing the motion of aircraft. Milliken studied aircraft dynamics and stability under Otto Koppen at MIT who taught Bryan's analytical methods, and then applied this expertise at Vought on World War II era aircraft such as the gull-winged Corsair navy fighter plane and at Boeing on the B17 and B29 bombers. Bill developed a research program in aircraft stability and control that resulted in frequency response characterization of aircraft-handling properties. This work led to variable stability aircraft making use of automatic controls and ultimately to flying quality specifications.

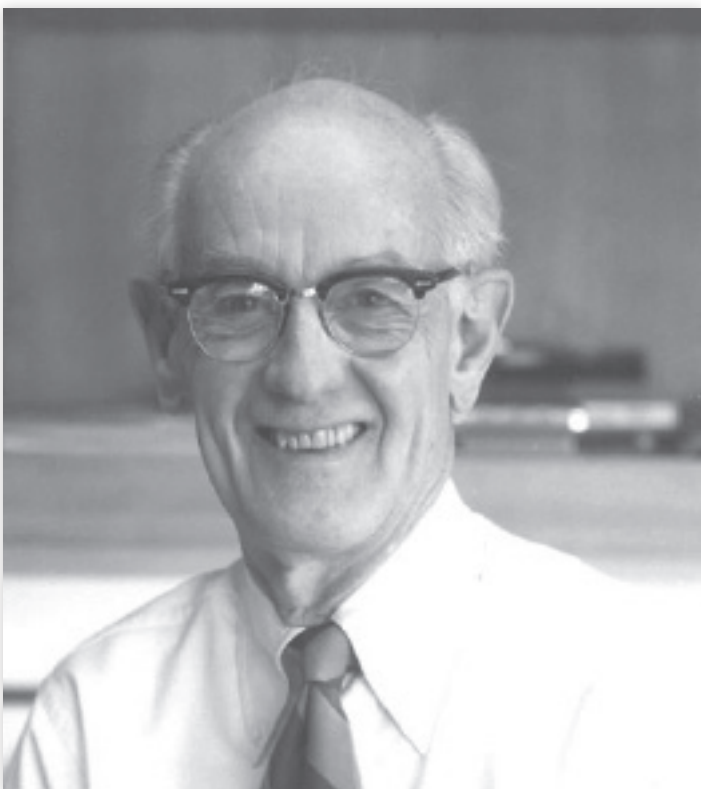
FIGURE 1.2 William (Bill) Milliken.

Photo Courtesy of John Z. Colt.

After the war, Milliken began racing automobiles and naturally started to apply his aircraft-handling expertise to ground vehicles. As the automobile had been around longer than aircraft, Bill was surprised to find only “a single reference to a technical paper by Maurice Olley.” By this time, Maurice Olley was the head of Research and Development at General Motors and hired Bill Milliken and his associates to apply their dynamic handling analysis techniques to passenger cars. With sponsorship from General Motors, a colleague of Milliken’s wrote the dynamic equations of motion for a 1953 Buick [2]. As later noted by a contemporary, “the modern vehicle dynamics era began right then” [3]. In time, Bill led a group at Cornell Aeronautical Laboratories (later Calspan) dedicated to automotive research. He later founded Milliken Research Associates that continues to this day researching advanced automotive dynamics led by Bill’s son and coauthor of several important works, Doug Milliken.

This work owes a debt to many vehicle dynamicists, most of whom in turn are indebted to Milliken and Olley. Specifically, there are two individuals whose work was particularly influential. R.A. Ellis wrote a classic vehicle dynamics

text notable for its combination of rigor and practicality. Ellis' work illustrates the value of convention, notation, and relevant assumptions in creating parsimonious vehicle dynamic models. Professor Ellis spent many years at Cranfield Institute of Technology establishing it as a leader in European vehicle dynamics research.

After World War II, control theory evolved as a body of knowledge with a particular methodology in analyzing, modeling, and ultimately designing dynamic systems. The next generation of vehicle dynamicists, such as the University of Illinois' L. Daniel Metz—who received his PhD at Cornell and worked with Bill Milliken—combined the newly emerged control theoretic concepts of stability and feedback to vehicle dynamics. Once the vehicle dynamic problem was cast in these terms, it is a straightforward step to consider chassis control systems such as active suspension and rear axle steer explored later in this work. Professors Ellis and Metz deserve particular mention in shaping the ideas presented in this work.

We now consider these topics at the most exciting time in vehicle dynamics since Bill Milliken was considering the equations of motion of ground vehicles. Between then and now, much of the emphasis in vehicle engineering has been on cost, quality, emissions, and fuel economy. Vehicle dynamics supported and constrained these efforts, but vehicle dynamics often and unfairly seemed a primary concern only when apparently gotten wrong, such as the oversteering Chevrolet Corvair or the Ford Explorer rolling over.

Now chassis control systems extend a vehicle's functional envelope to make it safer and easier to drive. Great effort is placed in developing autonomous vehicles, financed both internally as with established manufacturers, and with tremendous venture capital flows at start-ups. Vehicle dynamics can now more than ever be considered as a solution to problems rather than problems to avoid. To date, vehicle dynamics has been concerned with human control. At first that might seem to make vehicle dynamics irrelevant to autonomous vehicles, but, on the contrary, knowledge of vehicle dynamics will be even more important in allowing the "virtual driver" to make the safest decisions while ensuring the human occupant the highest level of comfort. As it turns out, the human driver is a pretty good controller, aided by pretty good situational awareness. Most accidents have a component of driver error, but drivers do a remarkable job of avoiding untold accidents. Improving upon human control will require the application of vehicle dynamic principles.

It has been estimated that 20% of humans become carsick when not driving. This statistic could limit the use of autonomous vehicles. The capstone chapter on ride presents an active suspension system implemented on an actual vehicle that can address this issue. The capstone chapter on handling presents a redundant steering system that will allow vehicle operation upon failure of the primary steering system as well as improving vehicle functionality in

terms of maneuverability, tire wear, and load capacity. The vehicle dynamics developed in this work led to the control algorithm which was validated on an actual vehicle, and the control algorithm leads to improved vehicle functionality that can be quantified by the dynamics developed. In both ride and handling, vehicle dynamics enables autonomous vehicle solutions.

Larry Burns has demonstrated how the simultaneous trends of autonomy, electric propulsion, and ride sharing will create enormous value. Active suspension was not adopted because it negatively affected the primary value drivers of the day: cost, quality, and fuel economy/emissions. Tomorrow, active suspension could be seen as a key enabler to unlock the value identified by Burns. It will be hard to imagine how these new vehicles will look. So much of today's vehicle architecture is constrained or compromised by human control requirements [4].

1.3 Structure of the Text

The following chapter opens reviewing mathematical concepts used later in the text. Mathematicians are likely to be disappointed by the rigor in this chapter; the intent is not to derive relevant mathematics from first principles. Rather, this chapter is intended as a “refresher” to the reader of relevant mathematical concepts that will be used in later chapters. This material is typical of an undergraduate course in linear dynamic systems and control. The chapter is not essential; however, it is highly recommended that even the well-prepared reader skims the chapter to ensure general familiarity. This chapter uses the example of a simply suspended mass to review these concepts, and this example will be augmented to form the first major model presented.

The book is divided into two largely independent main sections: ride and handling. Ride is developed first, as it is a dynamic system that is intuitively familiar to the reader as a vibration isolation problem. Coupled second-order dynamics allow physical interpretation of resonances. This intuitive familiarity is most apparent in [Chapter 3](#), which develops the quarter-car ride model, perhaps the most useful yet simple model in vehicle dynamics. The model gets its name from passenger car application, where it is assumed that a quarter of the sprung mass can be distributed to each corner (resembling the simply suspended mass of the preceding chapter), and then the tire spring combines with the suspension spring and wheel hub mass to filter vertical road inputs from the sprung mass. Only vertical motion, or heave, is considered. From this simple model, fundamental ride resonances are identified and attributed to various stiffnesses and masses. The isolation function is introduced and shown to be effective in demonstrating parameter sensitivity. Damping is seen to be mostly objectionable, and yet ironically required. The quarter-car model simply describes behavior and trade-offs present at each corner of the vehicle

and as such exemplifies the notion of parsimony in modeling. Although the name presumes a passenger car application, the quarter-car model is revealing for any vehicle configuration.

Then “corners” on each side of the vehicle are combined to act together at the centerline of the vehicle in [Chapter 4](#). This allows the sprung mass to not only vertically heave, but also to rock fore and aft in a motion known as pitch. Together, heave and pitch motions characterize ride in a vehicle traveling in a straight line. Maurice Olley provided insight into the coupling of these motions to provide good vehicle ride. As it turns out, humans are particularly sensitive to pitch, and the result of Olley’s suggestions reduces pitch. As speed increases, the vehicle wheelbase filters pitching inputs from the road, so that the pitch plane model is particularly relevant for intermediate speeds or longer wheelbase vehicles. The pitch plane model is extended to vehicles with multiple axles with a new application of the Olley ride criteria. This extension is a foreshadowing of a generalized handling model.

Roll is considered as an independent degree of freedom in [Chapter 5](#). Roll is less important than pitch and heave in straight line driving that most vehicles encounter most of the time. Roll is more important, as will be shown later, in handling. Ideally, it would be desirable for the suspension to be stiff in roll and relatively soft in heave, creating a compromise. Anti-roll bars are an innovative way to avoid some of this compromise inherent in the roll mode. These bars also affect the roll moment distribution between the front and rear, and thereby alter handling characteristics. Anti-roll bars can affect handling and reduce roll displacement, but at the expense of single wheel input harshness.

In [Chapter 6](#), the three modes of rigid body sprung mass motion—heave, pitch, and roll—are combined and addressed by active suspension. Most active suspension strategies can be traced to Lotus Modal Control or skyhook damping and this work combines both. Active suspension allows ideal sprung mass behavior, while dynamically varying the roll moment distribution. As active suspension provides an excellent application of optimal control, an example is included. (This example can be skipped without loss relative to the rest of the book.) The active suspension control algorithm derived in this chapter provided the best ride measured by one passenger car original equipment manufacturer (OEM) while ensuring exceptional stable neutral handling characteristics.

There are inherent compromises between ride and handling. A softly sprung car generally rides well but does not handle well and vice versa. The second section of this book addresses handling. This section opens with a survey of vehicle kinematics in turning. At low speeds when lateral forces are negligible, geometry determines vehicle direction. The steering system is modeled and used to introduce the concept of understeer. The concept of understeer is intentionally introduced prior to full vehicle dynamic development to develop conceptual intuition of this important concept.

Chapter 8 formally introduces reference frames. The vehicle experiences external forces with respect to a reference fixed to its center of gravity. For rudimentary vehicle dynamics, this intuition will suffice. For more complicated analysis, rigor is required for at least two theoretical reasons. First, the most common consumer handling mode of operation is lanekeeping, and lane position requires a coordinate transformation from a body fixed frame to an inertial frame. Second, when body roll is considered another Euler angle transformation is required and demands rigor. Pragmatically, a formal development of reference frames enables appreciation of the implicit assumptions present in the conventional yaw-plane bicycle model, and further formal reference frames motivate assumptions when roll is considered.

Chapter 9 is relatively short but introduces two conventions that result in the unique results presented in this work. First, steering error should be measured relative to the vehicle heading and not steering displacement. This concept will be developed in detail. Second, the position of axles should be located by signed rather than absolute numbers. On their own, these assumptions are quite simple. Taken together, in the context of vehicle dynamics they allow powerful results to be derived in later chapters.

At this point, in Chapter 10, the two-axle yaw-plane (or “bicycle”) vehicle model is developed. As in more standard works, external forces acting through the tire-road interface act in a reference frame fixed to the rotating vehicle. The two-axle yaw-plane model is well appreciated with conventional assumptions, but this work builds on the assumptions stated in Chapter 9. It will be appreciated in this chapter that these new conventions add no complexity to the conventional yaw-plane model. The concept that yaw rate is the vehicle response to a steering input is developed in this chapter. Steady-state yaw rate response is uniquely characterized by the vehicle wheelbase and understeer characterization in steady state. This chapter will be a key for the vehicle dynamicists, as the once familiar two-axle bicycle model is recast. Chapter 10 provides the background for the next three chapters that can largely be read in any order.

Next, the two-axle yaw-plane model is appended with additional states corresponding to an Euler angle transformation from motion in the vehicle fixed frame to an inertially fixed frame. Using small-angle approximations allows consideration of lateral displacement of the vehicle within an inertially defined traffic lane. Thus, the vehicle in this lanekeeping mode can be modeled as a dynamic transformation from a steering input to a lane position. A simple and intuitive driver model is used to determine the steering input based on a previewed lane position error, and the rear wheels are steered to shape the open loop of the driver/vehicle system. This control law on the rear steer is nonlinear and speed sensitive. It not only improves high-speed lanekeeping as designed but offers a surprising (and yet satisfying) result at low-speed consistent with Chapter 7.

[Chapter 12](#) begins with the two-axle yaw-plane model of [Chapter 10](#) and adds body roll as a degree of freedom. The rigorous treatment of reference frames pays dividends in this chapter, as a judicious choice recommended by Ellis results in a simple yet reasonably representative model. Ellis included a similar chapter in his vehicle dynamics texts, but more recent texts have omitted this topic. Roll mode dynamics in ride were introduced in [Chapter 5](#), and here they are coupled to the yaw-plane model for handling. It is a shame that more vehicle dynamic texts do not include the roll mode, as the compromises it imposes between ride and handling are fundamental to the practice of vehicle dynamics.

The third appendage to [Chapter 10](#) develops the yaw-plane model for a three-axle vehicle. Although not as common as the two-axle configuration, there are many three-axle vehicles around, mostly used for commercial purposes. This chapter develops several key innovations that will be useful later. First, it introduces nomenclature that when combined with the new conventions in this work simplifies these increasingly complex equations. Second, it develops the concept of equivalent wheelbase. In [Chapter 10](#), understeer and wheelbase characterize the steady-state yaw rate response. Understeer is a calculation from more basic vehicle parameters, but in the two-axle model of [Chapter 10](#) wheelbase is trivial. This chapter develops a function for the three-axle model that is equivalent to the trivial two-axle wheelbase, and therefore is called the “equivalent wheelbase.” Thus, there is no theoretical difference between the two-axle model and the three-axle model.

[Chapter 14](#) is the apex of theoretical development presented in the work. Steps taken in [Chapter 13](#) to add an axle to [Chapter 12](#) are generalized, resulting in a vehicle model that describes the dynamic yaw-plane behavior of a vehicle with an arbitrary number of axles, any of which can be steered. Furthermore, if the axles are steered in proportion to a single steering command, the two-axle rear steer of [Chapter 11](#) is generalized, and expressions of understeer and equivalent wheelbase are derived. Given that generalized yaw-plane model, the addition of roll applied in [Chapter 12](#) to the two-axle model is repeated here for the generalized yaw-plane model. The result is a generalized yaw-plane model including roll for a vehicle with an arbitrary number of axles, any of which can be steered. As such, it is the most general vehicle dynamic model presented to date. The section on ride included a generalized pitch plane model that complements this generalized yaw plane resulting in ride and handling characterization of a wheeled vehicle of arbitrary complexity.

Just as the ride section was concluded with a capstone case study of active suspension, this handling section is concluded with a case study relevant to autonomous vehicle handling. Autonomous vehicles require redundancy to all allow operation in the event of hardware component failure in a way that manually controlled vehicles do not. (If power steering fails in a conventional

vehicle, the driver retains directional control.) This chapter uses models developed previously in this work to suggest a method of steering redundancy that also allows the autonomous vehicle to have greater functionality than its manually controlled counterpart.

This work will derive many equations, some of them quite complicated, and requiring many parameters. More parameters, in fact, than are available in the alphabet. Furthermore, some parameters have a standard usage in the literature that is continued in this work wherever possible. Consequently, some parameters and variable names are reused, and the hope is that they are reused in ways that are obvious in the context. A good example is using t for both time, and the vehicle track width.

There was an attempt to make the chapters reasonably free-standing. The chapters open with a brief review of previously presented concepts that will be used, and close with a summary that will give the reader an idea of the important concepts just presented.

The reader will find several brief diversions into the history of science, mathematics, and engineering. These are presented in such a way so that they hopefully do not distract from an uninterested reader. It is hoped that some readers appreciate this context. Looking at the vehicle as a system has several important side benefits. One is that as drivers we can continually perceive the dynamics we are describing, and furthermore as engineers we can not only perceive but appreciate the changes that we have made. Another benefit is that the systems approach pulls together contributions from many influential historical figures. These two benefits have often occurred simultaneously for the author, and it is hoped for the reader as well. Enjoy the ride (and the handling)!

References

- [1] Milliken, W.F. and Milliken, D.L., "Chassis Design Principles and Analysis," Society of Automotive Engineers, Warrendale, PA, 2002.
- [2] Segal, Leonard, "Theoretical Prediction and Experimental Substantiation of the Response of the Automobile to Steering Control," Institution of Mechanical Engineers, London, 1956.
- [3] Milliken, Bill, "Equations of Motion," Bentley Publishers, Cambridge, MA, 2008.
- [4] Burns, Lawrence D., "Autonomy," HarperCollins, New York, 2018.

Simple Suspension as a Linear Dynamic System

“Everything turns into mathematics.”

—*Descartes*

2.1 Introduction

Ride is the response of a vehicle to changes in the road surface. The goal is to isolate the passenger as much as possible from the undulating road surface. It is a very interesting problem for at least three reasons. First, it is an incredibly fascinating application of mechanical filtering. Dynamic filtering is a concept most associated with electrical engineering, where certain frequency components of a dynamic input are considered valuable and allowed to pass, and other frequencies are considered to be a nuisance and are not allowed to pass through to the output. Rarely is there found a filtering application with such “seat of the pants” value as vehicle ride. This first chapter will apply linear systems analysis techniques to a simple example. These tools, used in electronics and control theory, were applied by Bill Milliken to aircraft dynamics, and then to ground vehicles. As such, this chapter can serve as a quick review for readers not immediately familiar with these techniques that will be used throughout the book in applications that are perhaps not as “seat of the pants” as vehicle ride.

Second, because of the “seat of the pants” effect of vehicle ride, it requires an understanding of human factors. In the end, vehicles are designed to provide a pleasant experience for humans. As with the mechanical filtering, human factors affecting ride are well understood in terms of our sensitivity to vibration in various modes. We will apply human factors to quantify ride and use them again as we discuss handling.

Third, and most important, ride is very often the dominant feature of a car in the eyes of the average purchaser drawn from the general public. It pains me greatly to say this, as I personally favor stiffly suspended vehicles that ride (and handle) like go-carts. Others do not sufficiently share my exhilaration when throwing a vehicle around a “round-about” to put up with feeling every bump in the road. But as professionals, we design vehicles for others, not for ourselves. (This was an early lesson of mine learned from working in active suspension, more on that later.) But the feature of vehicle design that is most captivating to the passionate designers is the idea that there are many inherent vehicle design compromises: purchase price, performance, physical appearance, interior utilization, luxury, and fuel economy, and someplace there is an optimum for the target market segment. In addition to these general aspects, the vehicle dynamic concepts of ride and handling are considered. Each vehicle is designed to appeal to a particular portion of the “general public.” Everybody would prefer a “cheaper car,” a “better” riding car, a “better” handling car, and so on. But different people value these attributes differently. Most people value ride greatly, but it will be at least somewhat valued by all people. At the end of the day a superior design expands the achievable envelope, including ride. The advent of autonomy is sure to change the performance criteria of vehicles, but as long as vehicles convey humans, ride will be important.

In fundamental ways, as we shall see, ride is specifically compromised by handling (in addition to these two vehicle dynamic attributes compromised by more general aspects of cost, quality, etc.). The trade-off between ride and handling is mostly found in the suspension. The primary purpose of the suspension is to isolate the human occupants from variations in the road, but in doing so it can degrade handling. Before we can explore this compromise, we must understand the dominant vehicle dynamic attribute as seen by the general public—ride. The first step is to look at the simplest mass suspended on a spring.

The simply suspended mass is not chosen to reveal any particular insight into vehicle ride. That will come later with a more complicated model. The simply suspended mass is chosen to review the basic mathematical techniques that will be used throughout this book. The simple model allows the techniques to be used in an intuitive and easily understood application, so that the focus can be on the techniques and not on the model.

2.2 The Simply Suspended Mass and Linear Systems Theory

Complexity will be incrementally added to the simply suspended mass to form the quarter-car model. In its simplest embodiment, the suspended mass allows the introduction of linear dynamic systems analysis techniques that will prove

useful throughout this book as applied to more complicated models. This will serve as a review for a reader who has perhaps not thought of such things for a while, and gradually introduces conventions and nomenclature that will be carried forward.

In general, vehicle dynamic models in this work will be of a particular idealized type. The models are generally linear, meaning that variables are multiplied by parameters. Variables are not squared, inverted, or form other “nonlinear” functions. In practice, this assumption can be valid, usually under specific circumstances. For example, for small vertical deflections a tire behaves like a linear spring. For large deflections, this assumption might not hold. For extremely large deflections, the tire could be sufficiently compressed that the hub contacts the road, significantly raising the stiffness. In the other extreme, when the tire is lifted off the road its force producing capability is lost, and it makes no sense to talk about a stiffness. But for moderate deviations about the mean position, the tire can be thought of as a linear spring. Fortunately, many parameters are like this—linear about some useful nominal range.

The models we will examine are generally time-invariant, meaning that these linear parameters do not change with time. Variables do, otherwise our system would not be dynamic, and this is the difference between variables and parameters. In reality, the mass of a vehicle varies with time as fuel is burned. We will see that the sprung mass of the vehicle bounces around 1 Hz, and in this time scale a very small mass of fuel is lost. For the purpose of this work, parameters such as mass are assumed to be constant, and therefore said to be “time-invariant.”

The final gross assumption made is that our system properties are “lumped” into parameters. For example, the mass of a vehicle is distributed throughout its structure. To simplify the model, we “lump” all the mass at a particular point, so that the dynamically relevant properties of the actual mass are somehow preserved.

These assumptions are largely justified by the mathematically tractable models they produce. Superposition is a property of a linear system that allows a reaction to complex inputs to be predicted by the system’s response to simpler inputs. System responses to a simple input can be scaled: twice the input yields twice the output. Another feature of linear systems is that they respond with a sinusoidal output when they receive a sinusoidal input. We know from Fourier that any input can be constructed with a number (possibly a large number) of sinusoidal inputs, so using superposition we can anticipate the output of linear systems to even nonsinusoidal inputs. These models result in differential equations that can be solved using Laplace transforms. Laplace transforms turn differential equations into algebraic equations that are readily solved with matrix methods. Linear systems expressed in the Laplace domain can be described by block diagrams that provide considerable intuitive value to

control theorists. To the extent that relevant system properties are preserved under these assumptions, the result is models that are simple and useful. The simplest dynamic model we start with is a simply suspended mass. This can be thought of as a quarter of the car's mass suspended on a load spring that in reality is the composite of the suspension and tire stiffness. In a basic sense this occurs at each corner of a four wheeled vehicle.

In [Figure 2.1](#), a quarter of the car's mass m_1 is lumped at the top of a load spring K_s . A displacement z_1 of the mass is allowed. This suspended mass is commonly referred to as the sprung mass. We consider a downward displacement to be positive. This application of Newton's second law (NSL) can be written. (In many ways, most of vehicle dynamics is merely repeated application of NSL.)

$$m_1 \ddot{z}_1 = -K_s z_1, \quad (2.1)$$

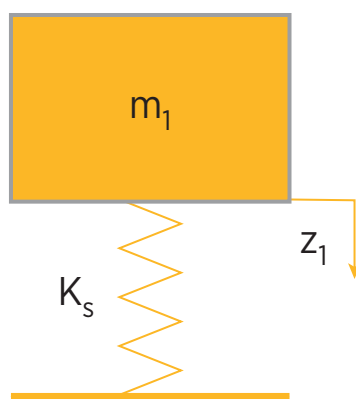
Equation 2.1 shows that the force produced by a positive displaced spring accelerates the sprung mass in a negative direction. Equation 2.1 is trivially solved for zero.

$$m_1 \ddot{z}_1 + K_s z_1 = 0. \quad (2.2)$$

At this point, it is assumed that the displacement of the sprung mass varies sinusoidally. Intuition or experience might inform the reader that this is a good assumption, but at this point there is no certainty attached to this provisional hypothesis.

$$z_1 = A \sin(\omega t). \quad (2.3)$$

FIGURE 2.1 A simply suspended mass.



Equation 2.3 assumes displacement as a simple sine wave with amplitude A and frequency, ω , varying as a function of time t . Displacement z_1 can vary with time, as it is a variable, it is only parameters like m_1 and K_s that are time invariant in our assumptions. Equation 2.3 can be once differentiated with respect to time,

$$\dot{z}_1 = A\omega \cos(\omega t) \quad (2.4)$$

and again twice differentiated.

$$\ddot{z}_1 = -A\omega^2 \sin(\omega t). \quad (2.5)$$

Equations 2.3 and 2.5 are inserted into Eq. 2.2.

$$m_1(-A\omega^2 \sin(\omega t)) + K_s(A \sin(\omega t)) = 0. \quad (2.6)$$

Equation (2.6) is simplified.

$$(K_s - m_1\omega^2)(A \sin(\omega t)) = 0. \quad (2.7)$$

So indeed we see that our provisional hypothesis—that the sprung mass moves sinusoidally—is justified. There exists a specific nonzero frequency where Eq. 2.7 is satisfied. This particular frequency is very significant and is referred to as the natural frequency.

$$\omega = \sqrt{\frac{K_s}{m_1}}. \quad (2.8)$$

When Eq. 2.8 is satisfied, Eq. 2.7 is true. Physical insight is gained from Eq. 2.6 in this condition. At this frequency, energy is transformed from potential in the displaced spring to kinetic in the accelerating mass.

We have shown that sinusoidal motion is a possible solution to differential Eq. 2.2, but is it the only solution? The sinusoidal hypothesis worked out well, while we are hot let's take another guess. Perhaps, the suspended motion can also be described as a complex exponential function,

$$z_1 = Ae^{-j\omega t}, \quad (2.9)$$

which as before can be once differentiated with respect to time,

$$\dot{z}_1 = -j\omega Ae^{-j\omega t} \quad (2.10)$$

and again twice.

$$\ddot{z}_1 = -\omega^2 A e^{-j\omega t}. \quad (2.11)$$

As before, Eq. 2.9 and Eq. 2.11 are inserted into Eq. 2.2,

$$m_1(-\omega^2 A e^{-j\omega t}) + K_s(A e^{-j\omega t}) = 0 \quad (2.12)$$

and simplified.

$$(K_s - m_1 \omega^2)(A e^{-j\omega t}) = 0. \quad (2.13)$$

So it seems our luck continues, and differential equation Eq. 2.2 is also satisfied by an exponential function. Of course Eq. 2.9 is not just any exponential function, it has an imaginary exponent. Maybe this game of guessing solutions to differential equations is not so difficult. (I know I have just aroused some unpleasant repressed memories of some of my readers having taken a formal course in differential equations.)

Try some other time varying functions of your own as potential solutions to Eq. 2.2. You will find the game is not so easy. In fact, the game is rigged. Equations 2.3 and 2.9 are related. Euler's identity famously shows how the sine function is equated to complex exponentials.

So we have applied NSL to the simple suspended mass model of [Figure 2.1](#) and found Euler's identity. In this quick introduction, we have already met two giants of physics and mathematics. One of the truly captivating features of our topic is that the vehicle system is so rich, that we will encounter many luminaries, and we will feel their contributions "in the seat of our pants."

The previous discussion was based on [Figure 2.1](#), a suspended mass that is somehow mysteriously excited, and it responds with oscillation. We now consider a more realistic example, where the input to the system is identified as a displacement of the supporting base.

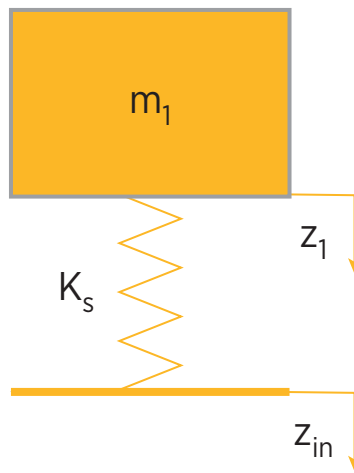
With a little imagination [Figure 2.2](#) starts to bear resemblance to a vehicle dynamic model. The mass can be assumed to be the roughly quarter of the mass that is supported by each corner suspension. The stiffness is a composite term that incorporates the effect of suspension stiffness in series with tire stiffness. The new feature of [Figure 2.2](#) is that the road now moves vertically. Equation 2.2 needs be modified to apply NSL with a moving base.

$$m_1 \ddot{z}_1 = K_s(z_{in} - z_1). \quad (2.14)$$

Equation 2.14 is simply a restatement of NSL. The left side is the product of mass and acceleration, the right side is the force. Note the signs in the right side of

FIGURE 2.2 The simply suspended mass excited by base displacement.

© Dan E. Williams.



Eq. 2.14 as compared with Eq. 2.1. The reason Eq. 2.1 has a negative sign on the right is that it is a special case of Eq. 2.14 when the input is zero. In the general case, the difference between the road input and the sprung mass response deflects the spring, and that spring deflection produces a force in the appropriate direction of the input deflection, assuming a positively defined stiffness.

Instead of assuming a solution of Eq. 2.14, we now take the Laplace transform. Simply stated, for appropriate differential equations (of the type produced by our assumptions), the time derivative of a variable can be represented by the symbol s . In convenient occurrence, the s can be treated as an algebraic variable. Terms of s can be collected, and powers of s can be formed. The reciprocal of s can be formed, and that, of course, represents integration with respect to time. (In this work, the Laplace transform of a variable is written in the upper case.)

$$(m_1 s^2 + K_s)Z_1(s) = K_s Z_{in}(s). \quad (2.15)$$

Equation 2.15 can be algebraically manipulated so solve for the ratio of $Z_1(s)$, the output, to $Z_{in}(s)$, the input.

$$\frac{Z_1(s)}{Z_{in}(s)} = \frac{K_s / m_1}{\left(s^2 + \frac{K_s}{m_1} \right)}. \quad (2.16)$$

Equation 2.16 expresses the Laplace transform of the ratio of the system output to the input as a function of s , the Laplace variable. Equation 2.16 is referred to as the transfer function of the system shown in [Figure 2.2](#).

In another happy occurrence in mathematics, it is possible to express the Laplace variable as a complex function of frequency.

$$s = j\omega. \quad (2.17)$$

Looking at Eqs 2.9, 2.10, and 2.11 and remembering that the Laplace variable is differentiation with respect to time, you can see how this works.

Equation 2.17 is inserted into Eq. 2.16.

$$\frac{Z_1(\omega)}{Z_{in}(\omega)} = \frac{\cancel{K_s/m_1}}{\left(-\omega^2 + \frac{K_s}{m_1}\right)}. \quad (2.18)$$

Equation 2.18 is referred to as the transmissibility of the system shown in [Figure 2.2](#) and is very similar to the transfer function of Eq. 2.16. Transmissibility is a function of the real variable ω , whereas the transfer function is a function of the complex Laplace variable s . In this simple example, the only time the Laplace variable is present, it is squared, so the imaginary part becomes a negative sign. We will not always be so lucky.

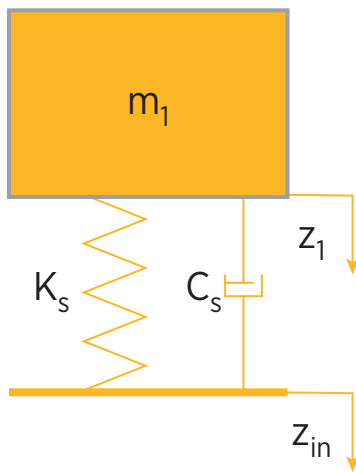
Equation 2.18 is worthy of comment. At low frequencies, $\omega \sim 0$, the output follows the input identically. This is visualized in [Figure 2.2](#). At high frequencies, when $\omega \gg 0$, the output does not move despite an input. What separates the low frequency regime from high frequencies? The natural frequency originally identified in Eq. 2.8. The natural frequency serves two purposes: (1) it determines when the denominator goes to zero, and therefore the transfer function goes to infinity, and (2) it separates low frequency behavior (output follows input) from high-frequency behavior (output attenuates input).

2.3 A Suspended Mass with Damping

[Figure 2.3](#) is very similar to [Figure 2.2](#). The only difference is that a linear damper is now in parallel with the load supporting spring. The linear damper produces a force proportional to the velocity difference between the input and the output, just as the spring produces such a force based on displacement differences. This new damping term is seen as an additional term in Eq. 2.1 upon application of NSL to the mass of [Figure 2.3](#).

FIGURE 2.3 A suspended mass with damping.

© Dan E. Williams.



$$m_1 \ddot{z}_1 = K_s (z_{in} - z_1) + C_s (\dot{z}_{in} - \dot{z}_1). \quad (2.19)$$

The Laplace transform of Eq. 2.19 is algebraically manipulated to collect like terms.

$$(m_1 s^2 + C_s s + K_s) Z_1(s) = (C_s s + K_s) Z_{in}(s). \quad (2.20)$$

The transfer function ratio of the output Laplace variable to the input Laplace variable is formed.

$$\frac{Z_1(s)}{Z_{in}(s)} = \frac{(C_s s + K_s) / m_1}{\left(s^2 + \frac{C_s}{m_1} s + \frac{K_s}{m_1} \right)}. \quad (2.21)$$

The effect of adding the linear damper is evident by comparing Eq. 2.21 with Eq. 2.16. Just as before, the Laplace variable can be replaced by a complex frequency of Eq. 2.17 to form transmissibility.

$$\frac{Z_1(\omega)}{Z_{in}(\omega)} = \frac{(C_s j\omega + K_s) / m_1}{\frac{K_s}{m_1} - \omega^2 + \frac{C_s}{m_1} j\omega}. \quad (2.22)$$

Our luck in the preceding paragraphs has run out. Equation 2.22 is more complex than Eq. 2.18 (pun intended). The cause of this complexity is immediately seen to be the damper added in [Figure 2.3](#). When a system is comprised of only a spring and mass as in [Figure 2.2](#), the sinusoidal solution can be written in the form of Eq. 2.3. The system simply transfers energy from the accelerating mass (kinetic) to the displaced spring (potential). No energy is dissipated; however, the mass is initially set into motion, it will oscillate forever. The damped system described by Eq. 2.22 will tend to oscillate if excited at something like the natural frequency of the undamped system we previously calculated, but the time domain solution is not described by something like Eq. 2.3 as the amplitude will now be a decaying function of time.

Both the numerator and denominator of Eq. 2.22 can be multiplied by the complex conjugate of the denominator.

$$\frac{Z_1(\omega)}{Z_{\text{in}}(\omega)} = \frac{\left(\frac{K_s}{m_1} + j \frac{C_s}{m_1} \omega \right) \left(\frac{K_s}{m_1} - \omega^2 - j \frac{C_s}{m_1} \omega \right)}{\left(\frac{K_s}{m_1} - \omega^2 + j \frac{C_s}{m_1} \omega \right) \left(\frac{K_s}{m_1} - \omega^2 - j \frac{C_s}{m_1} \omega \right)}. \quad (2.23)$$

Equation 2.23 can be separated into real and imaginary parts.

$$\frac{Z_1(\omega)}{Z_{\text{in}}(\omega)} = \frac{\frac{K_s}{m_1} \left(\frac{K_s}{m_1} - \omega^2 \right) + \frac{C_s^2}{m_1^2} \omega^2 - \frac{C_s}{m_1} \omega^3}{\left(\frac{K_s}{m_1} - \omega^2 \right)^2 + \left(\frac{C_s}{m_1} \omega \right)^2} + j \frac{-\frac{C_s}{m_1} \omega^3}{\left(\frac{K_s}{m_1} - \omega^2 \right)^2 + \left(\frac{C_s}{m_1} \omega \right)^2}. \quad (2.24)$$

For any input frequency ω in the system of [Figure 2.3](#), the sprung mass response is complex. This response can be located on a complex axis.

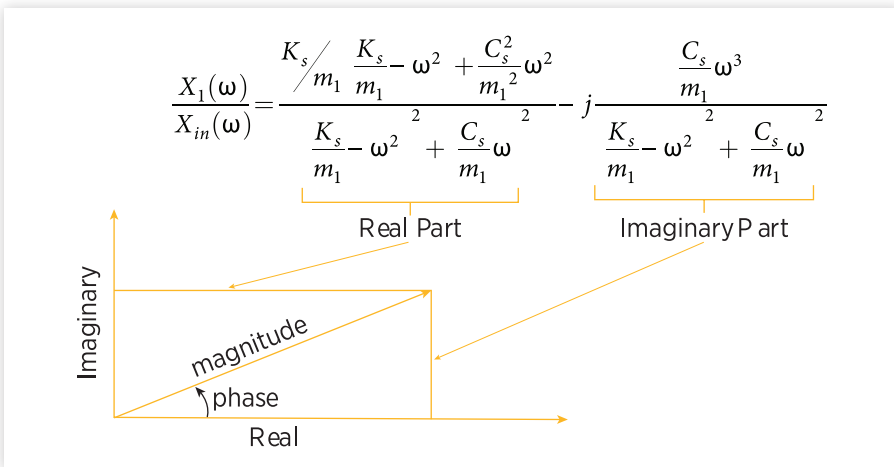
For different input frequencies both the real and complex coordinates vary. As seen in [Figure 2.4](#), a complex point could also be located by its magnitude and phase. So Eq. 2.24 locates the response in terms of real and complex components, and through trigonometry we can calculate the magnitude and phase angle of the response.

The magnitude,

$$\left| \frac{Z_1(\omega)}{Z_{\text{in}}(\omega)} \right| = \sqrt{ \left(\frac{\frac{K_s}{m_1} \left(\frac{K_s}{m_1} - \omega^2 \right) + \frac{C_s^2}{m_1^2} \omega^2}{\left(\frac{K_s}{m_1} - \omega^2 \right)^2 + \left(\frac{C_s}{m_1} \omega \right)^2} \right)^2 + \left(\frac{-\frac{C_s}{m_1} \omega^3}{\left(\frac{K_s}{m_1} - \omega^2 \right)^2 + \left(\frac{C_s}{m_1} \omega \right)^2} \right)^2 } \quad (2.25)$$

FIGURE 2.4 Response mapped to complex plane.

© Dan E. Williams.

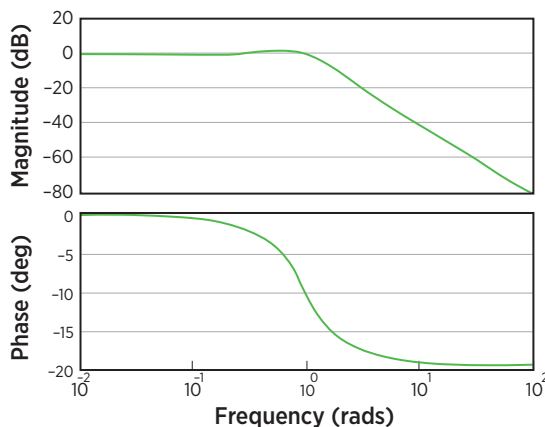


and the phase can be written.

$$\angle \frac{Z_1(\omega)}{Z_{in}(\omega)} = \tan^{-1} \frac{\left(\frac{C_s \omega^3}{m_1} \right)}{\left(\frac{(K_s - \omega^2)^2}{m_1^2} + \left(\frac{C_s \omega}{m_1} \right)^2 \right)}. \quad (2.26)$$

Equations 2.25 and 2.26 tell us a lot about the system shown in [Figure 2.3](#). For any given input frequency of the “road,” we know the ratio of the output displacement to the input, and we call this the “amplitude ratio.” We also know that the output will lag the input, and the amount of that lag is called the “phase lag.” We could repeat these calculations for a variety of input frequencies, and plot the amplitude ratio and the phase lag for an entire range of input frequencies.

When the amplitude ratio is plotted in decibels against the log of the input frequency, and placed above a plot of the phase lag against the same log of input frequency, the result is termed a Bode plot. To review our steps in constructing a Bode plot, we started with a transfer function of Eq. 2.21. We substituted the complex frequency variable, used algebra to separate the real and imaginary parts, and then used trigonometry to calculate the magnitude and phase.

FIGURE 2.5 Bode plot.

© Dan E. Williams.

Bode plots are extremely useful in the fields of dynamics and particularly controls. They are sometimes referred to as the frequency response of a system. No matter how useful they might be, Bode plots might seem to be terribly impractical given all the work we went to just to construct such a Bode plot of a very simple system. The good news is that analysis packages like MATLAB can produce Bode plots directly from a transfer function such as Eq. 2.21. You will never have to perform this calculation, but it is important to know the information contained in Bode plots because we will use them directly to infer system properties. We will also use Bode plots to determine how complex systems will behave given a knowledge of simpler system components. In practice, frequency responses are often used opposite of this development. The dynamic system is inferred from measured frequency responses in a process termed System ID.

2.4 Basic Frequency Responses

We will determine the frequency responses for five basic functions: proportional gain or multiplication, a differentiator, an integrator, a first-order lag, and a second-order lag. Many complicated systems can be built with these components, and an understanding of the frequency response of the components is helpful to understanding a more complicated composite system.

Gain

In the time domain, an input signal can be multiplied by a constant k to give a proportional output signal.

$$x_{\text{out}}(t) = kx_{\text{in}}(t). \quad (2.27)$$

The Laplace transform of Eq. 2.27 is taken

$$X_{\text{out}}(s) = kX_{\text{in}}(s) \quad (2.28)$$

and the ratio of output to input forms the transfer function.

$$\frac{X_{\text{out}}(s)}{X_{\text{in}}(s)} = k. \quad (2.29)$$

The amplitude ratio

$$\left| \frac{X_{\text{out}}(\omega)}{X_{\text{in}}(\omega)} \right| = k \quad (2.30)$$

and phase are trivially constructed.

$$\angle \frac{X_{\text{out}}(\omega)}{X_{\text{in}}(\omega)} = 0. \quad (2.31)$$

In the complex plane, the simple gain multiplier has no phase and a constant magnitude. Its locating vector is on the real axis. Because the amplitude does not vary with frequency, the frequency response or Bode plot is flat. As the amplitude ratio is conventionally plotted as decibels on the Bode plot, a gain of $k = 1$ results in $20 \log 10(1) = 0$ dB. Thus, the amplitude ratio of unity gain is 0 dB, a gain of 2 results in 6 dB, and a gain of $\frac{1}{2}$ results in -6 dB.

Differentiator

As it turns out, the differentiator is only slightly more complex than the proportional gain. A time domain input signal can be differentiated to produce an output signal,

$$x_{\text{out}}(t) = \frac{d}{dt} x_{\text{in}}(t) \quad (2.32)$$

and Laplace transformed,

$$X_{\text{out}}(s) = sX_{\text{in}}(s) \quad (2.33)$$

and forming the transfer function.

$$\frac{X_{\text{out}}(s)}{X_{\text{in}}(s)} = s. \quad (2.34)$$

The complex frequency is substituted for the Laplace variable,

$$\frac{X_{\text{out}}(j\omega)}{X_{\text{in}}(j\omega)} = j\omega \quad (2.35)$$

the amplitude ratio is simply written,

$$\left| \frac{X_{\text{out}}(\omega)}{X_{\text{in}}(\omega)} \right| = \omega \quad (2.36)$$

and the phase.

$$\angle \frac{X_{\text{out}}(\omega)}{X_{\text{in}}(\omega)} = 90^\circ. \quad (2.37)$$

On the imaginary plane, the differentiator is similar to the gain, in that it has a fixed phase, only the differentiator's phase is a constant 90° rather than zero. The differentiator's magnitude is simply the frequency. In terms of decibels on the Bode plot, the differentiator magnitude rises by 20 dB for every decade on the logarithmic frequency axis. (This slope is a function of the definition of decibel.)

Integrator

Similar to the differentiator, a time domain input signal can be integrated to form an output signal,

$$x_{\text{out}}(t) = \int x_{\text{in}}(t) dt. \quad (2.38)$$

Laplace transformed,

$$X_{\text{out}}(s) = \frac{1}{s} X_{\text{in}}(s) \quad (2.39)$$

to yield the transfer function of the integrator.

$$\frac{X_{\text{out}}(s)}{X_{\text{in}}(s)} = \frac{1}{s}. \quad (2.40)$$

The complex frequency variable is substituted for the Laplace variable,

$$\frac{X_{\text{out}}(j\omega)}{X_{\text{in}}(j\omega)} = \frac{1}{j\omega} X_{\text{in}}(j\omega) = j \frac{-1}{\omega} X_{\text{in}}(j\omega) \quad (2.41)$$

the amplitude ratio is written,

$$\left| \frac{X_{\text{out}}(\omega)}{X_{\text{in}}(\omega)} \right| = \frac{1}{\omega} \quad (2.42)$$

and when plotted on a Bode plot the slope is -20 dB/dec , and the phase angle can also be calculated.

$$\angle \frac{X_{\text{out}}(\omega)}{X_{\text{in}}(\omega)} = -90^\circ. \quad (2.43)$$

First-Order Lag

A particular transfer function with a first-order Laplace variable in the denominator is called a first-order lag.

$$\frac{X_{\text{out}}(s)}{X_{\text{in}}(s)} = \frac{1}{s+a}. \quad (2.44)$$

The complex frequency is substituted for the Laplace variable.

$$\frac{X_{\text{out}}(j\omega)}{X_{\text{in}}(j\omega)} = \frac{1}{j\omega + a}. \quad (2.45)$$

Equation 2.45 is manipulated to eliminate the complex denominator,

$$\frac{X_{\text{out}}(j\omega)}{X_{\text{in}}(j\omega)} = \frac{1}{a+j\omega} \left(\frac{a-j\omega}{a-j\omega} \right) \quad (2.46)$$

to result in positive and real parts.

$$\frac{X_{\text{out}}(j\omega)}{X_{\text{in}}(j\omega)} = \frac{a}{a^2 + \omega^2} + j \frac{-\omega}{a^2 + \omega^2}. \quad (2.47)$$

It is apparent when looking at Eq. 2.47 that at low frequencies, when ω approaches 0, the real part is $1/a$, and the imaginary part is 0. Thus at low frequencies the first-order lag appears as a gain of $1/a$. At high frequencies, when ω is much greater than a , the gain real part is 0 and the imaginary part is $-1/\omega$. Thus at high frequencies, the first-order lag appears as an integrator. It hindsight this behavior is obvious in looking at Eqs 2.44 and 2.45. This behavior is also apparent when looking at the magnitude,

$$\left| \frac{X_{\text{out}}(j\omega)}{X_{\text{in}}(j\omega)} \right| = \frac{\sqrt{a^2 + \omega^2}}{a^2 + \omega^2} \quad (2.48)$$

and the phase.

$$< \frac{X_{\text{out}}(j\omega)}{X_{\text{in}}(j\omega)} = \tan^{-1} \frac{-\omega}{a}. \quad (2.49)$$

It is worth noting that the separation between this “high”-frequency and “low”-frequency behavior is $\omega=a$. At this special frequency, the magnitude of the response is the low-frequency gain of $1/a$ divided by the square root of 2. Said another way, the amplitude function is approximately 70% of its value at very low frequencies. A 70% gain is -3 dB. Therefore, this characteristic frequency of the first-order lag frequency response can be found by looking at the frequency corresponding to a -3 dB reduction in gain from the “steady-state” low-frequency value. The value of a is perhaps even easier to ascertain from the phase plot. It is evident from Eq. 2.49 that when $\omega = a$, the phase is -45 . This makes perfect sense, halfway between the low-frequency phase of 0° and the high-frequency phase of -90° .

Second-Order Dynamics

The previous section developed a transfer function that had a first-order Laplace variable in its denominator. In this section, we look at a typical transfer function with a second-order denominator.

$$\frac{X_{\text{out}}(s)}{X_{\text{in}}(s)} = \frac{1}{s^2 + as + b}. \quad (2.50)$$

Replacing the Laplace variable with complex frequency,

$$\frac{X_{\text{out}}(j\omega)}{X_{\text{in}}(j\omega)} = \frac{1}{(j\omega)^2 + aj\omega + b} \quad (2.51)$$

and with a bit more algebraic effort Eq. 2.51 is separated into real and imaginary parts.

$$\frac{X_{\text{out}}(j\omega)}{X_{\text{in}}(j\omega)} = \left(\frac{(b - \omega^2)}{(b - \omega^2)^2 + (a\omega)^2} \right) - j \left(\frac{a\omega}{(b - \omega^2)^2 + (a\omega)^2} \right). \quad (2.52)$$

The magnitude of the second-order transfer function of Eq. 2.50 can be found,

$$\left| \frac{X_{\text{out}}(j\omega)}{X_{\text{in}}(j\omega)} \right| = \frac{1}{\sqrt{(b - \omega^2)^2 + (a\omega)^2}} \quad (2.53)$$

and its phase.

$$< \frac{X_{\text{out}}(jw)}{X_{\text{in}}(jw)} = \tan^{-1} \frac{-aw}{(b - w^2)}. \quad (2.54)$$

As with the first-order lag dynamics, it is useful to make some generalizations about the second-order dynamics, and we begin by assuming that $\omega = 0$. For this condition, the amplitude Eq. 2.53 becomes $1/b$, and the phase Eq. 2.54 becomes 0. Similar to the first-order lag, at low frequencies the second-order lag appears like a simple real valued gain. At high frequencies, when ω is large, the gain Eq. 2.53 appears to be $1/\omega^2$, and the phase Eq. 2.54 is 180° . At high frequencies, second-order dynamics appear as a “double integrator.”

The lag transfer function of Eq. 2.44 had only one parameter, but the second-order dynamics of Eq. 2.50 has two parameters. Let us consider a very interesting frequency in between the two extremes above, where $\omega^2 = b$. The amplitude equation from Eq. 2.53 becomes,

$$\left| \frac{X_{\text{out}}(j\omega)}{X_{\text{in}}(j\omega)} \right| = \sqrt{\left(\frac{0}{(0)^2 + (a\omega)^2} \right)^2 + \left(\frac{a\omega}{(0)^2 + (a\omega)^2} \right)^2} = \frac{1}{a\omega} = \frac{1}{a\sqrt{b}} \quad (2.55)$$

and the phase from Eq. 2.54.

$$< \frac{X_{\text{out}}(j\omega)}{X_{\text{in}}(j\omega)} = \tan^{-1} \frac{0}{-\frac{1}{a\sqrt{b}}} = -90^\circ. \quad (2.56)$$

It is interesting to further consider that while $b = \omega^2$, $a = 0$. In this condition, the amplitude of Eq. 2.55 becomes infinite. The second-order dynamic behavior we have just explored is relevant to the suspended mass. With a bit of algebraic manipulation the transfer function of Eq. 2.22 can resemble Eq. 2.50.

$$\frac{Z_1(s)}{Z_{\text{in}}(s)} = \frac{(C_s s + K_s) / m_1}{\left(s^2 + \frac{C_s}{m_1} s + \frac{K_s}{m_1} \right)}. \quad (2.57)$$

So when $\omega^2 = \frac{K_s}{m_1}$ and $0 = C_s$ we would expect Eq. 2.57 to have an infinite response. This is equivalent to saying that when the suspended mass of [Figure 2.3](#) is excited at its natural frequency and there is no damping, the amplitude response is infinite. If there is the slightest bit of damping, the response is not infinite, but large. The larger the damping, the more attenuated the

response at the natural frequency. We will see that this is the prime function of shock absorbers. More aptly named dampers, their primary purpose is to damp the sprung mass natural frequency. Without this damping, the response of the sprung mass would be quite large when excited at its natural frequency by road inputs.

First- and second-order dynamics can be found in the numerator of a transfer function as well as a denominator. These occurrences can be easily interpreted in terms we have previously discussed. It is important to be able to recognize the frequency responses of these basic linear dynamic functions. As we go forward, we will see that many more complicated vehicle dynamic systems can be built from these functions, or alternatively can be approximated by these functions. Over time and with experience, controls engineers start to think more in terms of the frequency domain (post Laplace transform) than the time domain. Instead of thinking of an integrator described by Eq. 2.38, Eq. 2.41 becomes favored. Both expressions are saying the same thing mathematically, but like two different languages, you tend to think with one or the other. A time domain thinker would say that an integrator has a slope of -20 db/sec on a Bode plot. A frequency domain thinker would say that a -20 dB/sec slope on a Bode plot is an integrator.

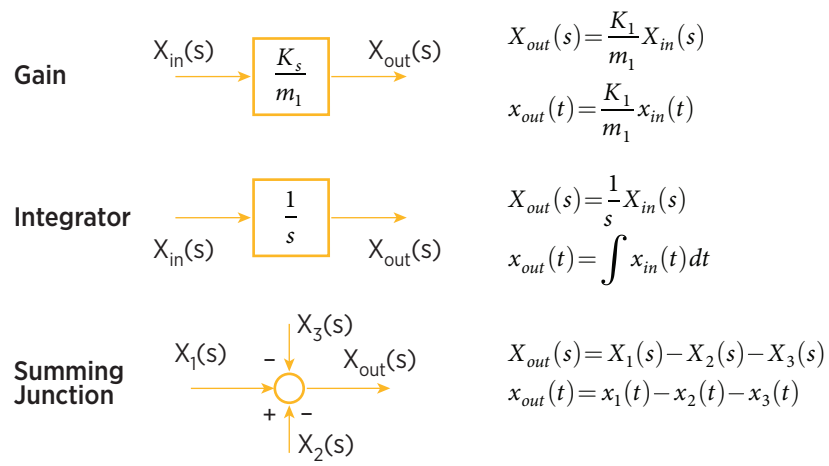
Why -20 dB/dec ? We have seen that to be a product of plotting the vertical axis of the Bode plot in decibels. This is really just a way to plot the amplitude data in log/log format, incorporating the vertical log transformation in preprocessing the data, and the horizontal log on the common frequency axis shared with the accompanying phase plot. From our perspective, it would have been better if Mr. Bode would have made his initial amplitude plot simply log/log. In that case, a differentiator would have a positive slope of dec/dec, and an integrator $-dec/dec$. Conventions such as these are important. Just like language, we tend to take conventions for granted as we use them symbolically in thought. On a positive note, they allow efficient communication between people. Just as we agree on what language we are going to use, we also agree on the conventions we use. Once established, conventions tend to stick around because they are so useful. Sometimes they outlive their usefulness, and end up creating more problems than they solve. Sometimes conventions constrain our thoughts to paradigms.

2.5 State Space and Block Diagram Algebra

Block diagram algebra is a technique that can mathematically describe complex systems with simple components, some of which have already been introduced as we discussed basic frequency responses.

FIGURE 2.6 Basic block diagram algebra elements.

© Dan E. Williams.



When the gain and integrator of [Figure 2.6](#) are connected in series, the amplitude, or gain, multiplies, and the phase delay adds. Because we plot the log of gain on Bode plots, both the amplitude and phase of the series connected Bode plots add to yield the resulting connected Bode plot.

The frequency response of the transfer function between $Z_2(s)$ and $X(s)$ as shown in [Figure 2.7](#) is the generic single integrator with a magnitude reducing at -20 dB/sec and a phase of -90° . This is the same frequency response of the transfer function between $Z_1(s)$ and $Z_2(s)$. When we consider the overall frequency response of the double integrator transfer function between $Z_1(s)$ and $X(s)$, we find a magnitude declining at -40 dB/dec and a phase of -180 . The amplitude of a series connected differentiator and integrator is -20 and $+20$ dB/dec or 1 , and the phase is $+90^\circ - 90^\circ$, or 0 , in other words unity gain. This series combination of transfer functions can be generalized as shown in [Figure 2.8](#).

FIGURE 2.7 Double integrator combination.

© Dan E. Williams.

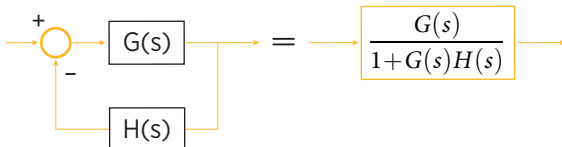
**FIGURE 2.8** Series combination of transfer functions.

$$\rightarrow \boxed{G(s)} \rightarrow \boxed{H(s)} \rightarrow = \rightarrow \boxed{G(s)H(s)} \rightarrow$$

© Dan E. Williams.

In a similar way, classic feedback of transfer functions can be formed.

FIGURE 2.9 Transfer function of feedback.



© Dan E. Williams.

Figure 2.9 is a common block diagram operation in control systems. In general, an input is compared with an output (negative feedback) in the summing junction to form an error signal that drives feedforward dynamics. A commonly occurring form of this general feedback system is when $H(s)$ is one, in which case the output of the $G(s)$ dynamics is directly compared with the input. In such systems, the output will track the input, which is one of the reasons why feedback control systems are so useful. In this case, the feedback is subtracted from the command, forcing an error signal. The higher the gain on the error signal, the more the output will act to reduce the error. This “loop gain” is practically limited by stability, and this is the basis of control theory.

At this point, it is interesting to briefly contemplate the stiffness convention, in terms of the standard form of feedback system shown in **Figure 2.9**. Careful inspection of Eq. 2.1 repeated below shows that when the suspended mass is displaced, the spring generates a restoring force.

$$m_1 \ddot{z}_1 = -K_s z_1.$$

In Eq. 2.1, the restoring nature of the spring is shown explicitly in the negative sign attached to K_s . Alternatively, it is possible to consider the actual K_s negative, as was actually the spring contemplated by Robert Hooke. Hooke was a contemporary of Newton and a rival. He developed alternative theories of refraction and gravity. Hooke was also a colleague of Newcomen, famous for the steam engine, and coined the term cell to describe what he saw looking at plant tissue in a microscope.

Equation 2.1 was derived from **Figure 2.1**, but the same notion of a Hooke’s restoring force could be applied to **Figure 2.2**, where the base displaces to moderate the effect of the displaced mass.

$$m_1 \ddot{z}_1 = -K_s (z_1 - z_{in}). \quad (2.58)$$

Equation 2.58 can be compared with Eq. 2.14, which was previously derived to describe the effect of the input of the base.

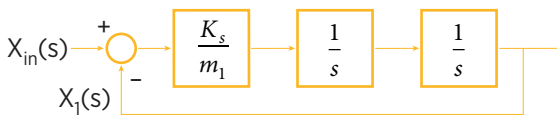
$$m_1 \ddot{z}_1 = K_s (z_{in} - z_1).$$

Algebraically, the difference is merely how a negative sign is distributed. Intuitively, however, the difference is greater. On one hand, the spring is a restoring force, serving to oppose a displacement of the sprung mass, and moderated if the base moves. On the other hand, the spring serves to urge the sprung mass as the base moves and moderate the urge if the sprung mass actually moves. If the mass is somehow displaced and allowed to freely respond the first convention is appropriate, but if the base is displaced, the second convention is more intuitive to describe the sprung mass response.

It is interesting to compare the block diagram formed by Eq. 2.14.

FIGURE 2.10 Block diagram from Newton's Second Law (NSL) of suspended mass.

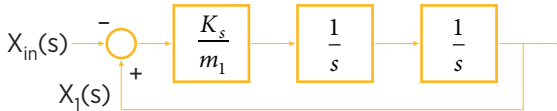
© Dan E. Williams.



A block diagram can be formed from Eq. 2.58.

FIGURE 2.11 Block diagram from Hooke's spring law and suspended mass.

© Dan E. Williams.



The block diagrams of [Figures 2.10](#) and [2.11](#) are equivalent when one considers that K_s in [Figure 2.11](#) is negative. In both cases, a positive displacement of the base produces a positive force on the mass, and conversely a positive displacement of the mass produces a negative force on it. However, [Figure 2.10](#) clearly is in keeping with the conventional closed loop feedback form of [Figure 2.9](#). This form is more reflective of the notion that the spring isolates the mass from known inputs in the base, and intuitively presents the notion of transmissibility. The negative stiffness is really only intuitive for a fixed base and initially displaced mass, begging the question of what unknown force initially displaces the mass? [Figure 2.10](#) better describes a relevant input. Conventions are clearly important. While insignificant for mathematical correctness, they can dramatically affect clarity of thought. The importance of convention will be a recurring theme in this work. Proper selection of convention and nomenclature makes the problem more intuitive.

The double integrator shown in [Figure 2.7](#) is used in [Figures 2.10](#) and [2.11](#). When looking at [Figures 2.10](#) and [2.11](#) and Eqs 2.14 and 2.58 that describe the figures, it is evident that the double integrator comes from the acceleration term in NSL, and the summing junction feeding the double integrator is basically the equal sign in NSL.

We return to Eq. 2.19 that describes [Figure 2.3](#),

$$m_1 \ddot{z}_1 = K_s(z_{\text{in}} - z_1) + C_s(\dot{z}_{\text{in}} - \dot{z}_1)$$

that is solved for the highest-order derivative.

$$\ddot{z}_1 = \frac{K_s}{m_1}(z_{\text{in}} - z_1) + \frac{C_s}{m_1}(\dot{z}_{\text{in}} - \dot{z}_1) \quad (2.59)$$

Equation 2.59 is Laplace transformed.

$$s^2 Z_1(s) = \left(\frac{K_s + C_s s}{m_1} \right) Z_{\text{in}}(s) - \frac{K_s}{m_1} Z_1(s) - \frac{C_s}{m_1} s Z_1(s). \quad (2.60)$$

A new temporary variable is defined.

$$s^2 Z_1(s) = X(s). \quad (2.61)$$

Equation 2.61 is integrated once in the Laplace domain,

$$s Z_1(s) = \frac{1}{s} X(s) \quad (2.62)$$

and again twice.

$$Z_1(s) = \frac{1}{s^2} X(s) \quad (2.63)$$

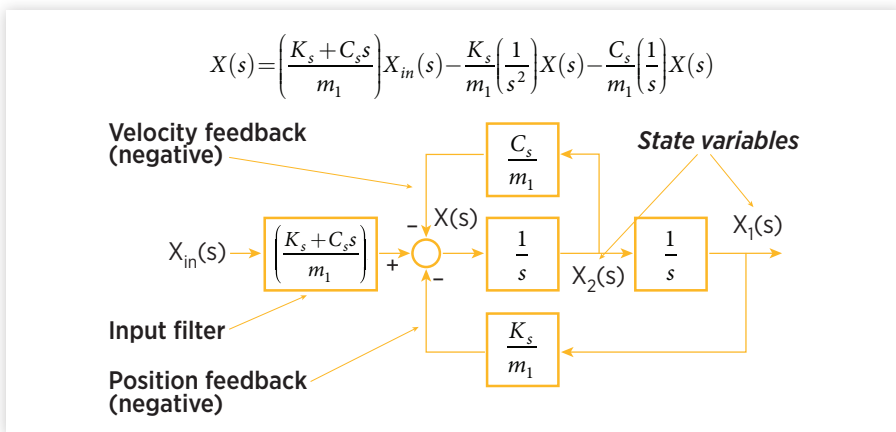
Equations 2.61, 2.62, and 2.63 are inserted into Eq. 2.60.

$$X(s) = \left(\frac{K_s + C_s s}{m_1} \right) Z_{\text{in}}(s) - \frac{K_s}{m_1} \left(\frac{1}{s^2} \right) X(s) - \frac{C_s}{m_1} \left(\frac{1}{s} \right) X(s). \quad (2.64)$$

Recalling Eq. 2.61, Eq. 2.64 is really an expression for the Laplace transform of the acceleration of Z_1 . Why do we go to all this trouble? Equations 2.60 and 2.64 appear in some sense equivalent, one is written in terms of s , the other in $1/s$. Integration is a more numerically stable process, as will be shown shortly.

FIGURE 2.12 Complete block diagram of suspended mass.

© Dan E. Williams.



When the temporary variable $X(s)$ is known from Eq. 2.64, the velocity of the original variable is given by Eq. 2.62, and the original displacement by Eq. 2.63. Together, Eqs 2.62, 2.63, and 2.64 are equivalent to Eq. 2.60. We have taken the original second-order differential equation of Eq. 2.60 and replaced it with two first-order integrators of Eqs 2.62 and 2.63, and an algebraic Eq. 2.64.

[Figure 2.12](#) displays some generic properties of a general block diagram. The double integrator provides velocity and position from acceleration. The acceleration is calculated at a summing junction that subtracts a displacement term and a velocity term from a filtered input. It is evident that [Figure 2.12](#) is consistent with the positive stiffness assumption of [Figure 2.10](#), and with this form can be simplified with the block diagram algebra of [Figure 2.9](#) to yield an overall transfer function from input to output displacements, which can be used to find transmissibility.

2.6 State Space Realization

The outputs of the integrators in [Figure 2.12](#) are called state variables. State variables are not unique for a given system, but for mechanical systems that we will be discussing it is very intuitive to cast the system as we have, so that the state variables are displacement and position. If you know the state variables at any instant in time, and know the future inputs after that initial time, the future state variables are known. So the state variables describe the “state” of the system. (“State variable” is simply the formal name for the “variable” term that we introduced at the beginning of the chapter.)

It is almost trivial, but ultimately very powerful, to write Eq. 2.59, a second-order differential equation, as two first-order differential equations, in keeping with the state variables identified in [Figure 2.12](#).

$$\dot{z}_1 = z_2, \quad (2.65)$$

$$\dot{z}_2 = \frac{K_s}{m_1}(z_{in} - z_1) + \frac{C_s}{m_1}(\dot{z}_{in} - \dot{z}_1). \quad (2.66)$$

Equations 2.65 and 2.66 can be Laplace transformed.

$$sz_1 = z_2, \quad (2.67)$$

$$sz_2 = \frac{K_s}{m_1}(z_{in} - z_1) + \frac{C_s}{m_1}(sz_{in} - sz_1). \quad (2.68)$$

Equations 2.67 and 2.68 can be written in matrix form:

$$\begin{bmatrix} \dot{z}_1 \\ \dot{z}_2 \end{bmatrix} = \begin{bmatrix} 0 & 1 \\ \frac{-K_s}{m_1} & \frac{-C_s}{m_1} \end{bmatrix} \begin{bmatrix} z_1 \\ z_2 \end{bmatrix} + \begin{bmatrix} 0 & 0 \\ \frac{K_s}{m_1} & \frac{C_s}{m_1} \end{bmatrix} \begin{bmatrix} z_{in} \\ \dot{z}_{in} \end{bmatrix}. \quad (2.69)$$

If we assume that the mass is somehow displaced with an initial value of z_1 or z_2 (initial displacement or velocity) and there is no input, Eq. 2.69 becomes,

$$\begin{bmatrix} \dot{z}_1 \\ \dot{z}_2 \end{bmatrix} = \begin{bmatrix} 0 & 1 \\ \frac{-K_s}{m_1} & \frac{-C_s}{m_1} \end{bmatrix} \begin{bmatrix} z_1 \\ z_2 \end{bmatrix}. \quad (2.70)$$

The Laplace transform of the matrix Eq. 2.70 can be taken.

$$\begin{bmatrix} s & 0 \\ 0 & s \end{bmatrix} \begin{bmatrix} z_1 \\ z_2 \end{bmatrix} = \begin{bmatrix} 0 & 1 \\ \frac{-K_s}{m_1} & \frac{-C_s}{m_1} \end{bmatrix} \begin{bmatrix} z_1 \\ z_2 \end{bmatrix}. \quad (2.71)$$

If the matrix \mathbf{A} is defined.

$$\mathbf{A} = \begin{bmatrix} 0 & 1 \\ \frac{-K_s}{m_1} & \frac{-C_s}{m_1} \end{bmatrix}. \quad (2.72)$$

Equation 2.71 can be written,

$$[sI]\mathbf{x} = \mathbf{Ax} \quad (2.73)$$

and terms collected for the state vector \mathbf{x} .

$$[\mathbf{sI} - \mathbf{A}] \mathbf{x} = \mathbf{0}. \quad (2.74)$$

Equation 2.74 is in some way the matrix equivalent of the free responses of Eqs 2.7 and 2.13. Equations 2.7 and 2.13 are simpler because they did not include the damping term present in [Figure 2.3](#). Without damping, both the displacement and the twice differentiated acceleration are real numbers. When damping is considered, the differential equation cannot be so simplified, and needs to be written as either a second-order differential equation or two first-order differential equations to be expressed in real numbers.

But the principle used in the solution of Eqs 2.7 and 2.13 is the same for Eq. 2.74. It is possible to find a matrix \mathbf{A} such that Eq. 2.74 holds. Equation 2.74 is similar to the classic eigenvalue problem of $[\lambda \mathbf{I} - \mathbf{A}]$. So the values of s that satisfy Eq. 2.74 are similar to the $j\omega$ that satisfies Eqs 2.7 and 2.13. This condition is expressed as the eigenvalue of $[\mathbf{sI} - \mathbf{A}]$. If there is no damping in \mathbf{A} , the eigenvalue of Eq. 2.74 is Eq. 2.8.

Specifically, the eigenvalue of Eq. 2.74 can be found.

$$s_{1,2} = \frac{-C_s + / - \sqrt{C_s^2 - 4K_s m_1}}{2m_1}. \quad (2.75)$$

When damping is 0,

$$s_{1,2} = + / - j \sqrt{\frac{K_s}{m_1}} \quad (2.76)$$

and if $s = j\omega$ Eq. 2.76 is equivalent to Eq. 2.8.

2.7 First-Order Matrix Differential Equations

It was just shown how a second-order system can be expressed as two first-order differential equations. In general complex linear differential equations can be expressed as first-order differential equations. A system of coupled linear differential equations can be algebraically reduced to the following form where x_i is considered to be a dynamic state variable, and u_i is considered to be an input and the dot notation is used to denote a derivative with respect to time.

$$\begin{aligned}\dot{x}_1 &= a_{11}x_1 + a_{12}x_2 + \dots + a_{1n}x_n + b_{11}u_1 + b_{12}u_2 + \dots + b_{1m}u_m \\ \dot{x}_2 &= a_{21}x_1 + a_{22}x_2 + \dots + a_{2n}x_n + b_{21}u_1 + b_{22}u_2 + \dots + b_{2m}u_m \\ &\vdots \\ \dot{x}_n &= a_{n1}x_1 + a_{n2}x_2 + \dots + a_{nn}x_n + b_{n1}u_1 + b_{n2}u_2 + \dots + b_{nm}u_m.\end{aligned}$$

This system of first-order differential equations can be expressed in matrix form:

$$\begin{bmatrix} \dot{x}_1 \\ \vdots \\ \dot{x}_n \end{bmatrix} = \begin{bmatrix} a_{11} & \cdots & a_{1n} \\ \vdots & \ddots & \vdots \\ a_{n1} & \cdots & a_{nn} \end{bmatrix} \begin{bmatrix} x_1 \\ \vdots \\ x_n \end{bmatrix} + \begin{bmatrix} b_{11} & \cdots & b_{1m} \\ \vdots & \ddots & \vdots \\ b_{n1} & \cdots & b_{nm} \end{bmatrix} \begin{bmatrix} u_1 \\ \vdots \\ u_m \end{bmatrix} \quad (2.77)$$

and further condensed by using symbolic vectors and matrices.

$$\dot{\mathbf{x}} = \mathbf{Ax} + \mathbf{Bu}. \quad (2.78)$$

The operation of the Laplace variable s is combined with the structure of an identity matrix \mathbf{I} .

$$s\mathbf{Ix} = \mathbf{Ax} + \mathbf{Bu} \quad (2.79)$$

and solved for the state vector \mathbf{x} .

$$\mathbf{x} = [s\mathbf{I} - \mathbf{A}]^{-1} \mathbf{Bu}. \quad (2.80)$$

The inverse of a matrix is its adjoint scaled by its determinant, where the adjoint is the transpose of the matrix of cofactors. In general, this requires the evaluation of a determinant of order one fewer than the original matrix for each element. In the special case of a two-dimensional system these “minor determinants” are trivial,

$$[s\mathbf{I} - \mathbf{A}]^{-1} = \frac{\begin{bmatrix} a_{11} & -a_{21} \\ -a_{12} & a_{22} \end{bmatrix}}{\Delta}, \quad (2.81)$$

where Δ is the characteristic polynomial. For the special case of a two dimensional system, the state vector can thus be simply expressed.

$$\mathbf{x} = \frac{\begin{bmatrix} a_{11} & -a_{21} \\ -a_{12} & a_{22} \end{bmatrix} \mathbf{Bu}}{\Delta}. \quad (2.82)$$

It is also possible that the final outputs of interest are linear combinations of state variables

$$\mathbf{y} = \mathbf{Cx} \quad (2.83)$$

and this output vector can be written in terms of the input vector.

$$\mathbf{y} = \frac{\mathbf{C}[\mathbf{sI} - \mathbf{A}]^{-1} \mathbf{Bu}}{\Delta}. \quad (2.84)$$

Recall that \mathbf{u} and \mathbf{y} are input and output vectors respectively. Therefore the polynomial elements of the matrix

$$\frac{\mathbf{C}[\mathbf{sI} - \mathbf{A}]^{-1} \mathbf{B}}{\Delta} \quad (2.85)$$

can be considered transfer functions from the respective input to the respective output. By using the Laplace transform of linear time invariant differential equations, complex systems can be considered as coupled first-order differential equations, where output can be predicted using linear algebra techniques.

2.8 Summary

Assumptions leading to linear systems allow efficient mathematical tools to be used to simplify dynamic systems. Fortunately, many physical systems to some degree resemble linear systems. Simple linear elements can be connected to form more complicated physical linear systems. It is possible to put a linear differential equation into block diagram form, and from there into state space form.

Conventions are important. With properly chosen convention, the simply suspended mass is seen to be a closed loop, with the error between the input (command) and the displacement of mass forming an error that is multiplied by the stiffness. The downward positive z -axis might add a bit of confusion; however, this is common in vehicle models and allows for a more convenient right-handed axis to deal with handling.

This has been a quick survey of the landscape of linear systems theory. The intent of this chapter was not to convey the complete subject matter of this extremely rich theory. Rather, the purpose was to refresh the memory of a reader who was previously exposed to linear systems theory by developing the suspended mass example that will be further developed in the next chapter. If the reader is uncomfortable with the material discussed in this chapter, a quick read of a linear system dynamics book might be a good idea.

The Quarter-Car Model

“

All models are wrong, some
are useful.

—George E.P. Box

”

3.1 Introduction

George E.P. Box famously quipped that “all models are wrong, but some are useful.” Albert Einstein once said that “make things as simple as possible … but not simpler.” Taken together, these two thoughts capture the art of modeling dynamic systems. Models are judged by the standards of simplicity and usefulness. The convergence of these two concepts is a wonderful word: parsimony. A parsimonious model efficiently conveys understanding of a dynamic system. There are two fundamental parsimonious models in vehicle dynamics, and the first useful in ride is the quarter-car model.

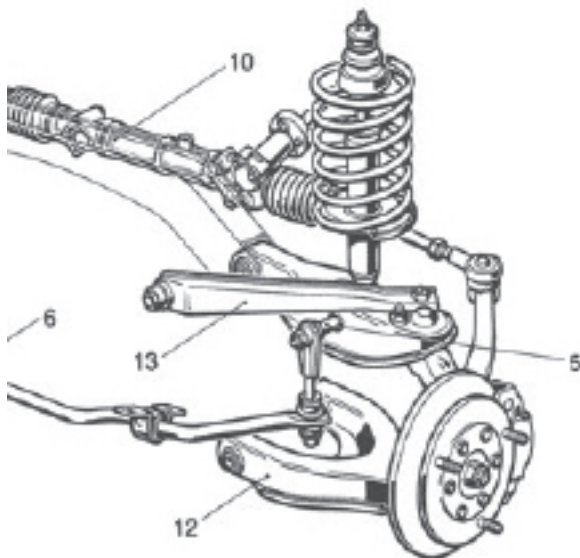
In the previous chapter, a simply suspended mass was analyzed with various techniques from linear system analysis. Those same techniques will be utilized in this chapter, only with a more realistic corner model. By introducing an unsprung mass distinct from the sprung mass, we will identify two fundamental resonant frequencies, compare these with human sensitivity, and develop a method to evaluate the effect of parameter variation.

3.2 Representing Reality with the Quarter-Car Model

This chapter builds on the previous model of a simply suspended mass that combines the tire and suspension springs at each corner. Now, the tire and suspension springs are separated by the wheel hub mass. Many complicated real-world suspension systems can be approximated by this method.

In [Figure 3.1](#), Rempell and Stoll show a typical independently suspended front corner [1]. Independent suspension implies no mechanical coupling across axles. A dynamically coupled front suspension would be a solid axle across both front corners so that input motions on one side are felt on the other. In independent suspensions, there is no real axle, and input motions at one corner do not directly affect other corners.

FIGURE 3.1 Typical multilink suspension.

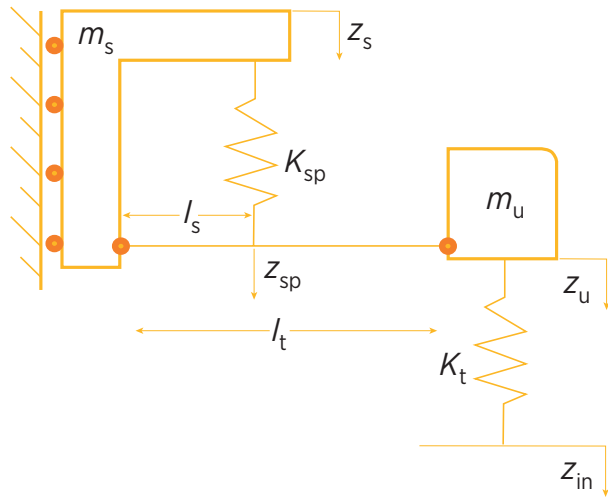


Reprinted with permission from © SAE International.

In the independent front suspension (IFS) shown in [Figure 3.1](#), two mechanical links locate the wheel hub to which the tire is fixed. One side of the links is attached to the hub with means allowing rotation (ball joints), and the other side of the links, also allowing rotation, is attached to the sprung mass. The suspension spring is attached to one locating link, midway between the hub and spring mass. The other end of the spring is attached to the sprung mass. The quarter-car IFS shown pictorially in [Figure 3.1](#) can be redrawn schematically.

FIGURE 3.2 Schematic of multilink suspension.

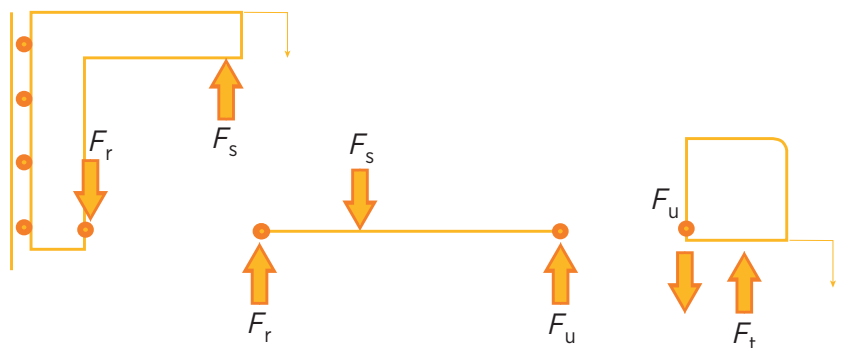
© Dan E. Williams.



In [Figure 3.2](#), the road input deflects a tire spring that acts upon the hub mass. The hub mass is connected to the sprung mass by a link that is roughly horizontal and free to rotate at each end. Therefore, the link can directly transmit a lateral force from the hub to the sprung mass. A vertical force on the hub, however, is more complex. It creates not only a compression in the load spring, but also a reaction on the link attachment to the sprung mass. The sprung mass is constrained to move vertically. These three forces, the tire spring force, the load spring force, and the reaction force, can be identified relative to their respective masses, as shown in [Figure 3.3](#).

FIGURE 3.3 Forces and reaction forces on multilink suspension.

© Dan E. Williams.



The tire force on the unsprung mass can be calculated. The deflection of the tire spring is the vertical road input minus the unsprung mass displacement. This deflection multiplied by the vertical stiffness of the tire produces a positive force on the unsprung mass.

$$F_t = K_t (z_{in} - z_u). \quad (3.1)$$

Similarly, the suspension spring force can be calculated from the spring deflection. The suspension spring deflection is the vertical motion of the lower spring attachment to the suspension link z_{sp} , minus the vertical deflection of the sprung mass.

$$F_s = K_{sp} (z_{sp} - z_s). \quad (3.2)$$

The deflection of the lower suspension spring attachment can be written as follows:

$$z_{sp} = \left(1 - \frac{l_s}{l_t}\right) z_s + \frac{l_s}{l_t} z_u. \quad (3.3)$$

Equation 3.3 is inserted into Eq. 3.2, and simplified to express the suspension spring force in terms of sprung and unsprung mass displacements.

$$F_s = \frac{l_s}{l_t} K_{sp} (z_u - z_s). \quad (3.4)$$

The reaction force of the unsprung mass on the massless suspension link can be written by summing moments about the sprung mass attachment point of the link,

$$F_u = F_s \frac{l_s}{l_t} \quad (3.5)$$

and inserting Eq. 3.4 into Eq. 3.5 the unsprung mass reaction force can be written in terms of unsprung mass, link geometry, and sprung mass displacements.

$$F_u = \left(\frac{l_s}{l_t}\right)^2 K_{sp} (z_u - z_s). \quad (3.6)$$

Vertical forces on the suspension link can be equated,

$$F_s = F_r + F_u \quad (3.7)$$

and solved for the reaction force F_r of the suspension link on the sprung mass.

$$F_r = F_s - F_u. \quad (3.8)$$

Inserting Eq. 3.5 into Eq. 3.8,

$$F_r = F_s \left(1 - \frac{l_s}{l_t} \right), \quad (3.9)$$

which allows Eq. 3.2 to be inserted into Eq. 3.9.

$$F_r = \left(1 - \frac{l_s}{l_t} \right) \frac{l_s}{l_t} K_{sp} (z_u - z_s). \quad (3.10)$$

Newton's second law can be written for the sprung mass,

$$m_s \ddot{z}_s = F_s - F_r \quad (3.11)$$

and Eqs 3.4 and 3.10 inserted and simplified.

$$m_s \ddot{z}_s = \left(\frac{l_s}{l_t} \right)^2 K_{sp} (z_u - z_s). \quad (3.12)$$

Similarly, Newton's second law can be written for the unsprung mass,

$$m_u \ddot{z}_u = F_t - F_u \quad (3.13)$$

and Eqs 3.1 and 3.6 inserted,

$$m_u \ddot{z}_u = K_t (z_{in} - z_u) - \left(\frac{l_s}{l_t} \right)^2 K_{sp} (z_u - z_s) \quad (3.14)$$

and simplified in terms of sprung and unsprung mass displacements.

$$m_u \ddot{z}_u = K_t z_{in} - \left(K_t + \left(\frac{l_s}{l_t} \right)^2 K_{sp} \right) z_u + \left(\frac{l_s}{l_t} \right)^2 K_s z_s. \quad (3.15)$$

It is evident from inspection of Eqs 3.12 and 3.15 that the suspension spring term always appears with a dimensionless function of the suspension link geometry. Therefore, we can redefine the load spring stiffness as the original stiffness times the dimensionless function.

$$K_s = \left(\frac{l_s}{l_t} \right)^2 K_{sp}. \quad (3.16)$$

With this simplification allowing an “effective” K_s to be used, differential Eq. 3.14 from Newton’s second law can be written as

$$m_u \ddot{z}_u = K_t (z_{in} - z_u) - K_s (z_u - z_s) \quad (3.17)$$

and similarly the differential Eq. 3.12 from Newton’s second law applied to the sprung mass can be written.

$$m_s \ddot{z}_s = K_s (z_u - z_s). \quad (3.18)$$

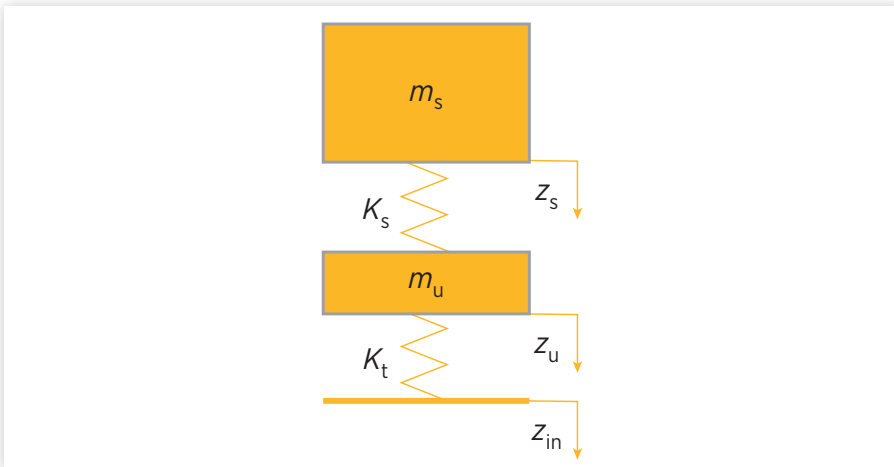
Equations 3.17 and 3.18 describe a simple system that can be shown pictorially in [Figure 3.4](#).

[Figure 3.4](#) shows schematically the celebrated quarter-car model. This is the first of two fundamental vehicle dynamic models explored in this work (the second is the yaw-plane or bicycle model that plays a similarly fundamental role in vehicle handling). These fundamental models combine the twin precepts of usefulness and simplicity. Specifically, their value lies in describing basic behavior present in real systems of interest. We study such models in engineering because they describe characteristics that are not just curiosities, but properties whose understanding are essential to improvement of the system.

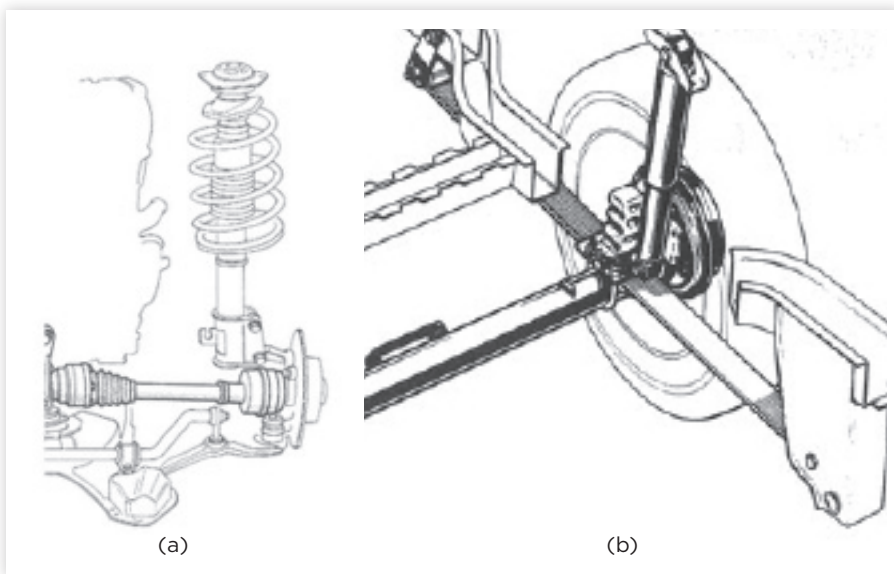
[Figure 3.4](#) is a clear simplification of [Figure 3.1](#) that will allow us in time to make certain conclusions about the dynamics of the multilink suspension.

FIGURE 3.4 Quarter-car schematic model.

© Dan E. Williams.

**FIGURE 3.5** McPherson and leaf suspensions.

Reprinted with permission from © SAE International.



If that were its sole purpose, the model would be somewhat useful. However, it can be shown that the model of [Figure 3.4](#) can similarly describe the fundamental dynamics of other real-world suspensions, such as the McPherson strut and with a little more work the solid axle both shown in [Figure 3.5](#).

3.3 Two Fundamental Frequencies of Interest

Considering the widely applicable two-mass quarter-car model of [Figure 3.4](#), we initially consider the input to be zero to describe unforced vibrations.

$$z_{\text{in}} = 0. \quad (3.19)$$

Newton's second law describes the effects of the spring force on the sprung mass, similar to the suspended mass of the previous section,

$$m_s \ddot{z}_s = -K_s z_s + K_s z_u \quad (3.20)$$

and for the hub or unsprung mass,

$$m_u \ddot{z}_u = z_s K_s + z_u (-K_t - K_s). \quad (3.21)$$

The Laplace transform of Eq. 3.20 can be written as

$$m_s s^2 Z_s(s) = -K_s Z_s(s) + K_s Z_u(s) \quad (3.22)$$

and similarly for Eq. 3.21.

$$m_u s^2 Z_u(s) = K_s Z_s(s) + (-K_t - K_s) Z_u(s). \quad (3.23)$$

Equations 3.22 and 3.23 can be set to 0,

$$m_s s^2 Z_s(s) + K_s Z_s(s) - K_s Z_u(s) = 0, \quad (3.24)$$

$$m_u s^2 Z_u(s) - K_s Z_s(s) + (K_t + K_s) Z_u(s) = 0, \quad (3.25)$$

and put in matrix form.

$$\begin{bmatrix} m_s s^2 & 0 \\ 0 & m_u s^2 \end{bmatrix} \begin{bmatrix} Z_s(s) \\ Z_u(s) \end{bmatrix} + \begin{bmatrix} K_s & -K_s \\ -K_s & K_t + K_s \end{bmatrix} \begin{bmatrix} Z_s(s) \\ Z_u(s) \end{bmatrix} = 0 \quad (3.26)$$

Just as with the simply suspended mass, $s = j\omega$ can be inserted into Eq. 3.26.

$$\begin{bmatrix} K_s - m_s \omega^2 & -K_s \\ -K_s & (K_t + K_s) - m_u \omega^2 \end{bmatrix} \begin{bmatrix} Z_s(\omega) \\ Z_u(\omega) \end{bmatrix} = 0. \quad (3.27)$$

The eigenvalues of the 2×2 matrix in Eq. 3.27 can be found from the determinant of the following matrix:

$$\det[\lambda I - A] = \det \begin{bmatrix} \lambda - K_s + m_s \omega^2 & K_s \\ K_s & \lambda - (K_t + K_s) + m_u \omega^2 \end{bmatrix} = 0. \quad (3.28)$$

A frequency ω that makes Eq. 3.28 true is called the eigenfrequency or natural frequency of the system shown in [Figure 3.4](#). Eigenvalues of Eq. 3.28 can be calculated,

$$\omega_1^2, \omega_2^2 = \frac{1}{2} \left(\frac{m_s(K_t + K_s) + m_u K_s}{m_u m_s} \right) \pm \frac{1}{2} \sqrt{\frac{(m_s(K_t + K_s) - m_u K_s)^2 + 4m_u m_s K_s^2}{m_u^2 m_s^2}} \quad (3.29)$$

and somewhat simplified.

$$\omega_1^2, \omega_2^2 = \frac{1}{2m_u m_s} \left(m_s(K_t + K_s) + m_u K_s \pm \sqrt{(m_s(K_t + K_s) + m_u K_s)^2 - 4m_s m_u (K_s K_t)} \right) \quad (3.30)$$

Typical approximate and “round” values for the parameters shown in [Figure 3.4](#) are $K_s = 150$ lbs/in, $K_t = 1000$ lbs/in, $W_s = 1000$ lbs, and $W_u = 100$ lbs.

With these typical parameters, eigenfrequencies satisfying Eq. 3.28 are $\omega_1 = 10.588$ Hz and $\omega_2 = 1.1249$ Hz. These frequencies were calculated using approximate parameter values for mass and stiffness. It is worth noting that these natural frequencies are separated by an order of magnitude.

Insight into these two fundamental frequencies can be obtained by forming approximations made from assumptions to the system shown in [Figure 3.4](#), justified by the reasonable parameter values. First we notice that the unsprung mass m_u is very small relative to the sprung mass m_s , so that we might assume that m_u is 0. In this case, the sprung mass is supported by the series combination of the tire and suspension springs.

$$\omega_{\text{ride}} = \sqrt{\frac{K_s K_t / (K_s + K_t)}{m_s}} \quad (3.31)$$

Equation 3.31 defines the natural frequency of the sprung mass shown in [Figure 3.4](#). When our typical parameters are applied to Eq. 3.31, we get a ride natural frequency of 1.1273 Hz, differing from the exact value calculated from Eq. 3.30 by less than 0.25%.

The next assumption follows similar reasoning. Now given the differences in the masses, we assume that the sprung mass is infinite compared to the nonzero unsprung mass. With this assumption, the sprung mass is considered to be inertially grounded. Therefore, the unsprung mass is located by the parallel combination of the suspension and tire stiffnesses.

$$\omega_{\text{wheel hop}} = \sqrt{\frac{K_s + K_t}{m_u}} \quad (3.32)$$

Equation 3.32 reports the natural frequency of the unsprung mass, popularly referred to as the “wheel hop” frequency. As before, when our typical parameters are applied to Eq. 3.32, the wheel hop frequency is found to be 10.5848 Hz, again with even better agreement with Eq. 3.30.

Although the actual frequencies of the two-mass system are coupled and their exact computation is complicated, intuitive approximations are quite good. It is convenient that the complicated linkage of [Figure 3.1](#), as well as other actual corner suspension mechanisms, can be accommodated in the general quarter-car model of [Figure 3.4](#) by using leverage ratios, and that the natural frequencies of [Figure 3.4](#) are so closely approximated by intuitive idealized spring and mass combinations, yielding a very simple intuitive understanding of the ride and wheel hop frequencies.

Furthermore, we will see that the ride and wheel hop frequencies are fairly constant across a wide range of motor vehicles, and we will discuss the reason why this is the case. At this point, however, the quarter-car model’s simplicity and usefulness is already apparent.

3.4 The Conventional Quarter-Car Model

The free response quarter-car model developed in Sections 3.2 and 3.3 is an idealization. Plato would appreciate this model, as the ideal form of the quarter-car model with two masses, forever oscillating at their ideal frequencies isolated from all contamination from the real world. On the other hand, Aristotle was

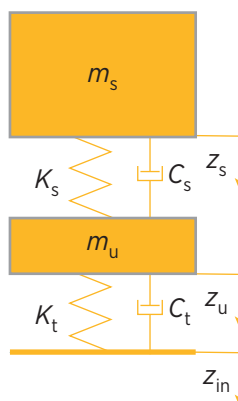
more concerned with the real world, and specifically interested in causation and how systems are actually observed rather than idealized. In this section, we will follow Aristotle's lead. One of the contaminants of Plato's ideal quarter-car model is energy dissipating damping.

The quarter-car model discussed so far and shown in [Figure 3.4](#) is the result of Eqs 3.20 and 3.21. These differential equations are linear and time invariant, allowing Laplace transforms to be taken, but they also are notable as they do not include any terms proportional to the first time derivative—velocity. Without a velocity term, when jw is substituted for the Laplace variable, the result is two coupled second-order differential equations whose unforced solution is described by Eq. 3.27. This has led to a very simple and general solution, but at the same time we have sacrificed much in terms of the generality of our model. First, in considering the unforced response, we are not able to calculate responses to specific road inputs. The fundamental frequencies of ride and wheel hop that we have determined will remain significant as the model's response to a specific road input, such as a step, will be considered. Second, we will allow our model of [Figure 3.4](#) to contain linear dampers in parallel with the suspension springs. As such the effect of the lever arms applies equally to the springs and dampers to transform the mechanical system of [Figure 3.1](#) to a new model. If the dampers are not parallel with the springs, the same methodology applies, but the equations are more complicated.

Newton's second law can be applied to the sprung mass of [Figure 3.6](#),

$$m_s \ddot{z}_s = K_s(z_u - z_s) + C_s(\dot{z}_u - \dot{z}_s) \quad (3.33)$$

FIGURE 3.6 Ideal quarter-car model with damping.



and to the unsprung mass.

$$m_u \ddot{z}_u = K_t (z_{in} - z_u) + C_t (\dot{z}_{in} - \dot{z}_u) - K_s (z_u - z_s) - C_s (\dot{z}_u - \dot{z}_s). \quad (3.34)$$

As seen in Eqs 3.33 and 3.34, the suspension (spring and damper) forces push the sprung mass in the positive direction, and the unsprung mass in the negative direction. As anticipated in Newton's third law, a suspension force on the sprung mass is reacted as an opposing force on the unsprung mass. The tire forces (from stiffness and damping) push the unsprung mass in the positive direction. (Of course the tires impose a reaction force on the road pavement that is important to Civil Engineers, but not so much to Vehicle Dynamicists—when considering ride.)

By inspection and a bit of contemplation, it is evident that we cannot proceed with this new model to develop two coupled second-order differential equations without introducing imaginary coefficients. When assumed sinusoidal signals are twice differentiated with respect to time they can be expressed as a real function of the frequency; however, once differentiated sinusoids are imaginary functions of frequency as seen in the previous chapter. Therefore, to "keep it real," we must go a different direction and use Laplace transforms exclusively. Equations 3.33 and 3.34 are rewritten in terms of positions and displacements.

$$\ddot{z}_s = -\frac{K_s}{m_s} z_s - \frac{C_s}{m_s} \dot{z}_s + \frac{K_s}{m_s} z_u + \frac{C_s}{m_s} \dot{z}_u, \quad (3.35)$$

$$\ddot{z}_u = \frac{K_s}{m_u} z_s + \frac{C_s}{m_u} \dot{z}_s + \frac{(-K_t - K_s)}{m_u} z_u + \frac{(-C_t - C_s)}{m_u} \dot{z}_u + \frac{K_t}{m_u} z_{in} + \frac{C_t}{m_u} \dot{z}_{in}. \quad (3.36)$$

Equations 3.35 and 3.36 can be written in matrix form:

$$\begin{bmatrix} \dot{z}_s \\ \ddot{z}_s \\ z_u \\ \ddot{z}_u \end{bmatrix} = \begin{bmatrix} 0 & 1 & 0 & 0 \\ \frac{-K_s}{m_s} & \frac{-C_s}{m_s} & \frac{K_s}{m_s} & \frac{C_s}{m_s} \\ 0 & 0 & 0 & 1 \\ \frac{K_s}{m_u} & \frac{C_s}{m_u} & \frac{-(K_s + K_t)}{m_u} & \frac{-(C_s + C_t)}{m_u} \end{bmatrix} \begin{bmatrix} z_s \\ \dot{z}_s \\ z_u \\ \dot{z}_u \end{bmatrix} + \begin{bmatrix} 0 & 0 \\ 0 & 0 \\ 0 & 0 \\ \frac{K_t}{m_u} & \frac{C_t}{m_u} \end{bmatrix} \begin{bmatrix} z_{in} \\ \dot{z}_{in} \end{bmatrix}. \quad (3.37)$$

Equation 3.37 can be compared with the previously derived matrix Eqs 3.26 and 3.27. Earlier, we had described the frequencies present when two suspended masses were somehow excited, with no damping and no input. Equation 3.37 allows damping and a known input to excite the system, but at the expense of the system becoming four coupled first-order differential equations, rather than two coupled second-order differential equations.

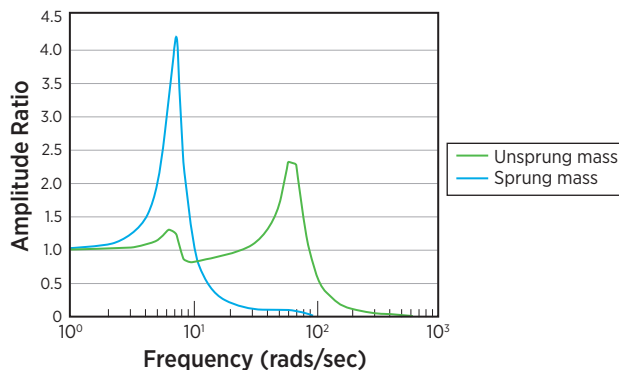
There is actually an inconsistency in Eq. 3.37. The vertical displacement of the road and its time derivative, the vertical road velocity, are both considered as independently specified inputs. That is not correct. Once one is known, the other is specified. If the road velocity is known, road displacement must be its integral, and if road displacement is known, road velocity is its derivative. Going forward both inputs will be used in different applications, and it will begin to be evident that in many applications an acceptable assumption can be made.

The theoretically correct method is to treat the road velocity as an input to be specified. This adds an additional dynamic state to the system, where the road input velocity is integrated to yield road displacement, which is used by the other existing state equations. In terms of formal control theory definitions, this new state is “uncontrollable” from an input to the suspension. The suspension does nothing to change the simple mathematical relationship between road velocity and road displacement. Typically vertical tire damping is quite small, so an acceptable approximation is to neglect it and treat road displacement as the system input. On the other hand, we will see that road velocity has a very convenient statistical property.

If road displacement is the system input, it is interesting to look at the response of the unsprung and sprung mass at various frequencies. A characteristic of any quarter-car suspension is a transfer function between sprung mass displacement and road displacement.

$$G_{\text{susp}}(s) = \frac{z_s}{z_{\text{in}}} = \frac{sz_s}{sz_{\text{in}}} = \frac{s^2 z_s}{s^2 z_{\text{in}}} \quad (3.38)$$

As evident in Eq. 3.38, when such a transfer function is established for a suspension, it trivially serves as the transfer function between sprung mass velocity and road input velocity, and sprung mass acceleration and road input acceleration. Thus, this transfer function generally describes how the suspension mechanically filters road inputs to the sprung mass. Similarly, the transfer function from road input to unsprung mass velocity can be found.

FIGURE 3.7 Transmissibility of quarter-car model.

© Dan E. Williams.

Typically, these displacements are plotted against the log of frequency, similar to bode plots, although the amplitude ratio can be linear. These plots are referred to as transmissibilities, and one of the advantages of this approach is that they report dimensionless ratios of output to input, so they describe equally well displacement, velocity or acceleration. [Figure 3.7](#) shows such a plot for the system of [Figure 3.4](#), with the typical parameters previously considered.

In general, at low frequencies the ratio of output to input is one, and at high frequencies it is very small. Both the ride frequency and wheel hop frequencies are apparent. The ride frequency dominates the sprung mass response, and the wheel hop frequency dominates the unsprung mass response. The wheel hop frequency is hardly noticeable on the sprung mass, but the ride frequency is little more prominent on the unsprung mass. If there were not close to a decade separation in the two frequencies, there would be more effect of one on the other. This frequency separation is why the previous intuitive approximations are so effective.

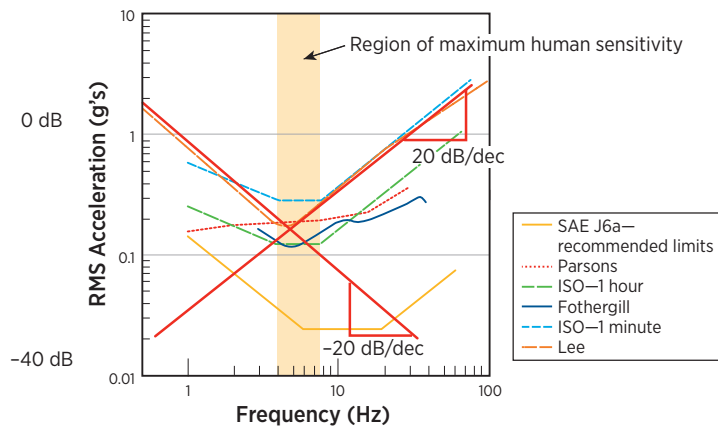
This frequency separation of nearly a decade is well placed. [Figure 3.8](#) summarizes several studies and standards that report the limits of human tolerance for vertical vibrations of various frequencies. In five of the six studies, the region of maximum intolerance of vertical vibrations is roughly between 4 and 8 Hz. In the sixth study, the limit is a bit higher and broader [2].

Thus, it can be seen in comparing [Figures 3.7](#) and [3.8](#) that the ride frequency and the wheel hop frequency straddle this region of maximum sensitivity to vertical vibration. Furthermore, it is seen that in all studies the sensitivity decreases by 20 dB/decade moving away from the region of minimum tolerance.

Transmissibility can be used to describe the effect of variation of the typical parameters previously identified. Often the variation is best illustrated when the parameter in question is halved and doubled. In general, the objective is

FIGURE 3.8 This plot needs to be cleaned up a bit.

Reprinted with permission from © John Wiley and Sons.



to minimize sprung mass transmissibility in the 4–8 Hz region of maximum sensitivity to vertical accelerations.

In this manner, **Figure 3.9** illustrates the variation of the suspension stiffness. As seen in the ride frequency of Eq. 3.31 and the wheel hop frequency of Eq. 3.32, both fundamental natural frequencies increase with suspension stiffness. This is anticipated in the approximations of Eqs 3.31 and 3.32. It appears that increased suspension stiffness slightly improves transmissibility in the critical region of 4–8 Hz, but at great expense of amplifying higher ride frequency. Variation of the suspension stiffness has a greater effect on the ride than wheel hop modes. From Eq. 3.31, the suspension spring is the softest in a series combination of stiffnesses, and therefore dominates. In Eq. 3.32, the suspension spring is the softest in a parallel combination, and therefore has less effect.

FIGURE 3.9 Transmissibility for various suspension stiffnesses.

© Dan E. Williams.

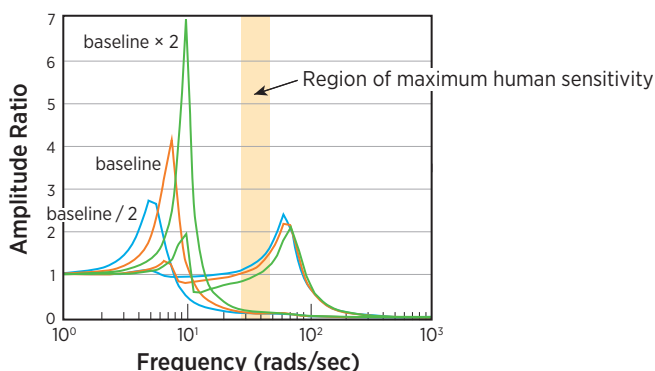
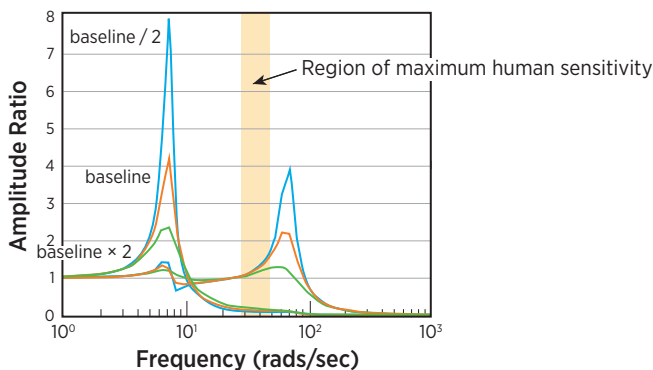
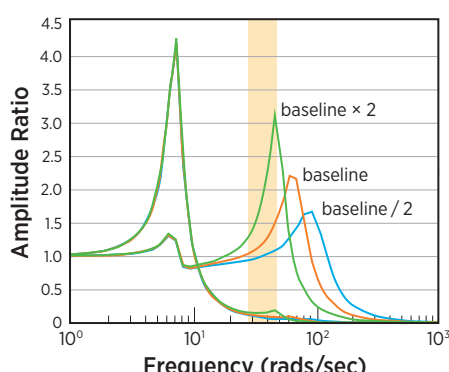


FIGURE 3.10 Transmissibility for various damping.

© Dan E. Williams.

In [Figure 3.10](#), suspension damping is varied. Both the ride and wheel hop resonances are decreased with added damping, but transmissibility in the critical frequency range is slightly degraded.

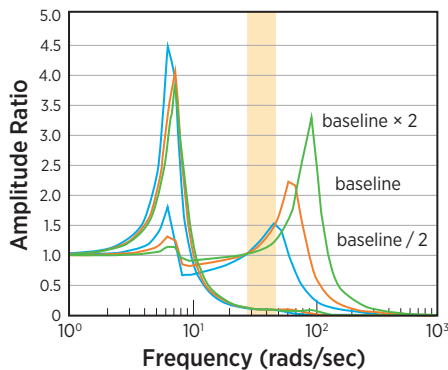
As expected, variation in the unsprung mass has no effect on the ride resonance as shown in [Figure 3.11](#). However, as unsprung mass increases the wheel hop frequency impinges on the critical frequency range. As human passengers are located on the sprung mass, an increased motion of the unsprung is not necessarily objectionable, but on closer inspection it is seen that this lower frequency, higher amplitude wheel hop resonance degrades the sprung mass transmissibility in the critical range.

FIGURE 3.11 Transmissibility for various unsprung mass.

© Dan E. Williams.

FIGURE 3.12 Transmissibility for various tire stiffnesses.

© Dan E. Williams.



Similarly, variation of the tire stiffness affects the wheel hop resonance more than ride as would be expected in the parallel stiffness approximation as shown in [Figure 3.12](#). If the tire frequency is reduced the wheel hop frequency is again in the critical range. However, unlike increased unsprung mass of [Figure 3.11](#), as tire stiffness decreases the wheel hop amplitude is decreased, and the net effect on sprung mass transmissibility is negligible.

3.5 Stochastic Road Input and Human Sensitivity to Vibration

[Figure 3.13](#) shows how the transmissibility filters road acceleration to yield sprung mass response.

FIGURE 3.13 Effect of suspension to isolate road acceleration.

Reprinted with permission from © SAE International.

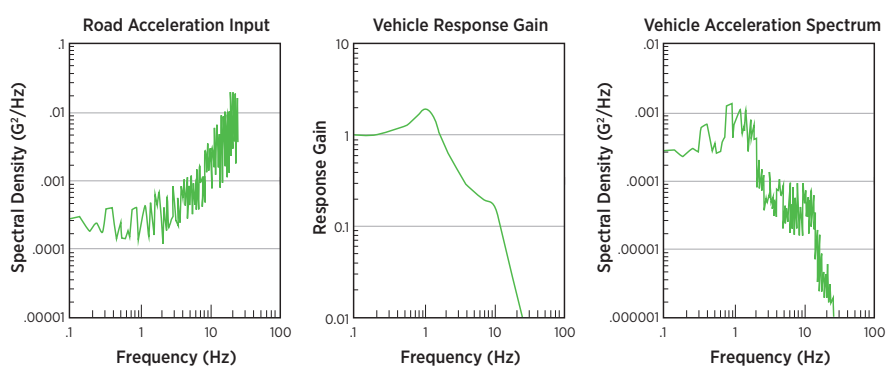
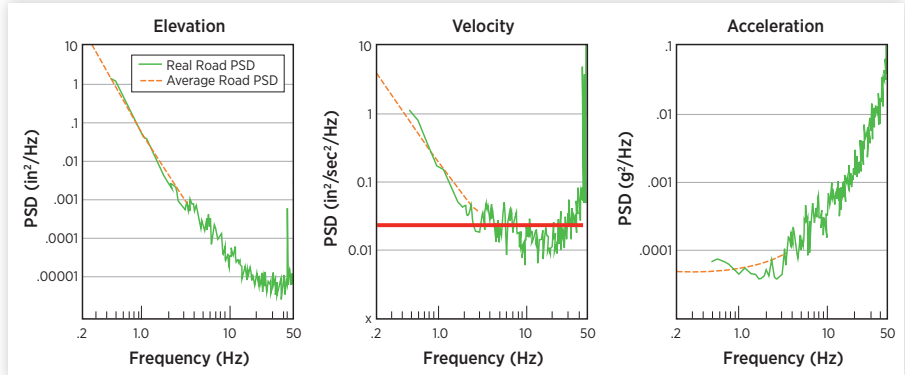


FIGURE 3.14 Power spectra of road elevation, vertical velocity, and acceleration.



Reprinted with permission from © SAE International.

Of particular interest is the road acceleration input power spectral density. The vertical axis is in units of acceleration (g) squared, and the slope at higher frequencies is approximately 40 dB/dec. If the square of acceleration is increasing at 40 dB/dec, acceleration is actually increasing at 20 dB/dec. Therefore, if the road acceleration were integrating—to form road velocity—it would be reasonably flat. In fact, we see this to be the case in [Figure 3.14](#).

Road displacement power falls with frequency, road acceleration power rises with frequency, and road velocity power is relatively constant between 1 and 40 Hz, conveniently containing the typical ride and wheel hop natural frequencies, and the frequency of maximum vertical acceleration sensitivity.

When all frequencies are present with roughly the same energy, the power spectrum is flat. This condition is called “white” as the perceived color white actually contains all colors—all frequencies. Therefore, it is proposed that road surfaces can generally be approximated by white vertical input velocity in the range of frequencies relative to the quarter-car model dynamics and human sensitivity. Rough roads generally increase amplitude across the frequency spectrum. Speed changes make little difference as there is as much energy in the higher frequency inputs as the lower. When the road input is assumed to be white, it becomes uninteresting, and only the transfer function from road velocity to sprung mass acceleration determines human ride perception. We are therefore interested in how the suspensions transform white road velocity to sprung mass acceleration.

$$sZ_{\text{in}}(s)G_{\text{desired}}(s) = s^2 Z_s(s). \quad (3.39)$$

Using Eq. 3.38,

$$G_{\text{desired}}(s) = \frac{s^2 Z_s(s)}{s Z_{\text{in}}(s)} = \frac{s Z_s(s)}{Z_{\text{in}}(s)} = s G_{\text{susp}}(s), \quad (3.40)$$

the desired transfer function that yields sprung mass acceleration from road velocity input is simply the derivative of the transmissibility. The desired transfer function of Eq. 3.40 introduced in this work can be referred to as the “isolation function” of the quarter-car model. If we assume that tire damping is negligible, the desired transfer function of Eq. 3.40 can be written in state space form using Eq. 3.37.

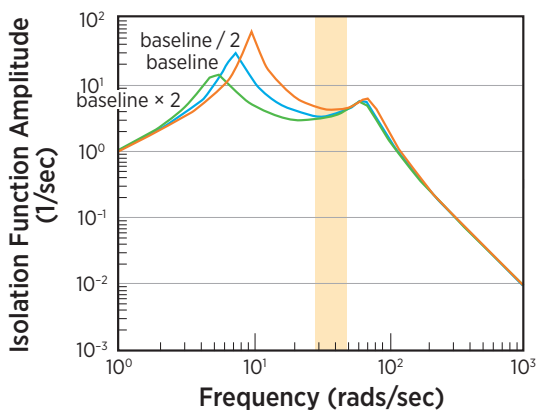
$$\begin{bmatrix} \dot{z}_s \\ \ddot{z}_s \\ \dot{z}_u \\ \ddot{z}_u \end{bmatrix} = \begin{bmatrix} 0 & 1 & 0 & 0 \\ -K_s & -C_s & K_s & C_s \\ \frac{m_s}{m_s} & \frac{m_s}{m_s} & \frac{m_s}{m_s} & \frac{m_s}{m_s} \\ 0 & 0 & 0 & 1 \\ \frac{K_s}{m_u} & \frac{C_s}{m_u} & \frac{-(K_s + K_t)}{m_u} & \frac{-(C_s + C_t)}{m_u} \end{bmatrix} \begin{bmatrix} z_s \\ \dot{z}_s \\ z_u \\ \dot{z}_u \end{bmatrix} + \begin{bmatrix} 0 \\ 0 \\ 0 \\ \frac{K_t}{m_u} \end{bmatrix} \begin{bmatrix} x_{\text{in}} \end{bmatrix} \quad (3.41)$$

$$y = \begin{bmatrix} 0 & 1 & 0 & 0 \end{bmatrix} \begin{bmatrix} z_s \\ \dot{z}_s \\ z_u \\ \dot{z}_u \end{bmatrix}$$

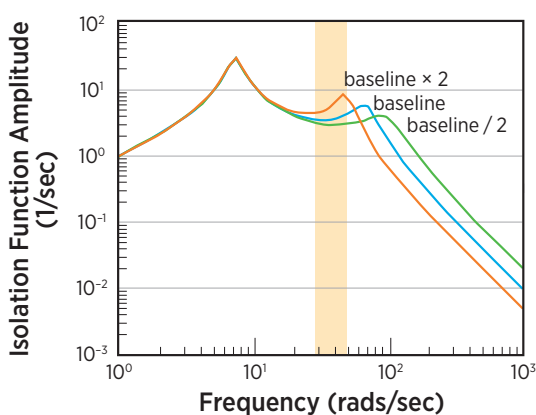
Equation 3.41 describes the quarter-car system shown in [Figure 3.7](#), with a displacement road input and a sprung mass velocity output, as desired in Eq. 3.40. This transfer function can be plotted similar to the transmissibilities of [Figure 3.9](#) to show sensitivity to variation of key parameters. The vertical axis is plotted on a log scale as opposed to earlier linear plots.

As shown in [Figure 3.15](#), variation in suspension stiffness has an effect in the frequency band of highest sensitivity; it significantly affects the ride frequency that is an important adjacent resonance. By reducing the ride natural frequency, it moves farther away from the frequency range of highest sensitivity, and is therefore favorable. It is worth noting that there appears to be a point near the wheel hop frequency where the desired transfer function is not affected by changing this parameter. Karl Hedrik first identified these “invariant points” in the quarter-car model, and showed how they limit the performance of optimal controllers [3].

As seen in [Figure 3.16](#), increasing the unsprung mass can move the wheel hop frequency into the region of vibration sensitivity. Similar to what was seen in [Figure 3.15](#), as we decrease the sprung mass we can move the wheel hop resonance away from the frequency of greatest interest, thereby improving the isolation seen in the desired suspension transfer function.

FIGURE 3.15 Isolation function for various suspension stiffness.

© Dan E. Williams.

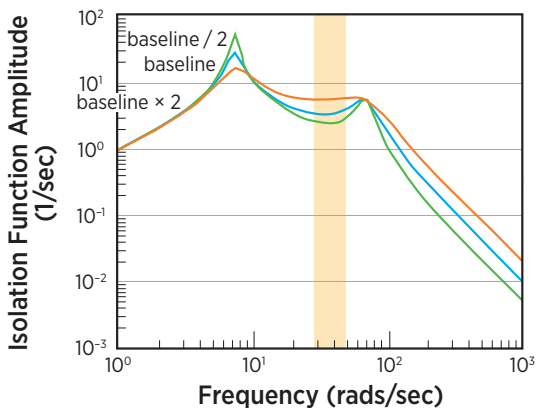
FIGURE 3.16 Isolation function for various unsprung mass.

© Dan E. Williams.

It is reasonable to ask why some of the parameters we have looked at do not have a more optimal baseline value. Suspension damping is seen to improve vibration isolation at the ride frequency, but at the expense of degrading the isolation in the frequency range of maximum sensitivity, as shown in [Figure 3.17](#). Decreasing the suspension stiffness improves vibration isolation by reducing the ride frequency and moving it away from the frequency band of maximum sensitivity, as shown in [Figure 3.18](#). Such low stiffnesses are generally achieved by lower rate suspension springs. These low rate springs must still support the static weight on that corner of the vehicle, leading to long free

FIGURE 3.17 Isolation function for various suspension damping.

© Dan E. Williams.

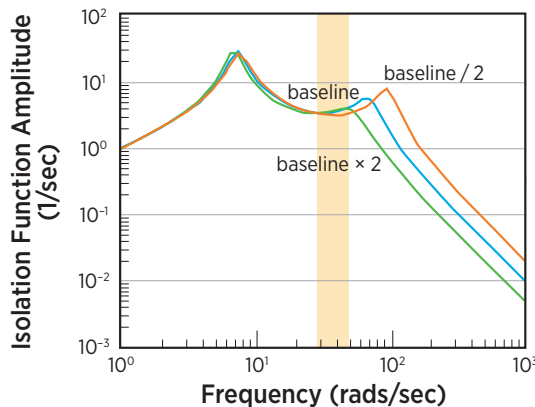


lengths and significant installed allowance for coil-to-coil contact. In short, low rate suspension springs are constrained by packaging.

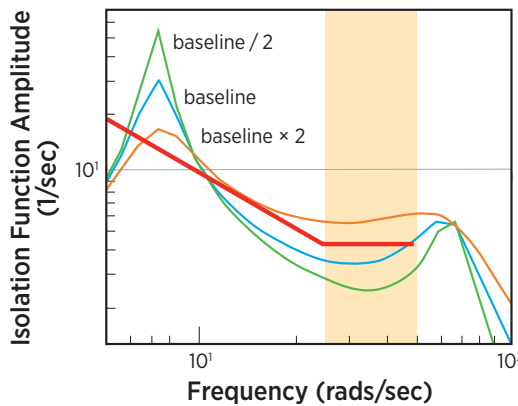
Similarly, suspension isolation properties can be uniformly improved by reducing the unsprung mass. Ideally, zero unsprung mass would completely eliminate the wheel hop resonance, and the tire and suspension spring would truly be in series, so the suspension would increasingly attenuate frequencies at 40 dB/decade away from the ride frequency. Unfortunately, the unsprung mass is mechanically required to locate and mount the tire, and allow it to freely roll. Decreasing unsprung mass is the most effective way to move the wheel hop resonance away from the frequencies of human sensitivity; however, this is usually accomplished with exotic materials and therefore expense. This is a reason why the wheel hop frequency is so constant across diverse vehicle types. From a dynamic performance standpoint the unsprung mass should be as low as possible, but it is pragmatically constrained by its kinematic function and cost, so it sits just beyond the region of maximum human sensitivity.

[Figure 3.18](#) shows that tire stiffness has a marginal effect in the frequency range of interest.

[Figure 3.19](#) shows the effect of varying suspension damping in a more narrow frequency range. Variation of suspension damping, along with variation of unsprung mass, has the most significant effects on the desired isolation function in the frequency range of maximum sensitivity. There is an interesting trade-off shown in [Figure 3.19](#), as referenced by the contour of constant sensitivity shown in bold red. Higher suspension damping produces greater acceleration in the sensitive frequency range, and lower damping produces less high-sensitivity vibrations. However, the whole story is not so simple. Even though humans are less sensitive at the ride frequency, there is still some amount of sensitivity.

FIGURE 3.18 Isolation function for various tire stiffness.

© Dan E. Williams.

FIGURE 3.19 Key compromise in isolation function damping.

© Dan E. Williams.

At the ride frequency, higher damping produces lower objectional vibrations, and lower damping is more objectionable. Therefore, we observe a fundamental trade-off. Higher suspension damping decreases the ride frequency resonance, but unfortunately increases vibrations in the most sensitive frequency region. Variation in suspension damping is seen to dramatically change the isolation function, but in ways that are not uniformly favorable. Therefore, suspension damping is a highly tunable parameter. The isolation function displays this sensitivity and associated trade-offs much more effectively than the corresponding conventional transmissibility shown in [Figure 3.10](#).

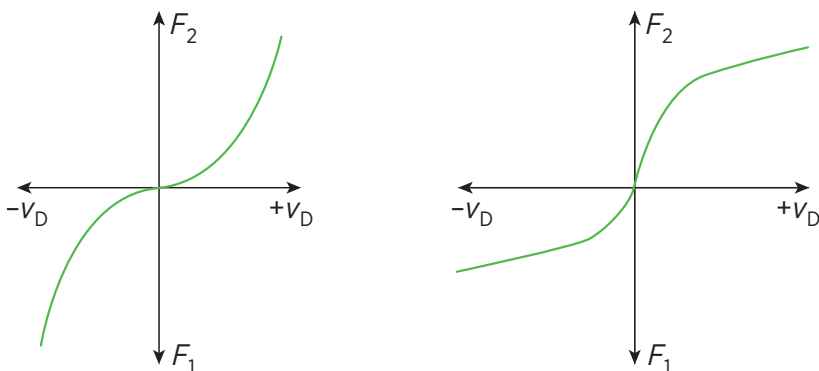
3.6 Nonlinear Damping

We have seen how suspension damping stands alone among the parameters examined as having significant tradeoffs apparent in the simplest dynamic analysis. Other dynamically sensitive parameters such as suspension stiffness and unsprung mass are constrained by external factors such as economics, kinematics, or packaging. Compromises in linear systems can sometimes be stretched by adding nonlinearities.

Dampers are typically constructed by using a piston moving relative to a containing sleeve to pump fluid, either from one side of the piston to the other, or to an auxiliary volume. In a fundamental sense, such devices are governed by the physics of stiction and flow through orifices, both of which are nonlinear. When these two phenomena are present, the system can be somewhat approximated by linear damping as before. From a pure frequency domain analysis this approximation is not bad, as it is reasonable to find a linear approximation that dissipates the correct energy for a range of frequencies and amplitudes, and that is what is important for an analysis of linear stability and performance. In transient cases, however, that describe the effect of a particular event such as a pothole, the effect of nonlinear damping should be studied. The downside of such nonlinear analysis is that they are typically relevant to only a particular input event, whereas conclusions drawn from linear analysis are good for a range of inputs—as long as linearity is preserved.

The simplest nonlinearity that is used in dampers is different damping rates for compression (jounce) and extension (rebound). In mathematical terms the damping rate is dependent upon the sign of the velocity. The idea is usually to provide less damping in compression to allow the unsprung mass to absorb an upward bump, and then apply more damping (and thus energy dissipation) as the damper rebounds to its correct ride height. With a road input of the opposite direction, the unsprung mass would be significantly damped as it falls into a pothole.

A second nonlinearity is used in damper design, to vary the damping with stroke. As seen in [Figure 3.20](#), this kind of damping can be digressive, which is higher on-center than away from center, or progressive where the damping increases away from center. In mathematical terms, the damping rate is varied with the absolute value of suspension displacement. With road velocity being more or less white, that means at lower frequencies there are higher amplitudes. There progressive damping would do more to desirably damp inputs at lower frequencies such as the ride frequency, as evident in [Figure 3.19](#), while providing less objectional damping at higher frequencies that are more objectionable. Digressive damping is usually not desirable as it provides the opposite effect. The only reason digressive damping would help if a massive amount of energy dissipation is needed.

FIGURE 3.20 Nonlinear progressive and regressive damping.

© SAE International.

In most cases the functional dynamic characteristics of dampers are determined by their internal physics—flow through orifices, sliding friction, spring loaded blow-off valves, and so on. Usually there are “crashout stops” or “bump rubbers” that provide extreme progressivity at the end of travel to prevent metal to metal contact.

Nonlinear damper behavior is important for handling, which will be discussed later in the ride section. For now the effect can be appreciated when understanding: (1) that the more normal force on a tire, the more lateral force it can generate, and (2) a rolling sprung mass is opposed by suspension stiffness and damping. When a car enters a turn and the sprung mass is rolling toward the outside, the rolling of the sprung mass is best opposed by compression damping on the outside corners of the car. Because body roll rates are of the opposite sign entering and exiting a turn, nonlinear damping terms can determine a different behavior when a car enters or exits a turn.

3.7 Summary

The widespread use of the quarter-car model can now be appreciated. Most realizable vehicle suspensions can be addressed by the quarter-car model. It identifies the two key natural frequencies in the vertical direction that must be located outside of the region of maximum sensitivity to vertical vibration. An important method of analyzing the quarter-car model was presented. With the understanding that the road input can typically be approximated by white road velocity, and that humans are most sensitive to accelerations at certain frequencies, the first derivative of the well-known transfer function of the suspension was shown to be quite revealing. The white road input allows all

road frequencies to be accounted for with the simplest stochastic input, but perhaps more importantly the derivative tends to flatten the transfer function and make it more sensitive to parametric variation. This derived transfer function allows the effect of suspension parameters to be better understood. Compromises in the linear quarter-car dynamic model can be loosened by introducing nonlinearities.

The quarter-car model also reveals handling properties. The ability of the tire to generate side force is proportional to the weight or load supported by the tire, transmitted through the contact patch where the “rubber meets the road.” Neglecting tire damping, the load through the contact patch is proportional to the deflection of the tire. As the unsprung mass oscillates at its wheel hop frequency, load varies, and therefore so does the lateral force the tire can generate. Nonlinear damping can also affect lateral force generation when turning and accelerating. We will study handling in detail later, and these will be seen to be important second order effects. We will develop active suspension in the capstone chapter of this ride section, and in doing so the quarter-car model will be an important starting place.

The quarter-car model is the most extensive treatment we will see of the unsprung mass resonance, or “wheel-hop.” This chapter compares wheel-hop with the primary vertical ride frequency (heave). In practice wheel-hop is seen virtually wherever you care to measure accelerations in a vehicle, especially on roads with input disturbances that excite the hubs. We will soon see that the other sprung mass rigid body frequencies are closer to the ride frequency in this chapter, so “wheel-hop” is distinctive.

References

- [1] Reimpell, J., and H. Stoll. “The Automotive Chassis: Engineering Principles, Society of Automotive Engineers, Warrendale.” (1996), ISBN: 9780080527734.
- [2] Wong, J.Y., Theory of Ground Vehicles, Wiley, New York, 1978. ISBN: 978-0-470-17038-0.
- [3] Hedrik, J.K., and Butsuen. T., “Invariant Properties of Automotive Suspensions,” Proceedings of the Institution of Mechanical Engineers, Part D: Journal of Automotive Engineering, Vol 201 Issue 1, January 1990, p. 21–27.

The Pitch-Plane Model

“ Things should be made as simple as possible, but not simpler.
—Albert Einstein (paraphrased)

4.1 Introduction

The two-mass quarter-car model was developed to understand the response of a corner of a car to a vertical road input. If all four corners of the car experience an equal simultaneous vertical road input, a composite quarter-car model will anticipate the sprung mass vertical motion, known as heave. Thus, the two-mass model is a simple approximation of the vertical reaction of the sprung mass to road inputs with its ride frequency, describes the unsprung mass resonance known as wheel hop, and demonstrates the mechanical filtering properties of the suspension for vertical inputs. The ride frequency was located relative to human sensitivity to vertical vibrations, and trade-offs among the suspension parameters were explored. For many purposes, the quarter-car model derived in the previous chapter is a parsimonious solution justifying its widespread use. In some cases, additional complexity is required for usefulness.

There are basic limitations of a “heave only” model when applied to the complete vehicle. First vehicles travel with predominately longitudinal motion. The front wheels will encounter a vertical disturbance before the rear wheels. It is unlikely that all four wheels will experience the same simultaneous input, which would excite the sprung mass in pure heave. There are many vertical disturbances that run completely across and roughly perpendicular to the path of the vehicle. When the front wheels encounter these disturbances, and then some distinct period of time later the rear wheels encounter them, there is a fore-and-aft rocking input superimposed upon the pure heave input.

This fore-and-aft rocking motion is referred to as pitch. The second limitation of the “heave-only” model is that the human body is very sensitive to these pitching motions. The time between the front tires impacting a bump and the rear tires impacting the same bump decreases with increased vehicle speed, thus the pitching inputs are greater at low and moderate vehicle speeds.

Finally, it is possible to have different suspension parameters describing the front and rear suspensions. Sometimes these are because of packaging constraints, but often they are by design. The human body has different sensitivities to heave and pitch, and just as we saw with the quarter-car model, it is possible to move resonances away from frequencies of maximum sensitivity. In these cases, adding complexity to the quarter-car model is warranted.

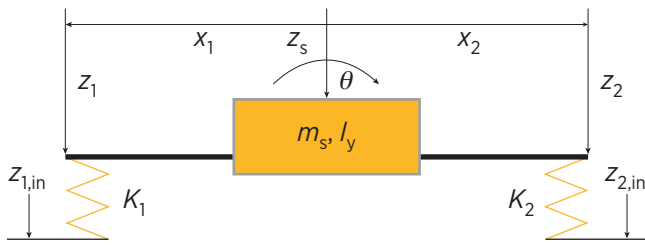
4.2 Basic Pitch-Plane Model

Because it is common that the front wheels simultaneously experience the same road displacement input, and sometime later based on wheelbase and vehicle speed, the rear wheels experience an identical input, when considering vertical inputs the two wheels on the front axle can be combined, as can the two rear wheels. (We speak of “axles” metaphorically. In many cases with independent suspensions, there are no actual axles, but wheels on the front and rear, respectively, rotate about a common axis and are referred to as an “axle.”). In [Chapter 3](#), we introduced unsprung mass dynamics. They are neglected in the pitch-plane model as the natural frequencies of heave (as has already been shown) and pitch (which will be shown to be even lower than heave) are roughly an order of magnitude lower than unsprung mass dynamics. The quarter-car model examines the relationship between the sprung mass and unsprung mass natural frequencies in the vertical direction, and the pitch-plane model of this chapter looks at the relationship between the heave and the pitch natural frequencies of the sprung mass.

Two degrees of freedom of the suspended mass are allowed in [Figure 4.1](#), heave or vertical displacement z_s , as was developed in the quarter-car model, and pitch Θ , which is the sprung mass rocking fore and aft about its center of gravity. The sprung mass is defined by mass m_s and rotational moment of inertia I_y . The unsprung masses are considered negligible compared with the sprung mass and its inertia, so the tire and the suspension stiffnesses are combined in series. Right and left suspension stiffnesses are in parallel and are combined to form composite front and rear stiffnesses, K_1 and K_2 , respectively. The front and rear axles are located by the signed displacements x_1 and x_2 , respectively. Vertical displacements at the front and rear axles are z_1 and z_2 , respectively, and the inputs are $z_{1,in}$ and $z_{2,in}$, respectively.

FIGURE 4.1 Pitch-plane model schematic.

© Dan E. Williams.



It is possible that through suspension kinematics the sprung mass does not actually rotate in pitch about its center of gravity. This condition of kinematically constrained rotation is perhaps more relevant in roll and will be discussed in following chapters. In this chapter, we will assume that pitch motion of the sprung mass is kinematically unconstrained.

A reference frame is fixed to the center of sprung mass. As earlier mentioned, the z -axis in [Figure 4.1](#) is pointed downward. The x -axis is pointing out the front of the vehicle along its longitudinal axis. Consistent with a right-hand coordinate system, the y -axis is directed into the page. As pitch is a rotation about the y -axis, it is clockwise in [Figure 4.1](#).

Newton's second law is applied to the vertical or heave motion of the sprung mass in [Figure 4.1](#) caused by vertical forces at the axles.

$$m_s \ddot{z}_s = F_1 + F_2. \quad (4.1)$$

Vertical forces at the front axle of [Figure 4.1](#) are produced by the displacement of composite stiffnesses at the front axle,

$$F_1 = K_1(z_{1,in} - z_1) \quad (4.2)$$

and similarly for the rear axle.

$$F_2 = K_2(z_{2,in} - z_2). \quad (4.3)$$

Displacement of the sprung mass at the front axle is the superposition of heave and pitch sprung mass displacements,

$$z_1 = z_s - x_1 \theta \quad (4.4)$$

and similarly for the rear.

$$z_2 = z_s - x_2 \theta. \quad (4.5)$$

Note the similarity of Eqs 4.4 and 4.5, and the negative sign of x_2 insuring that a positive pitch displacement adds positively to the sprung mass displacement at the rear, as expected from the axis shown in [Figure 4.1](#). In previous literature, the axle location is an unsigned or absolute number, and therefore the sign in Eq. 4.5 is changed. Equations 4.4 and 4.5 are inserted into Eqs 4.2 and 4.3.

$$F_1 = K_1(z_{f,in} - z_s + x_1 \theta), \quad (4.6)$$

$$F_2 = K_2(z_{r,in} - z_s + x_2 \theta). \quad (4.7)$$

Finally, Eqs 4.6 and 4.7 are inserted into Eq. 4.1.

$$m_s \ddot{z}_s = K_1(z_{1,in} - z_s + x_1 \theta) + K_2(z_{2,in} - z_s + x_2 \theta). \quad (4.8)$$

Equation 4.8 can be solved for sprung mass acceleration and written in terms of displacements.

$$\ddot{z}_s = \left(\frac{-K_1 - K_2}{m_s} \right) z_s + \left(\frac{K_1 x_1 + K_2 x_2}{m_s} \right) \theta + \left(\frac{K_1}{m_s} \right) z_{1,in} + \left(\frac{K_2}{m_s} \right) z_{2,in}. \quad (4.9)$$

Newton's second law can also be applied to the pitch mode as the vertical axle forces of Eqs 4.6 and 4.7 act through lever arms to create pitching moments.

$$I_y \ddot{\theta} = -x_1 F_1 - x_2 F_2 \quad (4.10)$$

Equations 4.6 and 4.7 are inserted into Eq. 4.10.

$$I_y \ddot{\theta} = -x_1 K_1(z_{1,in} - z_s + x_1 \theta) - x_2 K_2(z_{2,in} - z_s + x_2 \theta). \quad (4.11)$$

Equation 4.11 is solved for pitch acceleration in terms of displacements.

$$\ddot{\theta} = \left(\frac{K_1 x_1 + K_2 x_2}{I_y} \right) z_s + \left(\frac{-K_1 x_1^2 - K_2 x_2^2}{I_y} \right) \theta + \left(\frac{-x_1 K_1}{I_y} \right) z_{1,in} + \left(\frac{-x_2 K_2}{I_y} \right) z_{2,in}. \quad (4.12)$$

Equations 4.9 and 4.12 can be written in matrix form:

$$\begin{bmatrix} \ddot{z}_s \\ \ddot{\theta} \end{bmatrix} = \begin{bmatrix} \frac{-K_1 - K_2}{m_s} & \frac{K_1 x_1 + K_2 x_2}{m_s} \\ \frac{K_1 x_1 + K_2 x_2}{I_y} & \frac{-K_1 x_1^2 - K_2 x_2^2}{I_y} \end{bmatrix} \begin{bmatrix} z_s \\ \theta \end{bmatrix} + \begin{bmatrix} \frac{K_1}{m_s} & \frac{K_2}{m_s} \\ \frac{-x_1 K_1}{I_y} & \frac{-x_2 K_2}{I_y} \end{bmatrix} \begin{bmatrix} z_{1,\text{in}} \\ z_{2,\text{in}} \end{bmatrix}. \quad (4.13)$$

Nomenclature is introduced, which will significantly streamline future computations.

$$K_a = K_1 + K_2, \quad (4.14)$$

$$K_b = x_1 K_1 + x_2 K_2, \quad (4.15)$$

$$K_c = x_1^2 K_1 + x_2^2 K_2. \quad (4.16)$$

Equations 4.14, 4.15, and 4.16 are used to simplify Eq. 4.13.

$$\begin{bmatrix} \ddot{z}_s \\ \ddot{\theta} \end{bmatrix} = \begin{bmatrix} \frac{-K_a}{m_s} & \frac{K_b}{m_s} \\ \frac{K_b}{I_y} & \frac{-K_c}{I_y} \end{bmatrix} \begin{bmatrix} z_s \\ \theta \end{bmatrix} + \begin{bmatrix} \frac{K_1}{m_s} & \frac{K_2}{m_s} \\ \frac{-x_1 K_1}{I_y} & \frac{-x_2 K_2}{I_y} \end{bmatrix} \begin{bmatrix} z_{1,\text{in}} \\ z_{2,\text{in}} \end{bmatrix}. \quad (4.17)$$

4.3 Pitch-Plane-Free Response

Similar to what was done in [Chapter 3](#) with the quarter-car model, we can look at how the pitch-plane model behaves when there is no road displacement input, and the model oscillates in response to some unspecified input by taking the Laplace transform of Eq. 4.17.

$$\begin{bmatrix} m_s s^2 & 0 \\ 0 & I_y s^2 \end{bmatrix} \begin{bmatrix} x_s(s) \\ \theta(s) \end{bmatrix} = \begin{bmatrix} -K_a & K_b \\ K_b & -K_c \end{bmatrix} \begin{bmatrix} x_s(s) \\ \theta(s) \end{bmatrix}. \quad (4.18)$$

Equation 4.18 can be solved for zero, and the Laplace variable s is replaced by $j\omega$.

$$\begin{bmatrix} 0 \\ 0 \end{bmatrix} = \begin{bmatrix} m_s \omega^2 - K_a & K_b \\ K_b & I_y \omega^2 - K_c \end{bmatrix} \begin{bmatrix} x_s(s) \\ \theta(s) \end{bmatrix}. \quad (4.19)$$

Equation 4.19 is satisfied for the trivial condition when there is no displacement, and more interestingly when the determinant of the matrix multiplying the Laplace variables is zero.

$$\det = (m_s \omega^2 - K_a)(I_y \omega^2 - K_c) - K_b^2 = 0. \quad (4.20)$$

As previously, the goal is to find a frequency ω that makes the determinant zero. At that frequency, Eq. 4.19 is satisfied for nonzero displacements. It is interesting to note that K_b is found in the off-diagonal terms of Eq. 4.19. When the determinant is found in Eq. 4.20, K_b is seen to make the result more complicated. If K_b were 0, Eq. 4.19 would be diagonal. Upon inspection of Eq. 4.19, a diagonal matrix implies that heave motion does not affect pitch, and vice versa, and in the diagonal form the oscillating modes are decoupled. The determinant of Eq. 4.20 can be evaluated.

$$\det = m_s I_y \omega^4 - (K_c m_s + K_a I_y) \omega^2 + (K_a K_c - K_b^2) = 0. \quad (4.21)$$

When multiplied out, the determinant is seen to be quadratic in ω^2 . Therefore, the quadratic equation can be applied to find the roots of Eq. 4.21.

$$\omega^2 = \frac{(K_c m_s + K_a I_y) + / - \sqrt{(K_c m_s + K_a I_y)^2 - 4 m_s I_y (K_a K_c - K_b^2)}}{2 m_s I_y}. \quad (4.22)$$

The terms in the radical of Eq. 4.22 can be multiplied out,

$$\omega^2 = \frac{(K_c m_s + K_a I_y) + / - \sqrt{K_c^2 m_s^2 + 2 K_c m_s K_a I_y + K_a^2 I_y^2 - 4 m_s I_y (K_a K_c - K_b^2)}}{2 m_s I_y} \quad (4.23)$$

and then simplified.

$$\omega^2 = \frac{(K_c m_s + K_a I_y) + / - \sqrt{(K_c m_s - K_a I_y)^2 + 4 m_s I_y K_b^2}}{2 m_s I_y} \quad (4.24)$$

The coupling effect of K_b is again apparent in Eq. 4.24, as previously referenced in Eq. 4.19. Recall from Eq. 4.15, it is possible that K_b could be small or even zero, as the distance to the front axle must be positive and the distance to the rear axle must be negative. If the coupling of K_b is negligible, Eq. 4.24 is greatly simplified.

$$\omega^2 = \frac{(K_c m_s + K_a I_y) + / - (K_c m_s - K_a I_y)}{2 m_s I_y}. \quad (4.25)$$

Equation 4.25 actually defines two frequencies. The first is when the terms in numerator added,

$$\omega_1^2 = \frac{2 K_a I_y}{2 m_s I_y} \quad (4.26)$$

that is simplified are the square root taken,

$$\omega_1 = \sqrt{\frac{K_a}{m_s}} \quad (4.27)$$

and Eq. 4.14 is used to express the frequency in terms of the original stiffnesses.

$$\omega_1 = \sqrt{\frac{K_1 + K_2}{m_s}}. \quad (4.28)$$

The first decoupled frequency expressed in Eq. 4.28 is seen to be the natural frequency of the sprung mass supported vertically on the parallel combination of the front and rear suspension stiffnesses. In the quarter-car model, this was referred to as the ride frequency with the total mass of the vehicle supported vertically on the parallel combination of the front and rear composite stiffnesses. This is therefore an important connection between the quarter-car and pitch-plane models.

A second frequency is possible in Eq. 4.25 when the numerator is subtracted,

$$\omega_2^2 = \frac{2 K_c m_s}{2 m_s I_y} \quad (4.29)$$

and simplified,

$$\omega_2 = \sqrt{\frac{K_c}{I_y}} \quad (4.30)$$

and Eq. 4.16 is used to express the second frequency in terms of the axle stiffnesses and locations.

$$\omega_2 = \sqrt{\frac{x_1^2 K_1 + x_2^2 K_2}{I_y}}. \quad (4.31)$$

Equation 4.31 is referred to as the pitch frequency, as it describes oscillatory pitching rotation about the center of sprung mass.

Similar to the free response of the two masses in the quarter-car model, the free response analysis of the pitch plane defines two key natural frequencies with a coupling term that can plausibly be small. Conversely, to the extent that coupling is significant, these approximations are not as good.

By assuming the coupling term K_b to be negligible, natural frequencies for pure heave (ride) and pitch are found. Another interesting special case of Eq. 4.24 can be found when the radical vanishes and both frequencies are equal. Thus, the condition for equal frequencies can be written.

$$(K_c m_s - K_a I_y)^2 + 4m_s I_y K_b^2 = 0. \quad (4.32)$$

Because of the squared terms, for Eq. 4.32 to hold conditions are imposed upon K_a , K_b , and K_c .

$$K_b = 0. \quad (4.33)$$

$$\frac{K_c}{K_a} = \frac{I_y}{m_s}. \quad (4.34)$$

When Eqs 4.33 and 4.34 hold, Eq. 4.24 becomes

$$\omega^2 = \frac{K_a}{m_s} = \frac{K_c}{I_y}, \quad (4.35)$$

which is a plausible situation. Therefore, the pitch-plane and ride frequencies can be close together. This convergence can be shown in an idealized vehicle if half the mass is placed on either axle, and the front and rear stiffnesses are equal. In this special case $I_y = m_s x^2$ and $K_c = 2Kx^2$.

4.4 Road Inputs to the Pitch-Plane Model

The previous development described how the system would continue to freely oscillate given some initial unspecified perturbation. From the free response, key natural frequencies were derived in a process similar to the quarter-car model. In practice, again similar to the quarter-car model, the pitch-plane

model receives inputs from an undulating road. The key assumption in the pitch-plane model is that both wheels on a given axle receive the same input.

Rather than consider road inputs at the axles as two vertical inputs, it is possible to consider their average as a heave input.

$$z_{\text{in}} = \frac{z_{1,\text{in}} + z_{2,\text{in}}}{2}. \quad (4.36)$$

Similarly, it is possible to construct a pitch input from the two vertical axle inputs.

$$\theta_{\text{in}} = \frac{z_{1,\text{in}} - z_{2,\text{in}}}{2(x_1 - x_2)}. \quad (4.37)$$

Equations 4.36 and 4.37 can be written in matrix form:

$$\begin{bmatrix} z_{\text{in}} \\ \theta_{\text{in}} \end{bmatrix} = \begin{bmatrix} 1 & 1 \\ 2 & 2 \\ 1 & -1 \\ 2(x_1 - x_2) & 2(x_1 - x_2) \end{bmatrix} \begin{bmatrix} z_{1,\text{in}} \\ z_{2,\text{in}} \end{bmatrix}. \quad (4.38)$$

So any two vertical inputs at the axles can be transformed to a pure heave input and a pure pitch input.

Equation 4.38 is written so that the front and rear axle inputs are generally independent. In fact, these inputs are highly dependent. The front axle experiences an input, and sometime later the rear axle experiences the same input. The time delay is the vehicle wheelbase divided by the speed.

$$z_{2,\text{in}}(t) = z_{1,\text{in}} \left(t - \frac{x_1 - x_2}{u} \right). \quad (4.39)$$

In Eq. 4.39, the road is expressed as function of time, t . The vehicle can experience a sinusoidal road input with unitary amplitude and frequency ω .

$$z_{1,\text{in}}(t) = \sin(\omega t). \quad (4.40)$$

Using Eq. 4.39, the sinusoidal rear axle road input can be written.

$$z_{2,\text{in}}(t) = \sin \left(\omega \left(t - \frac{x_1 - x_2}{u} \right) \right). \quad (4.41)$$

The frequency of the input can be distributed:

$$z_{2,\text{in}}(t) = \sin\left(\omega t - \omega \frac{x_1 - x_2}{u}\right), \quad (4.42)$$

yielding two terms in the argument of the sin function of the second axle. The first is the expected product of frequency and time. The second is not a function of time and is therefore recognized as a phase angle. If this phase angle is a multiple of 2π , a relationship between the road input undulation frequency and the vehicle dynamic properties of wheelbase and speed can be written, so that both axles experience the same input.

$$\frac{2\pi n}{\omega} = \frac{x_1 - x_2}{u}. \quad (4.43)$$

In this condition, in view of Eq. 4.36, the vertical input is the unit amplitude of the sinusoidal input (and obviously would be scaled with the sinusoidal input). From Eq. 4.37, the pitch input is zero.

Similarly, the phase angle can be a multiple of π .

$$\frac{\pi n}{\omega} = \frac{x_1 - x_2}{u}. \quad (4.44)$$

When Eq. 4.44 is satisfied, the axle inputs at the rear are opposite those at the front. In this special case, in view of Eq. 4.36, the vertical heave input is zero. For the unitary input, Eq. 4.37 is more interesting.

$$\theta_{\text{in}} = \frac{1}{(x_1 - x_2)}. \quad (4.45)$$

When the condition imposed by Eq. 4.44 holds, there is no heave input and a pure pitch input.

Equations 4.43 and 4.44 are written in general terms to allow multiple sine waves between the front and the rear axles. In practice only at the lowest speeds are multiple input sine waves between the axles are possible.

Equation 4.43 can be solved for the undulating road frequency required to cancel the pitch input for a single wave.

$$\frac{u}{x_1 - x_2} = \frac{\omega}{2\pi} = f. \quad (4.46)$$

The ratio of speed to wheelbase thus defines the input frequency in hertz that provides a pure heave input. However, we would like to express the frequency not as a function of time, but as a function of longitudinal displacement to relate the occurrence of heave cancellation to a road profile. If the frequency is divided by the longitudinal velocity, the result is a road profile in units of cycles per unit displacement.

$$\frac{1}{x_1 - x_2} = \frac{f}{u} = \text{cycles per displacement.} \quad (4.47)$$

Equation 4.47 is an intuitively pleasing result that the pitch canceling input is the wavelength of the wheelbase. This simple conclusion is not relevant, however. We have seen that a fundamental attribute of the pitch-plane model is a ride frequency defined by Eq. 4.28, and we have previously seen from the quarter-car model that the ride frequency is commonly around 1–2 Hz. Road inputs in excess of this natural frequency are attenuated by the suspension. The speed required for this ride frequency can be found from Eq. 4.46.

$$u = f(x_1 - x_2). \quad (4.48)$$

For a ride frequency of 2 Hz and a wheelbase of 8 ft, a speed of 16 ft/sec (11 mph) will result in inputs that will excite the pure ride frequency, and speeds beyond this will provide inputs that will be increasingly attenuated. From Eq. 4.48, it is evident that the speed at which the ride resonance is excited varies with wheelbase, leading to the term “wheelbase filtering.” From Eq. 4.44, the pure pitch input is at a wavelength half of what excites the heave input, corresponding to the front axles in a trough when the rear are on peak, and vice versa. It will be seen shortly that the pitch natural frequency is ideally close to the ride natural frequency. A general rule of thumb is that frequencies beyond an order of magnitude of the resonance are filtered to the point they can be neglected. Therefore, at highway speeds, wheelbase filtering has practically eliminated the pitch input and attenuated the ride input. This ties up with experience, as pitching motions resulting from road inputs are not noticed at highway speeds.

From Eq. 4.48, it is evident that as the vehicle wheelbase is longer, the speed at which the road undulation frequency is excited is also higher. So, longer wheelbase vehicles can experience pitching inputs at higher speeds than shorter wheelbase vehicles. This situation is mitigated by Eq. 4.45 that shows the pure pitch input is inversely proportional to the wheelbase. So, a longer wheelbase allows pitching inputs at higher vehicle speeds; however, those pitching inputs will be of smaller amplitude.

It is unlikely that a vehicle will experience sustained sinusoidal inputs over a number of cycles. More likely, the vehicle will experience an isolated near sine wave that will momentarily excite a frequency (heave or pitch), and then return to more complicated stochastic inputs.

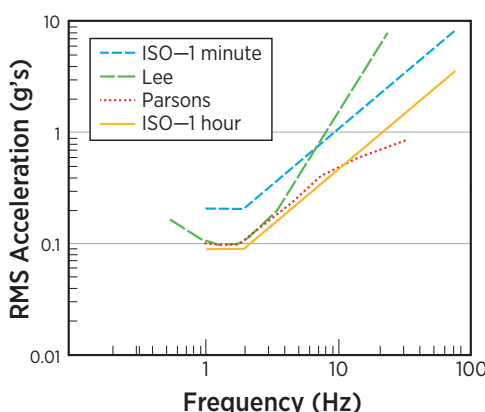
4.5 Pitch-Plane Ride Quality and the Olley Ride Criteria

Through the phenomena of wheelbase filtering, we have seen that inputs to the pitch-plane model are predominantly heave at highway speeds. However, at low to moderate speeds, and with vehicles with longer wheelbases, both the pitch and the heave modes of the vehicle can be excited.

We have seen previously in the quarter-car model how passengers located on the sprung mass are sensitive to vertical or heave accelerations. These passengers also experience pitch accelerations. The passengers can experience pure pitch rotation, and they can also experience pitch as a fore-and-aft acceleration if they are seated above the center of gravity or a pitch axis kinematically imposed by the suspension.

Compared with the heave acceleration sensitivity shown in the quarter-car section, it is seen in [Figure 4.2](#) that the maximum sensitivity for the fore-and-aft direction is at a lower frequency (1–2 Hz) than the heave mode maximum sensitivity (6–8 Hz). In terms of amplitude, the maximum sensitivities are roughly the same. As we have just seen, the actual pitch input is reduced by wheelbase, and the fore-and-aft vibration is increased as the passengers are elevated.

FIGURE 4.2 Human tolerance for fore-and-aft vibrations.



This presents a dilemma for suspension designers. In general, softer springs provide lower natural frequencies. We saw in the quarter-car model that a relatively soft suspension can move the ride frequency lower than the frequency of maximum heave sensitivity. Such soft suspensions risk putting the pitch resonance at a sensitive frequency. But, the soft springs provide the best ride isolation at highway speeds where the inputs are generally only heave, and most vehicles spend most of their time at highway speed.

Maurice Olley, introduced in the first chapter, was a legendary figure in the emergence of vehicle dynamics and described a method to optimize the pitch-plane ride performance. We will see Olley's work again in the handling section; the ride criteria are as follows:

1. *Both ride natural frequencies, heave and pitch, should be below 1.3 Hz.* The heave natural frequency has been derived in Eq. 4.28 and the pitch natural frequency in Eq. 4.31.

$$2\pi \sqrt{\frac{K_1 + K_2}{m_s}} < 1.3. \quad (4.49)$$

$$2\pi \sqrt{\frac{x_1^2 K_1 + x_2^2 K_2}{I}} < 1.3. \quad (4.50)$$

2. *The pitch and heave natural frequencies should be close together. The bounce frequency should be less than 1.2 times the pitch frequency.* For simplicity in fulfilling the Olley ride criteria we recall the conditions for the pitch and heave frequencies to be equal have been derived in Eq. 4.33,

$$x_1 K_1 + x_2 K_2 = 0 \quad (4.51)$$

and Eq. 4.34.

$$\frac{x_1^2 K_1 + x_2^2 K_2}{K_1 + K_2} = \frac{I}{m_s}. \quad (4.52)$$

3. *The front suspension deflection should be at least 30% greater than the rear. This is equivalent to the spring center 6.5% of the wheelbase to the rear of the center of gravity.*

The location of the spring center c relative to the center of mass can be expressed.

$$c = (x_1 K_1 + x_2 K_2) / (K_1 + K_2) \quad (4.53)$$

4. *The roll frequency should be close to the heave and pitch frequencies.* Roll is not considered in the pitch-plane model, and so this criterion is not considered here.

The first three conditions imposed by Olley can be used to determine the front and rear suspension stiffnesses. It would be nice if the suspension stiffness values could be determined independently for any vehicle parameters. Unfortunately, the Olley criteria cannot directly define the suspension stiffnesses, as they impose three independent constraints (if Eqs 4.51 and 4.52 hold, the ride frequencies will be equal, and then only one of Eqs 4.48 and 4.49 is required), and therefore overdetermine the two stiffnesses. To achieve the Olley criteria, the vehicle dynamic parameters such as axle location and inertia properties need to be considered as potential design variables. For a two-axle vehicle, the Olley ride criteria often impose design constraints throughout the vehicle.

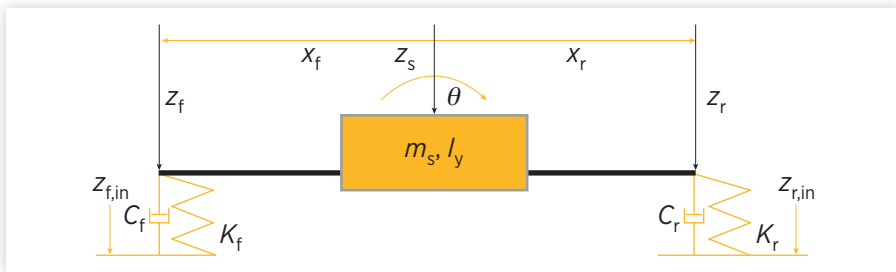
A bit later, the Olley ride criteria will be demonstrated on a three-axle vehicle. Then, it will be shown quantitatively how ride is improved with the Olley criteria. For now, a qualitative explanation must suffice. The key to such an intuitive understanding is found in the third criteria, Eq. 4.53. The front suspension is softer than the rear. So, when the front axle experiences a step input, it responds relatively slowly, and then the rear axle experiences the step a bit later, and it responds more quickly. At slow and moderate speeds where the pitch input is excited by the time delayed inputs, the Olley criteria tends to attenuate the initial pitch input. For the initial overshoot of the undamped pitch-plane response, pitch is reduced. Therefore, the heave natural frequency can be placed to optimize the more important response to heave inputs Eq. 4.49 and the Olley criteria then minimizes the pitch inputs that fall in the region of human sensitivity. To summarize, because wheelbase filtering is more effective on pitch, the axle stiffnesses are optimized for heave and the Olley effect can attenuate the residual pitch discomfort. The ghost of Plato tells us, in terms of a free response this reasoning is problematic, as all it addresses is the initial pitch overshoot and subsequent ringing will produce a beat effect. But in reality, the ghost of Aristotle counters that we can rely on damping in the system to attenuate subsequent ringing such that it is more important to attenuate the first overshoot of the step.

4.6 Pitch-Plane Model with Damping

The Olley criteria attenuated the initial pitch overshoot, but with a substantial difference between the front and the rear spring rates, pitch could reappear in subsequent oscillations. The reason this is a preferable trade-off is that subsequent pitch-plane oscillations are damped. As was shown in the quarter-car model, at each corner dampers are in parallel with the suspension springs and can accommodate the same leverage ratio. Similar to the suspension stiffness,

FIGURE 4.3 Pitch-plane model schematic with damping.

© Dan E. Williams.



these dampers can be combined across axles to result in front and rear damping values. Therefore, in [Figure 4.3](#), damping is added to the pitch-plane model of [Figure 4.1](#).

Equations 4.2 and 4.3 are replaced by similar equations which include the composite damping at each axle and allow a road input to extend the springs and dampers.

$$F_1 = K_1(z_{1,\text{in}} - z_s + x_1\theta) + D_1(\dot{z}_{1,\text{in}} - \dot{z}_s + x_1\dot{\theta}). \quad (4.54)$$

$$F_2 = K_2(z_{2,\text{in}} - z_s + x_2\theta) + D_2(\dot{z}_{2,\text{in}} - \dot{z}_s + x_2\dot{\theta}). \quad (4.55)$$

Recalling Eq. 4.1, some of the axle forces create a vertical acceleration.

$$m_s \ddot{z}_s = F_1 + F_2.$$

Equations 4.54 and 4.55 are inserted into Eq. 4.1 and solved for vertical heave acceleration.

$$\ddot{z}_s = \left(\frac{-K_1 - K_2}{m_s} \right) z_s + \left(\frac{-D_1 - D_2}{m_s} \right) \dot{z}_s + \left(\frac{x_1 K_1 + x_2 K_2}{m_s} \right) \theta + \left(\frac{x_1 D_1 + x_2 D_2}{m_s} \right) \dot{\theta} + \left(\frac{K_1}{m_s} \right) z_{1,\text{in}} + \left(\frac{K_2}{m_s} \right) z_{2,\text{in}} + \left(\frac{D_1}{m_s} \right) \dot{z}_{1,\text{in}} + \left(\frac{D_2}{m_s} \right) \dot{z}_{2,\text{in}}. \quad (4.56)$$

Similarly, Eq. 4.10 describes how axle moments create pitch accelerations.

$$I_y \ddot{\theta} = -x_1 F_1 - x_2 F_2$$

Equations 4.54 and 4.55 can be inserted into Eq. 4.10 and solved for pitch acceleration.

$$\ddot{\theta} = \left(\frac{x_1 K_1 + x_2 K_2}{I_y} \right) z_s + \left(\frac{x_1 D_1 + x_2 D_2}{I_y} \right) \dot{z}_s + \left(\frac{-x_1^2 K_1 - x_2^2 K_2}{I_y} \right) \theta + \left(\frac{-x_1^2 D_1 - x_2^2 D_2}{I_y} \right) \dot{\theta} \\ + \left(\frac{-x_1 K_1}{I_y} \right) z_{1,in} + \left(\frac{-x_1 D_1}{I_y} \right) \dot{z}_{1,in} + \left(\frac{-x_2 K_2}{I_y} \right) z_{2,in} + \left(\frac{-x_2 D_2}{I_y} \right) \dot{z}_{2,in} \quad (4.57)$$

Equations 4.56 and 4.57 can be written in matrix form:

$$\begin{bmatrix} \dot{z}_s \\ \ddot{z}_s \\ \dot{\theta} \\ \ddot{\theta} \end{bmatrix} = \begin{bmatrix} 0 & 1 & 0 & 0 \\ \frac{-K_1 - K_2}{m_s} & \frac{-D_1 - D_2}{m_s} & \frac{x_1 K_1 + x_2 K_2}{m_s} & \frac{x_1 D_1 + x_2 D_2}{m_s} \\ 0 & 0 & 0 & 1 \\ \frac{x_1 K_1 + x_2 K_2}{I_y} & \frac{x_1 D_1 + x_2 D_2}{I_y} & \frac{-x_1^2 K_1 - x_2^2 K_2}{I_y} & \frac{-x_1^2 D_1 - x_2^2 D_2}{I_y} \end{bmatrix} \begin{bmatrix} z_s \\ \dot{z}_s \\ \theta \\ \dot{\theta} \end{bmatrix} + \\ \begin{bmatrix} 0 & 0 & 0 & 0 \\ \frac{K_1}{m_s} & \frac{D_1}{m_s} & \frac{K_2}{m_s} & \frac{D_2}{m_s} \\ 0 & 0 & 0 & 0 \\ \frac{-x_1 K_1}{I_y} & \frac{-x_1 D_1}{I_y} & \frac{-x_2 K_2}{I_y} & \frac{-x_2 D_2}{I_y} \end{bmatrix} \begin{bmatrix} z_{f,in} \\ \dot{z}_{f,in} \\ z_{r,in} \\ \dot{z}_{r,in} \end{bmatrix}. \quad (4.58)$$

Compared with Eq. 4.13 which is two coupled second-order differential equations, Eq. 4.58 is four coupled first-order differential equations, and includes road input velocity input as previously discussed in [Chapter 2](#).

It is possible to simplify Eq. 4.58 using nomenclature for functions of axle stiffness of Eqs 4.14, 4.15, and 4.16, and similar functions for axle damping.

$$D_a = D_1 + D_2, \quad (4.59)$$

$$D_b = x_1 D_1 + x_2 D_2, \quad (4.60)$$

$$D_c = x_1^2 D_1 + x_2^2 D_2. \quad (4.61)$$

Equation 4.58 is thus simplified.

$$\begin{bmatrix} \dot{z}_s \\ \ddot{z}_s \\ \dot{\theta} \\ \ddot{\theta} \end{bmatrix} = \begin{bmatrix} 0 & 1 & 0 & 0 \\ -\frac{K_a}{m_s} & -\frac{D_a}{m_s} & \frac{K_b}{m_s} & \frac{D_b}{m_s} \\ 0 & 0 & 0 & 1 \\ \frac{K_b}{I_y} & \frac{D_b}{I_y} & -\frac{K_c}{I_y} & -\frac{D_c}{I_y} \end{bmatrix} \begin{bmatrix} z_s \\ \dot{z}_s \\ \theta \\ \dot{\theta} \end{bmatrix} + \begin{bmatrix} 0 & 0 & 0 & 0 \\ \frac{K_1}{m_s} & \frac{D_1}{m_s} & \frac{K_2}{m_s} & \frac{D_2}{m_s} \\ 0 & 0 & 0 & 0 \\ -\frac{x_1 K_1}{I_y} & -\frac{x_1 D_1}{I_y} & -\frac{x_2 K_2}{I_y} & -\frac{x_2 D_2}{I_y} \end{bmatrix} \begin{bmatrix} z_{i,in} \\ \dot{z}_{i,in} \\ z_{i,in} \\ \dot{z}_{i,in} \end{bmatrix} \quad (4.62)$$

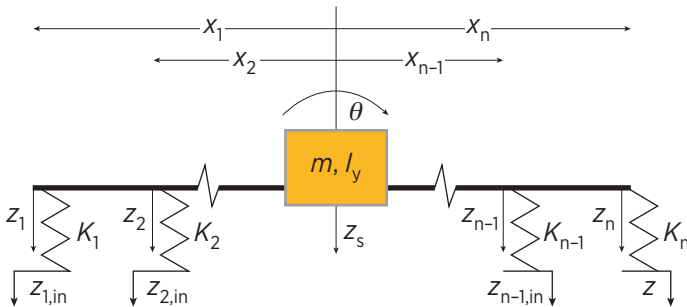
Equation 4.62 describes the behavior of a pitch-plane model including damping with general road inputs. As previously discussed, in practice, the road inputs in the pitch plane are not general for two reasons. First, as discussed in the quarter-car model, the road input velocity and the road input position are not independent, and in fact the integrated road input velocity will form the road input position. Second, as just seen in the pitch-plane model, the rear axle position and velocities are time-phased equivalents of front axle position and velocity. Therefore, from a practical standpoint, instead of the four independent road inputs as shown in Eq. 4.62, there is really only one, which is integrated/differentiated and/or time phased. From a theoretical standpoint, it is better to use a road input velocity and integrate; however, road position is perhaps more accessible. The physics of the tire rolling over a sharp step input (not considered here) will soften the step, and therefore minimize the necessity to differentiate a sharp input and therefore allow reasonable differentiation of road displacement input.

4.7 Generalized Pitch-Plane Model and Olley Solution

A generalized multiaxle pitch-plane model is possible through the change in convention used to locate axles [1]. In past vehicle models, consistent with two-axle vehicle precedent, axles are located by their absolute location from the vehicle center of mass. In the present work an axle is located by the signed distance along the longitudinal axis of the vehicle, therefore an axle in front of the center of mass is located with a positive number, and an axle behind the center of mass is located with a negative number. Thus for the two-axle vehicle, x_1 locating the front axle would be positive, and x_2 locating the rear axle negative. A more general multiaxle vehicle model is shown in [Figure 4.4](#).

With this change in convention, the vertical displacement of the sprung mass at each axle i can be written for the heaving and pitching vehicle,

$$z_i = z_s - x_i \theta, \quad (4.63)$$

FIGURE 4.4 Generalized pitch-plane model schematic.

© Dan E. Williams.

where x_i is the signed displacement of the i th axle. The corresponding vertical force through the suspension on the sprung mass is a function of the combined stiffness of the suspension on both axle ends, K_i .

$$F_i = K_i(z_{i,in} - z_i). \quad (4.64)$$

Considering the free response $z_{i,in}$ is zero and Eq. 4.63 is inserted in Eq. 4.64.

$$F_i = -K_i(z_s - x_i\theta). \quad (4.65)$$

Vertical suspension forces can be summed and equated to the product of the sprung mass and heave acceleration.

$$m_s \ddot{z}_s = \sum -K_i(z_s - x_i\theta). \quad (4.66)$$

Vertical suspension moments can be summed and equated to the product of sprung mass inertia and pitch acceleration.

$$I_y \ddot{\theta} = \sum -x_i K_i(z_s - x_i\theta). \quad (4.67)$$

Equations 4.66 and Eq. 4.67 can be written in matrix form to yield a general pitch-plane model for a vehicle with an arbitrary number of axles.

$$\begin{bmatrix} m_s \ddot{z}_s \\ I_y \ddot{\theta} \end{bmatrix} = \begin{bmatrix} -\sum K_i & \sum x_i K_i \\ \sum x_i K_i & -\sum x_i^2 K_i \end{bmatrix} \begin{bmatrix} z_s \\ \theta \end{bmatrix}. \quad (4.68)$$

Taking the Laplace transform of Eq. 4.68,

$$\begin{bmatrix} m_s s^2 & 0 \\ 0 & I_y s^2 \end{bmatrix} \begin{bmatrix} x(s) \\ \theta(s) \end{bmatrix} = \begin{bmatrix} -\sum K_i & \sum x_i K_i \\ \sum x_i K_i & -\sum x_i^2 K_i \end{bmatrix} \begin{bmatrix} x(s) \\ \theta(s) \end{bmatrix} \quad (4.69)$$

and a useful bit of nomenclature is adopted.

$$K_a = -\sum K_i, \quad (4.70)$$

$$K_b = \sum x_i K_i, \quad (4.71)$$

$$K_c = -\sum x_i^2 K_i. \quad (4.72)$$

The change of the axle location convention makes the introduction of generalized stiffness parameters K_a , K_b , and K_c of Eqs 4.70, 4.71, and 4.72 possible. Not only do these generalized stiffness parameters simplify the generalized pitch-plane model, but they convey physical insight with K_a and K_c as the decoupled heave and pitch stiffnesses, and K_b as a modal coupling term.

Using Eqs 4.70, 4.71, and 4.72 and the definition of the Laplace variable,

$$\begin{bmatrix} 0 \\ 0 \end{bmatrix} = \begin{bmatrix} m_s \omega^2 - K_a & -K_b \\ -K_b & I_y \omega^2 - K_c \end{bmatrix} \begin{bmatrix} z_s(j\omega) \\ \theta(j\omega) \end{bmatrix} = 0. \quad (4.73)$$

The two natural frequencies of the two-axle pitch-plane model are described by the ω^2 that solves Eq. 4.73. Specifically, this ω^2 can be expressed using the determinant of the matrix in Eq. 4.73.

$$\omega^2 = \frac{\left(K_c m + K_a I_y \right) + / - \sqrt{K_c^2 m^2 + 2K_c m K_a I_y + K_a^2 I_y^2 - 4mI_y \left(K_a K_c - K_b^2 \right)}}{2mI_y}. \quad (4.74)$$

The previously derived two-axle Eq. 4.24 is a special case of Eq. 4.74, and Eq. 4.74 can be algebraically simplified.

$$\omega^2 = \frac{\left(K_c m + K_a I_y \right) + / - \sqrt{\left(K_c m - K_a I_y \right)^2 + 4mI_y K_b^2}}{2mI_y}. \quad (4.75)$$

Similar to the two-axle model, in view of Eq. 4.73, the K_b defined in Eq. 4.71 is a coupling term and axle stiffnesses K_1, K_2, \dots, K_n can be selected so that the two modes are approximately decoupled. When this is done, the two solutions of Eq. 4.75 can be written.

$$\omega_1 = \sqrt{\frac{K_a}{m}}, \quad (4.76)$$

$$\omega_2 = \sqrt{\frac{K_c}{I_y}}. \quad (4.77)$$

Equation 4.76 can be recognized as the decoupled heave natural frequency, and Eq. 4.77 as the decoupled pitch natural frequency.

Maurice Olley originally described desirable relationships between natural frequencies for use in selecting the front and rear stiffness values [2]. Tom Gillespie summarized them as follows with a slight restatement of the first criteria that will be computationally useful [3]:

- (1) The front suspension should have a 30% lower ride rate than the rear suspension, or the spring center should be at least 6.5% of the wheelbase behind the center of gravity.
- (2) The pitch and bounce frequencies should be close together.
- (3) Neither frequency should be greater than 1.3 Hz.

For the two-axle vehicle, Olley's ride criteria thus impose three constraints on the selection of two parameters, the front and rear stiffnesses K_f and K_r . It is therefore probable that the two-axle system is overconstrained. (The problem is somewhat mitigated as most two-axle passenger cars are close to a 50/50 weight distribution, allowing the Olley criteria to generally approximate.) It will be shown that vehicles with three or more axles have more degrees of freedom to satisfy the Olley criteria.

The first criteria can be addressed as the spring center x_{sp} can be written using algebraic manipulation of the static free body analysis [4].

$$x_{sp} = \frac{-K_b}{K_a}. \quad (4.78)$$

Because it is desired that the spring center be behind the vehicle center of gravity, x_{sp} is negative.

The second criteria can be addressed by examining Eq. 4.75. Ideally, the two natural frequencies would be equal if the discriminant of Eq. 4.75 is zero. Unfortunately, this is not possible for real parameter values as it is comprised of two squared terms. The second term is a function of K_b and cannot be zero with adherence to the first Olley criteria. Given a nonzero K_b , the smallest the discriminant (and thus the closest the natural frequencies) can be is if the value within the parenthesis of the discriminant goes to zero. This allows the second Olley criteria to be quantified.

$$K_c m = K_a I_y. \quad (4.79)$$

The second Olley Criteria—that pitch and bounce frequencies be close together—is not directly achievable in view of Eq. 4.75 and the first criteria of Eq. 4.78 implying a nonzero K_b . However, a modification of the second Olley criteria—that the *decoupled* pitch and bounce frequencies are equal as implied in Eq. 4.79—can be achieved, with the understanding that the actual coupled frequencies will differ. Equations 4.78 and 4.79 are inserted into Eq. 4.75. The third Olley criteria is stated when the result is solved for the largest natural frequency.

$$\omega^2 = \frac{K_a I_y - K_a x_{sp} \sqrt{m_s I_y}}{m_s I_y} = K_a \left(\frac{1}{m_s} - \frac{x_{sp}}{\sqrt{m_s I_y}} \right). \quad (4.80)$$

The three equations derived from Olley criteria, Eqs 4.78, 4.79, and 4.80 can be expressed in matrix form:

$$\begin{bmatrix} \left(\frac{1}{m_s} - \frac{x_{sp}}{\sqrt{m_s I_y}} \right) & 0 & 0 \\ x_{sp} & 1 & 0 \\ I_y & 0 & -m_s \end{bmatrix} \begin{bmatrix} K_a \\ K_b \\ K_c \end{bmatrix} = \begin{bmatrix} \omega^2 \\ 0 \\ 0 \end{bmatrix} \quad (4.81)$$

The inverse of the matrix in Eq. 4.81 is used to find the generalized stiffness parameters.

$$\begin{bmatrix} K_a \\ K_b \\ K_c \end{bmatrix} = \begin{bmatrix} \left(\frac{m_s}{1 - x_{sp} \sqrt{\frac{m_s}{I_y}}} \right) & 0 & 0 \\ \left(\frac{-x_{sp} m_s}{1 - x_{sp} \sqrt{\frac{m_s}{I_y}}} \right) & 1 & 0 \\ \left(\frac{I_y}{1 - x_{sp} \sqrt{\frac{m_s}{I_y}}} \right) & 0 & \frac{-1}{m_s} \end{bmatrix} \begin{bmatrix} \omega^2 \\ 0 \\ 0 \end{bmatrix}. \quad (4.82)$$

Equation 4.82 reports generalized stiffness parameters K_a , K_b , and K_c in terms of vehicle inertial parameters m_s and I_y and ω and x_{sp} selected according to the Olley criteria.

Generalized stiffness parameters K_a , K_b , and K_c are defined in Eqs 4.70, 4.71, and 4.72 as functions of the axle location with respect to the vehicle center of mass and axle stiffnesses. It is likely that axle locations are defined by other vehicle considerations, and only the stiffnesses can be varied to achieve desirable ride. In this case the axle stiffnesses of a three-axle vehicle can be found by putting Eqs 4.70, 4.71, and 4.72 in matrix form. (The negative second row is the result of the negative sign attached to Eq. 4.71.)

$$\begin{bmatrix} K_a \\ K_b \\ K_c \end{bmatrix} = \begin{bmatrix} 1 & 1 & 1 \\ -x_1 & -x_2 & -x_3 \\ x_1^2 & x_2^2 & x_3^2 \end{bmatrix} \begin{bmatrix} K_1 \\ K_2 \\ K_3 \end{bmatrix}. \quad (4.83)$$

Hence for only the three-axle vehicle, Eq. 4.83 can be inverted and combined with Eq. 4.82 to yield unique three-axle stiffnesses as a function of basic vehicle inertial properties, axle locations, and Olley parameters.

$$\begin{bmatrix} K_1 \\ K_2 \\ K_3 \end{bmatrix} = \begin{bmatrix} 1 & 1 & 1 \\ -x_1 & -x_2 & -x_3 \\ x_1^2 & x_2^2 & x_3^2 \end{bmatrix}^{-1} \begin{bmatrix} \frac{m_s}{1-x_{sp}\sqrt{\frac{m_s}{I_y}}} \\ \frac{-x_{sp}m_s}{1-x_{sp}\sqrt{\frac{m}{I_y}}} \\ \frac{I_y}{1-x_{sp}\sqrt{\frac{m_s}{I_y}}} \end{bmatrix} \begin{bmatrix} 0 & 0 \\ 1 & 0 \\ 0 & \frac{-1}{m_s} \end{bmatrix} \begin{bmatrix} \omega^2 \\ 0 \\ 0 \end{bmatrix} \quad (4.84)$$

Equation Eq. 4.84 can be evaluated and simplified,

$$\begin{bmatrix} K_1 \\ K_2 \\ K_3 \end{bmatrix} = \begin{bmatrix} \frac{-x_2 x_3}{x_1 x_2 + x_1 x_3 - x_2 x_3 - x_1^2} & \frac{-x_2 - x_3}{x_1 x_2 + x_1 x_3 - x_2 x_3 - x_1^2} & \frac{-1}{x_1 x_2 + x_1 x_3 - x_2 x_3 - x_1^2} \\ \frac{-x_1 x_3}{x_1 x_2 - x_1 x_3 + x_2 x_3 - x_2^2} & \frac{-x_1 - x_3}{x_1 x_2 - x_1 x_3 + x_2 x_3 - x_2^2} & \frac{-1}{x_1 x_2 - x_1 x_3 + x_2 x_3 - x_2^2} \\ \frac{x_1 x_2}{x_1 x_2 - x_1 x_3 - x_2 x_3 + x_3^2} & \frac{x_1 + x_2}{x_1 x_2 - x_1 x_3 - x_2 x_3 + x_3^2} & \frac{1}{x_1 x_2 - x_1 x_3 - x_2 x_3 + x_3^2} \end{bmatrix} \begin{bmatrix} \frac{m_s \omega^2}{1 - x_{sp} \sqrt{\frac{m_s}{I_y}}} \\ \frac{-x_{sp} m_s \omega^2}{1 - x_{sp} \sqrt{\frac{m_s}{I_y}}} \\ \frac{I_y \omega^2}{1 - x_{sp} \sqrt{\frac{m_s}{I_y}}} \end{bmatrix} \quad (4.85)$$

and multiplied to solve for individual axle stiffnesses.

$$K_1 = \frac{\omega^2 (-mx_2 x_3 + x_{sp} m(x_2 + x_3) - I_y)}{\left(1 - x_{sp} \sqrt{\frac{m}{I_y}}\right)(x_1 x_2 + x_1 x_3 - x_2 x_3 - x_1^2)}, \quad (4.86)$$

$$K_2 = \frac{\omega^2 (-mx_1 x_3 + x_{sp} m(x_1 + x_3) - I_y)}{\left(1 - x_{sp} \sqrt{\frac{m}{I_y}}\right)(x_1 x_2 - x_1 x_3 + x_2 x_3 - x_2^2)}, \quad (4.87)$$

$$K_3 = \frac{\omega^2 (-mx_1 x_2 - x_{sp} m(x_1 + x_2) + I_y)}{\left(1 - x_{sp} \sqrt{\frac{m}{I_y}}\right)(x_1 x_2 - x_1 x_3 - x_2 x_3 + x_3^2)}. \quad (4.88)$$

For a two-axle vehicle with a fixed wheelbase, the matrix mapping axle stiffnesses to generalized stiffness parameters in Eq. 4.83 is not invertible. In this case the axle stiffnesses are overdetermined, and it is not likely that front and rear axle stiffness can be selected to precisely satisfy the Olley parameters selected.

For the three-axle vehicle, the Olley criteria as stated by Gillespie cannot be precisely achieved. However, this criterion can be achieved if slightly restated—that the *decoupled* pitch and heave natural frequencies equate. With this modification, Eqs 4.86, 4.87, and 4.88 yield the three axle stiffnesses that will result in equal decoupled pitch and heave natural frequencies and both coupled ride frequencies below ω and as close together as possible, a spring center of x_{sp} , for a vehicle of mass m_s and pitch moment of inertia I_y , with axles located by x_1 , x_2 , and x_3 .

If there are more than three axles, again the matrix mapping axle stiffnesses to K_a , K_b , and K_c in Eq. 4.83 is not invertible. In this case, however, the axle stiffnesses are underdetermined, and there could be multiple combinations of axle stiffnesses that would satisfy the selected Olley parameters equally well. In this case the extra degree of freedom could be used for design flexibility. For example, if the vehicle had four axles another row could be added to Eq. 4.83 describing a desired function of the four-axle stiffnesses (e.g., K_2 and K_3 equal). In general such a function could specify a relationship between particular axle stiffnesses. This would make the matrix of Eq. 4.83 invertible in the case of four axles, and allow the same methodology to be repeated.

4.8 Three-Axle Vehicle Example

The individual axle stiffnesses can be calculated for a specific vehicle knowing its axle locations and inertial properties. This exercise will both illustrate the prior theoretical development for the interesting three-axle case with a unique solution, and provide insight into the generally applied Olley criteria for all vehicle configurations. The following parameters are representative of an actual development vehicle shown in [Figure 4.5](#).

$$x_1 = 4.256\text{m}; W_1 = 29,460 \text{ N}$$

$$x_2 = -0.524\text{m}; W_2 = 78,560 \text{ N}$$

$$x_3 = -2.144\text{m}; W_3 = 39,280 \text{ N}$$

$$m_s = 15000 \text{ kg}$$

$$I_y = 4343\text{kg}\cdot\text{m}\cdot\text{sec}^2 = 42648 \text{ kg}\cdot\text{m}^2$$

The desired Olley parameters can be selected.

$$\omega = 1.3 \text{ Hz} = 8.2 \text{ rads/sec}$$

$$x_{sp} = -0.065*(4.26+2.144) \text{ m} = -0.416\text{m}$$

FIGURE 4.5 Test vehicle.

© SAE International.



Using Eqs 4.85, 4.86, and 4.87, the generalized stiffness parameters can be calculated.

$$K_a = 809,000 \text{ N/m}$$

$$K_b = 336,500 \text{ N}$$

$$K_c = 2,300,200 \text{ N-m}$$

Several observations can be made from the generalized stiffness parameter values. The decoupled heave and pitch natural frequencies are around 7.3 rad/sec. Equal decoupled pitch and heave natural frequencies are a product of the second Olley criteria, as described in Eq. 4.79. Unfortunately K_b , while small is significant, and the actual natural frequencies differ.

Using these values, it can be shown that the desired Olley ride criteria parameters are achieved. From Eq. 4.78, the value of the spring center can be found.

$$x_{sp} = -336,500/809,000 = -0.416 \text{ m}$$

This was in fact the desired design value for the spring center, and it is this Olley parameter that drives the significant value of K_b that serves to couple the pitch and heave modes.

The largest natural frequency is found from Eq. 4.80,

$$\omega = \sqrt{809800 \left(\frac{1}{15000} - \frac{-0.416}{\sqrt{(15000)(42648)}} \right)} = 8.2 \text{ rads/sec},$$

which is the design value for the largest natural frequency. Note that it is higher than the decoupled pitch and heave natural frequencies. Equation 4.75 can likewise be solved for the lower natural frequency.

$$\omega = \sqrt{809,000 \left(\frac{1}{15000} + \frac{-0.416}{\sqrt{(15000)(42648)}} \right)} = 6.4 \text{ rads/sec.}$$

Owing to the structure of Eq. 4.75, it can be seen that this is the closest the two natural frequencies of the pitch-plane model can be, although not as close as Gillespie suggests [5]. The K_b required to move the spring center rearward results in coupled natural frequencies. Note the first Olley criterion is stated as a percentage of the overall wheelbase. Therefore, for long vehicles the spring center will move more, resulting in more coupling between the pitch and heave modes.

When the generalized stiffness parameters K_a , K_b , and K_c are inserted into Eq. 4.33 values for the axle stiffnesses can be calculated.

$$K_1 = 75,550 \text{ N/m}$$

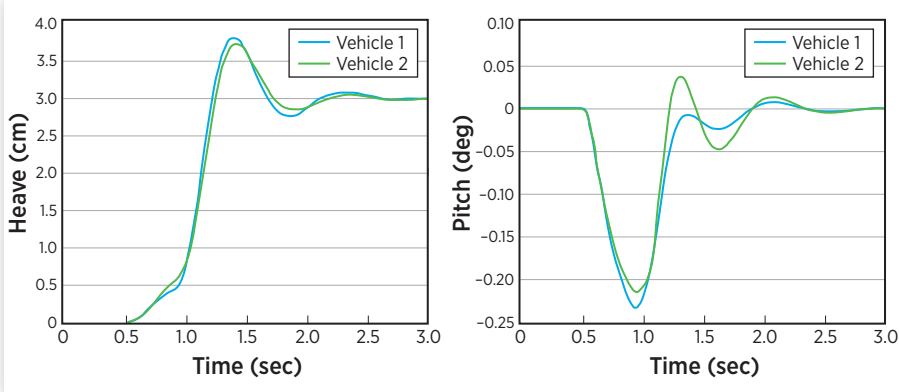
$$K_2 = 564,480 \text{ N/m}$$

$$K_3 = 168,980 \text{ N/m}$$

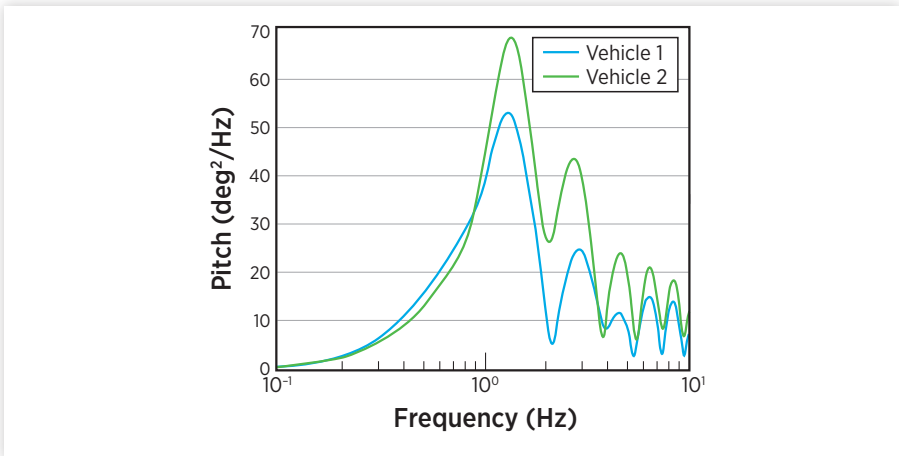
An “equivalent natural frequency” can be used to normalize these stiffnesses by the weight carried by each axle. When this is done, the front axle is 5 rad/sec, the second 8.4 rads/sec, and the third 6.5 rad/sec. The front axle stiffness is even lower than would be expected because of carrying less weight. By moving the spring center to the rear, the Olley ride criterion effectively lowers the front axle natural frequency.

As explained previously, the Olley ride criteria does indeed soften the front suspension relative to the rear, so that the front hits the bump first and reacts slower relative to the rear axles that hit the bump later, and the initial reaction of the sprung mass through the first overshoot is more heave than pitch.

The desirability of a three-axle vehicle conforming to the Olley ride criteria is evident when compared to a second vehicle similar to the vehicle shown in [Figure 4.3](#) except with the second and third axle stiffnesses equal—a common configuration. A time domain simulation was performed where the vehicle encountered a 3.0-cm step when traveling at 50 kph.

FIGURE 4.6 Heave and pitch step responses of Olley and benchmark vehicles.

Reprinted with permission from © Inderscience Enterprises Limited (UK).

FIGURE 4.7 Pitch FFT for Olley and benchmark vehicles.

Reprinted with permission from © Inderscience Enterprises Limited (UK).

The first vehicle configuration conforming to the Olley ride criteria has virtually the same heave-mode response as the second vehicle with equal rear suspension stiffnesses, as seen in [Figure 4.6](#). The effect of the Olley criteria, however, is apparent when looking at the pitch response. There is slightly greater initial magnitude, but the desired effect of the Olley ride criteria is seen in the attenuation of subsequent overshoots/undershoots.

As shown in [Figure 4.7](#), the net result is a significant decrease in pitch acceleration at frequencies between 1 and 2 Hz—where the human body is most sensitive [5], and as seen in the fore-and-aft tolerance shown in [Figure 4.2](#).

4.9 Summary

The pitch degree of freedom is added to heave to form the pitch-plane model. Unsprung mass dynamics developed in the preceding quarter-car chapter are neglected. In the pitch-plane model two idealized natural frequencies were identified: the heave mode familiar from the quarter-car model, and the new pitch mode. Both the right and left sides of an axle experience the same road input, so their stiffness and damping can be combined. The rear axle experiences the same time phased input as the front, so as vehicle speeds increase road inputs excite the pitch mode less. At highway speeds vehicle ride is mostly dominated by the heave mode.

Maurice Olley suggested properties of a vehicle that would result in a good qualitative ride. Most of these properties are relevant to the pitch-plane model. The basic idea is that at low and moderate speeds where pitch is relevant, ride can be improved with a relatively softer front suspension. In this case, pitch is reduced as the rear responds quicker to the time phase input.

The well-known pitch-plane vehicle ride model was slightly modified so that axles are located by a signed parameter. This change in convention allowed the pitch-plane model to generalize to any number of arbitrary axles. Nomenclature was suggested so that the pitch-plane model can be more simply expressed in terms of summations of functions of axle stiffnesses and locations. These summations were found to have physical significance as well as simplifying the equations. This change in convention and nomenclature can be used to solve for axle stiffnesses that uniquely provide good vehicle ride according to the long appreciated Olley criteria for three-axle vehicles. Vehicles with more than three axles can generally achieve the Olley ride criteria with a number of axle stiffness combinations.

The quarter-car model developed in the previous chapter is perhaps more generally appreciated as it defines the primary heave and wheel-hop vertical natural frequencies that recur in ride applications. These frequencies provide, as was shown, constraints and trade-offs on fundamental vehicle dynamic parameters (e.g., suspension damping). The pitch-plane model is more limited in its application. As pitch is less excited by undulating roads at higher speeds, the pitch-plane model is more relevant for low-speed and off-highway vehicle use cases. As this is a common use case for many multi-axle vocational commercial and military vehicles, the generalized model allowed by the conventions change is valuable.

References

- [1] Williams, D.E., and Nhila, A., "Generalized Pitch-Plane Vehicle Model Satisfying Olley Ride Criteria," *Int. J. Heavy Vehicle Systems*, IJHVS-112416, Vol. 23, No. 3, 2016.

- [2] Milliken, W.F. and Milliken, D.L., "Chassis Design Principles and Analysis," Society of Automotive Engineers, Warrendale, PA, 2002.
- [3] Gillespie, T.D., "Fundamentals of Vehicle Dynamics," Society of Automotive Engineers, Warrendale, PA, 1992.
- [4] Milliken, W.F. and Milliken, D.L., "Chassis Design Principles and Analysis," Society of Automotive Engineers, Warrendale, PA, 2002.
- [5] Gillespie, T.D., "Fundamentals of Vehicle Dynamics," Society of Automotive Engineers, Warrendale, PA, 1992.

The Roll-Plane Model

“ So if you’re tired of the same
old story
Oh, turn some pages
I’ll be here when you are ready
To roll with the changes

—REO Speedwagon

5.1 Introduction

In the previous chapter, the pitching motion of the vehicle was described. In typical vehicles, the rear wheels follow in the tracks of the front, and therefore experience a time delayed input. It is common, particularly on highways, that a road disturbance runs across the width of the lane, such as a railroad track perpendicular to the lane. It is less common, although still possible, that only one side of the vehicle experiences an input from the road. This would produce an input to the sprung mass that would tend to rotate the vehicle about its longitudinal axis, commonly referred to as roll. Perhaps the most common cause of vehicle roll is because of the “centrifugal force” acting on the sprung mass of the vehicle during a turn. In general, we would like the vehicle to appear soft in response to uneven pavement inputs, and yet stiff in roll in response to lateral acceleration.

Typically in vehicle dynamics, roll and pitch are considered independently. The real world insures no such decoupling; however, it is useful to acquire a fundamental understanding of each mode independently. We will begin by applying the quarter-car model at each corner of the sprung mass similar to what was done in the previous chapter in the pitch plane, only here combining equivalent stiffness on the left and ride sides of the car. In [Chapter 4](#), advantages were shown for different suspension stiffness in the front and rear of the vehicle. These stiffnesses combine to get the same roll resisting stiffness on

either side of the vehicle, but the proportion of roll moment carried on the front relative to the rear can affect handling. Antiroll bars or stabilizer bars will be considered as a significant difference between the pitch and the roll planes as they can increase roll stiffness without increasing suspension stiffness—sort of. The distribution of roll moment resistance between the front and the rear axles has a second-order effect on the vehicle turning behavior.

The phenomena of interest in the pitch plane were the dynamic interactions of the pitch and heave modes when excited by road inputs, as described by Olley. In this chapter, the focus will be on how stabilizer bars address a compromise in roll mode behavior as excited by road inputs or by the centrifugal force experienced as the vehicle turns. While the pitch plane was shown to be interesting off-highway and at speeds less than highway speeds, the compromise seen in the roll plane is evident on the highway, and at highway speeds—a big component of many vehicle's duty cycle.

Roll is often omitted in vehicle dynamics work. It is introduced here so that it can be used in the next chapter when active suspension is presented as a case study. It will be again used and a bit further developed in the second section on handling. We will see in this later section that roll is an important source of coupling between ride and handling. As such, it produces constraints on (and opportunities for) vehicle dynamics and is worth considering. In this chapter, roll is introduced in an intuitive way. In the following section on handling, it is developed more formally. Much of the vehicle dynamics literature omits roll. The following chapter on active suspension and the following section on handling will continue to develop the importance of roll. So to paraphrase REO Speedwagon, if you are tired of the same old story in vehicle dynamics, keep reading, and by the later chapters in the book you will see roll included with some new changes. The present chapter will introduce a basic roll mode model, and develop a basic analysis of the stabilizer bar, an important device used to mitigate inherent compromises in vehicle design.

5.2 Simple Two-Axle Roll-Plane Model

The pitch plane was best envisioned by looking at the side of the vehicle and simplified by combining corner suspensions across an axle. The simplification was justified as suspensions are typically the same on the right and left hand sides of the vehicle. For the roll plane analysis, we similarly look at the front (or rear) of the vehicle. But we cannot simplify the model by simply combining front and rear suspensions across one side of the vehicle, as front and rear suspensions are often quite different. Recall that this very characteristic is specified in the Olley criteria.

Just as with the pitch-plane model, unsprung mass dynamics are ignored. The roll mode, similar to what we have seen earlier in the sprung mass modes

of heave and pitch, has a natural frequency significantly lower than the wheel hop frequency (recall the Olley ride criteria). A two-axle vehicle will initially be considered, with the front axle denoted as axle 1 and the rear as axle 2. Assuming the vehicle has a similar track t across all axles, the differential equation describing the roll mode behavior in response to vertical inputs can be written where l and r denote the left and right corners of a given axle as seen by the driver.

$$I_{\emptyset} \ddot{\emptyset} = \frac{t}{2} F_{1,r} - \frac{t}{2} F_{1,l} + \frac{t}{2} F_{2,r} - \frac{t}{2} F_{2,l}, \quad (5.1)$$

$$m_s \ddot{x}_s = F_{1,r} + F_{1,l} + F_{2,r} + F_{2,l}. \quad (5.2)$$

As a first approximation the corner forces on the sprung mass in response to road inputs were simply described in the quarter-car chapter, with the assumption that unsprung mass dynamics had a negligible effect on sprung mass dynamics. With this assumption, the suspension stiffness at each corner is displaced by the road input to provide an input to the rolling sprung mass,

$$F_{i,j} = \frac{K_{i,t} K_{i,s}}{(K_{i,t} + K_{i,s})} (z_{i,j,in} - z_{i,j}), \quad (5.3)$$

where i is the axle number (i.e., 1 for front, 2 for rear of a two axle vehicle, and j is the side— l for left and r for right, relative to the seated driver. Similarly, each axle i is allowed its own tire stiffness $K_{i,t}$ and suspension stiffness $K_{i,s}$. For an unconstrained rolling vehicle, the sprung mass displacement at each corner can be written as follows:

$$z_{1,r,s} = x_s + \frac{t}{2} \emptyset, \quad (5.4)$$

$$z_{1,l,s} = x_s - \frac{t}{2} \emptyset, \quad (5.5)$$

$$z_{2,r,s} = x_s + \frac{t}{2} \emptyset, \quad (5.6)$$

$$z_{2,l,s} = x_s - \frac{t}{2} \emptyset. \quad (5.7)$$

Equations 5.4–5.7 can be inserted into Eq. 5.3 to yield sprung mass forces on each corner.

$$F_{1,r} = \frac{K_{1,t} K_{1,s}}{(K_{1,t} + K_{1,s})} \left(z_{1,r,\text{in}} - z_s - \frac{t}{2} \emptyset \right), \quad (5.8)$$

$$F_{1,l} = \frac{K_{1,t} K_{1,s}}{(K_{1,t} + K_{1,s})} \left(z_{1,l,\text{in}} - z_s + \frac{t}{2} \emptyset \right), \quad (5.9)$$

$$F_{2,r} = \frac{K_{2,t} K_{2,s}}{(K_{2,t} + K_{2,s})} \left(z_{2,r,\text{in}} - z_s - \frac{t}{2} \emptyset \right), \quad (5.10)$$

$$F_{2,l} = \frac{K_{2,t} K_{2,s}}{(K_{2,t} + K_{2,s})} \left(z_{2,l,\text{in}} - z_s + \frac{t}{2} \emptyset \right). \quad (5.11)$$

The sprung mass forces of Eqs 5.8–5.11 can be inserted into the heave mode differential Eq. 5.1.

$$\begin{aligned} \ddot{z}_s = & \frac{2}{m_s} \left(-\frac{K_{1,t} K_{1,s}}{(K_{1,t} + K_{1,s})} - \frac{K_{2,t} K_{2,s}}{(K_{2,t} + K_{2,s})} \right) z_s + \frac{K_{1,t} K_{1,s}}{m_s (K_{1,t} + K_{1,s})} (z_{1,r,\text{in}}) \\ & + \frac{K_{1,t} K_{1,s}}{m_s (K_{1,t} + K_{1,s})} (z_{1,l,\text{in}}) + \frac{K_{2,t} K_{2,s}}{m_s (K_{2,t} + K_{2,s})} (z_{2,r,\text{in}}) \\ & + \frac{K_{2,t} K_{2,s}}{m_s (K_{2,t} + K_{2,s})} (z_{2,l,\text{in}}). \end{aligned} \quad (5.12)$$

Similarly, the sprung mass forces of Eqs 5.8–5.11 can be inserted into the roll mode differential Eq. 5.2.

$$\begin{aligned} \ddot{\emptyset} = & \frac{t^2}{2} \left(-\frac{K_{1,t} K_{1,s}}{I_\emptyset (K_{1,t} + K_{1,s})} - \frac{K_{2,t} K_{2,s}}{I_\emptyset (K_{2,t} + K_{2,s})} \right) \emptyset + \frac{t}{2} \frac{K_{1,t} K_{1,s}}{I_\emptyset (K_{1,t} + K_{1,s})} (z_{1,r,\text{in}}) \\ & - \frac{t}{2} \frac{K_{1,t} K_{1,s}}{I_\emptyset (K_{1,t} + K_{1,s})} (z_{1,l,\text{in}}) + \frac{t}{2} \frac{K_{2,t} K_{2,s}}{I_\emptyset (K_{2,t} + K_{2,s})} (z_{2,r,\text{in}}) \\ & - \frac{t}{2} \frac{K_{2,t} K_{2,s}}{I_\emptyset (K_{2,t} + K_{2,s})} (z_{2,l,\text{in}}) \end{aligned} \quad (5.13)$$

and written in matrix form.

$$\begin{bmatrix} \dot{z}_s \\ \ddot{z}_s \\ \dot{\emptyset} \\ \ddot{\emptyset} \end{bmatrix} = \begin{bmatrix} 0 & 1 & 0 & 0 \\ \frac{2}{m_s} \left(-\frac{K_{1,t} K_{1,s}}{(K_{1,t} + K_{1,s})} - \frac{K_{2,t} K_{2,s}}{(K_{2,t} + K_{2,s})} \right) & 0 & 0 & 0 \\ 0 & 0 & 0 & 1 \\ 0 & 0 & t^2 \left(-\frac{K_{1,t} K_{1,s}}{I_{\emptyset} (K_{1,t} + K_{1,s})} - \frac{K_{2,t} K_{2,s}}{I_{\emptyset} (K_{2,t} + K_{2,s})} \right) & 0 \end{bmatrix} \begin{bmatrix} z_s \\ \dot{z}_s \\ \emptyset \\ \dot{\emptyset} \end{bmatrix} \quad (5.14)$$

$$+ \begin{bmatrix} 0 & 0 & 0 & 0 \\ \frac{K_{1,t} K_{1,s}}{m_s (K_{1,t} + K_{1,s})} & \frac{K_{1,t} K_{1,s}}{m_s (K_{1,t} + K_{1,s})} & \frac{K_{2,t} K_{2,s}}{m_s (K_{2,t} + K_{2,s})} & \frac{K_{2,t} K_{2,s}}{m_s (K_{2,t} + K_{2,s})} \\ 0 & 0 & 0 & 0 \\ \frac{t}{2 I_{\emptyset} (K_{1,t} + K_{1,s})} & -\frac{t}{2 I_{\emptyset} (K_{1,t} + K_{1,s})} & \frac{t}{2 I_{\emptyset} (K_{2,t} + K_{2,s})} & -\frac{t}{2 I_{\emptyset} (K_{2,t} + K_{2,s})} \end{bmatrix} \begin{bmatrix} z_{1,r,in} \\ z_{1,l,in} \\ z_{2,r,in} \\ z_{2,l,in} \end{bmatrix}.$$

The general matrix expression in Eq. 5.14 does not produce a directly valuable result because the road inputs are unrealistically general, but closer examination provides insight into the roll-plane model. First, assuming an equal front and rear track, the rear wheels experience a time delayed input of the front, similar to the pitch plane analysis. The phenomena of wheelbase filtering discussed in the previous chapter applies to the roll plane. The result of wheelbase filtering in the pitch-plane model was that pitching inputs were increasingly filtered at higher speeds. In the roll plane at low speeds, an event on one side of the vehicle produced a bit of a combined heave, pitch and roll input biased toward heave, until the rear wheel experiences the same event, and the input is a decomposition of the input into roll and heave. If the inputs on either side of the vehicle are considered simultaneous, the road input can be considered as a heave input—both sides of the vehicle see the same input, and a roll input—either side of the vehicle sees an opposite input. With this reasoning, the roll plane is less sensitive to speed variation than the previous pitch plane. Roll remains relevant at high speeds in a way that pitch does not, but to the extent high-speed roads are straight and do not provide roll inputs (road inputs on one side of the vehicle track but not the other), the roll mode is not usually excited. This is why the pitch-plane model of Chapter 4 is considered more useful in understanding ride. However, in high-performance driving or emergency maneuvers roll most certainly is excited, but generally through handling inputs and not road inputs.

Furthermore, the observation that road inputs can be decomposed into pure heave inputs and pure roll inputs can be combined with the observation that Eq. 5.14 is partitioned so that the heave-mode dynamics are decoupled from the roll-mode dynamics. If the inputs can be decomposed and the dynamics are decoupled, the modes can be treated independently. It should be noted that suspension kinematics could modify this statement. A key assumption to the roll-plane model as now presented is that the vehicle rolls about its center of mass. As we will see in following section of the book, this is not always the case.

A final comment can be made regarding Eq. 5.14. The stiffness terms in the heave mode and roll mode are similar. From Eq. 5.14, the heave stiffness can be identified,

$$K_h = 2 \left(\frac{K_{1,t} K_{1,s}}{(K_{1,t} + K_{1,s})} + \frac{K_{2,t} K_{2,s}}{(K_{2,t} + K_{2,s})} \right) \quad (5.15)$$

and similarly the roll stiffness.

$$K_r = \frac{t^2}{2} \left(\frac{K_{1,t} K_{1,s}}{(K_{1,t} + K_{1,s})} + \frac{K_{2,t} K_{2,s}}{(K_{2,t} + K_{2,s})} \right). \quad (5.16)$$

In many ways, it would be advantageous to be soft in heave and stiff in roll, particularly when the dominant roll-mode excitation is from turning and not the road. Clearly in light of Eq. 5.14 this is not possible, and there is a compromise between high roll stiffness and low heave stiffness. With the conventional quarter-car model at each corner of the car, it is not possible for the vehicle to be stiff in roll and compliant in heave. This is a key consideration that sizes the overall suspension stiffness (and damping, given that desirable critical damping is a function of stiffness) values. From Eqs 5.15 and 5.16, it is evident that the only way to make a vehicle more stiff in roll than heave, is to increase the track width. Track width is practically limited by road lane width, and by fuel economy because of its effect on frontal area.

5.3 The Roll Mode for a Single Axle

It has previously been shown that the inputs to the general roll-plane model can be decomposed, and the dynamics are decoupled. Therefore, now it is appropriate to consider the roll mode independent of other sprung mass modes of motion. As we do so, it must be considered that there is another input to the isolated roll mode, completely independent of the road inputs we have previously considered in ride. We will see in the second section of this book on handling that this rolling motion can have an effect on the lateral and yaw dynamics, but it also must be considered in the ride section as it affects human perception of ride.

As the vehicle turns, the sprung mass experiences a lateral centrifugal force that causes roll. This lateral force is transferred through the suspension linkage to the tires and is ultimately reacted by lateral forces on the tires in the ground plane. This centrifugal force acting on the center of sprung mass, thus induces a coupling moment that acts as an input to the roll mode that is defined by the product of the centrifugal force and the height of the center of sprung mass.

This reasoning sounds better than it is. The precise flaw is a difficulty often encountered in dynamics: the phantom notion of centrifugal force. There is no such force, rather there is an acceleration experienced when a body rotates while it translates, in this case referred to as centripetal acceleration. To precisely deal with this phenomena, we need a yaw degree of freedom to capture the input, and we need a lateral displacement degree of freedom to completely capture the output. These are the two degrees of freedom that comprise the basic handling model of the next section. Thus, the coupling of ride and handling through the roll mode. We will again be haunted by this phantom of centrifugal force in an even more sinister way.

Equation 5.1 is appended to allow a lateral acceleration input from a moment derived from “centrifugal force” in turning. Rolling moments are summed about a point below the center of mass on the ground plane. As such, the lateral forces turning the vehicle are not considered to produce a rolling moment,

$$I_{\phi} \ddot{\phi} = \frac{t}{2} F_{1,r} + \frac{t}{2} F_{2,r} - \frac{t}{2} F_{1,l} - \frac{t}{2} F_{2,l} + mha_y, \quad (5.17)$$

where h is the height of the sprung mass above the ground plane. Implicit in this development is that the vehicle rolls about the point on the ground plane and the roll moment of inertia is appropriately referenced. As will be shown in the following section, this is not a terrible approximation, but through a more rigorous development it can be loosened.

The new convention used in the pitch plane analysis could apply to the roll plane, making the signs consistent in Eq. 5.1 but it adds little value as the track is typically relatively consistent across all axles. It is useful to consider the roll moment produced at each axle of Eq. 5.17.

$$M_1 = \frac{t}{2} F_{1,r} - \frac{t}{2} F_{1,l}, \quad (5.18)$$

$$M_2 = \frac{t}{2} F_{2,r} - \frac{t}{2} F_{2,l}. \quad (5.19)$$

Inserting Eqs 5.18 and 5.19 into Eq. 5.17.

$$I_{\phi} \ddot{\phi} = M_1 + M_2 + mha_y. \quad (5.20)$$

The front and rear axles of a vehicle can be modeled separately as shown in [Figure 5.1](#) to determine the passive roll stiffnesses $K_{\phi 1}$ and $K_{\phi 2}$. An assumption is made that is appropriate for McPherson strut suspensions and solid axle suspensions, and perhaps somewhat less appropriate for independent suspensions, namely that tire stiffnesses can be scaled to approximate their effect at the point where the suspension forces are transmitted to the sprung mass or body of the vehicle.

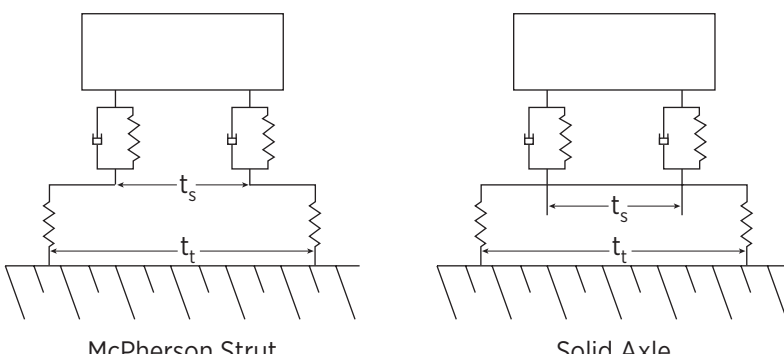
Independent suspensions typically have several load paths from the tire to the sprung mass, and the ensuing analysis is complicated by the multiple lever arms various suspension forces act on to produce roll moments. As discussed earlier, unsprung mass dynamics have been neglected. Referring to [Figure 5.1](#), the effective tire stiffness can be written as:

$$K'_t = K_t \left(\frac{t_t}{t_s} \right)^2, \quad (5.21)$$

where K'_t is the effective tire stiffness acting at the suspension attachment point to the sprung mass, K_t is the actual tire stiffness, t_t is the track width of the tire (also known as the ‘tread width’), and t_s is the track width of the suspension. To the extent the tire track is wider than the suspension track, the tire stiffness appears to be stiffer in roll. This roll stiffness amplification is not present in heave and pitch. (Note the similarity of the effect of the ratio of track widths to the leverage ratio of the quarter-car model.)

Now, it is useful to consider the roll stiffness of a suspension employing a simple primary suspension spring in series with the effective tire spring on one side of the axle, in parallel with that same-series stiffness combination on the other side of the axle.

FIGURE 5.1 McPherson strut and solid axle suspensions in roll plane.



$$K_{\emptyset,i} = -t^2 \left(\frac{K_{i,t} K_{i,s}}{(K_{i,t} + K_{i,s})} \right). \quad (5.22)$$

At a single-axle Eq. 5.22 is consistent with the full vehicle and both sides have the same stiffness. The axle suspensions shown in [Figure 5.1](#) lack an important component sometimes present on an axle, that is a key factor in the compromise between road and handling inputs in the roll plane.

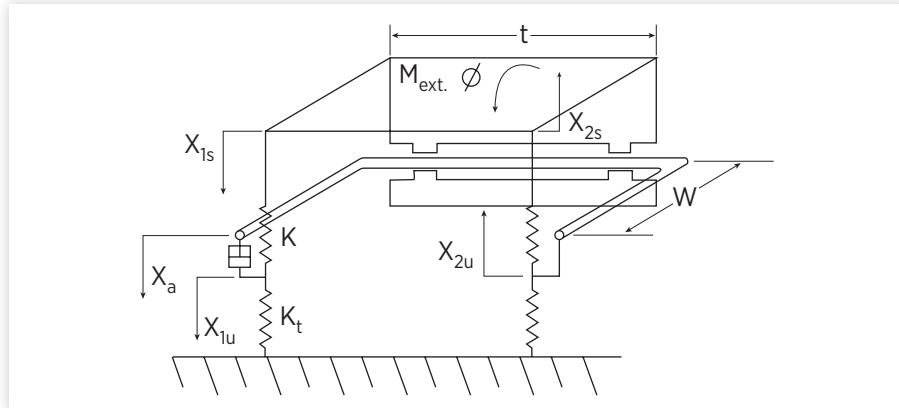
5.4 The Roll-Plane Model with Stabilizer Bar

A stabilizer bar (sometimes imprecisely referred to as a “roll bar”) is most commonly a “U” shaped rod. The two ends of the “U” are fastened to and move with opposing unsprung masses on a given axle. The middle part of the “U” is located by the sprung mass, where it is positionally attached by effective hinge joints and allowed to freely rotate. As the two ends move together (e.g., the opposing wheels on an axle experience the same input event) the ends move up together and freely rotate in the sprung mass hinge connection, and there is no effect of the stabilizer bar on the sprung mass or the unsprung masses. If one of the ends moves relative to the other, the input to the sprung mass is more complicated. The value of a stabilizer bar is that it increases roll stiffness while not affecting the response to an event experienced simultaneously by both wheels on an axle. This is a reasonably common input, for example, railroad tracks perpendicular to the vehicle direction of travel. The disadvantage of stabilizer bars is that they increase the apparent stiffness in response to single wheel inputs (e.g., pothole). Stabilizer bars also significantly affect handling, and that is sometimes their primary function.

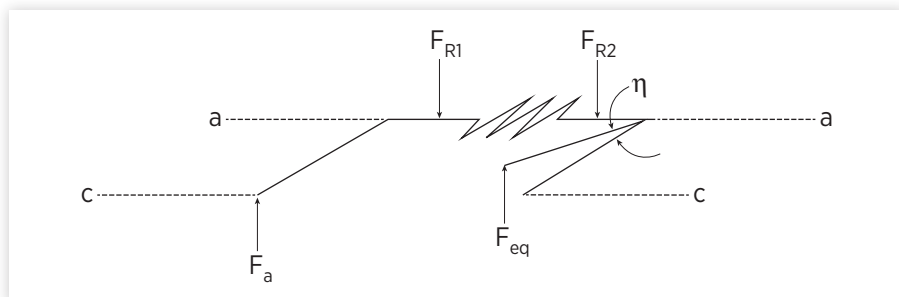
This work uses [Figure 5.2](#) to generate the effective roll stiffness of axle i in terms of tire stiffness K_t , suspension stiffness K_s , stabilizer bar stiffness K_r , and an externally applied moment M_{ext} . The roll displacement is Φ and z_{rs} , z_{ls} , z_{ru} , and z_{lu} are vertical displacements at various points, t is the effective track, and w is the effective stabilizer bar lever arm.

Summing moments acting on the various axes of the free body diagram of the massless stabilizer bar shown in [Figure 5.3](#), values can be assigned to the forces shown. An applied force to the end of the stabilizer bar F_a is balanced by an equivalent opposing force, F_{eq} .

The opposing reaction forces are scaled by the effective track widths, similar to how the roll moment produced by the tires was scaled,

FIGURE 5.2 Suspension schematic with stabilizer bar.

© Dan E. Williams.

FIGURE 5.3 Stabilizer bar forces.

© Dan E. Williams.

$$F_{r1} = -F_{r2} = -F_a \frac{t}{t_r}, \quad (5.23)$$

where t_r is the distance between stabilizer support mounts. This reaction force produces a moment on the sprung mass at the reaction points.

$$M_r = -tF_a. \quad (5.24)$$

The applied force F_a produces a positively defined moment accelerating the sprung mass in roll, and so the opposing reaction moment is negative.

Assuming roll displacement about an axis parallel to the centerline of the vehicle, and neglecting any resulting horizontal motion, by summing the

moments arising from spring forces and stabilizer bar reaction forces the differential equation describing roll behavior of the half car model can be written as,

$$I_{\phi} \ddot{\phi} = M_{ext} + \frac{tK_s}{2}(z_{r,s} - z_{r,u} - z_{l,s} + z_{l,u}) - tF_a, \quad (5.25)$$

where I_{ϕ} is the roll moment of inertia of half the sprung mass about the center-line projected on the ground plane.

Assuming that vertical displacements arise solely from the roll mode (i.e., a single degree of freedom model excited by lateral acceleration), and making several small angle approximations, the sprung mass displacements can be written for both sides of an axle i just as they were previously for the front and rear axles in Eqs 5.4–5.7, and with no heave motion the sprung mass motion of the right side of an axle can be written,

$$z_{i,r,s} = \frac{t}{2}\phi \quad (5.26)$$

and similarly for the left side.

$$z_{i,l,s} = -\frac{t}{2}\phi. \quad (5.27)$$

Eq. 5.27 can be subtracted from Eq. 5.26,

$$z_{i,r,s} - z_{i,l,s} = t\phi \quad (5.28)$$

inserted into Eq. 5.25.

$$I_{\phi} \ddot{\phi} = M_{ext} - \frac{t^2 K_s}{2} \phi + \frac{tK_s}{2}(z_{i,r,u} - z_{i,l,u}) - tF_a. \quad (5.29)$$

Summing forces at the unsprung mass (assumed massless), the following expressions for unsprung mass displacements can be written, with the applied force from the stabilizer bar F_a acting positively on one side and negatively on the other. On the right side (driver side) of the i th axle,

$$K_s(z_{i,r,s} - z_{i,r,u}) + F_a + K_t(-z_{i,r,u}) = 0 \quad (5.30)$$

and similarly for the left side of the axle.

$$K_s(z_{i,l,s} - z_{i,l,u}) - F_a + K_t(-z_{i,l,u}) = 0. \quad (5.31)$$

Solving Eq. 5.30 for the right-side unsprung mass displacement and inserting Eq. 5.26,

$$z_{i,r,u} = \frac{1}{(K_t + K_s)} F_a + \frac{tK_s}{2(K_t + K_s)} \emptyset \quad (5.32)$$

and similarly Eq. 5.31 for the left-side unsprung mass displacement.

$$z_{i,l,u} = -\frac{1}{(K_t + K_s)} F_a - \frac{tK_s}{2(K_t + K_s)} \emptyset. \quad (5.33)$$

Sprung mass displacement on the left side of an axle i is subtracted from the right side.

$$z_{i,r,u} - z_{i,l,u} = \frac{2}{(K_t + K_s)} F_a + \frac{tK_s}{(K_t + K_s)} \emptyset. \quad (5.34)$$

Inserting these values of vertical displacements into the roll mode differential Eq. 5.29,

$$I_\emptyset \ddot{\emptyset} = M_{\text{ext}} + \frac{tK_s}{2} \left(\frac{2}{(K_t + K_s)} F_a + \frac{tK_s}{(K_t + K_s)} \emptyset - tF_a \right) - tF_a \quad (5.35)$$

and simplified.

$$I_\emptyset \ddot{\emptyset} = M_{\text{ext}} + \left(\frac{-tK_t}{(K_t + K_s)} \right) F_a - \frac{t^2 (K_s K_t)}{2(K_t + K_s)} \emptyset. \quad (5.36)$$

From [Figure 5.2](#), it is seen that an applied force F_a on one hub is reacted by an opposing force on the opposite hub. The force applied to the hub acts at the end of the stabilizer bar, and works through a lever arm to displace the torsional stiffness of the bar,

$$F_a w = K_r \eta, \quad (5.37)$$

where η is the torsional stabilizer bar displacement, K_r is the torsional stabilizer bar stiffness, and w is the moment arm of the equivalent forces acting at the hub. Using a small angle approximation for η , angular torsion bar displacement can be converted to linear suspension displacement,

$$\eta w = z_{i,r,u} - z_{i,l,u}. \quad (5.38)$$

Equations 5.37 and 5.38 are combined to form,

$$F_a = \frac{K_r}{w^2} (z_{i,r,u} - z_{i,l,u}). \quad (5.39)$$

Equation 5.34 is inserted into Eq. 5.39.

$$F_a = \frac{K_r}{w^2} \left(\frac{2}{(K_t + K_s)} F_a + \frac{tK_s}{(K_t + K_s)} \emptyset \right). \quad (5.40)$$

In a change of notation, the effective stiffness of the stabilizer bar, K'_r , is formed,

$$K'_r = \frac{K_r}{w^2}, \quad (5.41)$$

where K_r is the actual torsional stiffness, and w is the lever arm connecting the bar to the wheel. Although it is simplest to consider K_r as the torsional rigidity of the stabilizer bar, experience has shown that stiffness characteristics of the end attachments and of the bushings where the stabilizer bar is attached to the sprung mass are not negligible. For the purposes of this work, K'_r is used as the effective suspension stiffness of the stabilizer bar, which includes torsional stiffness of the stabilizer bar, attachment bushing stiffnesses, and the cantilever stiffness of the stabilizer bar lever arm and is best determined experimentally. In a manner similar to Eq. 5.21, the equivalent suspension stiffness of a stabilizer bar can be transformed to an equivalent wheel stiffness.

As the stabilizer bar is restrained on the sprung mass as shown in [Figure 5.2](#), it is actually the suspension deflections that are tied together. The applied force F_a opposes the deflection of the right side (where it is assumed positive) and is mitigated by suspension deflection on the opposing left side.

$$F_a = -K'_r ((z_{i,r,u} - z_{i,r,s}) - (z_{i,l,u} - z_{i,l,s})), \quad (5.42)$$

Inserting Eqs 5.28 and 5.34 into Eq. 5.42,

$$F_a = -K'_r \left(\frac{2}{(K_t + K_s)} F_a + \frac{tK_s}{(K_t + K_s)} \emptyset - t\emptyset \right) \quad (5.43)$$

and solving for F_a .

$$F_a = \frac{tK'_r K_t}{K_t + K_s + 2K'_r} \emptyset. \quad (5.44)$$

Inserting Eq. 5.44 into Eq. 5.36,

$$I_{\emptyset} \ddot{\emptyset} = M_{ext} - \frac{tK_t}{(K_t + K_s)} \left(\frac{tK'_r K_t}{K_t + K_s + 2K'_r} \emptyset \right) - \frac{t^2 (K_s K_t)}{2(K_t + K_s)} \emptyset \quad (5.45)$$

and simplifying.

$$I_{\emptyset} \ddot{\emptyset} = M_{ext} - t^2 \frac{K_s K_t}{(K_t + K_s)} \left(\frac{K'_r \left(\frac{K_t}{K_s} + 2 \right) + (K_t + K_s)}{(K_t + K_s + 2K'_r)} \right) \emptyset. \quad (5.46)$$

Using Eq. 5.46, roll stiffness for an axle i including a stabilizer bar can be written as

$$K_{\emptyset,i} = -t^2 \left(\frac{K_{i,t} K_{i,s}}{(K_{i,t} + K_{i,s})} \right) \left(\frac{K_{i,t} K'_{i,r}}{K_{i,s} (K_{i,t} + K_{i,s} + 2K'_{i,r})} + 1 \right). \quad (5.47)$$

If $K'_r = 0$, Eq. 5.47 reverts the previously derived Eq. 5.22.

$$K_{\emptyset,i} = -t^2 \left(\frac{K_{i,t} K_{i,s}}{(K_{i,t} + K_{i,s})} \right).$$

If K'_r is infinitely stiff,

$$K_{\emptyset,i} = -t^2 \left(\frac{K_{i,t} K_{i,s}}{(K_{i,t} + K_{i,s})} \right) \left(\frac{K_{i,t}}{2K_{i,s}} + 1 \right). \quad (5.48)$$

Equation 5.48 contains a term equal to the roll stiffness of the axle without the stabilizer bar. This term is multiplied by a term that is function of the tire and suspension stiffness so that regardless of these actual stiffness values the overall roll stiffness of the axle with an infinitely stiff stabilizer bar is greater than that axle would have been without the stabilizer bar. Typically, the tire stiffness is an order of magnitude greater than the suspension stiffness, and at the extreme the infinitely stiff stabilizer bar increases the roll stiffness of an axle by approximately a factor of 5. In these limits, Eq. 5.48 is in keeping with intuition.

5.5 Single-Wheel Inputs

Single-wheel inputs on one side of an axle with a stabilizer are a bit difficult to consider. Unlike the simple quarter-car model, the stabilizer bar provides a load path to both sides of the axle. To consider the single wheel input, the sprung mass is considered fixed, and the road input to the opposite side of the axle is fixed, as shown in [Figure 5.4](#).

On the opposite side of the axle, with these assumptions, the tire and suspension spring are in parallel, as shown in [Figure 5.5](#).

FIGURE 5.4 Roll-plane suspension schematic with stabilizer bar.

© SAE International.

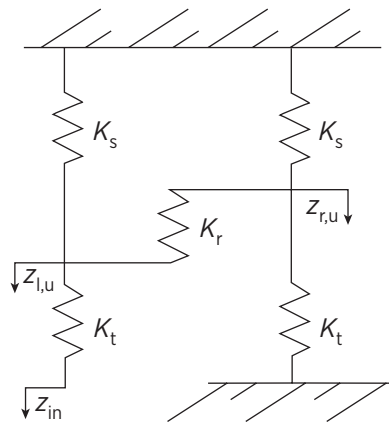
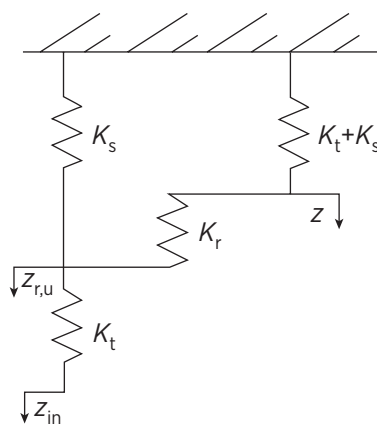


FIGURE 5.5 Single-wheel input to suspension with stabilizer bar.

© SAE International.



The parallel combination of the opposite tire and suspension stiffness is in series with the stabilizer bar. This combination can be written.

$$K_{\text{eq}} = \frac{K_r(K_s + K_t)}{(K_r + K_s + K_t)}. \quad (5.49)$$

The equivalent stiffness of Eq. 5.49 is in parallel with the suspension spring on the input side,

$$K_{\text{eq}} = K_s + \frac{K_r(K_s + K_t)}{(K_r + K_s + K_t)} \quad (5.50)$$

and rewritten for further simplification.

$$K_{\text{eq}} = \frac{2K_s K_r + K_s^2 + K_s K_t + K_r K_t}{K_r + K_s + K_t}. \quad (5.51)$$

Equation 5.51 is in series with the tire stiffness on the input side.

$$K_{\text{eq}} = \frac{\left(\frac{2K_s K_r + K_s^2 + K_s K_t + K_r K_t}{K_r + K_s + K_t} \right) K_t}{\left(\frac{2K_s K_r + K_s^2 + K_s K_t + K_r K_t}{K_r + K_s + K_t} \right) + K_t}. \quad (5.52)$$

Equation 5.52 is simplified,

$$K_{\text{eq}} = \frac{K_s K_t \left(2K_r + K_s + K_t + \frac{K_r K_t}{K_s} \right)}{(K_s + K_t)(2K_r + K_s + K_t)} \quad (5.53)$$

and written to isolate the single-wheel equivalent stiffness and a term dependent on the stabilizer bar stiffness that modifies it.

$$K_{\text{eq}} = \left(\frac{K_s K_t}{K_s + K_t} \right) \left(\frac{K_s + K_t + 2K_r \left(1 + \frac{K_t}{2K_s} \right)}{(K_s + K_t + 2K_r)} \right). \quad (5.54)$$

Equation 5.54 describes the effect of the stabilizer bar on single wheel stiffness. In the limiting case of $K_r = 0$, the single-wheel stiffness is the simple series

combination of the tire and suspension spring. In the other limiting case of an infinitely stiff stabilizer bar, the single-wheel stiffness is modified as a function of the tire and suspension stiffness. Typically, the tire stiffness is nearly an order of magnitude greater than the suspension stiffness. In general terms, an infinitely stiff stabilizer bar can increase the independent single wheel stiffness by an approximate factor of five. Thus a trade-off exists between desirably high roll stiffness and desirably low single-wheel stiffness using a stabilizer bar.

5.6 Passenger Car Roll

The previously derived roll-plane model can be applied to the front and rear axles of a two-axle passenger car. All the mass is assumed to be lumped at the center of sprung mass. The sprung mass is assumed to be rigid in roll, so that the same roll angle is experienced at the front and rear. Since all the mass is assumed lumped at the center of sprung mass, there is no inertia attached to the individual axles. Equation 5.47 can be written for the front axle referred to as axle 1.

$$M_1 = t^2 \left(\frac{K_{1,t} K_{1,s}}{(K_{1,t} + K_{1,s})} \right) \left(\frac{K'_{1,r} \left(\frac{K_{1,t}}{K_{1,s}} + 2 \right) + (K_{1,t} + K_{1,s})}{(K_{1,t} + K_{1,s} + 2K'_{1,r})} \right) \emptyset. \quad (5.55)$$

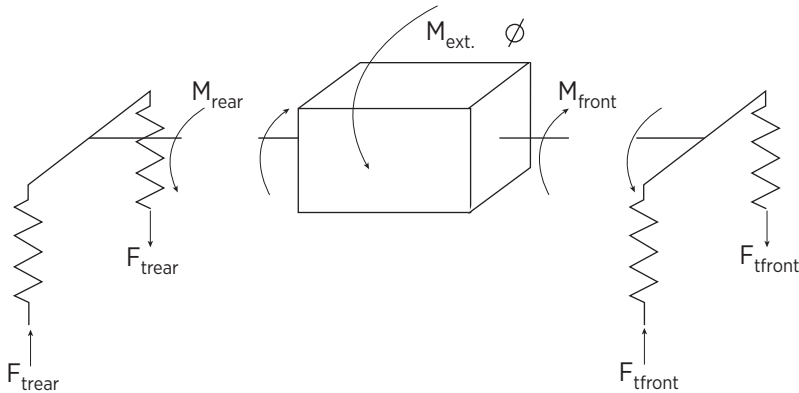
Similarly, for the second axle at the rear of the passenger car,

$$M_2 = t^2 \left(\frac{K_{2,t} K_{2,s}}{(K_{2,t} + K_{2,s})} \right) \left(\frac{K'_{2,r} \left(\frac{K_{2,t}}{K_{2,s}} + 2 \right) + (K_{2,t} + K_{2,s})}{(K_{2,t} + K_{2,s} + 2K'_{2,r})} \right) \emptyset. \quad (5.56)$$

The external moments M_1 and M_2 acting on the front and rear roll-plane models are created by the rolling lumped sprung mass. These moments acting on the axles serve to compress the suspension described in the roll-plane model. The reaction to these moments, acting on the sprung mass, serves to restrain the roll motion of the sprung mass, as shown in [Figure 5.6](#).

The previously derived differential Eq. 5.20 continues to derive the roll mode behavior of the sprung mass.

$$I_{\emptyset} \ddot{\emptyset} = M_1 + M_2 + mha_y. \quad (5.57)$$

FIGURE 5.6 Free body diagram of vehicle roll model.

© Dan E. Williams.

The moments on each axle can be expressed as a roll stiffness from Eq. 5.47,

$$K_{1,\phi} = t^2 \left(\frac{K_{1,t} K_{1,s}}{(K_{1,t} + K_{1,s})} \right) \left(\frac{K'_{1,r} \left(\frac{K_{1,t}}{K_{1,s}} + 2 \right) + (K_{1,t} + K_{1,s})}{(K_{1,t} + K_{1,s} + 2K'_{1,r})} \right), \quad (5.58)$$

$$K_{2,\phi} = t^2 \left(\frac{K_{2,t} K_{2,s}}{(K_{2,t} + K_{2,s})} \right) \left(\frac{K'_{2,r} \left(\frac{K_{2,t}}{K_{2,s}} + 2 \right) + (K_{2,t} + K_{2,s})}{(K_{2,t} + K_{2,s} + 2K'_{2,r})} \right) \quad (5.59)$$

multiplied by roll and inserting Eqs 5.55 and 5.56 into Eq. 5.20,

$$I_\phi \ddot{\phi} = (K_{1,\phi} + K_{2,\phi}) \phi + mha_y. \quad (5.60)$$

From the steady state of Eq. 5.60, the ratio of roll displacement to lateral acceleration can be formed.

$$\frac{\phi}{a_y} = \frac{mh/t^2}{K_{1,\phi} + K_{2,\phi}}. \quad (5.61)$$

5.7 Generalized Roll-Plane Model

Just as the roll-plane model applied to the front and rear axles of the passenger car produce a vehicle roll-plane model, the same process can be used for vehicles with any number of axles. Just as Eq. 5.54 for the front axle, and Eq. 5.55 for the rear axle, a roll stiffness for the i th axle can be written.

$$K_{\phi,i} = t^2 \left(\frac{K_{i,t} K_{i,s}}{(K_{i,t} + K_{i,s})} \right) \left(\frac{K'_{i,r} \left(\frac{K_{i,t}}{K_{i,s}} + 2 \right) + (K_{i,t} + K_{i,s})}{(K_{i,t} + K_{i,s} + 2K'_{i,r})} \right). \quad (5.62)$$

Using Eq. 5.62, Eq. 5.60 can be written for an arbitrary number of axles.

$$I_{\phi} \ddot{\phi} = \sum K_{i,\phi} \dot{\phi} + mha_y. \quad (5.63)$$

In steady state, the ratio of roll to lateral acceleration can be written as

$$\frac{\phi}{a_y} = \frac{mh/t^2}{\sum K_{i,\phi}}. \quad (5.64)$$

As more axles are considered, the vehicle tends to get longer and the assumption of sprung mass torsional rigidity should be considered.

5.8 Roll and Handling

The distribution of roll stiffness among axles on a vehicle has an effect on handling, as will be discussed in greater detail in the next chapter. For now a superficial understanding is helpful. Because of nonlinearities in tire properties, an axle that is generating a larger roll moment cannot generate as much side force. Tire side force and roll both occur with lateral acceleration.

When a vehicle has more than one axle, there can be a design decision to distribute the roll stiffness unequally between axles. For a two-axle vehicle, if more roll moment is on the front, the front generates less side force to turn the vehicle, and the driver needs to apply more steering input. This is called understeer. Conversely, if the roll moment is biased toward the rear, the rear axle cannot generate the side force and it will tend to slide out, this is called oversteer. Usually some degree of understeer is desired, as oversteering vehicles require driving skill.

The Olley criteria of the pitch-plane model suggest that the rear stiffness should be greater than the front. This being the case, the Olley criteria would induce objectional oversteer in the vehicle if no stabilizer bars are used. By using a stabilizer bar at the front, front roll stiffness is increased, inducing desirable understeer, without detrimental effect on the Olley ride criteria as the stabilizer bar has no effect for pitch plane inputs seen by both wheels on the front axle. Only when there is a single-wheel event does the stabilizer bar increase the vertical stiffness.

This chapter has not considered the effect of dampers at each corner. Just as roll stiffness can be distributed between front and rear axles, suspension dampers combine to provide roll mode damping that can also be distributed between front and rear. The sprung mass rolls as lateral acceleration is built up entering a turn. If this rolling is resisted by damping at the front, the vehicle will understeer more entering turns. Just as the roll mode in general, these effects of roll damping are more relevant in high-performance driving and emergency maneuvers. They can be a source of competitive advantage (or disadvantage) in racing. For vehicles designed to be operated by the general public, the “rule of thumb” is to avoid oversteering.

5.9 Summary

A simplified roll-plane model was developed to describe rolling motion of a vehicle. The roll mode can be excited by uneven road inputs or lateral acceleration. Ideally, the vehicle should be soft in heave and stiff in roll. Using a simple model of independent suspensions at each corner, it was shown that heave and roll stiffness are highly correlated, and that the only way to increase roll stiffness without adversely affecting heave stiffness is to increase the track width of the vehicle. Furthermore, this simplified model showed that the heave and roll modes are dynamically decoupled, so to the extent inputs can be decoupled, roll can be considered independently. Because of wheelbase filtering the pitch motion tends to reduce at highway speeds, but the roll motion can be induced independent of vehicle speed. Therefore at high speeds roll is more important than pitch. It is relatively unusual for the roll mode to be excited by highway road inputs. More commonly, the roll mode is excited by high performance or emergency driving maneuvers.

When the roll mode is excited by lateral acceleration inputs, a stabilizer bar can increase roll stiffness with no adverse effect on heave stiffness for inputs experienced by both wheels on an axle. When only one wheel of the axle experiences the input, the stabilizer bar increases the single wheel stiffness, thereby degrading ride. Front stabilizer bars increase the possibility for vehicles to understeer while achieving the Olley ride criteria.

A theoretical roll stiffness has been calculated for an axle using a stabilizer bar. In practice roll stiffness, especially when considering a stabilizer bar, can be experimentally determined and will include effects not considered in this analysis. Assuming a torsionally rigid connection, any number of axles can be combined to result in composite roll stiffness for the entire vehicle and a generalized differential equation for the roll mode can be written.

The roll mode can affect vehicle handling by distributing the resistance to roll between axles. These affects can be used by vehicle designers to minimize oversteering in emergency passenger car maneuvering, also for competitive advantage in racing.

The discussion of roll is a valuable opportunity to treat the vehicle as a system that must simultaneously ride and handle well. This chapter began this discussion, and it will be continued in both the next chapter and the following section of the book.

6

Active Suspension to Optimize Ride

“ From the beginning the problem of supplying a smoother and softer ride has been one of the most complex in automotive engineering.

—Alfred P. Sloan

6.1 Introduction

Suspensions transmit forces from the suspended or sprung mass of the vehicle to the road through the tires. Historically, such suspensions were comprised of springs and dampers as introduced in the quarter-car model of [Chapter 3](#). These elements are said to be “passive” from the standpoint that they either dissipate or store energy that ultimately comes from the vehicle traveling over a rough and/or curvy road. The suspension serves several purposes: (1) to locate the sprung and unsprung masses; (2) to isolate the sprung mass from vertical vibrations; and (3) to transmit horizontal forces that serve to accelerate, brake, and turn the vehicle. These sometime conflicting goals, as well as practical constraints, have led to a variety of suspension configurations. Given the stated purposes of suspensions and the presence of practical constraints, suspensions have typically imposed interesting compromises between ride and handling.

These compromises generally involve the roll mode, as steering inputs create a lateral acceleration, lateral acceleration causes a roll moment, and how the sprung mass responds to the roll moment is a function of the suspension and can affect handling. We have seen in previous chapters that a well-designed suspension places the ride and wheel-hop frequencies on either side of the frequency range of greatest human sensitivity to vertical vibration. The Olley ride criteria result in softer front suspensions creating an understeering tendency that can be mitigated with front stabilizer bars, at the expense of single-wheel events.

On one hand, this chapter on active suspension could be placed as a concluding capstone of the entire book, as it involves both ride and handling. It is placed as a concluding chapter in the ride section, however. As most of the interesting development of active suspension is in the area of ride, handling is improved through secondary effects: (1) elimination of sprung mass roll; (2) actively distributing the roll moment distribution between the front and the rear axles; and (3) maintaining a more constant load through the contact patch of the tire. First-order coupling between ride and handling occurs as the tires ability to generate a lateral force varies linearly with body roll and will be discussed in the second section of this book on handling. The most interesting trade-offs between ride and handling in the roll mode are therefore eliminated by active suspension which eliminates roll, while active suspension retains the authority to improve second-order effects derived from roll moment distribution. Although the active roll moment distribution is a nonlinear second-order effect, because it can be actuated within a closed loop on yaw rate, it can provide a quite dramatic effect on vehicle handling, but owing more to the control system rather than the vehicle dynamics. Active roll moment distribution is more effective with an aggressive driving style. The greater the lateral acceleration the greater the roll moment, and the greater the authority to influence handling via active control.

In active suspension, additional components have the capability to add energy to the suspension. In essence, this added energy actively lifts the wheels up over bumps, rather than passively responding to the bumps. To justify the added cost and complexity, these systems reduce compromises inherent in passive suspensions. For example, for good vertical vibration isolation the spring elements should be soft as desired by Alfred Sloan, founder of General Motors. But to positively locate the sprung mass when turning or braking, they should be stiff. Ideally dampers should absorb energy only at resonant frequencies as we have seen with the quarter-car model. Vertical forces transmitted through the suspension should act in concert with the horizontal forces required to maneuver the vehicle. A given corner of the vehicle should isolate the sprung mass from vertical road disturbances while supporting vehicle dynamic induced inertia loadings (pitch and roll) without deflection, and provide the optimal vertical load through the tire's contact patch. Passive suspensions have been doing most of these things most of the time in a very cost-effective manner [1,2].

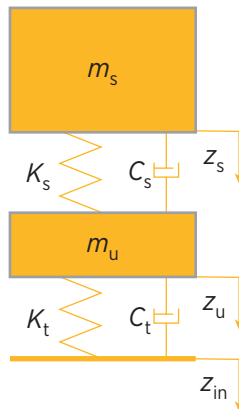
In a typical embodiment, a simple hydraulic damper that dissipates energy might be replaced by a hydraulic actuator: a cylinder whose internal pressures on either side of a piston are controlled by an electrically actuated servovalve. Because the servovalve is electrically actuated, it can be computer controlled. Active suspension is one application of a general movement in the latter part of the 20th century to apply the newly emerged control theory body of knowledge to ground vehicles, and more particularly to chassis control systems [3].

Professors Dean Karnopp and Don Margolis at the University of California-Davis developed the simple and yet powerful concept of inertial damping, and described it with the phrase “skyhook damping.” This chapter will introduce inertial damping with the quarter-car model, and then extend it to the full vehicle. The contributions of Lotus are presented at a high level to appreciate the difference relative to the simpler skyhook damping. The Lotus algorithm was more complicated than inertial damping, but also allowed for a better handling vehicle. Led by Peter Wright and David Williams, Lotus achieved early significant results that led all researchers into this new area. The independent concepts of Lotus modal control and skyhook damping will be combined, preserving the advantages of both as reported with actual vehicle results.

This chapter will serve as a capstone to the ride section. It will combine the notions of heave, pitch, and roll developed in the previous sections. It will be shown how the two major streams of active suspension research were merged to achieve unprecedented ride and handling improvements. The results will be interpreted relative to optimal controllers. Active suspension is well configured for the application of optimal control, and doing so provides insight on the advantages of optimal control relative to other more pragmatic control strategies. It is hoped that the reader will draw upon the quarter-car model, the pitch-plane model, and the roll-plane model to appreciate the real world benefit of active suspension.

6.2 Inertial Damping

The quarter-car model developed in [Chapter 2](#) and shown again in [Figure 6.1](#) exhibits utility by simply capturing many of the important vibration isolation properties that characterize a passive suspension earlier described, and serves as the starting point of the analysis of active suspension. To briefly review, the passive elements could be nonlinear; they are essentially energy dissipation and storage elements between discrete masses. In the most common uses of the quarter-car model, these elements are linear so that it is possible to speak of two natural frequencies, ride and wheel hop, as earlier derived in [Chapter 3](#). If one considers the sprung mass so large as to make the unsprung mass negligible, the sprung mass is supported by the series combination of the suspension and tire springs. This frequency is roughly around 1–2 Hz, and is termed the ride (or heave) frequency. Another natural frequency is found when the much heavier sprung mass is considered practically infinite, and the smaller unsprung mass is located by the parallel combination of the suspension and tire springs. This frequency is called the wheel-hop frequency and is usually between 10 and 12 Hz. The nearly one order of magnitude separation between these two frequencies allows the unsprung mass dynamics to filter road inputs to the sprung mass.

FIGURE 6.1 Quarter-car model with conventional damping.

© Dan E. Williams.

The tire is usually very lightly damped, so most of the damping present in the quarter-car model is in the suspension. Without this damping the sprung mass is undamped at the ride frequency and thus offensive to occupants. Unfortunately, the conventional damper creates a force based on relative motion between the sprung and unsprung masses, transmitting forces to the sprung mass at all frequencies. Passengers are located on the sprung mass and are sensitive to its movement. In the case of relative damping, there is a trade-off between damping the sprung mass resonance, and transmitting forces at other frequencies to the occupant cabin.

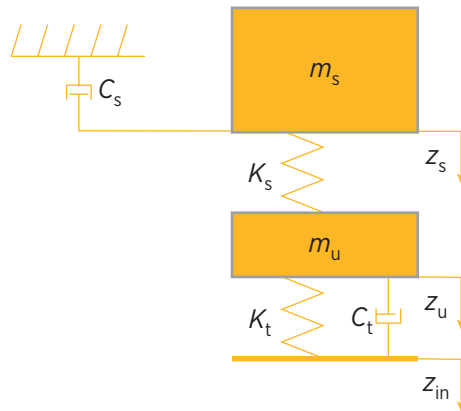
[Figure 6.2](#) shows an idealized situation where the sprung mass damper is inertially grounded. In this physically unrealizable case unsprung mass motion does not create a force on the sprung mass through the damper. There is no trade-off between sprung and unsprung masses, and inertial damping gains can be quite high. Dean Karnopp was the first to realize this, and coined the phrase “sky-hook” damping.

Such an inertially grounded damper attachment may sound like science fiction, but in fact it can be actualized to a large extent. Consider the replacement of the damper by a force actuator as shown in [Figure 6.3](#). In practice, this system is implemented by a force actuator driven by a sprung mass velocity signal, and the force actuator generates a reaction force on the unsprung mass.

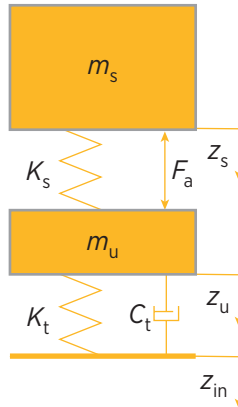
With knowledge of sprung and unsprung mass velocities such a force actuator can produce a linear damping force as earlier discussed, with the

FIGURE 6.2 Quarter-car model with inertial damping.

© Dan E. Williams.

**FIGURE 6.3** Quarter-car model with force actuator.

© Dan E. Williams.



positive damping term multiplied by the input velocity minus the output velocity (relative velocity).

$$F_a = C_s(\dot{z}_u - \dot{z}_s). \quad (6.1)$$

It is a seemingly easy thing to describe an inertial force actuator in a similar way.

$$F_a = -C_s \ddot{z}_s. \quad (6.2)$$

The problem with the inertial damping concept has nothing to do with Eq. 6.2, rather the system of [Figure 6.3](#). According to Newton's first law, the force actuator needs to push against something to create its force on the sprung mass. In [Figure 6.3](#), it pushes against the unsprung mass. Imagine what would happen if we tried to create such an active force on the sprung mass at the wheel-hop frequency. There would be nothing to push against. The transfer function of the force actuator is said to have a "zero" at the wheel-hop frequency. Therefore, even an active system cannot produce a pure inertial damper. But it can come very close to serving its intended purpose. It can create a force that can inertially damp the sprung mass resonances in heave, pitch, and roll.

[Figure 6.4](#) shows the desired isolation function for the quarter-car analysis derived in [Chapter 2](#). The desired isolation function is sprung mass acceleration as a result of vertical road velocity as earlier discussed. (Occupants sense acceleration, and the rate of change of vertical road displacements is relatively "white;" developed in [Chapter 3](#) as the "isolation function.") Just as we earlier saw in [Chapter 3](#), for the relative damping of [Figure 6.4](#), more damping decreases sprung mass accelerations at the ride frequency, but increases them elsewhere, thus the trade-off in relative damping. However, [Figure 6.5](#) shows a different and very interesting effect. More inertial damping is always better. It not only attenuates the ride frequency, but all other frequencies. Thus active inertial damping eliminates the compromise inherent in passive relative dampers.

From a control systems perspective, inertial damping can be thought of as a closed-loop on inertial velocity with a zero set point as shown in [Figure 6.6](#).

FIGURE 6.4 Relative damping isolation function.

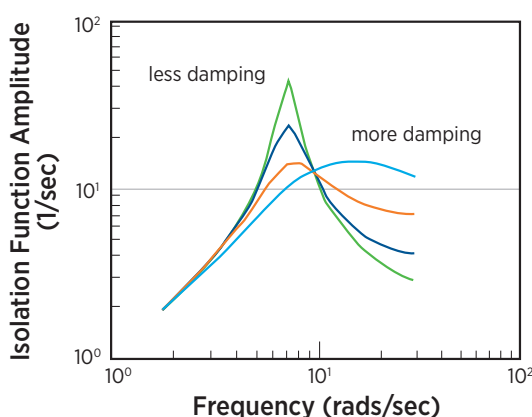
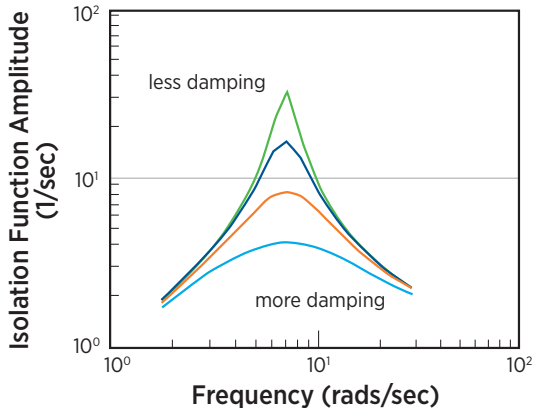
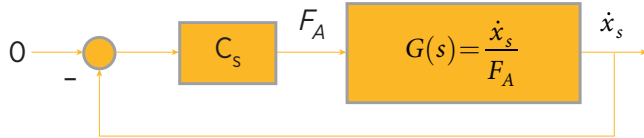


FIGURE 6.5 Inertial damping isolation function.

© Dan E. Williams.

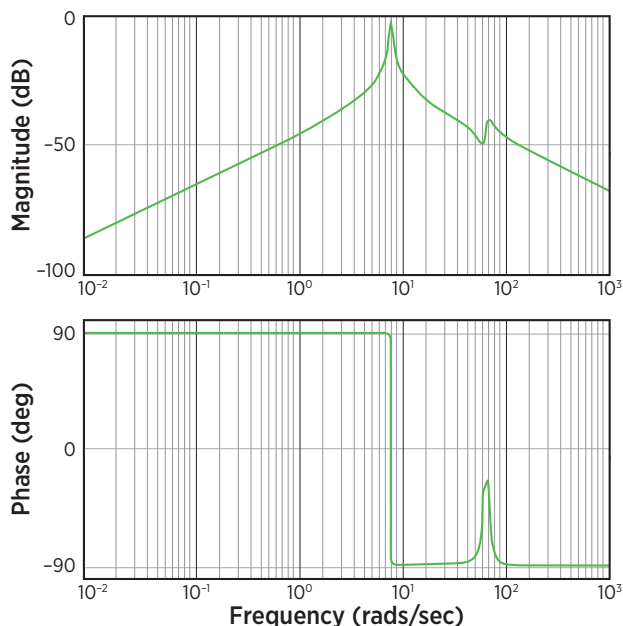
**FIGURE 6.6** Inertial damping as closed loop.

© Dan E. Williams.



From classical control theory we appreciate the closed-loop stability properties found in the examination of the open loop (the relationship between the output and input variables without the feedback loop being closed). As shown in [Figure 6.7](#) for typical quarter-car parameters, this open-loop transfer function produces a sprung mass acceleration output resulting from an actuator force input. As known from control theory, when this output is fed back in closed-loop form to drive the input, if there is a dynamic phase lag in the open loop of 180° or greater, and if the magnitude of the open loop is >1 , an instability will occur as there will be a self-reinforcing signal at the frequency defined by the 180° phase lag.

The sprung mass resonance is clearly seen in the magnitude part of the bode plot shown in [Figure 6.7](#), which is the open-loop frequency response of the inertially damped system of [Figure 6.3](#). The presence of the zero at the wheel hop frequency is evident. What is more insightful is the high-frequency phase lag. The inertial damping open-loop phase does not reach the 180° necessary for closed-loop instability. Inertial damping is in a class of dynamic systems referred to formally as positive real—characterized by their favorable stability [4,5].

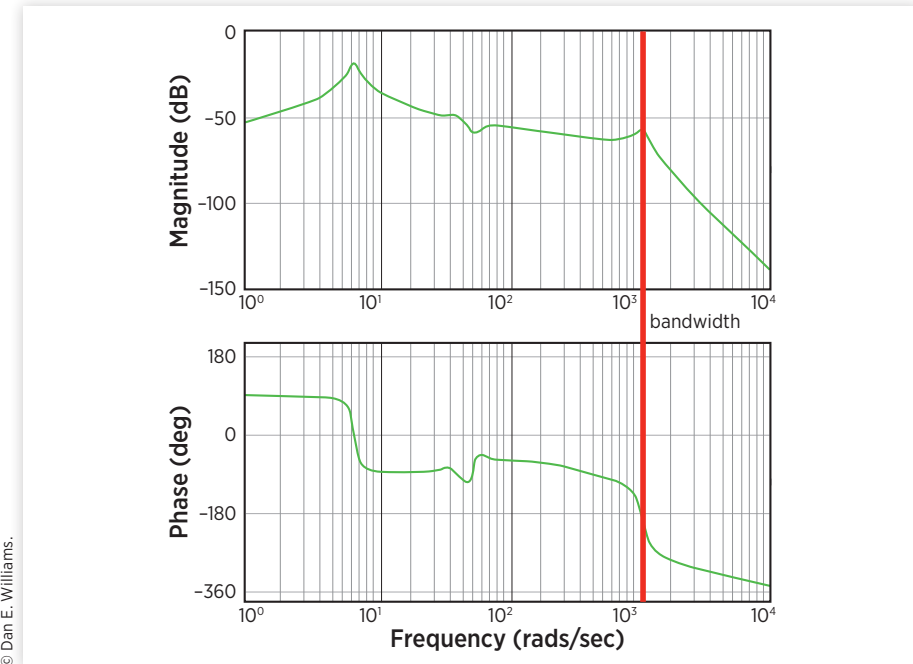
FIGURE 6.7 Ideal inertial damping open loop.

© Dan E. Williams.

Inertial damping is a very powerful concept with two important implications: (1) because there is no compromise in damping, desired inertial damping levels are quite high; and (2) because of the positive real stability properties of the skyhook damping configuration, the ideal inertial damping level is not bounded by system stability. Thus, high inertial damping is both desirable and theoretically realizable.

When the inertial damping principle is used in practice, the force actuator will have a bandwidth. Actuator dynamics will add phase lag, and at some point the open-loop response will cross the 180° point and the inertial damping gain will be limited by stability as shown in [Figure 6.8](#). One of the advantages of the inertial damping method in the quarter-car model is that this open-loop transfer function can be experimentally determined, and therefore robustly compensated with a stability margin using classical control methods. Fortunately, it is possible to find such actuators with sufficient bandwidth, and Karnopp's skyhook damper provides a very convenient tool to quickly characterize achievable 1/4 car model performance.

Mehdi Ahmadian suggested “groundhook damping” of the unsprung mass [6]. Rather than drive the force actuator with the sprung mass inertial velocity, it is possible to drive the force actuator with unsprung mass inertial velocity. This

FIGURE 6.8 Inertial damping open loop with actuator.

© Dan E. Williams.

has the advantage of damping the hub to provide a more constant friction circle to transmit horizontal forces through the contact patch of the tire. Of course the actuator generates its hub damping force by pushing against the sprung mass, thus degrading ride. In practice it would be possible to transition from Karnopp's skyhook to Ahmadian's groundhook based on lateral acceleration, degrading the ride only when handling is a priority.

Davor Hrovat, a graduate student of Prof. Karnopp, showed that such a skyhook damper placed at each corner of a sprung mass, will produce total vehicle vibration isolation results nearly equal to a full state optimal controller [7],

$$\begin{bmatrix} F_{1a} \\ F_{2a} \\ F_{3a} \\ F_{4a} \end{bmatrix} = \begin{bmatrix} C_{des} & 0 & 0 & 0 \\ 0 & C_{des} & 0 & 0 \\ 0 & 0 & C_{des} & 0 \\ 0 & 0 & 0 & C_{des} \end{bmatrix} \begin{bmatrix} \dot{z}_1 \\ \dot{z}_2 \\ \dot{z}_3 \\ \dot{z}_4 \end{bmatrix}, \quad (6.3)$$

where F_{1a} is the first corner force, \dot{z}_1 is the first corner velocity, and C_{des} is the desired damping.

Inertial damping provides a readily understandable 1/4 car solution that can be scaled up to the complete vehicle. Such a vehicle has some shortcomings. It has a “magic carpet” ride, that is somewhat disconnected from the road. To provide this magic carpet ride, the suspension travel must be large enough to accommodate bumps, theoretically even hills. At extreme levels, the skyhook damper will attempt to keep the sprung mass inertial velocity zero while the vehicle is climbing a hill, and eventually the suspension will run out of travel. If the vehicle is allowed to slowly recover its ride height, it will be perceived as disconnected, and if it recovers too fast, it will be transmitting discomforting accelerations to the occupants in the sprung mass. Furthermore, these disconnected inputs can send the wrong cues to the driver in a handling situation where pitch and roll moments are produced. Perhaps the biggest shortcoming of the use of independent skyhooks on each corner is that handling is not influenced. These practical issues aside, inertial damping is a very powerful concept for vibration isolation and will be revisited.

6.3 Lotus Modal Control

In the 1980s, Lotus pioneered practical active suspension. Peter Wright led a team at Lotus Engineering, and David Williams led a team at the Cranfield Institute of Technology. Between the two, Lotus set a performance standard for active suspension in F1 competition, and applied the same technology to prototype passenger cars. As applied to the quarter-car model, the Lotus algorithm determined the actuator velocity (relative velocity) that would result in desired second order dynamic behavior of the sprung mass. Knowing the sprung mass, desired second-order dynamic behavior was determined by selected stiffness and damping parameters. The calculated desired velocity drove a high-performance servovalve producing a highly accurate flow to the hydraulic cylinder so that the desired relative velocity was achieved. Thus, relative velocity was produced by an open-loop valve drive that was itself a function of desired parameters and sensor measurements. Of particular note was that the desired second-order dynamics were constructed from a “free response.” That is to say, somehow the system was disturbed so that there were displacements and velocities associated with the masses (i.e., initial conditions of the dynamic states), and the desired second-order dynamics determined the systems return to equilibrium. In actual practice, the system is disturbed through road inputs, and this is not considered in the ad hoc Lotus strategy.

The genius of the Lotus system was how it applied to the overall vehicle. Lotus assigned similar specific second-order dynamics to each rigid body sprung mass mode of motion. Through transforming modal coordinates to corner coordinates and using superposition, individual corner relative velocities

could be calculated to achieve the desired sprung mass rigid body dynamics. In this way, the vehicle could be stiff in pitch and roll, and soft in heave. Because individual corner relative velocities were comprised of both stiff pitch and roll parameters, and soft heave parameters, the stiffness apparent in single-wheel events was high. In a way this effort is similar to stabilizer bars introduced in the previous chapter that increasing roll-mode stiffness at the expense of single-wheel stiffness. Lotus modal control reduced compromises between different modes of rigid body motion, but at the expense of single-wheel events. Because Lotus modal control was so effective, it set an early performance standard and is very interesting to study in detail [8–10].

Because of aggressively pushing hardware into vehicles and thereby accumulating practical experience, Lotus led the development of active suspension. Lotus was able to apply nonlinear concepts appreciated by suspension engineers (such as progressivity of springing and damping) that were difficult for control theorists to consider. Most important for this work, Lotus was able to affect overall handling of the vehicle by indirectly influencing the roll moment distribution, as well as varying the second-order sprung mass dynamics by mode (e.g., dramatically decreasing roll).

Inertial damping provides near-optimal vertical vibration isolation and allows a highly stable closed loop to be formed. Inertial damping does not attempt to influence vehicle handling. Conversely, the Lotus modal control was shown to allow the ability to have the vehicle appear soft in heave, and more rigid for pitch and roll inertial inputs, and the ability to influence roll moment distribution. The Lotus modal control has relatively high single-wheel stiffnesses, provides relative heave damping, and has stability limits. Therefore, these two general active suspension systems were in many ways opposite—or complementary. The modal inertial damping presented in the following section was a combination of Lotus modal control and skyhook damping.

6.4 Modal Inertial Damping

It is possible to combine inertial damping and Lotus modal control in a way that preserves, and in some cases even improves upon the respective performance benefits of both. Given the same Lotus suspension hardware corner configuration, the hydraulic servovalve can be driven by the error between a demanded corner force and the force measured by the load cell. Therefore, a closed-loop force actuator is formed at each corner, as compared with the open-loop velocity produced by the Lotus modal control. In the actual implementation, this force loop was closed locally at each corner with analog compensation. This combination of analog compensation, no digital time delay, and high-quality Moog servovalve, resulted in a high-performance force actuator [11].

With such a high-quality force actuator, the Lotus hardware configuration could easily achieve independent skyhooks at each corner of the car. All that would be required is an accelerometer at each corner, whose output could be numerically integrated to yield inertial velocity of each corner. To preserve the benefits of the Lotus modal control, specifically in allowing distinctly parameterized responses to each rigid body mode of motion, forces at each corner could alternatively form products of heave, pitch, and roll modal inertial velocities and damping parameters.

$$C_{\text{heave}} \dot{z} = F_{1a} + F_{2a} + F_{3a} + F_{4a}, \quad (6.4)$$

$$C_{\text{roll}} \dot{\phi} = \frac{t}{2} (F_{2a} + F_{3a}) - \frac{t}{2} (F_{1a} + F_{4a}), \quad (6.5)$$

$$C_{\text{pitch}} \dot{\theta} = -x_1 (F_{1a} + F_{2a}) - x_2 (F_{3a} + F_{4a}), \quad (6.6)$$

where F_{ia} is the modal inertial damping active force at the i th corner.

Front and rear inertial roll dampings are defined by separating Eq. 6.5 into front and rear roll dampings,

$$C_{\text{roll,front}} \dot{\phi} = \frac{t}{2} (F_{2a} - F_{1a}), \quad (6.7)$$

$$C_{\text{roll,rear}} \dot{\phi} = \frac{t}{2} (F_{3a} - F_{4a}), \quad (6.8)$$

so that the total inertial roll damping of Eq. 6.5 is the sum of the front and rear roll dampings of Eqs 6.7 and 6.8.

$$C_{\text{roll}} = C_{\text{roll,front}} + C_{\text{roll,rear}}. \quad (6.9)$$

Equation 6.9 does not shed insight on how to determine the front and rear inertial roll dampings $C_{\text{roll,front}}$ and $C_{\text{roll,rear}}$. For this, we use the roll moment distribution parameter ε , where $\varepsilon = 1$ if all the roll moment is on the front, and $\varepsilon = -1$ if all on the rear, and continuously varied between these extremes. Using ε , the values for front and rear roll stiffness can be written as

$$C_{\text{roll,front}} = C_{\text{roll}} \left(\frac{1+\varepsilon}{2} \right), \quad (6.10)$$

$$C_{\text{roll,rear}} = C_{\text{roll}} \left(\frac{1-\varepsilon}{2} \right). \quad (6.11)$$

Using Eqs 6.4, 6.6, 6.10, and 6.11, a relationship between modal accelerations and corner forces can be written.

$$\begin{bmatrix} \dot{z} \\ \dot{\theta} \\ \left(\frac{1+\varepsilon}{2}\right)\dot{\phi} \\ \left(\frac{1-\varepsilon}{2}\right)\dot{\phi} \end{bmatrix} = \begin{bmatrix} \frac{1}{C_{\text{heave}}} & \frac{1}{C_{\text{heave}}} & \frac{1}{C_{\text{heave}}} & \frac{1}{C_{\text{heave}}} \\ \frac{-x_1}{C_{\text{pitch}}} & \frac{-x_1}{C_{\text{pitch}}} & \frac{-x_2}{C_{\text{pitch}}} & \frac{-x_2}{C_{\text{pitch}}} \\ \frac{t}{2C_{\text{roll}}} & \frac{-t}{2C_{\text{roll}}} & 0 & 0 \\ 0 & 0 & \frac{-t}{2C_{\text{roll}}} & \frac{t}{2C_{\text{roll}}} \end{bmatrix} \begin{bmatrix} F_{1a} \\ F_{2a} \\ F_{3a} \\ F_{4a} \end{bmatrix} \quad (6.12)$$

By using algebra to distribute ε , a relationship can be written to express corner forces as a function of modal inertial velocities.

$$\begin{bmatrix} F_{1a} \\ F_{2a} \\ F_{3a} \\ F_{4a} \end{bmatrix} = \begin{bmatrix} \frac{-x_2 C_{\text{heave}}}{2(x_1 - x_2)} & \frac{-C_{\text{pitch}}}{2(x_1 - x_2)} & \frac{(1+\varepsilon)C_{\text{roll}}}{2t} \\ \frac{-x_2 C_{\text{heave}}}{2(x_1 - x_2)} & \frac{-C_{\text{pitch}}}{2(x_1 - x_2)} & \frac{-(1+\varepsilon)C_{\text{roll}}}{2t} \\ \frac{x_1 C_{\text{heave}}}{2(x_1 - x_2)} & \frac{C_{\text{pitch}}}{2(x_1 - x_2)} & \frac{-(1-\varepsilon)C_{\text{roll}}}{2t} \\ \frac{x_1 C_{\text{heave}}}{2(x_1 - x_2)} & \frac{C_{\text{pitch}}}{2(x_1 - x_2)} & \frac{(1-\varepsilon)C_{\text{roll}}}{2t} \end{bmatrix} \begin{bmatrix} \dot{z} \\ \dot{\theta} \\ \dot{\phi} \end{bmatrix}. \quad (6.13)$$

On the surface this seems to have been done by inverting a nonsquare matrix; however, the four corner forces are still nonlinear functions of four variables, the three modal inertial velocities, and the roll moment distribution.

Some nomenclature is introduced for simplification.

$$C_h = \frac{-x_1 x_2 C_{\text{heave}}}{4(x_1 - x_2)^2}, \quad (6.14)$$

$$C_r = \frac{C_{\text{roll}}}{4t^2}, \quad (6.15)$$

$$C_p = \frac{C_{\text{pitch}}}{4(x_1 - x_2)^2}. \quad (6.16)$$

And using the definition of modal velocities a relationship between corner inertial velocities and corner forces can be constructed.

$$\begin{bmatrix} F_{1a} \\ F_{2a} \\ F_{3a} \\ F_{4a} \end{bmatrix} = \begin{bmatrix} \frac{-x_2}{x_1} C_h + (1+\epsilon) C_r + C_p & \frac{-x_2}{x_1} C_h - (1+\epsilon) C_r + C_p & C_h - (1+\epsilon) C_r - C_p & C_h + (1+\epsilon) C_r - C_p \\ \frac{-x_2}{x_1} C_h - (1+\epsilon) C_r + C_p & \frac{-x_2}{x_1} C_h + (1+\epsilon) C_r + C_p & C_h + (1+\epsilon) C_r - C_p & C_h - (1+\epsilon) C_r - C_p \\ \frac{-x_2}{x_1} C_h - (1-\epsilon) C_r - C_p & C_h + (1-\epsilon) C_r - C_p & \frac{x_1}{-x_2} C_h + (1-\epsilon) C_r + C_p & \frac{x_1}{-x_2} C_h - (1-\epsilon) C_r + C_p \\ \frac{-x_2}{x_1} C_h + (1-\epsilon) C_r - C_p & C_h - (1-\epsilon) C_r - C_p & \frac{x_1}{-x_2} C_h - (1-\epsilon) C_r + C_p & \frac{x_1}{-x_2} C_h + (1-\epsilon) C_r + C_p \end{bmatrix} \begin{bmatrix} \dot{z}_{1s} \\ \dot{z}_{2s} \\ \dot{z}_{3s} \\ \dot{z}_{4s} \end{bmatrix}. \quad (6.17)$$

A similar relationship using modal stiffness and actuator displacements to form a corner force component based on stiffness is used, but the modal inertial damping system of Eq. 6.17 has more authority as the inertial damping coefficients are desirably large.

Corner inertial velocities are not directly controlled, and in fact contain redundancy relative to the three rigid body modes of motion. The input vector of corner inertial velocities is measured—or more correctly integrated—from accelerometers at each corner. Therefore, Eq. 6.17 is the modal inertial damping control matrix from sensor measurements to force actuator commands. Equation 6.17 shows how modal inertial damping maps inertial corner velocities to corner force commands in a much richer relationship than the independent skyhooks of Eq. 6.3.

The modal inertial damping matrix of Eq. 6.17 has significant differences from the Lotus modal control. First, Lotus modal control tried to shape second-order dynamics of the various modes, but because inertial damping was not truly achieved, heave damping was relative and therefore desirably soft. In general, the Lotus modal control worked best when the heave mode was soft and the pitch and roll modes were stiff. In the Lotus control modal stiffnesses added together to produce a single-wheel stiffness, and that determined the responses to a single-wheel event (similar to a stabilizer bar). Therefore, despite the desire for a soft heave mode, for a single-wheel event the stiff roll and pitch modes added to the single-wheel stiffness, and the vehicle was perceived to be “harsh.” Although the heave natural frequency was quite low, this was only apparent when all four corners received the same simultaneous input. In the modal inertial damping matrix of Eq. 6.17 the modal dampings individually add to form the single-wheel inertial dampings on the diagonal. The difference is that modal damping is desirably high, so the addition of all the modal values for a single-wheel value is not a problem. The high-fidelity corner force loop deals with single-wheel events as a loop disturbance to be rejected; much more

effective than the Lotus modal control with open-loop valve drives based on a desired dynamic free response.

6.5 Sprung Mass Acceleration Feedforward

Road irregularities are not the only disturbances encountered by the vehicle suspension system. As the vehicle accelerates or decelerates pitching moments are induced, similarly as the vehicle turns, roll moments are induced as discussed in the previous chapter. These moments can be calculated by knowing the mass properties of the vehicle, center of mass location, roll and pitch center locations, desired roll moment distribution, and measuring lateral and longitudinal accelerations. Although the center of mass changes with vehicle loading, by knowing static corner load values it can be easily located. Without knowledge of the specific vehicle kinematics, it is assumed that the vehicle pitches and rolls about a point on the ground plane. Specifically,

$$a_x mh = x_1 F_{1f} + x_1 F_{2f} + x_2 F_{1f} + x_2 F_{4f}, \quad (6.18)$$

$$\frac{(1+\varepsilon)}{2} a_y mh = \frac{t}{2} (F_{1f} - F_{2f}), \quad (6.19)$$

$$\frac{(1-\varepsilon)}{2} a_y mh = \frac{t}{2} (F_{4f} - F_{3f}), \quad (6.20)$$

where a_x is longitudinal acceleration, a_y is lateral acceleration, h is the height of the vehicle center of gravity above the ground plane. x_i is the location of the i th axle with respect to the center of gravity, and F_{if} is the feedforward force associated with the i th corner.

Equations 6.18, 6.19, and 6.20 in addition to the trivial equation that the sum of all feedforward forces must be zero can be written in matrix form as

$$\begin{bmatrix} mha_x \\ \frac{(1+\varepsilon)}{2} mha_y \\ \frac{(1-\varepsilon)}{2} mha_y \\ 0 \end{bmatrix} = \begin{bmatrix} x_1 & x_1 & x_2 & x_2 \\ \frac{t}{2} & \frac{-t}{2} & 0 & 0 \\ 0 & 0 & \frac{-t}{2} & \frac{t}{2} \\ 1 & 1 & 1 & 1 \end{bmatrix} \begin{bmatrix} F_{1f} \\ F_{2f} \\ F_{3f} \\ F_{4f} \end{bmatrix}. \quad (6.21)$$

Inverting this system of linear equations the feedforward corner forces can be obtained in terms of the lateral and longitudinal accelerations and the roll moment distribution, that is,

$$\begin{bmatrix} F_{1f} \\ F_{2f} \\ F_{3f} \\ F_{4f} \end{bmatrix} = \begin{bmatrix} \frac{1}{2(x_1 - x_2)} & \frac{1}{2} & 0 & \frac{-x_2}{2(x_1 - x_2)} \\ \frac{1}{2(x_1 - x_2)} & \frac{1}{2} & 0 & \frac{-x_2}{2(x_1 - x_2)} \\ \frac{-1}{2(x_1 - x_2)} & 0 & \frac{1}{2} & \frac{x_1}{2(x_1 - x_2)} \\ \frac{-1}{2(x_1 - x_2)} & 0 & \frac{1}{2} & \frac{x_1}{2(x_1 - x_2)} \end{bmatrix} \begin{bmatrix} mha_x \\ \frac{(1+\varepsilon)}{2} mha_y \\ \frac{(1-\varepsilon)}{2} mha_y \\ 0 \end{bmatrix}. \quad (6.22)$$

Note that Eq. 6.22 can be used with the modal inertial damping and independent inertial damping controllers. The feedforward force terms expressed in Eq. 6.22 are added to the closed-loop force demands, F_{1a} , F_{2a} , F_{3a} , and F_{4a} in Eq. 6.17 so that,

$$F_i = F_{ia} + F_{if}, \quad (6.23)$$

where F_i is the total force on the i th corner and is the summation of the modal inertial damping active force F_{ia} and the feedforward force F_{if} of the i th corner.

It is interesting to note that using the feedforward control of Eq. 6.24 in conjunction with the independent inertial damping at each corner would yield near optimal ride isolation and still allow some dynamic roll moment distribution for handling. For optimal handling, maintaining very good ride isolation modal damping is still preferred [12]. Roll moment distribution derived from modal inertial damping has authority for transient maneuvers, while roll moment distribution derived from acceleration feedforward has authority for only steady-state conditions. The feedforward and feedback work together in a very effective way. Feedback control produces forces resisting rolling motion, but significantly the forces cannot arise without some motion that creates an error signal. Feedforward control creates these roll resisting forces from the lateral acceleration that cause them. Any practical system cannot work perfectly, so inevitable errors in the feedforward control could be rejected by the feedback control.

6.6 Quarter-Car Optimal Control

The quarter-car model developed in [Chapter 3](#) is a very good target application of optimal control theory. This rich method will be briefly introduced so that

subsequent active suspension results can be placed in the context of optimal control. This and the following sections can be skipped by readers uninterested in optimal control results with no loss of context for future chapters. Using the system shown in [Figure 6.3](#), sprung and unsprung mass positions and velocities are assumed available for a feedback control strategy to drive the force actuator. It is important to recall that sprung mass velocity required for inertial damping is one of these states, so the optimal controller will have access to this information plus more, so intuitively we would expect the optimal controller to be at least as good as inertial damping.

Newton's second law can be applied to the sprung mass of [Figure 6.3](#) which is similar to Eq. 2.36, except the damping force is replaced by the actuator force F_a and the input displacement and velocity are omitted.

$$m_s \ddot{z}_s = K_s(z_u - z_s) + F_a \quad (6.24)$$

and to the unsprung mass, which is similar to Eq. 2.37.

$$m_u \ddot{z}_u = -K_t(z_u) - C_t(\dot{z}_u) - K_s(z_u - z_s) - F_a. \quad (6.25)$$

Equations 6.24 and 6.25 are written in matrix form:

$$\begin{bmatrix} \dot{z}_s \\ \ddot{z}_s \\ \dot{z}_u \\ \ddot{z}_u \end{bmatrix} = \begin{bmatrix} 0 & 1 & 0 & 0 \\ -K_s & 0 & \frac{K_s}{m_s} & 0 \\ \frac{m_s}{m_s} & 0 & \frac{m_s}{m_s} & 0 \\ 0 & 0 & 0 & 1 \end{bmatrix} \begin{bmatrix} z_s \\ \dot{z}_s \\ z_u \\ \dot{z}_u \end{bmatrix} + \begin{bmatrix} 0 \\ \frac{1}{m_s} \\ 0 \\ \frac{1}{m_u} \end{bmatrix} [F_a] \quad (6.26)$$

For notational simplicity matrices are defined. The state vector is written as

$$\mathbf{x} = \begin{bmatrix} \dot{z}_s \\ \ddot{z}_s \\ \dot{z}_u \\ \ddot{z}_u \end{bmatrix} \quad (6.27)$$

The control vector is written as

$$\mathbf{u} = [F_a] \quad (6.28)$$

$$\mathbf{A} = \begin{bmatrix} 0 & 1 & 0 & 0 \\ -\frac{K_s}{m_s} & -\frac{C_s}{m_s} & \frac{K_s}{m_s} & \frac{C_s}{m_s} \\ 0 & 0 & 0 & 1 \\ \frac{K_s}{m_u} & \frac{C_s}{m_u} & -\frac{(K_s + K_t)}{m_u} & -\frac{(C_s + C_t)}{m_u} \end{bmatrix}, \quad (6.29)$$

$$\mathbf{B} = \begin{bmatrix} 0 \\ \frac{1}{m_s} \\ 0 \\ \frac{1}{m_u} \end{bmatrix}. \quad (6.30)$$

So Eq. 6.27 becomes

$$\dot{\mathbf{x}} = \mathbf{Ax} + \mathbf{Bu}.$$

The idea of optimal control is that the state deviations are optimally stabilized so that a performance criterion is minimized. The deviation of each state can be individually penalized.

$$\mathbf{R} = \begin{bmatrix} r_1 & 0 & 0 & 0 \\ 0 & r_2 & 0 & 0 \\ 0 & 0 & r_3 & 0 \\ 0 & 0 & 0 & r_4 \end{bmatrix}. \quad (6.31)$$

The deviation from zero of the control variable is also penalized.

$$\mathbf{P} = [\rho]. \quad (6.32)$$

Given numerical values for Eqs 6.29–6.32, an optimal gain matrix can be found so that the actuator is driven by a linear function of the states. Because the optimal control is based on a linear system, and the square of the states (Eq. 6.27) and the control (Eq. 6.28) are penalized (Eqs 6.31 and 6.32), the process is sometimes referred to as a Linear Quadratic Regulator (LQR). The details of LQR are beyond the scope of the present work, and its overall result will be used going forward. In our case the optimal gain matrix \mathbf{K} can be found with this process [13].

$$\mathbf{F}_a = -\mathbf{Kx}. \quad (6.33)$$

The optimal control methodology provides the best state feedback gain vector K to satisfy the selected performance criteria described in the state penalty matrix of Eq. 6.31 and the control penalty matrix of Eq. 6.32. It is optimal only relative to that particular weighing of state and control penalties. The selected performance criterion becomes the design decision. The control effort must be sufficiently penalized. If control is “cheap” the optimal controller will expend much effort to minimize the last bit of state variable activity. Alternatively, if control is “expensive” the system will allow more state variable activity. Therefore design decisions made in the weightings have a great effect on actual performance of the “optimal” controller. One way that optimal control is useful is to vary the control effort weightings and produce an envelope of theoretically achievable control for various control efforts.

In [Chapter 3](#), we discussed how the human body was sensitive to sprung mass accelerations. This is problematic because the states that we have for feedback, and states whose activity we can penalize, are sprung mass displacement and velocity—not acceleration. Certainly, as we see in Eq. 6.27 if the states of the systems are minimized, acceleration will be minimized, but there is no way to directly penalize only sprung mass acceleration. The situation is even more complicated than this, as we have learned in [Chapter 3](#) that the human body is most sensitive to vertical accelerations in the band of 4–8 Hz.

Within this complexity is a way forward. It is possible to construct a bandpass filter on sprung mass acceleration that transmits in its pass band the vertical vibration frequencies most sensitive to humans. This is in effect the inverse of [Figure 3.8](#) in [Chapter 3](#) and can be written as

$$\frac{\ddot{z}_{\text{est}}}{\dot{z}_s} = \left(\frac{s}{s+25} \right) \left(\frac{50}{s+50} \right), \quad (6.34)$$

where z_{est} is an estimated displacement and \ddot{z}_{est} is its acceleration. Equation 6.34 gives a nice effect of transmitting the offensive frequencies that we want to penalize and therefore minimize, but its input is sprung mass acceleration, which is not a state of the system (rather a derivative of a state), and as described by Eq. 6.25, it is a function of the control input, as well as the other states. We can get around this unfortunate reality by multiplying both sides of Eq. 6.34 by s .

$$\frac{\ddot{z}_{\text{est}}}{\dot{z}_s} = \left(\frac{s^2}{s+25} \right) \left(\frac{50}{s+50} \right). \quad (6.35)$$

Equation 6.35 is seen to be a high-pass filter, transmitting high frequencies with no theoretical attenuation. Therefore, a first-order low pass filter is applied at a frequency roughly an order of magnitude beyond the highest frequency of interest, which is the wheel-hop frequency,

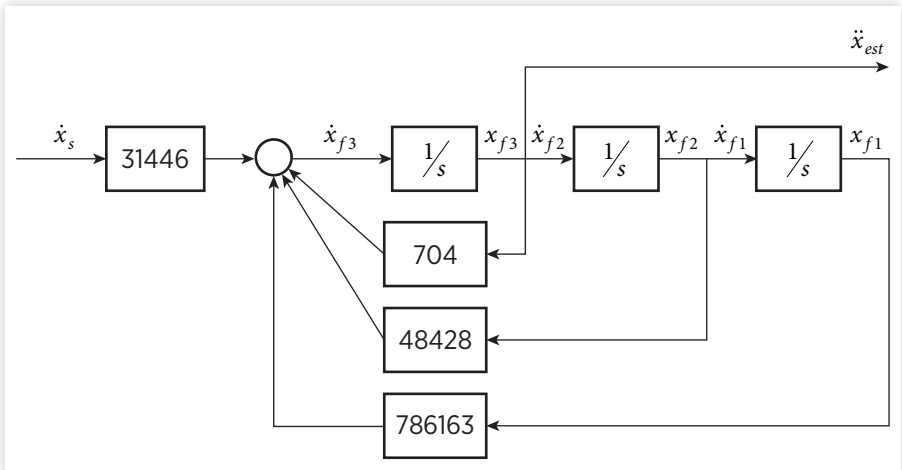
$$\frac{\ddot{z}_{\text{est}}}{\dot{z}_s} = \left(\frac{s^2}{s+25} \right) \left(\frac{50}{s+50} \right) \left(\frac{628}{s+628} \right) \quad (6.36)$$

and the denominator is multiplied out.

$$\frac{\ddot{z}_{\text{est}}}{\dot{z}_s} = \frac{s^2}{(3.18E-5)s^3 + (2.25E-2)s^2 + 1.54s + 25}. \quad (6.37)$$

Equation 6.37 is shown in block diagram form in [Figure 6.9](#).

FIGURE 6.9 Block diagram of filter providing estimate of vertical discomfort.



© SAE International.

This filter can be appended to the quarter-car model. [Figure 6.9](#) includes actual numerical values for the filter coefficients, rather than vehicle dynamic parameters. This is because the coefficients are based on the accepted bandwidth of human sensitivity to vertical vibrations, and a low-pass filter roughly an order of magnitude beyond the well-accepted general wheel-hop frequency. Therefore, this filter would be valid for any reasonable quarter-car model.

The filter dynamics shown in [Figure 6.9](#) are appended to Eq. 6.27, adding the three new filter states to the existing four states from the quarter-car model.

$$\begin{bmatrix} \dot{z}_s \\ \ddot{z}_s \\ \dot{z}_u \\ \ddot{z}_u \\ \dot{x}_{f3} \\ \dot{x}_{f2} \\ \dot{x}_{f1} \end{bmatrix} = \begin{bmatrix} 0 & 1 & 0 & 0 & 0 & 0 & 0 \\ -\frac{K_s}{m_s} & 0 & \frac{K_s}{m_s} & 0 & 0 & 0 & 0 \\ 0 & 0 & 0 & 1 & 0 & 0 & 0 \\ \frac{K_s}{m_u} & 0 & \frac{-(K_s + K_t)}{m_u} & \frac{-(C_t)}{m_u} & 0 & 0 & 0 \\ 31446 & 0 & 0 & 0 & 704 & 48428 & 786163 \\ 0 & 0 & 0 & 0 & 1 & 0 & 0 \\ 0 & 0 & 0 & 0 & 0 & 1 & 0 \end{bmatrix} \begin{bmatrix} z_s \\ \dot{z}_s \\ z_u \\ \dot{z}_u \\ x_{f3} \\ x_{f2} \\ x_{f1} \end{bmatrix} + \begin{bmatrix} 0 \\ \frac{1}{m_s} \\ 0 \\ \frac{1}{m_u} \\ 0 \\ 0 \\ 0 \end{bmatrix} [F_a] \quad (6.38)$$

When examining the filter of [Figure 6.9](#), it is evident that the addition of the low-pass filter at an order of magnitude beyond the wheel-hop frequency does more than just filter high-frequency noise. It allows the output we are interested in, \ddot{x}_{est} , to be a filter state, x_{f3} . As a state of the combined dynamic system, variation of \ddot{x}_{est} , the sprung mass acceleration most sensitive to humans, can be penalized, and therefore reduced by the optimal controller. In terms of accessing the theoretically optimal ride performance for a given cost of control, Eq. 6.38 is an excellent dynamic system for evaluation.

There has been much effort devoted to such theoretical optimal control studies of active suspension, and particularly the quarter-car model because of the elegance of the dynamic system. If some knowledge of future road inputs is available (preview) it is possible to improve system performance. It is also possible to optimize the system for other output functions of state variables, and to design reduced order controllers that are simpler but still in some sense theoretically optimal.

The dynamic system of Eq. 6.38 in many ways is a very compelling quarter-car model used as the basis for an optimal controller. There is a primary variable associated with quarter-car ride, and it is available as a state for optimal feedback control. But there are other more fundamental problems associated with the optimal control of the quarter-car active suspension, and in fact optimal control as applied to all active suspension. Physical actuators (and sensors) usually have an effective range of operation. Actuators can saturate and will not produce any more control effort, even if the control demands it. Actuator and sensor saturation is an example of a “hard nonlinearity,” but there are other “soft nonlinearities” in the system, such as the tire spring stiffness. The process to discover the optimal control gain vector of Eq. 6.34 from the dynamic system is based on assumed linear dynamic system behavior. Because the control is model based, real-world nonlinearities will cause suboptimal performance and can destabilize the feedback system.

Another issue with the classic quarter-car optimal control problem is that it assumes that all states are available for feedback. In practice, this is hardly ever the case, and particularly so with the quarter-car model. For example, both sprung and unsprung mass displacement are interesting to consider. On one hand, it is desirable that these measures are relative to the road. On the other hand, for mathematical consistency they need to be the double integration of the respective accelerations, which are inertially referenced. This issue is theoretically solved by using a method similar to the optimal LQR, which estimates the internal states of a model of the physical system that are necessary to produce an observed output. This theoretically elegant device is called a state observer or Kalman Filter.

The combined LQR/Kalman filter is not robust. We have already shown how quarter-car inertial damping is very robust until actuator dynamics are considered. Omitting such actuator dynamics from the LQR/Kalman filter will very likely result in instability when the simpler model is applied to real hardware. If hardware dynamics are considered the model becomes more complex. In the previous example of a hydraulic actuator, we saw that actuator dynamics adds three states to each corner. This added complexity, although regrettable, possess no real theoretical issues. Practical issues arise when parameters associated with these states are defined. For example, the bulk modulus of the hydraulic fluid varies with many things, among them cylinder displacement and air entrainment.

When all this is considered, the “optimal controller” must be in the end compared with the simple skyhook damper using only inertial velocity. As previously mentioned, sprung mass inertial velocity is a component of the state vector available for full state feedback, and so the optimal controller is expected to have better performance as it has access to more information. The question is, how much better? Without actuator dynamics we saw the inertial damping quarter car system to be extremely stable, accepting any amount of inertial damping gain. In terms of vibration isolation, the system could isolate the sprung mass to any degree desired given the cost of control effort, just as the full state optimal controller.

In the quarter-car problem, inertial damping has one very important practical advantage. If inertial velocity is available as a measurement of the system, driving the force actuator with inertial velocity is a Single-Input/Single-Output system. This system can be well-compensated from an experimental open-loop frequency response using well-known classical control techniques and not requiring exact parameter determination.

Optimal control techniques have thus been applied to the quarter-car model in many different ways over the past thirty years. An example has been presented, using a state filter to produce sprung mass acceleration that humans are most sensitive to that can be minimized by an optimal controller. While

intellectually satisfying, such controllers do not offer significant advantages over inertial (“skyhook”) damping. The biggest difference between the two is that the optimal controller is model based, and therefore can quickly produce a high-performing model of the closed-loop system. Inertial damping is based on experimental data and classical control theory, and can therefore more easily accommodate system nonlinearities and incorporate desirable and pragmatic stability margins.

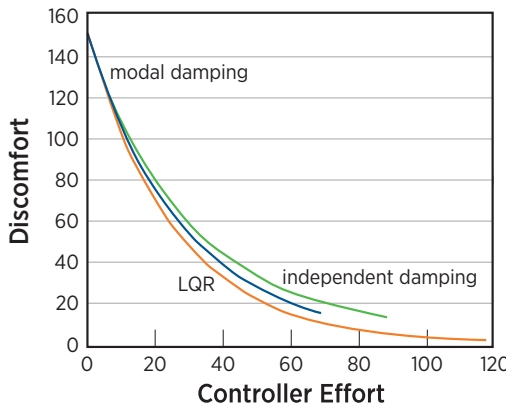
6.7 Full Vehicle Optimal Control

An optimal controller can be constructed to compare with modal inertial damping on the full vehicle. The active suspension ride problem sets up very well for a standard LQR/Kalman filter optimal control formulation as minimizing motion of a driver located on the sprung mass is an accepted performance criterion, and vertical road inputs are stochastically well defined. A model was constructed including 4 unsprung masses and 3 rigid body modes, yielding 14 mechanical states. Actuator dynamics were shown to be important, and second-order valve dynamics and oil compliance at each corner add 12 hydraulic actuator states for a total of 26 states [14].

Driver discomfort can be calculated knowing the driver’s location relative to the vehicle center of gravity and human sensitivity to vibration along the various axes. Inertial modal damping gains were selected to reflect the driver discomfort coefficients of the various modes.

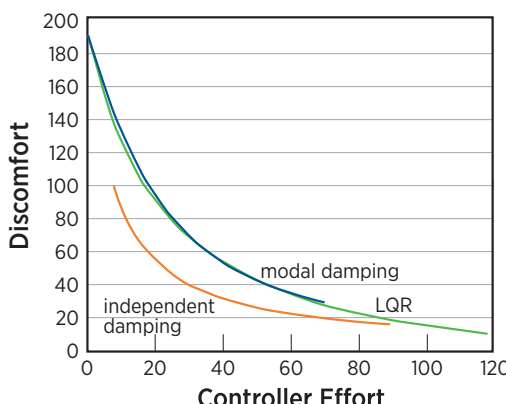
The cost of control in terms of RMS actuation can be varied from a relatively expensive control to cheap control, serving to define an envelope of possible optimal controllers. This is a particularly revealing approach for broad bandwidth active suspension (closed-center valve with constant pressure pump) as the control variable is valve drive, and therefore directly proportional to power consumption. This envelope can be generated for the optimal full state feedback LQR controller and is considered the benchmark against which all other controllers can be measured. This envelope of achievable isolation performance for various actuator efforts can also be generated for independent skyhook control and modal inertial damping as shown in [Figure 6.10](#). The lower left region is not feasible, and the upper right region is not optimal. Because actuator dynamics were included, the independent skyhook controller and the modal inertial damping controller both have a stability limit as the control effort grows. In [Figure 6.10](#), the inertial damping curves are terminated to preserve a 6-dB stability margin. In practice, it is not anticipated that the LQR controller could continue to achieve marginally better performance with more control effort (i.e., power), as unmodeled dynamics are often excited when higher control effort is expended.

FIGURE 6.10 Composite driver discomfort (similar to NASA ride index) for increasing control effort.



© Dan E. Williams.

FIGURE 6.11 Heave discomfort for increasing control effort.



© Dan E. Williams.

Until reaching its stability limit, the modal inertial damping approach performs better than the independent skyhooks, midway to the benchmark LQR controller as shown in the composite discomfort of [Figure 6.10](#). Modal inertial damping and the LQR algorithms can influence pitch and roll motions in ways that the independent skyhooks cannot. It is interesting that the maximum performance of both the independent skyhooks and modal inertial damping is equivalent, but the independent inertial damping requires more control effort.

In this basic application of optimal there is no effort to characterize the road input. The mathematics behind the LQR formulation assumes all four wheels of the vehicle are excited by white road noise, with the optimal controller ensuring a vehicle ride response that minimally excites the human occupant. We have seen from analyzing the pitch-plane ride model of [Chapter 3](#) that this is not a realistic road input configuration. On a paved road, it is likely that both front wheels will experience the same input, and the rear wheels will experience that input a bit later in time, with the time delay decreasing with vehicle speed. Therefore on paved roads the vehicle is less likely to experience a rolling input from the road than would be expected by random excitation at each corner, and as speed increases increasingly less likely to experience a pitching input. Therefore, the claim made by Hrovat that independent skyhooks make a fine vehicle control for ride isolation, particularly at high speed on paved roads is well founded. If the LQR control was reformulated with much higher state penalties on vertical motion, and not as much on pitch and roll, the LQR controller would be more similar to the independent damping envelope.

As expected, the independent skyhook dampers do a better job of isolating the pure heave mode as shown in [Figure 6.11](#). This makes sense, as heave is the only information used by the independent damping algorithm, so the entire authority and bandwidth of the force actuators in that system is used to isolate heave. In the modal inertial damping system pitch and roll are also controlled. As it turns out, based on the driver discomfort index selected, both the LQR and the inertial modal control placed heavy emphasis on controlling pitch, at the expense of heave (as anticipated by Maurice Olley). Recall the pure optimal controller does not account for wheelbase filtering, and therefore reduced pitching inputs at highway speed.

Optimal control is shown to be an effective way to design a good controller for a system described by a linear model. Optimal control is a bit of a mirage. It looks great from a distance, but the closer you get to it, the image of optimality tends to disappear. When the difference between inertial damping and optimal control is appreciated, the robust stability properties of inertial damping, and nature of road inputs appreciated, optimal control starts to look a lot like inertial damping.

Modal inertial damping was implemented on actual vehicles. Ride was assessed using the NASA ride quality index which calculated RMS accelerations along and around principal axis to yield a single number indicative of human discomfort. A general human can perceive a difference of 0.2 in this index. A midrange stock vehicle ride quality was measured to be 4.5 with its original equipment passive suspension on a specific route. The Lotus modal control improved this value to 3.3 when applied on this vehicle and duty cycle. Modal inertial damping further improved the ride of this vehicle to 2.6, with the best in class luxury vehicle ride of 2.8. Subsequent work has shown that this improvement could be increased [\[15\]](#).

6.8 Modal Inertial Damping and Handling

It has just been shown that the modal inertial damping concept produces a vehicle ride consistent with independent skyhook damping, and with optimal control. When installed on an actual midrange vehicle it exceeded the best in luxury class ride. The modal inertial damping matrix of Eq. 6.17 has been identified, and it includes a roll moment distribution parameter that will now be considered.

Suspension determines handling as well as ride, and the inertial damping matrix of Eq. 6.17 has significant handling advantages relative to alternative methods of active suspension control. It was earlier stated that the Lotus modal control roll moment distribution was determined by modal states and parameters. Thus, through judicious selection of the modal parameters, roll moment distribution could be affected, but only indirectly. In the modal inertial damping matrix of Eq. 6.17, the roll moment distribution parameter ε is independently selectable.

It is a well-known property of tires that the side forces they generate are dependent upon the normal force or the vertical load on the tire. The more vertical load, the greater the side force. However, the relationship between side force and load is nonlinear. As the vehicle turns, load is transferred from the inside tires to the tires on the outside of the turn. The tires on the outside that receive this load transfer increase their side force, but not by as much as is lost by the inside tires that lose the load. Therefore, when load is transferred across a vehicle, the net side force is reduced. This is in general an unfortunate situation, as the reason that there is a load transfer is the presence of a lateral acceleration, and as we saw in the roll-mode chapter the lateral force must be reacted by the tires. Therefore, when the tires are needed to react against the lateral acceleration, they will be less able to do it because of the very presence of the lateral acceleration and the nonlinear tire property.

Within this generally unfortunate circumstance is opportunity. Because there are generally three rigid body modes of sprung mass motion (heave, pitch and roll), and four actuators at each corner, the motion is “overdetermined” by the actuators. That is to say, with three actuators to control three rigid body modes, there would be a unique mapping between modal forces and actuators, and actuator forces would be uniquely determined. With four actuators there is an “extra” degree of control. It is this extra degree of control that allows the roll moment distribution parameter in Eq. 6.17.

If the roll moment is predominately carried on the front axle, it will lose its ability to generate a side force. The front of the car will drift out, and require an additional steering correction to hold a given radius. This is called understeer. Conversely, if too much roll moment is carried on the rear, it will lose its ability to generate a lateral force and drift out. In extreme cases the driver will have to counter steer just to hold the desired turning radius. This is oversteer. This effect can be produced by passive stabilizer bars introduced in the preceding chapter.

If the vehicle is not yawing enough relative to the steering command from the driver, we would like the roll moment distributed to the rear, allowing the front tires to bite and develop a higher vehicle yaw rate. Conversely, if the yaw rate is too high we would like to distribute the roll moment to the front axle and allow the rear tires to bite. Thus the roll moment can be distributed proportionally to the difference between the absolute value of measured yaw rate and the yaw rate required for neutral steer based on the ideal vehicle handling response referred to as the Ackermann relationship. The Ackermann relationship is initially derived in Eq. 7.4, and is expressed in a more relevant form in Eq. 7.35 in the following handling section. For now it is sufficient to consider the Ackermann relationship as the ideal transformation of steer angle to yaw rate. For any three modal velocities, given a desired roll moment distribution unique forces can be calculated for each corner.

$$\varepsilon = K_{\text{yaw}} \left(|r| - \frac{u}{a+b} |\delta| \right). \quad (6.39)$$

Although the construction of the control of Eq. 6.39 is relatively ad hoc, it has been shown to perform well relative to more rigorous nonlinear sliding mode controllers [16]. More complicated logic is required for an inherently oversteering vehicle above its critical speed.

The effect of varying the roll moment distribution can be seen on an actual vehicle, where the vehicle's trajectory was constrained to a 90° turn at 30 mph (a quarter-circle of constant radius). The passive vehicle required a large handwheel input to negotiate the defined trajectory as shown in [Figure 6.12](#). Varying degrees of static roll moment distribution from 1.0 (all on the front) to -1.0 (all on the rear) show that as the roll moment moves to the rear, the car becomes more oversteering and less handwheel input is required. Also shown in [Figure 6.12](#), the roll moment is distributed according to the closed-loop absolute yaw rate error of Eq. 6.39.

FIGURE 6.12 Steering input for various roll moment distributions.

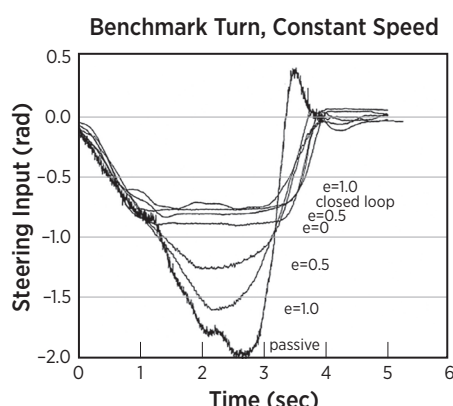
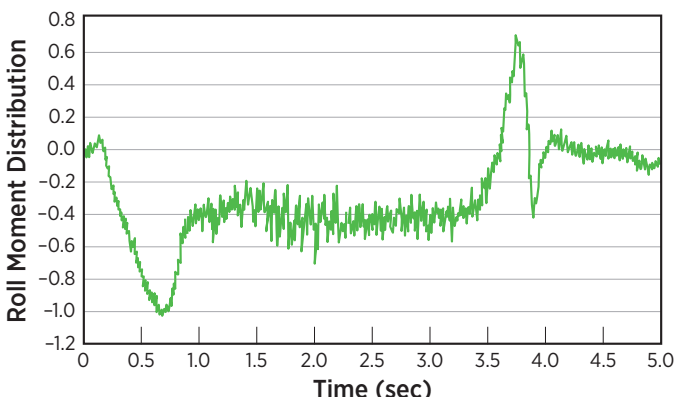


FIGURE 6.13 Closed-loop roll moment distribution.

© Dan E. Williams.

The time history of the dynamic roll moment distribution parameter shown in [Figure 6.13](#) reveals interesting closed-loop behavior. At the beginning of the turn, the roll moment is biased to the rear; at one point saturating at -1.0 to quickly initiate a yaw rate. Throughout the middle portion of the turn, the roll moment is relatively constant at approximately -0.5 . Finally, upon exit of the turn the roll moment is biased to the front, allowing the rear wheels to bite and stabilize the vehicle in its straight ahead position.

The driver's impression of this vehicle is quite dramatic. It is virtually impossible for this vehicle to spin out on a curve. If a driver enters a curve too fast, the car does not lose grip at the front (understeer) or the rear (oversteer), rather the car drifts out laterally away from the trajectory that requires more lateral force than the tires can generate.

6.9 Summary

In the previous chapters of this first section on ride, the quarter-car model was developed to identify fundamental characteristics of vertical motion. Then the pitch-plane model was developed to describe the combined heave and pitch motion of a vehicle encountering road inputs when traveling in a straight line. The roll mode was introduced, primarily excited by lateral forces experienced by the sprung mass during turning. It was shown that the presence of a stabilizer bar can determine roll stiffness somewhat independent of heave inputs to the axle. In this chapter we have looked at how all three rigid body modes of motion, heave, pitch, and roll, can be simultaneously controlled through active suspension.

In practice most active suspension efforts can trace their heritage to either skyhook damping or the Lotus modal control. Skyhook damping was shown to be very effective at vertical vibration isolation, whereas Lotus' modal control had the ability to modify vehicle handling.

The quarter-car model was cast as an optimal control problem, and results of a full vehicle simulation were shown that compares a full state feedback optimal controller, a vehicle with independent inertial damping at each corner, and modal inertial damping. Modal inertial damping generally compares with the vibration isolation properties of independent inertial damping at each corner, and a full state feedback optimal controller. Furthermore, modal inertial damping improves upon the best features of Lotus modal control: the ability to independently influence rigid body modes of motion and the ability to determine handling through roll moment distribution. Taken together, the improvements in ride and handling of the inertial modal control produced the best riding vehicle measured to that date, as well as dramatic direct closed-loop control of yaw rate to assure neutral steer (or any desired degree of understeer). Such a simultaneous improvement in both ride and handling, properties historically considered in conflict, was unprecedented [15].

Modal inertial damping influenced handling by exploiting a second order effect of load transfer on the side force generated by a tire. Despite its second-order nature, the roll moment distribution capability of modal inertial damping was shown to have a profound effect on vehicle handling. The angle of attack of a tire has a first-order effect on the lateral force a tire generates. The driver exploits this first order effect by changing this difference between the direction the tire is pointing and the direction it is moving. The following section of this book develops the notion of vehicle handling, and this first-order relationship between angle of attack and lateral force will be the fundamental origin of handling behavior. In addition to the driver changing the angle of attack of the wheels through steering, it will be shown that this angle of attack can change with vehicle roll.

Depending upon suspension kinematics, sprung mass roll can change the attack angle of the tires. Careful consideration of [Figure 6.12](#) allows a comparison of the first- and second-order effects. The figure shows the steering input required for a vehicle to negotiate a 90° turn at a fixed speed. Therefore, the more steering input required, the more understeering the vehicle. A passively suspended vehicle is reported as well as an identical active vehicle with a closed yaw rate loop of Eq. 6.39 and various static roll moment distributions. It is evident that as the vehicle carries more roll moment on the front axle, it becomes more understeering. It is important to remember that the actively suspended vehicle rolls very little even in such an aggressive maneuver. The passive vehicle rolls a great deal, with the roll resisted by both the front and rear axles. The passive vehicle with a split roll moment understeers more than the active vehicle

with the roll moment carried all on the front. This is because the first-order suspension kinematics of the vehicle are much more effective at producing desirable understeer than the second order roll moment distribution. In fact it is remarkable that the roll oscillation of the passive vehicle can be seen in [Figure 6.12](#). By eliminating sprung mass roll, active suspension eliminates much of the compromise between ride and handling that will be apparent in the second half of this book.

This chapter was in some ways the most challenging to write. The first 7 years of my career and my PhD research were exclusively devoted to active suspension. A huge body of knowledge at the intersection of vehicles dynamics and control systems, active suspension is an extremely interesting and instructive topic to delve into at a greater level of detail than is allowed in this work. After nearly 20 years of working on other vehicle control systems, I was invited by ASME to present the 2016 Milliken Lecture on vehicle dynamics, and specifically on active suspension. Preparing the lecture gave me the opportunity to revisit the topic and tie up some loose ends. This lecture was written into a SAE paper, and is recommended to anybody wanting a deeper look into active suspension, lessons learned from the development, and its potential for the future.

References

- [1] Gillespie, Thomas D., *Fundamentals of Vehicle Dynamics*, SAE International, Warrandale, PA, 1992.
- [2] Milliken, William F., and Douglas L. Milliken, *Chassis Design: Principles and Analysis*, SAE International, Warrandale, PA, 2002.
- [3] Milliken, William F., *Equations of Motion*, Bentley Publishers, 2006.
- [4] Benhabib, R.J., Iwens, R.P., and Jackson, R.L., “Stability of large space structure control systems using positivity concepts,” *Journal of Guidance, Control, and Dynamics*, 4:487–494, 1981.
- [5] Haddad, W.M., and Bernstein, D.S. “Explicit construction of quadratic Lyapunov functions for the small gain, positivity, circle, and Popov theorems and their application to robust stability. Part I: Continuous-time theory,” *International Journal of Robust and Nonlinear Control*, 1993.
- [6] Ahmadian, M., “Integrating electromechanical systems in commercial vehicles for improved handling, stability, and comfort,” *SAE International Journal of Commercial Vehicles*, 7(2): 535–587, 2014, DOI:[10.4271/2014-01-2408](https://doi.org/10.4271/2014-01-2408).
- [7] Hrovat, D., “Applications of optimal control theory to advanced automotive suspension design,” *ASME Journal of Dynamic Systems, Measurement, and Control*, 115:328–341, 1993.
- [8] Williams, D.A., and Wright, P.G., “Vehicle suspension system,” U.S. Patent 4625993, December 2, 1986.
- [9] Milliken, William F., Jr., *Active Suspension*, SAE paper 880799, Warrandale, PA, 1988.
- [10] Williams, D.A., and Wright, P.G., “Control system for controlling land vehicle,” U.S. Patent 5217246, June 8, 1993.

- [11] Williams, D.E., and Ghaphery, A.G., "Method and apparatus for controlling an active suspension system," U.S. Patent 6259982, July 10, 2001.
- [12] Williams, D.E., "Method for controlling an active suspension system," U.S. Patent 5510986, April 23, 1996.
- [13] Kwakernaak. H.S., and Sivan, R., *Linear Optimal Control Systems*, Wiley-Interscience, 1972.
- [14] Williams, D.E., and W.M. Haddad, "Active suspension control to improve vehicle ride and handling," *Vehicle System Dynamics*, July, 1997.
- [15] Williams, D.E., "Active suspension: Future lessons from the past," SAE International Journal of Vehicle Dynamics, Stability, and NVH, 2(2):147–165, 2018, DOI:[10.4271/10-02-02-0010](https://doi.org/10.4271/10-02-02-0010).
- [16] Williams, D.E., and W.M. Haddad, "Nonlinear control of roll moment distribution to influence vehicle yaw characteristics," IEEE Transactions on Control Systems Technology, 3:110–116, 1995.

Handling Basics

Long before the days of the skidpad. . . it was realized that the handling of a car, as contrasted for example with the steering of boat, was a very tricky business.

—Maurice Olley

7.1 Introduction

In the previous section on vehicle ride, the sprung mass was allowed to heave, pitch, and roll. The heave and pitch modes were primarily excited by vertical road inputs. Roll could likewise be excited by vertical road inputs but perhaps more commonly, at least on smooth highways, is that the roll mode is displaced by lateral acceleration when the vehicle is turning. In this case, the tires must generate a lateral force to balance the “centrifugal force” acting at the center of gravity of the vehicle. The previous section left open the question: How is such a centrifugal force generated? That question will now be addressed in this second section on vehicle handling.

The centrifugal force displacing the roll mode, as every driver realizes, is generated by a steering input. This first chapter of this section will look at the steering system, and how it can serve to turn the vehicle. This chapter will discuss steering kinematics, or the relationship between steered wheel displacements and forces, and how such forces originate. It will develop ideal low-speed relationships between the various wheels, will derive the steering forces required to turn the wheels, and will suggest a simple way to model the steering systems. Then, it will use the steering system to introduce the critical characteristic of vehicle handling—the yaw rate response. Finally, this chapter will introduce the notion of slip angle and how lateral forces generated by the tires can be described.

This chapter will broadly review the state of the art of vehicle handling as it is generally found in the literature. The chapter is not intended to be a detailed development of such state of the art; there are many fine referenced works that can provide that. This chapter will quickly develop the standard yaw plane model highlighting two key conventions that limit its generality. Future chapters will more rigorously develop the dynamics associated with steering and extend handling models beyond the conventional literature. Detailed development and discussion of the yaw plane will follow in these chapters where the conventions suggested later in this work allow more compact mathematics.

7.2 Ackermann Steering

We first consider the case of tires moving in the direction they are freely rolling. More formally this situation is described as the velocity vector of the tire coincides with the centerline of the tire. With this assumption, all tires must be tangent to the relevant radius of curvature. For this assumption to be accurate, there can only be negligible lateral force on the tires that would deflect the rolling tire from its centerline. Therefore this assumption is equivalent to stating that the vehicle is moving forward at very low speed, so that the lateral acceleration is effectively zero. Later the effect of “centrifugal force” will be considered.

With these conditions, one side of a conventionally steered two-axle vehicle can be pictured.

FIGURE 7.1 Steered wheel geometry.

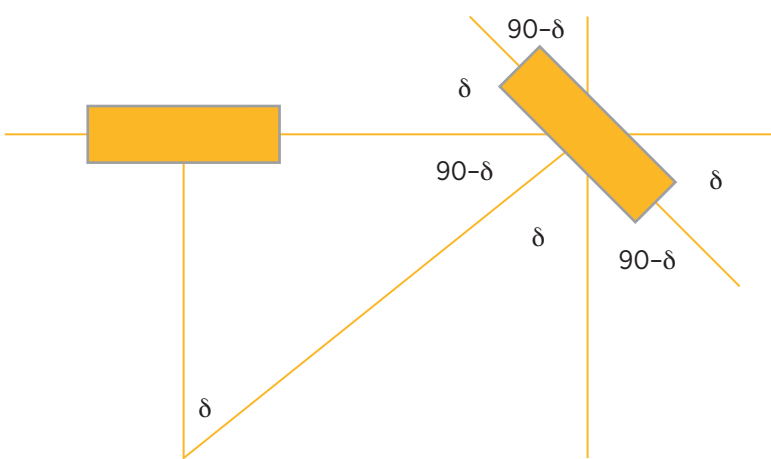
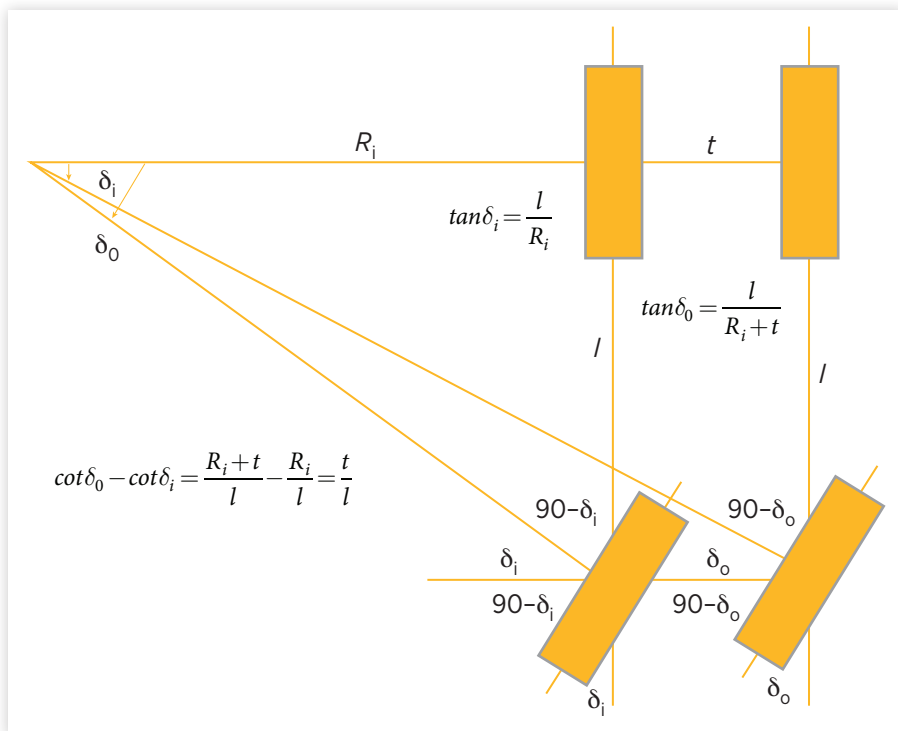


Figure 7.1 shows the geometry of a steered front wheel for relevant angles including the steer angle δ relative to the centerline of the vehicle. All angles are considered positive in the clockwise direction. With no lateral forces, the intersection of the perpendicular of the steered front wheel and the perpendicular of the unsteered rear wheel intersect to form the center of the turn. Thus, the radius of curvature of the steered front wheel is a bit longer than the radius of curvature of the unsteered rear wheel. (The perpendicular from the rear and the vehicle length form a convenient right angle.)

Figure 7.1 shows a single-track relationship between a front and a rear wheel. It is possible to duplicate this single-track model on either side of a two-axle vehicle, to show the ideal relationship of all four wheels to the center of curvature of the vehicle path. In this section, the geometric differences between the front and rear wheels will be described. Once understood, most of the future work assumes the two sides of the vehicle can be combined into a “single-track” model similar to **Figure 7.1**.

FIGURE 7.2 Two-axle vehicle kinematic model.



[Figure 7.2](#) shows the right and left sides of a two-axle vehicle, separated by a track width t . The radius of curvature R_i is the distance from the point the vehicle turns about to the inner rear wheel. The front and rear axles are separated by a wheelbase l . A significant feature of [Figure 7.2](#) is that different steering inputs are allowed for the inner steered wheel δ_i , and the outer steered wheel δ_o . It can be seen in [Figure 7.2](#) that this is necessary to allow the freely rolling wheels to orient to their respective tangents.

From [Figure 7.2](#), the relationship among the ideal inner steering input, the wheelbase and the track can be written as

$$\tan \delta_i = \frac{l}{R_i} \quad (7.1)$$

and similarly for the outer steering input.

$$\tan \delta_o = \frac{l}{R_i + t}. \quad (7.2)$$

Equations 7.1 and 7.2 can be combined to form a relationship between the ideal inner and the outer steer angles.

$$\cot \delta_o - \cot \delta_i = \frac{t}{l}. \quad (7.3)$$

If Eq. 7.3 is satisfied, all wheels on the vehicle are tangential to their instantaneous trajectory. Therefore, there is no side force developed by the freely rolling tires.

[Figure 7.3](#) shows a single-track model of [Figure 7.1](#) laid onto the center line of the full vehicle of [Figure 7.2](#). It is easily seen that using small-angle approximations, the average of the inner and outer steer angle is the ideal single-track steer angle. If a radius R is now defined as the distance from the center of curvature to the midpoint of the rear axle, a simple relationship can be formed.

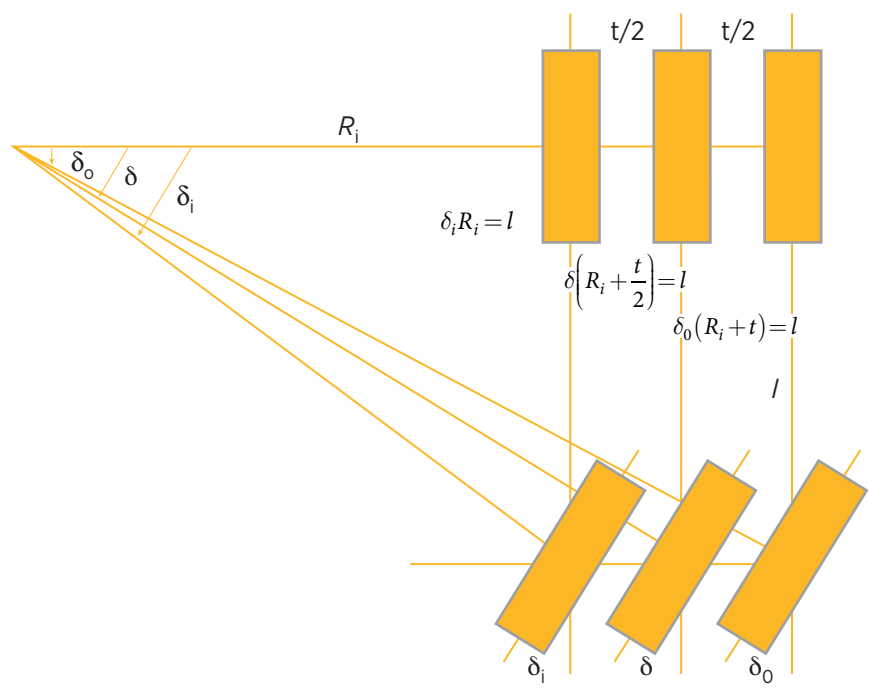
$$\delta_{ack} = \frac{l}{R}. \quad (7.4)$$

Equation 7.4 is the celebrated “Ackermann” steering relationship. The Ackermann ratio is the wheelbase divided by the turning radius and will be seen to be a fundamental parameter useful in vehicle dynamics at all speeds. This will be a recurring relationship throughout this handling section. In fact we already briefly used this term to define the roll moment distribution of active suspension in the previous chapter.

A common front axle configuration is that steering arms extending from the wheels are connected by a tie-rod, as shown in [Figure 7.4](#) looking down from

FIGURE 7.3 Comparison of single-track steering.

© Dan E. Williams.



above. This geometry was once widely used. More recently, the combination of front wheel drive, transverse short block engines, McPherson strut suspensions, and rack and pinion steering combine to provide better packaging and slightly different geometry, but general conclusions drawn from the linkage shown in [Figure 7.4](#) can still apply to other linkage configurations.

It is assumed that the left side wheel is displaced by a steering input δ_l . In this condition, the location of point B as shown in [Figure 7.5](#) can be written.

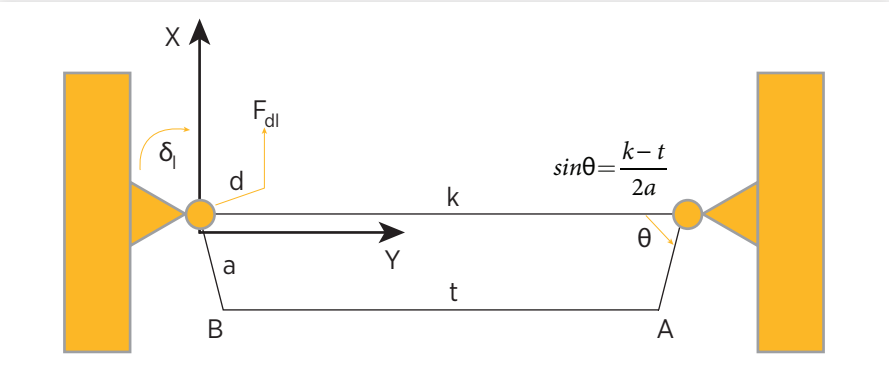
$$B_x = -a \sin(\delta_l + \theta), \quad (7.5)$$

$$B_y = a \cos(\delta_l + \theta). \quad (7.6)$$

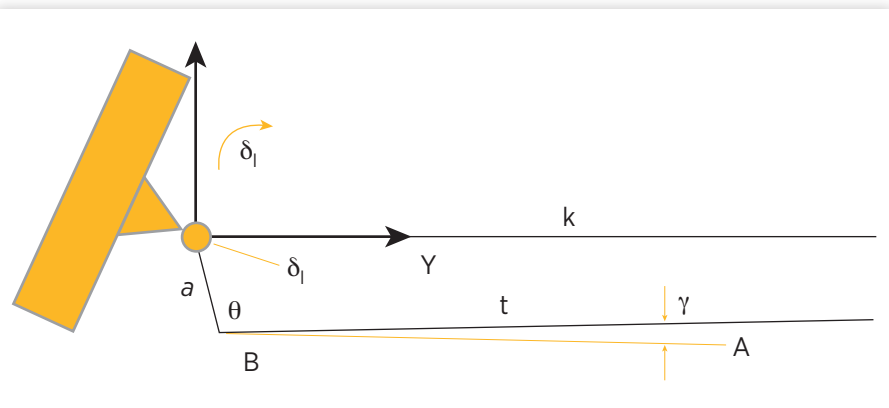
Theta is the angle the tie rod arms make with the solid axle at the center position of steering.

Given the location of Point B from Eqs 7.5 and 7.6, the location of Point A in [Figure 7.5](#) is displaced by the tie rod in [Figure 7.6](#) and can be written as

$$A_x = -a \sin(\delta_l + \theta) - ts \sin \gamma, \quad (7.7)$$

FIGURE 7.4 Conventional steering linkage with tie-rod.

© Dan E. Williams.

FIGURE 7.5 Left wheel displacement.

© Dan E. Williams.

$$A_y = a(\cos(\delta_l + \theta)) + t \cos \gamma. \quad (7.8)$$

Point A can also be referenced from a rotation about the right steered wheel.

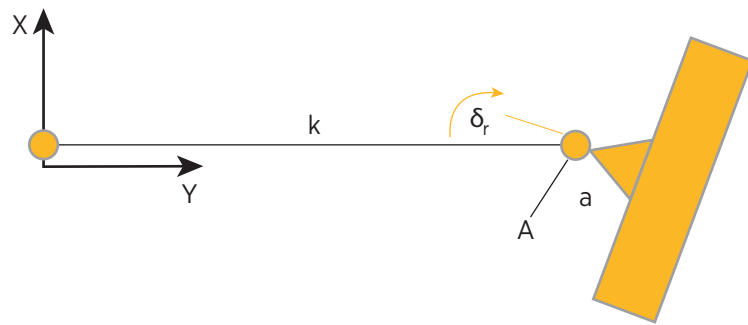
$$A_x = -a(\sin(\theta - \delta_r)), \quad (7.9)$$

$$A_y = k - a(\cos(\theta - \delta_r)). \quad (7.10)$$

Equation 7.7 can be equated with Eq. 7.9 as the longitudinal location of Point A and point B must be coincident.

FIGURE 7.6 Right wheel displacement.

© Dan E. Williams.



$$a(\sin(\theta - \delta_r)) = a(\sin(\delta_l + \theta)) + t \sin \gamma. \quad (7.11)$$

Similarly, as the lateral location of A must be coincident with that of point B, Eq. 7.8 equals Eq. 7.10.

$$a(\cos(\delta_l + \theta)) + t \cos \gamma = k - a(\cos(\theta - \delta_r)). \quad (7.12)$$

Equation 7.11 can be solved for the tie rod angle γ .

$$\begin{aligned} \sin \gamma &= \frac{a}{t} (\sin(\theta - \delta_r)) - \frac{a}{t} (\sin(\delta_l + \theta)), \\ \gamma &= \sin^{-1} \left(\frac{a}{t} (\sin(\theta - \delta_r)) - \frac{a}{t} (\sin(\delta_l + \theta)) \right). \end{aligned} \quad (7.13)$$

Equation 7.13 shows a tie rod angle for various steering inputs. Equation 7.13 can be inserted into Eq. 7.12 to yield a complex trigonometric relationship between the right side and the left side steering inputs. This complex relationship likely requires a numerical solution.

If the tie rod angle γ is small, Eq. 7.12 becomes

$$\frac{k-t}{a} - \cos(\theta - \delta_r) = \cos(\delta_l + \theta) \quad (7.14)$$

and using,

$$\cos \theta = \frac{k-t}{2a} \quad (7.15)$$

to yield a relationship between the steer arm angle, and the left and right steering inputs.

$$2\cos\theta = \cos(\delta_l + \theta) + \cos(\theta - \delta_r). \quad (7.16)$$

Equation 7.16 is significant in that the entire four-bar linkage of [Figure 7.4](#) is characterized by θ as the right and left steer angles are related. Eq. 7.16 can be solved for the right side steer input.

$$\delta_r = \theta - \cos^{-1}[2\cos\theta - \cos(\delta_l + \theta)]. \quad (7.17)$$

The ideal Ackermann relationship of Eq. 7.3 can be solved for the right and left side steering inputs.

$$\cot\delta_r = \cot\delta_l - \frac{t}{l}. \quad (7.18)$$

Equation 7.18 is solved for the right side steering input.

$$\delta_r = \cot^{-1}\left(\cot\delta_l - \frac{t}{l}\right). \quad (7.19)$$

The difference between the ideal right side steering input of Eq. 7.19 and the actual right side steering input of Eq. 7.17 can be considered the Ackermann error.

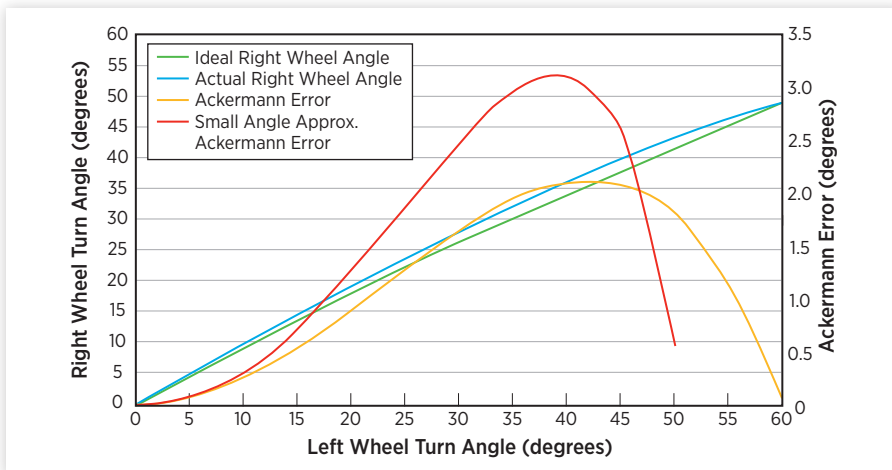
$$\Delta\delta_r = \theta - \cos^{-1}[2\cos\theta - \cos(\delta_l + \theta)] - \cot^{-1}\left(\cot\delta_l - \frac{t}{l}\right). \quad (7.20)$$

The Ackermann error calculated in Eq. 7.20 results in slip angles in the front tires at the opposite sides of the front axle that work against each other. The result can be compared with a more accurate result similar to the simultaneous solution of Eqs 7.12 and 7.13 as shown in [Figure 7.7](#). It should be noted that Eq. 7.20 is accurate only for small tie rod angles. Eq. 7.13 can be used to calculate the tie rod angle, and therefore determine the relevance of Eq. 7.20.

The Ackermann error approximation of Eq. 7.20 is good for steering inputs consistent with highway driving, where most vehicle operation occurs. Ackermann considerations are particularly important for commercial vehicles, with heavy axle loads and long wheelbases. Recall from Eq. 7.4 longer wheelbase requires more steering input to negotiate a given radius. Tire wear is known to be a higher order function of slip angle as well as tire load [1]. A typical

FIGURE 7.7 Ackermann steering error.

© Dan E. Williams.



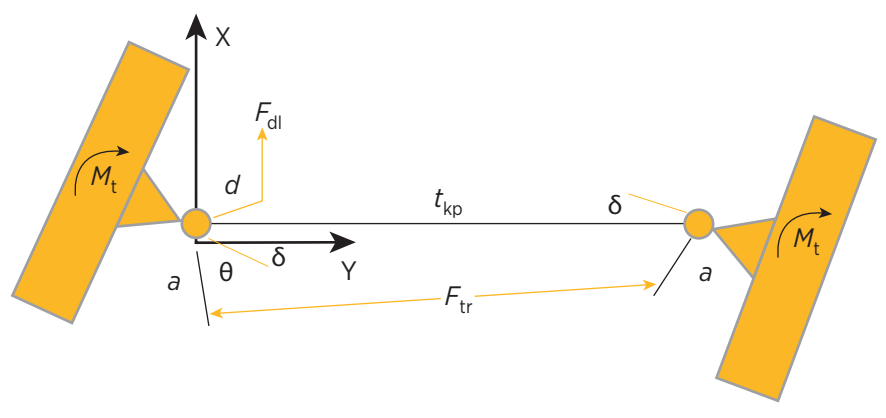
design goal is to keep Ackermann error below two degrees. The Ackermann error shown in [Figure 7.7](#) is typical, as the polynomial describing the error crosses zero in two places that can be determined by the designer. The two zero crossings are placed at straight ahead (where the vehicle spends most of its time), and near full steering input (where the steering can be in parking lot maneuvers), and there is typically an extreme value between these two zeros. The location of the zeros and the extreme value are a function of the tie-rod associated four-bar linkage. While the approximation of Eq. 7.20 is sufficient to predict performance for highway driving, a more accurate relationship should be used for actual system design.

7.3 Steering Efforts

The previous section described the geometric relationship between opposite wheels on a steered axle connected by a tie rod. Now the force required to create this displacement is developed. The vehicle is now assumed to be traveling at a significant forward speed so that when the steering wheel is turned a lateral force will be generated at the tires.

The one steered wheel input δ is on the left or driver's side. There is a moment M_t produced by lateral forces acting on each tire. There is drag link force F_{dl} , and a tie rod force F_{tr} . Moments about the left kingpin are summed.

$$aF_{tr} \sin(\theta + \delta) + M_t = F_{dl}d. \quad (7.21)$$

FIGURE 7.8 Drag link force displacing steered wheels.

© Dan E. Williams.

Likewise moments are summed about the right kingpin, assuming the moment M_t is experienced on either side of the axle.

$$aF_{\text{tr}} \sin(\theta - \delta) = M_t. \quad (7.22)$$

Equation 7.22 is solved for the tie rod force.

$$F_{\text{tr}} = \frac{M_t}{a \sin(\theta - \delta)}. \quad (7.23)$$

Equation 7.23 is inserted into Eq. 7.21.

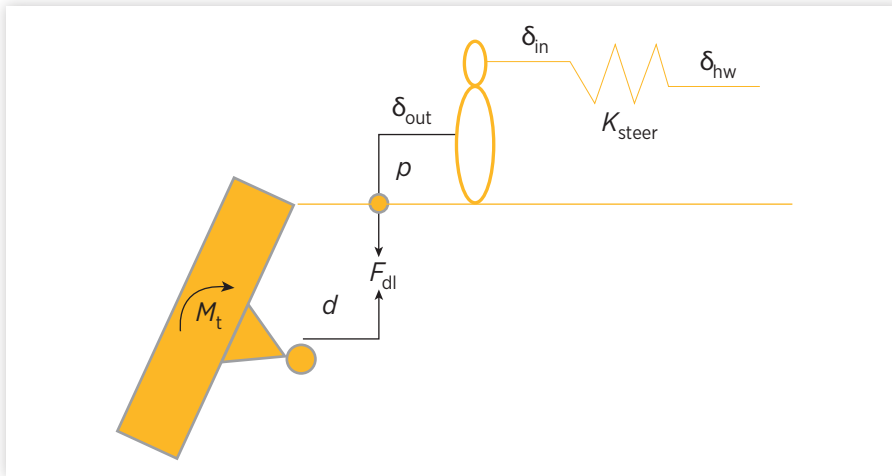
$$F_{\text{dl}} = \frac{M_t}{d} \left(1 + \frac{\sin(\theta + \delta)}{\sin(\theta - \delta)} \right). \quad (7.24)$$

Equation 7.24 describes the drag link force required to overcome the tire moments because of lateral forces. For small steer angles, the drag link force is twice the individual tire moments at each wheel divided by the lever arm d . For larger steer angles the drag link force is more than twice. This drag link force is generated by the steering system.

[Figure 7.9](#) is understood by considering that the steering system is actually rotated 90° to the plane of the drawing about the line intersecting the ball joint at the end of the pitman arm lever length p . The pitman arm is rotated by a gear

FIGURE 7.9 Drag link force from steering system.

© Dan E. Williams.



system described by output δ_{out} and input δ_{in} . The gear system is driven by the handwheel input δ_{hw} through a steering stiffness K_{steer} . The steering gearbox is characterized by a ratio of η ,

$$\eta = \frac{\delta_{\text{in}}}{\delta_{\text{out}}}, \quad (7.25)$$

where η is typically around 20 : 1 for commercial gearboxes and less for passenger cars. The efficiency ε is highly dependent upon the gear mechanism used,

$$\varepsilon = \frac{M_{\text{out}} \delta_{\text{out}}}{M_{\text{in}} \delta_{\text{in}}} \quad (7.26)$$

and can vary with direction. Typically, it is quite high—around 90%—in the forward direction, and less when the system is backdriven by road inputs. This bi-directional variability is desirable to smoothly transmit effort from the driver to the steered wheels while at the same time provide road input isolation.

The input torque to the gearbox is created by deflecting the steering stiffness.

$$M_{\text{in}} = K_{\text{steer}} (\delta_{\text{hw}} - \delta_{\text{in}}). \quad (7.27)$$

The output torque can be calculated by combining Eqs 7.25, 7.26, and 7.27.

$$M_{\text{out}} = \eta \varepsilon K_{\text{steer}} (\delta_{\text{hw}} - \eta \delta_{\text{out}}). \quad (7.28)$$

The gearbox outputs can be written in terms of wheel assembly parameters,

$$\delta_{\text{out}} = \delta \frac{d}{p} \quad (7.29)$$

where d is the drag link to kingpin lever arm and p is the pitman arm length, whose ratio is often approximately one.

$$M_{\text{out}} = p F_{\text{dl}} \quad (7.30)$$

Equations 7.29 and 7.30 are inserted into Eq. 7.28 and solved for the drag link force.

$$F_{\text{dl}} = \frac{\eta \varepsilon K_{\text{steer}}}{p} \left(\delta_{\text{hw}} - \delta \frac{\eta d}{p} \right). \quad (7.31)$$

Equation 7.31 is the drag link force “from above” and can be equated with Eq. 7.24, the drag link force “from below.”

$$\delta_{\text{hw}} = \frac{M_t p}{d \eta \varepsilon K_{\text{steer}}} \left(1 + \frac{\sin(\theta + \delta)}{\sin(\theta - \delta)} \right) + \delta \frac{\eta d}{p}. \quad (7.32)$$

Equation 7.32 relates the handwheel input to the tire moment and steered wheel input. Equation 7.32 contains the steered wheel input δ that must be eliminated through its relationship to M_t .

When a vehicle is going around a circle of radius R with a forward speed u , it completes one revolution in the time calculated by the forward speed divided by the circumference. In completing this cycle, not only has the center of gravity of the vehicle moved around the circle, but also the vehicle itself has rotated once. Therefore the yaw rate r can be calculated from the radius of turn and forward speed.

$$R = \frac{u}{r}. \quad (7.33)$$

From the single-track average of [Figure 7.3](#), the Ackermann relationship in Eq. 7.4 relates the steered input of the front wheels to the wheelbase and radius of turn. Equation 7.4 is combined with Eq. 7.33.

$$\delta = \frac{l}{u} r. \quad (7.34)$$

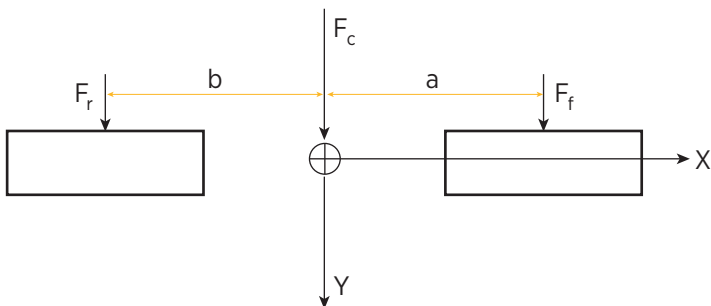
Equation 7.34 is a restated version of the Ackermann relationship introduced in Eq. 7.4. This relationship was derived under assumptions of negligible speed and therefore negligible lateral acceleration. It will be shown in later work that this relationship is also characteristic of “ideal” vehicle handling at high speeds. Therefore, Eq. 7.34 can be used as an ideal approximation for the steering input in Eq. 7.32.

Equation 7.34 can be rewritten in another very useful form.

$$\frac{r}{\delta} = \frac{u}{l}. \quad (7.35)$$

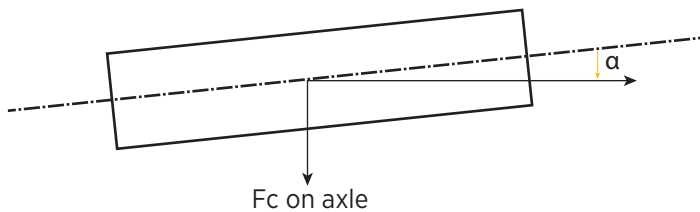
Equation 7.35 expresses the ratio of yaw rate to steering input and is called the yaw rate response. Its units are radians per second per radian, or simply inverse seconds, and when a vehicle has ideal Ackermann steering this yaw rate response is the ratio of the vehicle forward speed to wheelbase. Yaw rate is thus a response to the steering input. Yaw rate response will be shown later to be the fundamental transfer function that characterizes vehicle handling. Equation 7.34 allows us to write the steered wheel input in Eq. 7.32 as a ratio of vehicle parameters, but Eq. 7.32 still contains the tire moment M_t that is not quantified and further assumptions are required.

FIGURE 7.10 Centrifugal forces acting on tires.



Reprinted with permission from © SAGE Publications.

When a vehicle is making a constant radius turn at a constant forward speed, the vehicle is in a steady-state condition. There is said to be a centrifugal force based on the vehicle's mass, the forward speed, and the radius of turn (or yaw rate). Recall prior kinematic analysis assumed negligible centrifugal force. In the present condition, vehicle is performing a constant speed fixed radius turn and thus develops a centrifugal force.

FIGURE 7.11 Centrifugal force acting on rolling tire.

Reprinted with permission from © SAGE Publications.

The centrifugal force acting on the center of mass of the vehicle is decomposed into lateral force acting on each axle as shown in [Figure 7.10](#). In discussing conventions care must be taken with the signs of the variables. Positive centrifugal force acting on the center of mass of the vehicle is decomposed into two positive forces acting at the axles. It is important to note that rotations in the plane of [Figure 7.11](#) are positively defined to the right, in a clockwise direction. The centrifugal force F_c is assumed to be split between the front and the rear axles,

$$F_c = F_{c,f} + F_{c,r}, \quad (7.36)$$

while in the steady-state turn there is no net yaw moment as there is no yaw acceleration,

$$0 = aF_{c,f} - bF_{c,r}, \quad (7.37)$$

where a is the absolute distance between the front axle and the center of mass, b is the absolute distance between the rear axle and the center of mass, $F_{c,f}$ is the positively defined lateral force generated by the two tires on the front axle, and $F_{c,r}$ is the positively defined lateral force generated by the two tires on the rear axle. From Eqs 7.36 and 7.37, the steady-state lateral forces the vehicle experiences at each axle can be written as functions of the centrifugal force on the vehicle and axle locations.

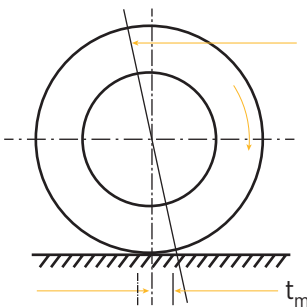
$$F_{c,f} = \left(\frac{b}{a+b} \right) F_c, \quad (7.38)$$

$$F_{c,r} = \left(\frac{a}{a+b} \right) F_c \quad (7.39)$$

Recall $a + b$ is the wheelbase l .

FIGURE 7.12 Mechanical trail.

© SAE International.



When steered, the front wheels actually rotate about a kinematically constrained axis that is usually not exactly vertical. This “kingpin” is inclined to the vertical axis primarily to introduce “returnability” to the steering system. The weight of the vehicle acting along the vertical axis produces a small torque about the inclined kingpin, serving to center the steered wheels. This returnability is an important characteristic of steering feel.

As shown in [Figure 7.12](#), mechanical trail t_m can be defined as the distance between the center of the tire, where the lateral force from the road is assumed to act, and the intersection of the kingpin axis and the road. Based on how the rubber in the tire deforms, the actual lever arm is lengthened by a term known as the pneumatic trail. Using small angle approximations, the lateral force on the tire creates a rotating moment about the kingpin.

$$M_t = t_m F_{c,f}. \quad (7.40)$$

The centrifugal force in [Figure 7.10](#) can be written as

$$F_c = mur. \quad (7.41)$$

Equation 7.32 can be rewritten assuming small steering inputs,

$$\delta_{hw} = \frac{2M_t p}{d\eta\varepsilon K_{steer}} + \delta \frac{\eta d}{p} \quad (7.42)$$

and Eqs 7.38, 7.40, and 7.41 can be inserted,

$$\delta_{hw} = \frac{2pt_m b mur}{d\eta\varepsilon K_{steer} l} + \delta \frac{\eta d}{p} \quad (7.43)$$

and using the ideal Ackermann relationship of Eq. 7.34.

$$\delta_{hw} = \left(\frac{2pt_m bmu}{d\eta \varepsilon K_{steer} l} + \frac{\eta dl}{pu} \right) r. \quad (7.44)$$

Eq. 7.44 can be solved in terms of handwheel yaw rate response.

$$\frac{r}{\delta_{hw}} = \frac{u}{\frac{d\eta l}{p} + \frac{2pt_m b}{d\eta \varepsilon K_{steer} l} mu^2}. \quad (7.45)$$

Equation 7.45 is immediately compared to the yaw rate response of Eq. 7.35 and provides significant insight into the physical properties of vehicle handling. Fundamentally, there are two terms in the denominator. One is dependent only upon vehicle parameters. The other is a function of the velocity squared and vehicle mass, which can be thought of as the vehicle energy. If the mechanical trail—the lever arm that lateral force acts through—goes to zero, the yaw rate response dependence upon the vehicle energy goes to zero.

Without the denominator dependence upon vehicle energy, Eq. 7.45 can be compared with the ideal Ackermann relationship of Eq. 7.35. If the two lever arms d and p are equal, and if the gear ratio η is one, Eq. 7.45 reverts to Eq. 7.35. So without the dependence on energy, the yaw rate response is the Ackermann relationship scaled by gear ratios.

Quite a number of parameters in addition to the mechanical trail can have an impact on the effect of vehicle energy on yaw rate response. The ratio of the lever arms and the gear ratio reduce the dependence on energy, as well as gear efficiency. An increased front weight bias increases the dependence on energy, and an increased steering stiffness decreases it.

As the dependence upon vehicle energy increases, the overall yaw rate response decreases as speed increases. Because the yaw rate response is decreased, the driver has to input more handwheel displacement for the vehicle to achieve a desired yaw rate. Simply said, in this condition the faster a given vehicle is moving, the more the driver must steer. This condition is known as “understeer.”

As seen in [Figure 7.8](#), this understeer occurs because the tire moment resulting from lateral acceleration in a turn winds up the steering compliance. It is important to develop an intuitive understanding of the physics captured in Eq. 7.45. As the centrifugal force grows, its lateral reaction on the front tires grows. This lateral reaction force works through various lever arms and gear ratios to require a handwheel torque. The handwheel torque winds up the steering compliance. The more the steering compliance is compressed, the more the handwheel needs to be turned to achieve a specific steered road wheel

position. This phenomenon can be exaggerated by different vehicle parameter values, but the basic mechanism remains.

Other sources of understeer will be developed in future chapters, but the driver's sensation will be the same. Therefore, to orient the front wheels properly in order to generate the centrifugal force that is required for a given vehicle trajectory and speed, the handwheel displacement must grow. This sensation felt by the driver, is what the vehicle dynamicist refers to as "understeer." The more compliant the steering system, the more the steering input must increase with vehicle speed for a given maneuver. All mechanical linkage trains will have some compliance. Most modern vehicles have power steering systems. Whether hydraulic or increasingly electric, power steering systems have sensors that determine steering torque by measuring the displacement of a known torsion bar. This compliance is a significant source of understeer.

The yaw rate response, first seen in Eq. 7.35, and revisited in a more complex form in Eq. 7.45, will be used repeatedly throughout the discussion of vehicle handling. The two terms in the denominator of Eq. 7.45 are defined by vehicle parameters and can be thought of as the vehicle's "wheelbase" and "understeer."

Steering systems are quite interesting as a confluence of vehicle dynamics and human factors. Simply stated, the human driver inputs a torque to the handwheel, but the vehicle responds to handwheel displacement, as shown in the yaw rate response. The steering system provides the mapping from handwheel torque to handwheel displacement. In parallel with this mapping from the steering system, the human driver proprioceptively closes a feedback loop between handwheel torque and handwheel position. These parallel relationships between handwheel torque and position determine the somewhat murky concept of "steering feel."

On-center steering feel is generally determined by nonlinearities in the mechanical steering linkage. Away from center feel is determined by axle geometry and power steering characteristics. An excellent analysis of power steering assist feel has been performed by Shapiro et. al. [2], and in the past few years artificial steering feel has been available [3]. Steering feel is a fascinating topic, but for the purposes of vehicle dynamics handwheel displacement can be considered the vehicle input. Most devices employed to modify steering feel increase steering system compliance, with an effect on the balance of the vehicle.

7.4 Slip Angles

Dean Karnopp provides a good description of how centrifugal force deforms the rolling tire to create a "slip angle."

"A tire mounted on a wheel subjected to no lateral force at all will generally roll along a surface in the direction the wheel is pointed . . . If now a small lateral force is applied to the wheel (axially), a corresponding lateral force will arise in the contact patch between the tire and the road surface due to friction . . . It will no longer be the case that the wheel continues to move in the direction it is pointed. Rather it will acquire a sideways or lateral velocity in addition to its forward velocity. Thus the total velocity vector of the wheel will point in a different direction than the direction of the center plane of the wheel. This angle between the wheel and the direction the wheel moves . . . is called the slip angle." [4]

Karnopp's description can be put into the context of this work. Equations 7.38 and 7.39 derived earlier represent the portion of the centrifugal force in the steady-state turn that is seen by the front and rear tires, respectively, through lateral forces transmitted by the suspension. When a positive lateral force is applied to the rolling tire (a component of the steady-state centrifugal force on the turning vehicle) there is a positive lateral velocity component of the tire as shown in [Figure 7.11](#). The lateral forces acting on the tire create a small lateral velocity, allowed and yet limited by compliance in the rubber tires. With the addition of this lateral force, the tire no longer rolls in the direction of its center line but is offset by the mechanism described by Karnopp. The vector result of this small lateral velocity in the direction of the centrifugal force, and the larger constant forward velocity of the vehicle combine to form the velocity vector of the tire. Slip angle is defined as the difference between the velocity vector and centerline of the tire.

A positively defined lateral (centrifugal) force creates a positively defined slip angle. So the slip angle must be defined as the velocity vector minus the angle of the centerline of the tire. Thus the velocity vector is the reference of the slip angle. It is important to realize that the tires are not truly slipping or sliding across the pavement. As the tires roll in the presence of a lateral force the tire deforms, and this deformation allows a small lateral velocity. The term "slip angle" does not clearly describe this deformation.

A simple linear tire model assumes that the slip angle can be found by multiplying the lateral force on the tire by the compliance, with compliance being the inverse of stiffness.

$$\alpha_f = \frac{1}{C_f} F_{c,f}, \quad (7.46)$$

$$\alpha_r = \frac{1}{C_r} F_{c,r}, \quad (7.47)$$

where C_f and C_r are the conventional cornering stiffnesses of the tires on the front and rear axles respectively. Thus, the cornering stiffness of a tire can be

thought of as the stiffness that a positively defined centrifugal force on the vehicle pushes into to generate a positively defined slip angle displacement, and therefore the stiffness term is positive. This slip angle definition is carried forward to the derivation of the conventional model.

Equations 7.38 and 7.39 are combined with Eqs 7.46 and 7.47.

$$\alpha_f = F_c \left(\frac{b}{a+b} \right) \frac{1}{C_f}. \quad (7.48)$$

$$\alpha_r = F_c \left(\frac{a}{a+b} \right) \frac{1}{C_r}. \quad (7.49)$$

Expressed more conventionally, the lateral force applied to the tires from centrifugal force in a steady-state turn equals the slip angle multiplied by the cornering stiffness. An interesting observation is made if Eq. 7.48 is equated with Eq. 7.49 yielding a condition that insures that front and rear slip angles are equal.

$$aC_f = bC_r. \quad (7.50)$$

When Eq. 7.50 is satisfied, and the slip angles at the front and the rear are equal, the vehicle is said to be “neutral steering.” One can extrapolate that when the slip angles are greater at the front, more steering input is required, and the vehicle is said to be understeering, and conversely if the slip angles are greater at the rear then it is called “oversteering.” As will be later shown, neutral steering results in a simple (and surprisingly familiar) relationship between steering input and yaw rate. Furthermore, as earlier mentioned tire wear is a higher order exponential function of slip angle, therefore a neutral steering vehicle will exhibit less overall tire wear [1].

It can be seen in [Figures 7.9](#) and [7.11](#) that a positively defined centrifugal force F_c produces a positively defined slip angle α . Centrifugal force creates a velocity vector at the tires out of the plane of the tire in the direction of the centrifugal force.

The preceding development shows generally how the centrifugal force in a steady-state turn results in slip angles at the tires. Although the axis and signs have been precisely defined, this development lacks the required rigor to be a model useful for quantitative analysis of the dynamic vehicle system. It has used forces, deflections, and stiffness, but not Newton’s second law.

In fact, the previous development is wrong when the vehicle is treated as a dynamic system. In steady-state one can consider the input of the system to be the centrifugal force. As we will see shortly, in a properly defined dynamic system the input is the steer angle, and the resulting accelerations in a rotating

reference frame, include a centripetal acceleration term that is commonly referred to as a centrifugal force when algebraically moved across the equation. This mixing of centripetal acceleration and “phantom” centrifugal force is a source of historical confusion in the vehicle dynamics literature and elsewhere.

7.5 Tire Forces

It has been previously established that the centrifugal force experienced by the vehicle in a turn is reacted by lateral forces on the tire. These forces are produced by adhesion between the tire and road as the rolling tire experiences an axial component of centrifugal force. The overall limit to the adhesive tire force is determined by the weight of the vehicle and the coefficient of friction between the tire and the road. Recalling Eq. 7.41 this limit can be written,

$$m u r < m g \mu, \quad (7.51)$$

where g is the acceleration because of gravity, and μ is the coefficient of friction. Equation 7.51 can be simplified,

$$\frac{u r}{g} < \mu \quad (7.52)$$

to yield the important result that the centrifugal force of the vehicle in g 's is limited by the coefficient of friction between the tires and the road. Sticky tires and adhesive road surfaces allow high centrifugal forces, and slippery tires and roads do not.

In haste to cancel the mass m on either side of Eq. 7.51, an important concept in physics is neglected. On the left side, mass is used in the context of Newton's second law, as a resistance to the acceleration of force. On the right side, mass is used as an element of weight influenced by gravity. Galileo was perhaps the first to wonder at these two magnificent seemingly independent characteristics of mass. Galileo found experimentally that acceleration of a test mass because of gravity is independent of the mass being accelerated. This is referred to as “weak equivalence.” Einstein's theory of general relativity provides a seeming irrefutable hypothesis explaining this coincidence as mass distorts space and leads to an acceleration. If this acceleration is constrained it is perceived as a force. This is said to be “strong equivalence.” Newton, in addition to Galileo and Einstein, are the three most influential physicists, and as stated earlier, vehicle dynamics is really just Newton's second law applied to vehicles. It is notable that we can appreciate Galileo, Newton, and Einstein as we consider vehicle dynamics.

Eq. 7.51 states that lateral accelerations are limited by tire adhesion. In fact longitudinal accelerations are similarly limited by tire adhesions, as are the vector sums of lateral and longitudinal forces. Thus if lateral accelerations are plotted on a horizontal axis and longitudinal accelerations on the vertical, these accelerations are contained within a circle whose radius is defined by the coefficient of friction between the tire and the road. In an overall sense, it is the job of a race car driver to maintain operation on the boundary of this friction circle, always getting the maximum out of the tires. The actual job of the race car driver is much more difficult, however, as in reality each tire has its own friction circle, that grows or shrinks with weight transfer [5,6]. This task is further complicated by other vehicles on the track constraining the correct line.

In the previous section, Eqs 7.5 and 7.6 show how slip angles are produced when the vehicle experiences a centrifugal force, as a result of the tire deforming. When the tire experiences a lateral force on its axle as it turns, the sidewall deforms, and allows a lateral velocity. The deformation is caused because the axial force derived from the centrifugal force is reacted against an opposing lateral force exerted by the road on the contact patch of the tire, and as the tire spins the sidewall is relaxed until it nears the contact patch, is deformed as it rotates through the contact patch, and resumes its undeformed state as it leaves the contact patch.

It stands to reason that if the centrifugal force is small, the deformation will be small, and if it is larger the deformation will grow. In fact for small forces the relationship is linear, as shown in Eqs 7.5 and 7.6, and the constant of proportionality is the cornering stiffness. It is interesting to note that this relationship between slip-angle and force depends on an instantaneous static adhesion between the tire and the road at the contact patch. Thus in a strange and unfortunate irony, the slip angle concept is invalid when slip occurs.

A positive axial force on the spinning tire results in a positive slip angle. But the axial force is opposed by the force the road exerts on the tire. It is this force that the road exerts on the tire that is relevant to the directional behavior of the vehicle. Early on people thought a positive centrifugal force produced a positive slip angle, and the positive centrifugal force was reacted against the road. In a proper vehicle dynamics model it will soon be shown that slip angles created by driver input produce lateral forces at the tires, and these lateral forces result in centripetal acceleration rather than caused by centrifugal force. Because this lateral tire force is opposite to the centrifugal force, the relationship between this lateral tire force and the slip angle is opposite. A negative slip angle is multiplied by a negative cornering stiffness to yield a positive lateral force on the vehicle at the tires and to create an apparent negative centrifugal force.

The reader should not worry if all these sign changes are confusing—they are and have been for decades. In future chapters a more intuitive convention will be used. But it is important to respect that the slip angle convention as now presented is commonly used and is the SAE standard [7].

Tire models more complicated than the linear relationship between slip angle and lateral force are possible. The linear relationship will be used through most of this work as it allows linear analysis techniques to be used, and stability to be simply studied. Analysis and synthesis are both required activities in engineering, and this work presents analysis techniques to support basic conceptual synthesis. As design concepts are refined in future iterations, the analysis techniques necessarily become more precise, and at some point the linear tire model needs revised. The linear tire model is accurate under constant loading and a few degrees of slip angle, but as loads change and slip angles are greater, more precise models are needed to predict absolute performance [8]. An important nonlinearity we have already seen in passing is that the tire stiffness is nonlinearly dependent upon tire normal force allowing handling to be affected by roll moment distribution.

7.6 The Conventional Bicycle Model

The general concepts discussed in the last section will be formalized. We have already just met Galileo and Einstein. In between was Newton. As was seen in the previous section on ride, vehicle dynamics is really nothing more than Newton's second law applied to vehicles. There are many vehicle dynamics texts that formally derive the yaw-plane model, none better than J.R. Ellis [9]. At this point, we will proceed with a less formal derivation of the simple yaw plane model that is consistent with accepted conventions. Lateral forces on the tires from the road at the front and rear of the vehicle are opposed to the centrifugal force and the difference accelerates the car laterally,

$$m\dot{v} = F_f + F_r - mur, \quad (7.53)$$

where m is vehicle mass, u is longitudinal velocity, r is yaw rate, and v is lateral velocity which once differentiated yields lateral acceleration.

Similarly, the lateral tire forces provide a yawing moment about the center of vehicle mass,

$$I_z \dot{r} = aF_f - bF_r, \quad (7.54)$$

where I_z is the yaw moment of inertia. Because the assumed centrifugal force acts on the center of gravity of the vehicle, it has no direct effect on the yaw moment summation.

The conventional yaw rate model assumes that an opposing lateral force is produced by a slip angle at the tire. As before the slip angle is defined as the difference between the direction the tire is moving and the direction it is

pointing. Stated precisely, it is the angle of the velocity vector minus the orientation of the tire with respect to the body fixed coordinate frame consistent with [Figure 7.11](#). For the rear tire this is easy, as the inclination is zero. Using small angle approximations,

$$\alpha_r = \frac{v - br}{u}, \quad (7.55)$$

where α_r is the slip angle of the rear tires. The overall vehicle has a “slip angle” of the lateral velocity v divided by the forward velocity u , but at the rear of the vehicle the slip angle of the wheels is increased by its yaw rate. The front slip angle is a bit more complicated. The front slip angle is increased by yaw rate. The steering input forms a reference that must be subtracted from the angle of the velocity vector,

$$\alpha_f = \frac{v + ar}{u} - \delta, \quad (7.56)$$

where α_f is the front slip angle and δ is the front steering input. Thus the conventionally defined slip angle is the steering input (the input to the control system) subtracted from the velocity vector (the system response to the input). Using a linear tire model, lateral force produced by the road on the tires is proportional to the slip angles,

$$F_f = C_f \alpha_f, \quad (7.57)$$

$$F_r = C_r \alpha_r. \quad (7.58)$$

It is tempting to relate Eqs 7.57 and 7.58 to Eqs 7.46 and 7.47 of the previous section. This is misleading. Equations 7.46 and 7.47 relate slip angles to positively defined centrifugal force that has been distributed to the two axles. Equations 7.57 and 7.58 define the lateral force produced at the axles by a slip angle of the tires. In steady state, the summation of the lateral force generated by the axles and the centrifugal force is zero. Only if the lateral acceleration in Eq. 7.53 is zero can Eq. 7.57 and Eq. 7.58 compare with Eq. 7.46 and Eq. 7.47.

It is important to distinguish this result from the previous section. Equations 7.38 and 7.39 identify a positively defined force on each axle that is derived from the overall steady-state centripetal force acting at the center of gravity of the vehicle. Equations 7.46 and 7.47 derive a positively defined slip angle of tires on each axle as a function of the positively defined centrifugal force of the vehicle. But that positive external force is balanced by an opposing

negative tire force. A positive centrifugal force on the vehicle creates a positive slip angle. But that positive slip angle creates a negative force on the tire from the road. Conversely, a negative slip angle creates a positive force on the tire from the road. Therefore, in the conventional model, the cornering stiffness must be negative.

Equations 7.57 and 7.58 can be inserted into Eq. 7.53, where C_f and C_r are often referred to as the cornering stiffness, which has just been shown to be negative.

$$\dot{v} = \left(\frac{C_f + C_r}{mu} \right) v + \left(\frac{aC_f - bC_r}{mu} - u \right) r - \frac{C_f}{m} \delta. \quad (7.59)$$

Similarly, Eqs 7.57 and 7.58 can be inserted into Eq. 7.54.

$$\dot{r} = \left(\frac{aC_f - bC_r}{I_z u} \right) v + \left(\frac{a^2 C_f + b^2 C_r}{I_z u} \right) r - \frac{aC_f}{I_z} \delta. \quad (7.60)$$

From [Figures 7.9](#) and [7.11](#), it is intuitively obvious that a positively defined front axle steering input should result in both a positive lateral velocity, and a positive yaw rate. The only way this can be achieved in Eqs 7.59 and 7.60 is if the cornering stiffness C_f is negative. Using Eqs 7.59 and 7.60, a steady-state relationship between steering input δ and yaw rate r can be found. It was earlier suggested that this yaw rate response is of fundamental importance to characterize vehicle handling.

$$\frac{r}{\delta} = \frac{u}{(a+b) + (mu^2) \frac{(aC_f - bC_r)}{C_f C_r (a+b)}}. \quad (7.61)$$

Equation 7.61 is a very useful product of the bicycle model that can parsimoniously characterize handling, both theoretically and experimentally. The summation of a and b are immediately recognized as the overall vehicle wheelbase, or the distance between the front and rear axles. If the quantity $(aC_f - bC_r)$ is zero, Eq. 7.61 is highly simplified, and the ratio of yaw rate to steer angle is simply the ratio of forward speed to wheelbase. This is often referred to as Ackermann steering, or neutral steering and was identified by Eq. 7.50 of the preceding section providing equal slip angles front and rear.

Equation 7.61 is the ratio between the yaw rate and steer angle. As such, yaw rate is the response to a steering input. The second term in the denominator

of Eq. 7.61 can be thought of as capturing the energy of the vehicle multiplied by a term composed of tire cornering coefficients and mass distribution. One must remain mindful that the cornering coefficients are actually negative in the conventional model. So when precisely considering signs, if $aC_f - bC_r$ is positive then the denominator will grow with vehicle energy, and the yaw rate response to steering input will decrease. If $C_f = C_r$ (i.e., the same tires throughout the vehicle), then this condition occurs when $b > a$, or the weight is biased toward the front. This situation is known as understeer. The opposite situation is known as oversteer, when the yaw rate response increases with vehicle energy. Because yaw rate is the fundamental response to steering input, an oversteering vehicle seems more sensitive to the driver at higher speeds. Variations of Eq. 7.61 are well known in vehicle dynamic literature and are generally accepted to capture fundamental handling characteristics of vehicles through the understeer term.

It is interesting to compare the yaw rate response to the road wheel steer angle of Eq. 7.61 with the previously defined yaw rate response to handwheel angle of Eq. 7.45. Clearly, the handwheel steer angle is related to the road wheel steer angle through the equations developed for the steering linkage. Both sides of Eq. 7.43 can be divided by yaw rate.

$$\frac{\delta_{hw}}{r} = \frac{2pt_m bmu}{d\eta \varepsilon K_{steer} l} + \left(\frac{\delta}{r} \right) \frac{\eta d}{p}. \quad (7.62)$$

Equation 7.61 can be inserted into Eq. 7.62,

$$\frac{\delta_{hw}}{r} = \frac{2pt_m bmu}{d\eta \varepsilon K_{steer} l} + \left(\frac{l + (mu^2) \frac{(aC_f - bC_r)}{C_f C_r l}}{u} \right) \frac{\eta d}{p} \quad (7.63)$$

and simplified.

$$\frac{r}{\delta_{hw}} = \frac{u}{\frac{d\eta}{p} l + \left(\frac{2pt_m b}{d\eta \varepsilon K_{steer} l} + \frac{d\eta (aC_f - bC_r)}{p C_f C_r l} \right) mu^2}. \quad (7.64)$$

Equation 7.64 is quite interesting. The understeering term of Eq. 7.45 because of steering compliance adds to the understeering term of Eq. 7.61 because of slip angles, to yield an overall sensitivity of the yaw rate response at the handwheel

to vehicle energy. The first term, dependent upon steering compliance, is always positive, meaning that the driver will have to input more steer angle as vehicle energy grows, to achieve a desired yaw rate. The second term, dependent upon tire cornering stiffness and weight distribution, can be positive or negative. Therefore, steering compliance can neutralize some amount of oversteer from the tires and weight distribution.

To summarize the progress so far, slip angles were originally defined as the proportional response of the tires to a steady-state centrifugal force. In a rigorously defined dynamic model, the lateral forces generated by the tire oppose the centrifugal force. Therefore, the tire stiffness is negative. A positively defined slip angle produces a negatively defined external lateral force on the tire that is transferred to the vehicle. If this discussion of positive and negative slip angles and tire coefficients seems confusing—that's because it is. We will now start to see that confusion more clearly. Equations 7.17 and 7.18 can be put into block diagram form.

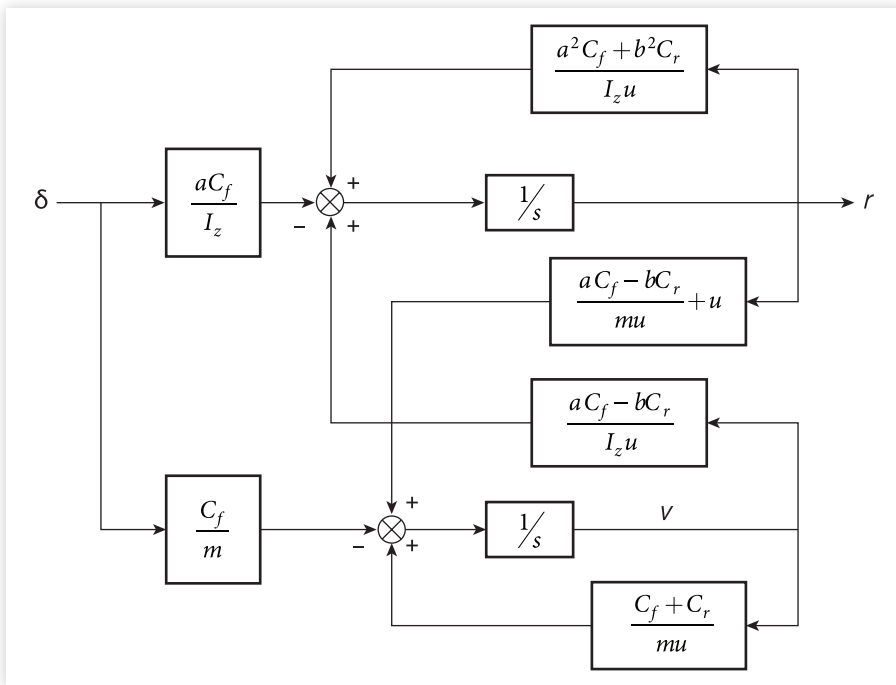
[Figure 7.13](#) is extremely interesting as it reveals several issues with the conventional model apparent to the control theorist. [Figure 7.13](#) shows the equations in block diagram form, both a representation of and to a certain extent a mathematical tool for general dynamic systems and particularly control systems. It clearly preserves the notion expressed in the classic steady-state Eq. 7.61 that yaw rate is a response to steering input. The general dynamics are seen to be two coupled first-order differential equations. Quite interestingly, the coupling is dependent upon the term that determined the steady-state understeer/oversteer properties of the vehicle. If the vehicle is neutral steering, the first-order dynamic systems are minimally coupled. The centripetal term ur provides a “force” causing a lateral velocity, but in this neutral steer condition the lateral velocity has no effect on the yaw rate. And recall the relationship between yaw rate and steer angle is the primary characterization of vehicle handling. In this way the dynamic system of [Figure 7.13](#) shows that in an ideal case (aka neutral steer) the yaw rate is determined simply as a first-order dynamic lag of the steering input, similar to the steady-state yaw rate gain of Eq. 7.61.

From a control systems standpoint the block diagram of the conventional yaw plane shown in [Figure 7.13](#) is unconventional. The input steer angle is subtracted from the feedback yaw rate, as opposed to the classic control system error formed by the feedback subtracted from the command. This occurs because the cornering stiffnesses of Eqs 7.57 and 7.58 are negative. Recall that these terms were negative because a positively defined slip angle in the tire produces a negatively defined lateral force. It is interesting to note that in [Figure 7.13](#) every signal—feedback and coupling—is multiplied by the tire stiffness terms. Because of this negative tire stiffness term, the unconventional block diagram is stable, and a positive steer angle results in a positive yaw rate.

The problem with [Figure 7.13](#) was injected at the start of the modeling process described above. Because early vehicle modeling treated the vehicles

FIGURE 7.13 Conventional yaw plane block diagram.

Reprinted with permission from © SAGE Publications.



response to steady-state centrifugal force, a positively defined lateral acceleration produced a positively defined slip angle. The very nomenclature reveals this thought process. The deformable tires are said to “slip” in response to a lateral force. When this phenomenon is preserved in a more formal system, it creates the confusing and unconventional block diagram of [Figure 7.13](#) that is objectionable to control theorists. The confusion occurs as slip angles are defined as a response to centrifugal force producing a negatively defined lateral force. In rigorous development attack angles cause lateral forces on the tire.

7.7 Summary

This chapter is actually a quick review of the conventional yaw plane kinematics and dynamics state of the art. This model has proven to be very useful for two-axle handling analysis, particularly in steady state. The yaw rate response characterizes steady-state handling with two parameters: a wheelbase term and an understeer term. These terms are easily obtained either through theory or experiments in steady-state cornering. Maurice Olley famously said that steady-state cornering tests “mean pretty much everything if we will just take

the trouble to interpret them.” To a large degree steady-state parameters determined on a vehicle dynamics pad characterize vehicle handling.

This chapter developed several basic concepts that will be important throughout following chapters as both complications and mathematical rigor increase. Ackermann steering was introduced and used to discuss steering errors and justify a single-track approximation of the vehicle. Using the ideal Ackermann steering, the effect of a steering system including gear ratio, gear efficiency, and steering compliance was presented.

The concept of yaw rate response was introduced and will be used in future chapters as the most descriptive characterization of vehicle handling. Using the yaw rate response, the notion of vehicle understeer was presented. The effect of steering system compliance is useful to convey an intuitive notion of understeer.

The concept of slip angle at the tires was presented as the result of a vehicle experiencing centrifugal force in a turn. The lateral force at the tires reacts against the centrifugal force, therefore a negative lateral force on the tire creates a positive slip angle. In a development of yaw plane dynamics, the negative relationship between slip angle and lateral force was seen to produce multiple negative terms in the equations that subsequently cancel, and further to produce unconventional block diagrams.

The combined effect of slip angle generated lateral forces at the tires with weight distribution of a two-axle vehicle was shown to develop the same understeering effect as steering systems compliance. In fact, the two terms were shown to add together to form an overall understeer of the vehicle.

This state-of-the art development of yaw plane dynamics included two critical conventions. One, is that the center of gravity of a vehicle is between the front and rear axles, and the second is that slip angles produce negative lateral forces on the tires. New conventions will be used in future chapters, that will allow a more general vehicle dynamic model.

References

- [1] Miller, G., Reed, R., and Wheeler, F., “Optimum Ackerman for improved steering axle tire wear on trucks,” SAE Technical Paper 912693, 1991, DOI:[10.4271/912693](https://doi.org/10.4271/912693).
- [2] Shapiro, J., McLaughlin, K., and Kwon, H., “Predicting and achieving objective steering performance measures,” SAE Technical Paper 2018-01-0696, 2018, DOI:[10.4271/2018-01-0696](https://doi.org/10.4271/2018-01-0696).
- [3] Williams, D.E. “Synthetic torque feedback to improve heavy vehicle drivability,” Proc. IMechE, Part D: *J. Automobile Engineering*, 2009, 223 (D12), DOI:[10.1243/09544070JAUTO960](https://doi.org/10.1243/09544070JAUTO960).
- [4] Karnopp, Dean, *Vehicle Dynamics, Stability and Control*, CRC Press, New York, 2nd Edition, 2013.
- [5] Van Valkenburgh, Paul, “What its really like out there: The concept of friction circle tells us scientifically,” Road and Track, October 1983, p. 67–69.

- [6] Wright, Peter, "Speed Graphic: The cornering styles of three great drivers as seen by a computer," *Road and Track*, July 1984 p 50–54.
- [7] SAE J 670_200801, "Vehicle Dynamics Terminology," SAE International, Warrendale, PA, 2008.
- [8] Pacejka, Hans B., "Tire and Vehicle Dynamics," Society of Automotive Engineers, Warrendale PA, 2002.
- [9] Ellis, J.R., *Vehicle Dynamics*, Business Books, London, 1969.

Reference Frames

“ Are the laws of acceleration and of the composition of forces only arbitrary conventions? Conventions, yes; arbitrary, no—they would be so if we lost sight of the experiments which led the founders of the science to adopt them, and which imperfect as they were, were sufficient to justify their adoption.

—Henri Poincaré

8.1 Introduction

In the previous chapter, vehicle steering was analyzed in several ways. The concept of yaw rate as the primary response to steering input was introduced and will be extensively used later. The standard yaw-plane model commonly found in the vehicle dynamic literature was quickly presented. It was suggested that the confusion relating to the signs of the slip angle and cornering stiffness came from an improper formulation of the vehicle dynamics in the yaw plane, specifically in treating centrifugal force as a steady-state input, rather than considering steering as the input. Several important topics were informally presented, such as Ackermann steering and understeer, which are fundamental concepts useful throughout the discussion of vehicle handling. These concepts were developed without mathematical rigor.

Two things made the discussion of vehicle ride more directly comprehensible to the reader than this present discussion of handling. First, the reader can immediately appreciate in a general sense that interconnected masses have inherent resonances. Second, road-induced vibrations are almost always detrimental to human comfort, but humans are sensitive to well-understood frequencies, and resonances amplify certain frequencies, so the intuitive notions of ride are pretty easily correlated with quantitative rigor. A third more subtle

reason handling is less intuitive than ride, is that in general ride can be described by the second-order dynamics found when masses are supported by springs. We will see that handling fundamentals are captured in coupled first-order differential equations, which are not as intuitive as masses and springs.

The handling discussion will be less intuitive. The modeling to be developed is elegant and allows interesting things to be said about the handling behavior of vehicles. But it is more difficult to intuitively relate quantitative models of handling to our experiences in the driver seat. That is why the concept of understeer was first introduced in the previous section as caused by a mechanical compliance in the steering system. We saw a second cause of understeer in the balance of cornering stiffness, and in fact in the coming chapters we will see several more. But all can be related to that fundamental feeling of steering compliance that hopefully the reader can well intuit.

In this chapter, we will formally define reference frames, and the relationship between reference frames that are rotating. This material can be found in any good dynamics text but it is repeated here so our own nomenclature can be used (this is confusing enough without trying to follow it in different nomenclatures), and more importantly so that we can make comments in the development that will be useful later when simplifying vehicle specific assumptions are made. As a result of these assumptions, the standard yaw-plane model will appear. A reader interested in a more formal definition of vehicle reference frames is encouraged to find the classic but out of print vehicle dynamics book from Ellis [1]. After reading that book, the influence of J.R. Ellis on this present work will be obvious. This chapter does not provide the thoroughness of Ellis, but is rather intended to show enough rigor so that key assumptions can be appreciated and support an eventual extension of the reference frame to allow roll.

This development is helpful to appreciate the assumptions behind the widely used yaw-plane model. This rigor is required, however, when a vehicle is allowed to have a suspension supporting a sprung mass, thereby allowing sprung mass roll. Allowing roll in addition to yaw adds much complexity and requires rigorous definitions of reference frames. And in fact we will see that judicious use of reference frames allows key simplifications making the roll mode tractable. Most vehicle dynamics texts do not consider roll, which is a shame because many interesting compromises that occur between ride and handling are because of roll mode constraints. This benefit justifies the effort of reference frame formality.

8.2 Reference Frames in General

The whole idea of reference frames implies the question of absolute or inertial reference. This has been a question of great philosophical debate throughout

the ages. Is there such a thing as absolute motion, or is all motion relative? If motion is absolute on a cosmic scale, what is the reference? A reasonable stance is that there is no absolute motion, all motion is relative, and therefore the only thing that is absolute is a change in motion, that is, acceleration. Fortunately for us in vehicle dynamics, these questions, while interesting, are not relevant. As vehicles dynamics are concerned, not only is the Earth a stable inertial anchor, it is the most relevant interface to the vehicle via the tires. Since it is rigid any point on the earth will do for an inertial reference point.

We must approach these “philosophical” considerations out of necessity. External forces that act on the vehicle to influence its motion act according to a reference frame on the vehicle. This reference frame fixed to the vehicle is what the driver experiences. Aerodynamic forces act to oppose the instantaneous forward velocity as seen by the driver. The car’s powertrain accelerates the vehicle forward, and the brakes decelerate, as seen by the driver. The tires generate lateral forces as seen by the driver. A spectator, however, sees the vehicle from an inertially fixed reference frame.

These external forces, acting in a reference frame experienced by the driver, result in accelerations that are inertially referenced. Translational motions can be easily mapped between the reference frame of the driver fixed to the car, and an inertially fixed reference frame. These external forces can just as easily produce rotations. When rotations are considered, however, the situation becomes less clear. In the previous chapter, we considered a “centrifugal force” in a turn that creates a lateral force on the tires. As will be shown, this “centrifugal force” is actually acceleration dependent upon the product of forward velocity and yaw rate.

The general properties of motion in rotating reference frames will be developed. In general, three translational velocities are allowed: longitudinal velocity u , lateral velocity v , vertical velocity w , and three angular velocities: roll rate p , pitch rate q , and yaw rate r , which together provide six degrees of freedom for general rigid body motion. The goal of this chapter is to derive the general expressions for the right half side of Newton’s second law ($F = ma$) for each mode.

As it turns out, these general motions of a vehicle are somewhat decoupled, and this decoupling allows the incremental evolution of ride. In many useful applications, vertical velocity alone describes vehicle motion. At low speed when surface irregularities are encountered, pitch motions can be superimposed to allow the traditional Olley ride criteria in the pitch plane. It will be shown that in a handling analysis, yaw and lateral acceleration are even more tightly coupled. In many cases ride and handling (and also the longitudinal dynamics of acceleration and braking) can be independently considered. This is to say, the combination of heave and pitch (ride) can be largely decoupled from the combination of lateral velocity and yaw (handling). This decoupling is possible both from the dynamics of the system and its inputs. Roll creates a problem,

as this mode is rightfully considered in both ride and handling studies. It is the eventual inclusion of the roll mode into the handling model of the tightly coupled yaw and lateral acceleration that requires this more formal treatment, but along the way we will develop an appreciation for the common yaw-plane or bicycle model.

8.3 Velocity of a Point Translating in a Rotating Reference Frame

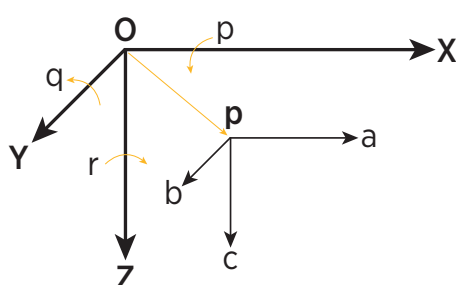
Figure 8.1 shows a point p that is moving with respect to a rotating reference frame. The reference frame is rotating about the X-axis with angular velocity p , about the Y-axis with angular velocity q , and about the Z-axis with angular velocity r . Eventually, this rotating reference frame will be fixed to the body of a vehicle, so that p will be recognized as roll, q as pitch, and r as yaw. We are interested in the motion of point p . Point p is located relative to the rotating reference frame XYZ by coordinates x , y , and z in the appropriate directions. Relative to the reference frame XYZ point p is translating with velocity a along X, b along Y, and c along Z. Thus the velocity of point p in an inertially grounded reference frame can be described as a function of the rotation of the reference frame, its location relative to the rotating reference frame, and its velocity relative to the rotating frame. The velocity of point p in a nonrotating reference frame whose origin coincides with the rotating reference frame XYZ in the X direction is:

$$u = a - ry + qz \quad (8.1)$$

and in the Y direction,

$$v = b - pz + rx \quad (8.2)$$

FIGURE 8.1 Point translating in rotating reference frame.



and in the Z direction.

$$w = c - qx + py. \quad (8.3)$$

So, if an inertially grounded observer was standing at point O , the velocity in the X direction would be given by Eq. 8.1, the Y direction Eq. 8.2, and the Z direction Eq. 8.3. From [Figure 8.1](#), the reader can see that a positive rotation r about the Z -axis multiplied by a positive displacement y along the Y -axis will result in a negative movement of p along the X -axis. Similarly, a positive rotation q about the Y -axis multiplied by a displacement z along the Z -axis yields a positive motion of p along the X -axis. So the velocity of p along any axis relative to an inertially grounded observer is the velocity along that axis in the rotating reference frame, plus rotations about the other two axes multiplied by the appropriate lever arms. This general formulation can be verified in Eqs 8.2 and 8.3.

8.4 Velocity and Acceleration of a Point in a Translating and Rotating Reference Frame

Now the rotating reference frame shown in [Figure 8.1](#) is allowed to translate in directions X , Y , and Z with velocities U , V , and W , respectively, as shown in [Figure 8.2](#).

As the rotating reference frame now translates, to the inertially fixed observer the motion of point p is simply the translational motion of the reference frame added to the previously calculated motion of p in Eqs 8.1, 8.2, and 8.3.

$$u = U + a - ry + qz, \quad (8.4)$$

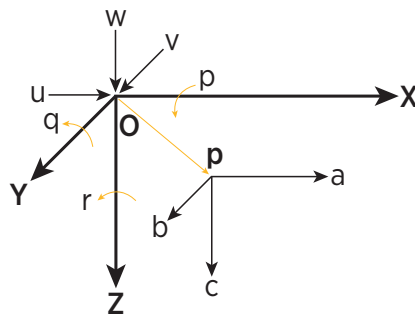
$$v = V + b - pz + rx, \quad (8.5)$$

$$w = W + c - qx + py. \quad (8.6)$$

Equations 8.4, 8.5, and 8.6 are general equations describing the velocity of an arbitrary point p that is moving in a translating and rotating reference frame. Now, we are concerned about a point p that is part of a rigid body (perhaps a vehicle) on which the rotating and translating reference frame is attached. Since the body is rigid, there is no relative motion between points on the body, and therefore no relative motion between p and the origin of the rotating and translating frame. With this condition [Figure 8.2](#) is simplified.

FIGURE 8.2 Point translating in a rotating and translating reference frame.

© Dan E. Williams.



In this special case, Eqs 8.4, 8.5, and 8.6 can be simplified.

$$u = U - ry + qz, \quad (8.7)$$

$$v = V - pz + rx, \quad (8.8)$$

$$w = W - qx + py. \quad (8.9)$$

Time derivatives of the velocities in Eqs 8.7, 8.8, and 8.9 can be formed.

$$\dot{u} = \dot{U} - r\dot{y} - \dot{r}y + q\dot{z} + \dot{q}z, \quad (8.10)$$

$$\dot{v} = \dot{V} - p\dot{z} - \dot{p}z + r\dot{x} + \dot{r}x, \quad (8.11)$$

$$\dot{w} = \dot{W} - q\dot{x} - \dot{q}x + p\dot{y} + \dot{p}y. \quad (8.12)$$

The time derivative of p in the X direction has already been found in Eq. 8.7,

$$\dot{x} = u = U - ry + qz, \quad (8.13)$$

and similarly for the time derivative in the Y direction,

$$\dot{y} = v = V - pz + rx \quad (8.14)$$

and the Z direction.

$$\dot{z} = w = W - qx + py. \quad (8.15)$$

Equations 8.13, 8.14, and 8.15 can be inserted into Eqs 8.10, 8.11, and 8.12.

$$\dot{u} = \dot{U} - rV + qW - (q^2 + r^2)x + (qp - \dot{r})y + (rp + \dot{q})z, \quad (8.16)$$

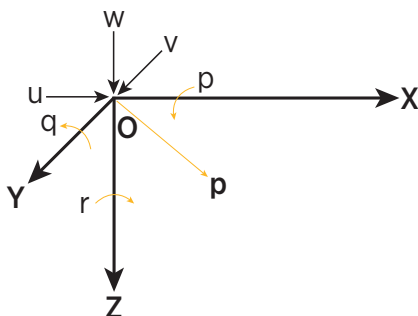
$$\dot{v} = \dot{V} - pW + rU - (p^2 + r^2)y + (rq - \dot{p})z + (pq + \dot{r})x, \quad (8.17)$$

$$\dot{w} = \dot{W} - qU + pV - (p^2 + q^2)z + (pr - \dot{q})x + (qr + \dot{p})y. \quad (8.18)$$

Equations 8.16, 8.17, and 8.18 are the accelerations of a point P that is rigidly connected to the origin of reference frame that is both translating and rotating relative to all three axes. Point p is located by (x,y,z) in the reference frame that translates with velocities U , V , and W in the XYZ axis, and rotates with angular velocities p , q , and r about the XYZ axis, as shown in [Figure 8.3](#). Equations 8.16, 8.17, and 8.18 will next be used to develop Newton's second law to describe the motion of the rigid body containing p as it experiences external forces.

FIGURE 8.3 Point located in a rotating and translating reference frame.

© Dan E. Williams.



8.5 External Forces and Inertia

The previous section derived acceleration of any point in a rotating and translating rigid body. In this section, Newton's second law will be completed with the development of forces and inertias. For each point of the rigid body, located by a specific x,y,z coordinate, Eq. 8.16 reports acceleration in the X direction. Now, we attach an infinitesimal mass δ_m to the point P , and the force to produce an acceleration of this point mass can be written.

$$F_{p,x} = \delta m \dot{u}_p. \quad (8.19)$$

Similar to Eq. 8.19, the force along the X axis required to accelerate each particle of mass in the rigid body can be calculated.

$$\sum F_x = \sum \delta m \dot{u}. \quad (8.20)$$

Equation 8.16 is substituted into Eq. 8.20.

$$\sum F_x = \sum \delta m \left(\dot{U} - rV + qW - (q^2 + r^2)x + (qp - \dot{r})y + (rp + \dot{q})z \right) \quad (8.21)$$

Some of the acceleration terms in Eq. 8.21 are experienced by all points in the rigid body, and some are varied dependent upon the specific point's location in the rigid body. The infinitesimal mass term can be distributed to the various acceleration terms.

$$\sum F_x = \sum \delta m (\dot{U} - rV + qW) - \sum \delta mx (q^2 + r^2) + \sum \delta my (qp - \dot{r}) + \sum \delta mz (rp + \dot{q}). \quad (8.22)$$

Equation 8.22 can be simplified by using identities of mass distribution. A summation of all the infinitesimal masses is simply the rigid body mass.

$$m = \sum \delta m. \quad (8.23)$$

Up to now, there has been no restriction on the rotating and translating reference frame, other than it is attached to the same rigid body that contains the point P . We now assume that the origin of the rotating and translating frame is located at the center of mass of the rigid body. With this condition, three identities follow from the definition of center of mass.

$$\sum \delta mx = 0, \quad (8.24)$$

$$\sum \delta my = 0, \quad (8.25)$$

$$\sum \delta mz = 0. \quad (8.26)$$

Using Eqs 8.23–8.26, the summation of all the forces on the rigid Eq. 8.22 can be simplified.

$$\sum F_x = m(\dot{U} - rV + qW). \quad (8.27)$$

By the same process, Newton's second law can be written for the rigid body motion in the Y and Z directions.

$$\sum F_y = m(\dot{V} - pW + rU), \quad (8.28)$$

$$\sum F_z = m(\dot{W} - qU + pV). \quad (8.29)$$

In addition to the three modes of translation, there are also three modes of rotary motion about each axis. Consider moments that cause rotation about the X-axis. As seen in [Figure 8.3](#), moments about the X-axis cause accelerations in particles of mass based on their distance from the X-axis. In responding to a positive moment about the X-axis, a particle of mass accelerating with \dot{w} has a moment arm of y . Similarly, a particle accelerating with \dot{v} has a moment arm of $-z$. (An acceleration of \dot{u} along the X-axis is not affected by a moment about the X-axis.) The effect of an external moment about the X-axis can be written as

$$\sum M_x = \sum \delta m(y\dot{w} - z\dot{v}). \quad (8.30)$$

Similar reasoning is applied for moments about the Y-axis and Z-axis.

$$\sum M_y = \sum \delta m(z\dot{u} - x\dot{w}), \quad (8.31)$$

$$\sum M_z = \sum \delta m(x\dot{v} - y\dot{u}). \quad (8.32)$$

As before in the translational modes, Eqs 8.17 and 8.18 are inserted into Eq. 8.30.

$$\begin{aligned} \sum M_x &= \sum \delta m(y(\dot{W} - qU + pV - (p^2 + q^2)z + (pr - \dot{q})x + (qr + \dot{p})y) \\ &\quad - z(\dot{V} - pW + rU - (p^2 + r^2)y + (rq - \dot{p})z + (pq + \dot{r})x)). \end{aligned} \quad (8.33)$$

As before, the infinitesimal mass terms are distributed to the various acceleration terms, but the result is more complicated.

$$\begin{aligned} \sum M_x &= \sum \delta my(\dot{W} - qU + pV) - \sum \delta myz(p^2 + q^2) + \sum \delta mxy(pr - \dot{q}) \\ &\quad + \sum \delta my^2(qr + \dot{p}) - \sum \delta mz(\dot{V} - pW + rU) + \sum \delta mzy(p^2 + r^2) \\ &\quad - \sum \delta mz^2(rq - \dot{p}) - \sum \delta mzx(pq + \dot{r}) \end{aligned} \quad (8.34)$$

Equation 8.34 is slightly simplified,

$$\begin{aligned}\sum M_x = & \sum \delta m y (\dot{W} - q U + p V) - \sum \delta m z (\dot{V} - p W + r U) + \sum \delta m z y (r^2 - q^2) \\ & + \sum \delta m x y (p r - \dot{q}) + \sum \delta m y^2 (q r + \dot{p}) - \sum \delta m z^2 (r q - \dot{p}) \\ & - \sum \delta m z x (p q + \dot{r})\end{aligned}\quad (8.35)$$

and further simplified by fixing the reference frame at the center of mass and using the properties of Eqs 8.24, 8.25, and 8.26.

$$\begin{aligned}\sum M_x = & \sum \delta m z y (r^2 - q^2) + \sum \delta m x y (p r - \dot{q}) + \sum \delta m y^2 (q r + \dot{p}) - \sum \delta m z^2 (r q - \dot{p}) \\ & - \sum \delta m z x (p q + \dot{r}).\end{aligned}\quad (8.36)$$

Equation 8.36 is a general equation describing how an external moment about the X-axis accelerates various mass particles in a rigid body. At this point notation is introduced regarding the inertia properties of rotating masses relative to a reference frame fixed to its center of mass. Moments of inertia relative to the three axes can be written.

$$I_x = \sum \delta m (y^2 + z^2), \quad (8.37)$$

$$I_y = \sum \delta m (x^2 + z^2), \quad (8.38)$$

$$I_z = \sum \delta m (x^2 + y^2). \quad (8.39)$$

In addition to the moments of inertia, products of inertia can be written as

$$P_{xy} = \sum \delta m x y, \quad (8.40)$$

$$P_{xz} = \sum \delta m x z, \quad (8.41)$$

$$P_{yz} = \sum \delta m y z. \quad (8.42)$$

Equations 8.37–8.42 can be used to simplify Eq. 8.36, where the sum of external moments acting on all the particles is the external moment.

$$\begin{aligned}\sum M_x = & P_{yz} (r^2 - q^2) + P_{xy} (p r - \dot{q}) + I_x \dot{p} + (\sum \delta m y^2 - \sum \delta m z^2) q r \\ & - P_{xz} (p q + \dot{r})\end{aligned}\quad (8.43)$$

and adding and subtracting a term and using Eqs 8.38 and 8.39,

$$\begin{aligned}\sum M_x = & P_{yz} (r^2 - q^2) + P_{xy} (pr - \dot{q}) + I_x \dot{p} \\ & + (\sum \delta my^2 + \sum \delta mx^2 - \sum \delta mz^2 - \sum \delta mx^2) qr - P_{xz} (pq + \dot{r}),\end{aligned}\quad (8.44)$$

the effect of an external moment about the X -axis on the acceleration of all mass particles in a rigid body, when the axis originates at its center of mass.

$$\sum M_x = I_x \dot{p} + (I_z - I_y) qr + P_{yz} (r^2 - q^2) - P_{xz} (pq + \dot{r}) + P_{xy} (pr - \dot{q}). \quad (8.45)$$

Similar equations can be derived from moments about the Y -axis and Z -axis.

$$\sum M_y = I_y \dot{q} + (I_x - I_z) rp + P_{xz} (p^2 - r^2) - P_{xy} (qr + \dot{p}) + P_{yz} (qp - \dot{r}), \quad (8.46)$$

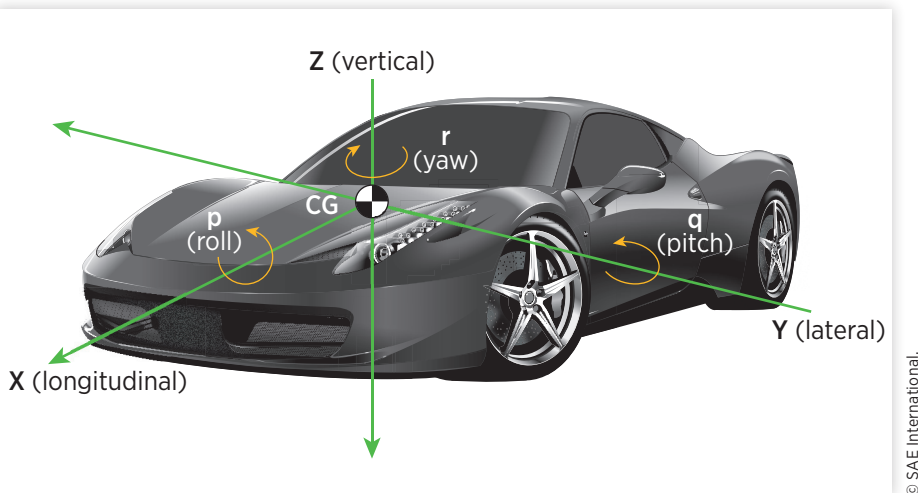
$$\sum M_z = I_z \dot{r} + (I_y - I_x) qp + P_{xy} (q^2 - p^2) - P_{yz} (rp + \dot{q}) + P_{xz} (rq - \dot{p}). \quad (8.47)$$

Equations 8.27, 8.28, and 8.29 describe accelerations caused by forces on a rigid body and Eqs 8.45, 8.46, and 8.47 describe accelerations caused by moments, when the reference axis is fixed to the center of mass. These are the general “right-hand sides” of Newton’s second law written for the six modes of rigid body motion, with a rotating and translating reference frame fixed to the center of mass of the moving body.

8.6 The Vehicle as a Rigid Body

Thus far, the mass that the translating and rotating reference frame is attached to is arbitrary. It has only been assumed that the reference frame originates at the center of mass. In this section, certain assumptions will be made consistent with a simple model of a road vehicle.

As a formality, it is assumed that a right-hand axis is fixed to the center of mass of the road vehicle, with the z -axis pointed downward, the x -axis longitudinally out the front of the vehicle, and the y -axis to the right of the driver. This coordinate system is reasonably intuitive, forward motion is positive, lateral motion to the right is positive, and clockwise rotation about the z -axis is positive. It is perhaps less intuitive that the positive vertical axis points down rather than up. This convention is borrowed from aircraft modeling, where many of the pioneers of vehicle dynamics—for example, Maurice Olley and Bill Milliken—got their start. Occasionally, vehicle dynamicists use an upward pointing z -axis, and that is fine if done consistently using a right hand axis, and positive lateral

FIGURE 8.4 Axis fixed to vehicle center of mass.

© SAE International.

motion will be to the left, and counter-clockwise rotation about the z -axis would be positive (such an axis might have appeal to NASCAR vehicle modelers).

The reference frame was intuitively selected so that the x -axis pointed along the centerline of the vehicle toward the front, and the y -axis point positively to the right side. In addition to being intuitively pleasing, there is another great analytical benefit to this axis choice—it is very close to the principle axis for reasonable vehicles.

The products of inertia present in the reference system shown in [Figure 8.4](#) can be rationalized in looking for planes of symmetry. First, consider the plane defined by the $x-z$ plane. It is quite easy to accept that the mass distribution of the vehicle is largely reflected about this vertical plane cutting the vehicle in half longitudinally. Said a bit more rigorously, for any mass particle located by a (x, y, z) coordinate, there is a corresponding particle at $(x, -y, z)$. In this case, in view of Eqs 8.40 and 8.42, we can state that P_{xy} and P_{yz} approach zero. Similar reasoning suggests a fair bit of symmetry about the $x-y$ plane. The roof line extends upward asymmetrically, and the tires below, but when you consider the relatively massive parts of the car's powertrain and structure, it is plausible to assume a degree of symmetry in this plane, therefore P_{xz} and P_{yz} approach zero. Note P_{yz} was previously shown to be zero, so this second plane of symmetry allows the third product of inertia, P_{xz} to be zero. These assumptions are reasonable for passenger cars, but should be revisited for specific commercial vehicle studies where cargo loads could be significant and asymmetrical.

This symmetry allows significant simplification of Eqs 8.45, 8.46, and 8.47, although complications remain. Recall in the previous section on ride, pitch and

roll motions were treated independently. Similar assumptions are made in this section on handling. Fundamentally handling is a study of vehicle behavior in the x - y plane, so vertical motions can be neglected. As with the independent treatment of the roll and pitch rotational modes in the first section, as the concern is now yaw, we initially assume roll and pitch motions are negligible. We can say for handling that all analysis is done at a relatively constant forward speed, so there is no acceleration and braking, and therefore no time derivative of longitudinal velocity. This gives solid support to neglecting pitch, as without vertical inputs and longitudinal acceleration, there is nothing to excite the vehicle in pitch. However, roll is bit more dubious. We have already seen that the primary vehicle response to a steering input is a yaw rate which produces vehicle motion in the x - y plane, but we also know that such a steering input will create “centrifugal force” that produces roll in the cars we drive. To eliminate the need to consider roll in our initial study of handling, we therefore assume that there is no suspension compliance, and therefore no possibility for roll displacement. Of course a driver of any passenger car knows this assumption is dubious, but it is made for simplification, with the rationalization that even if present, with the prior (and better) assumptions, roll is not significantly coupled to the degrees of freedom we are interested in the x - y or yaw plane.

With the above stated assumptions of symmetry and neglecting various modes of motion, the “right half” of Newton’s second law equations are a much simplified subset of Eqs 8.27–8.29 and Eqs 8.45–8.47.

$$\sum F_y = m(\dot{v} + ur), \quad (8.48)$$

$$\sum M_z = I_z \dot{r}. \quad (8.49)$$

Equations 8.48 and 8.49 describe the x - y axis yaw plane behavior of a vehicle with all the stated assumptions.

Because the vehicle is yawing about a vertical axis, a centripetal acceleration term is also present as the product of the constant longitudinal velocity and yaw rate Eq. 8.48. It is significant to note at this point the ur term in Eq. 8.48 this is an acceleration term derived from the vehicle having a simultaneous yaw rate and forward speed, and this acceleration would be present even with a steady-state constant forward speed and yaw rate. An accelerometer mounted on the yawing vehicle would record the lateral acceleration plus this centripetal acceleration. It is important to appreciate the sign on the centripetal term. A vehicle with a positive forward velocity and yaw rate will experience an apparent positive lateral acceleration relative to a right-hand axis toward the center of the turn. Through torturing the nomenclature, the mur term can be transferred across the equation and appear as an apparent negative “centrifugal force” on the

vehicle away from the center of the turn, to be summed along with the actual tire forces as was done in the previous section, in a steady-state analysis. The positively defined yaw rate and longitudinal velocity produce a positive centripetal acceleration (but a negative “centrifugal force”). Thus, when multiplied by m and moved across the equal sign, the centripetal acceleration becomes the “phantom” centrifugal force that so confused the slip angle convention.

In the following several chapters, the left-hand side of Eqs 8.48 and 8.49 will be developed. The left-hand side is the external lateral forces on the vehicle, exerted by the road on its tires. The yaw-plane model that will be developed using Eqs 8.48 and 8.49 is one of the fundamental models of vehicle dynamics, perhaps even exceeding the quarter-car model in its usefulness and applicability. It will be shown to capture fundamental transient and steady-state vehicle behavior. Recall the quote from GEP Box that “all models are wrong, and some are useful.” Then, recall Einstein’s famous muse that solutions should be “as simple as possible, but no simpler.” Just as with the quarter-car model, the yaw-plane model is extremely simple and useful, in word—parsimonious.

This comfort allowed by ignoring the roll mode is both significant and temporary. Eventually, it will be shown that roll-mode displacement has an effect on these lateral forces through the very suspension that was neglected. So while the roll mode is not dynamically hard-coupled to the lateral velocity and yaw modes through acceleration cross products, it is coupled through the mechanism by which external lateral forces are created. The roll mode will be present when motion is allowed relative to the rotating and translating reference frame. We will fix the frame translating and yawing with the vehicle, and then allow the suspended mass to roll relative to this frame.

8.7 Summary

Starting with a rigid body that generally rotates and translates, general expressions of accelerations were derived. Then many assumptions were made that allowed accelerations commonly expected in the standard yaw-plane model. Among these assumptions were: no pitch, heave or roll motion, no longitudinal acceleration, and symmetry in the x - y plane and x - z plane.

The derivation showed a centripetal term that when multiplied by mass forms the fictitious centrifugal force and produces unfortunate signs associated with the conventional yaw-plane model. An understanding of the difference between centripetal acceleration and centrifugal force is necessary to appreciate the convention changes suggested in the next chapter.

Of these assumptions that produce the standard yaw-plane model, perhaps the most problematic is that the vehicle has no roll motion amid handling

inputs. The other modes assumed motionless: namely pitch and heave, are ride modes and are not excited when a vehicle travels a smooth highway at constant speed. Experience with common passenger cars tells us the roll mode is known to displace with steering inputs, even on smooth roads at a constant speed. Therefore, the assumption of no roll is really an assumption of no suspension. This assumption will be revisited later in this section, with the benefit of the general acceleration equations derived in this chapter.

Reference

- [1] Ellis, J.R. Vehicle Dynamics, Business Books, London, 1969.

New Conventions

“ Scientists work from models acquired through education and through subsequent exposure to the literature often without quite knowing or needing to know what characteristics have given these models the status of community paradigms.

—Thomas Kuhn

9.1 Introduction

In the introductory chapter in the handling section, a simple yaw-plane or bicycle model was developed using standard conventions readily found in the vehicle dynamic literature. These conventions have led to a commonly accepted yaw-plane model that well describes many handling characteristics of a two-axle passenger car. As was shown at the end of that chapter, however, this model appears very “unconventional” when put in the block diagram form used by control theorists to analyze dynamic systems.

It was suggested in the chapter on reference frames that the problem with the conventional model is that originally forces at the tire were thought to be a response from centrifugal force on the vehicle when turning, resulting in an unfortunate sign convention. Equations of motion were derived for a general rigid body translating and rotating in all three dimensions. Then, using assumptions consistent with the yaw-plane model, the complexity of these equations was greatly reduced, resulting in an equation describing lateral acceleration in response to the summation of lateral forces, and yaw acceleration in response to the summation of lateral forces producing yaw moments about the z -axis. In this derivation, centripetal acceleration is seen to be the product of a longitudinal velocity and yaw rate and not an independent input to the vehicle. Thus, tires create lateral forces on the vehicle based on their orientation relative to vehicle motion. Those lateral forces create a yaw rate, which when combined with

longitudinal velocity creates a centripetal acceleration that is often mistakenly considered a force.

In the present chapter, we will suggest two new conventions that will slightly alter the nomenclature of the yaw-plane model. The two assumptions will be combined to produce a general model describing how the tires on an axle develop a lateral force which turns the vehicle. Assumptions will be made in this chapter that will initially appear superfluous to those familiar with the standard yaw-plane model. Patience is requested from those readers. It will be evident that the new conventions do not harm the two-axle vehicle model, but greatly enhance the ability to analyze more complicated vehicles. The product of these two assumptions is a general equation describing the lateral force produced for any axle location, steered, or unsteered.

9.2 State-of-the-Art Conventions

Conventions are important in science and engineering. They allow for efficient technical communication. We do not have to start from first principles when discussing a new development; we can use nomenclature, axis systems, reference frames, and so on, which can be assumed familiar to an informed reader. The yaw-plane model presented in [Chapter 7](#) results from conventions, but has itself become so accepted as to become conventional and is often presented without derivation.

In his seminal work “The Structure of Scientific Revolutions” [1], Thomas Kuhn developed a much broader role for conventions. He suggests that they actually constrain thought along certain paths, precisely because they determine communication within the scientific community. Conventions can be dangerous however, in that they can hide implicit assumptions that are not usually recognized. Often a change in convention is correlated with a paradigm change in theory.

Kuhn describes two modes of science. First, normal science proceeds using the accepted conventions, becoming increasingly better at describing nature. A good example of this is how Ptolemy’s earth centered astronomy had become very good at predicting events. By using eccentricities and circular orbits of celestial bodies centered on points that were themselves circling about the earth, effectively there were enough degrees of freedom in the model that over time it was optimized to very accurately reflect reality. When the Copernican model supplanted Ptolemy, it was not because it allowed better prediction of observations. Copernicus needed Kepler’s help for that. The Copernican model was adopted because it was easier to use, rather than because it was more accurate. And in fact in the last hundred years or so, we have come to appreciate that there really is no privileged reference point for uniform

motion, and therefore the only thing that Copernicus has to offer is efficient utility—but that is quite enough.

After that lofty philosophical waxing, a convention already established in this work is revisited briefly. Occasionally, elsewhere in the quarter-car model literature the upward direction was positive. This makes intuitive sense as in almost any chart or graph that we see, the vertical axis upwardly increases. The vehicle dynamics literature is split between upward and downward vertical axes. The reason we have chosen downward in this work is that it makes certain handling attributes more intuitive. So it's sort of a trade, intuitive handling versus intuitive ride, and also more consistent with prevailing aerodynamic conventions.

Keeping track of positive and negative is simple and seemingly arbitrary, but it is related to another convention change allowing unique results that will be presented throughout this work. Most vehicle dynamic theory starts out applied to two-axle vehicles. This makes sense for at least two reasons: (1) most vehicles are passenger cars, and most passenger cars are two-axle vehicles; and (2) passenger cars are the simplest of vehicles and that is usually a good place to start. You could claim that bicycles and motorcycles are perhaps simpler, but their dynamics are fundamentally different. An inherent assumption of two-axle vehicles—one that is almost so trivial that it avoids scrutiny—is that the center of gravity must be between the two axles. Innocently buried in Eq. 7.54 is this questionable convention. This equation implicitly assumes that the center of mass is between the first and the second axles, and therefore explicitly attaches a negative lever arm to the rear lateral tire force, and furthermore embeds this assumption in the equation, so that the distance b is absolute—always positive. This assumption is trivial in the special case of a two-axle vehicle, but exceedingly problematic for a general case of multiple axles.

An alternative is to use the signed position of the axles relative to the center of mass. In all vehicle models, the positive x -axis points longitudinally along the centerline of the car in its direction of travel. Therefore, the front axle is a positive direction from the sprung mass, and the rear axle is a negative location. This convention allowed a generalized pitch-plane model in [Chapter 4](#). In this current section on handling, it will be shown to have perhaps an even greater effect in allowing a generalized handling model.

A second convention will be changed in the following chapters. Slip angles will not be used to calculate tire forces, rather the opposite of the slip angle, called the attack angle will be used. As noted, this is a departure from SAE convention, warranted by the significant simplification it allows in a block diagram similar to [Figure 6.13](#) of [Chapter 6](#). In the vehicle dynamics community, there are others that have departed from this slip angle convention, but many very good and popular works adhere to it.

In his very popular “Fundamentals of Vehicle Dynamics,” Tom Gillespie defines the slip angle of a tire as the positively defined angular direction of travel minus the positively defined direction of heading. The idea is that the tire slips in the presence of a lateral force and does not actually travel in the direction it is heading, and this difference is defined as the slip angle. Gillespie notes “by the SAE convention, a positive slip angle produces a negative force on the tire.” As evidenced by (or perhaps because of) the popularity of his work, Gillespie’s view corresponds to the conventional understanding of the vehicle dynamic literature [2]. Dean Karnopp also uses the standard definition of slip angle, with the previously borrowed good description of how it arises [3]. Reimpell and Stoll use similar logic to define slip angle [4].

In his seminal “Vehicle Dynamics,” R.A. Ellis likewise uses slip angle [5]. Ellis’ work is the most rigorous early development of general vehicle dynamics found in the literature and has no doubt greatly influenced subsequent work (including the present work). Despite his admirable rigor in developing the equations of motion for vehicles—including a sprung mass allowed to roll—Ellis uses the slip angle convention in his development. In example problems he uses a negative cornering coefficient, but when showing tire data the cornering coefficient appears as a positive gradient. This statement should not be considered as critical of Ellis, in many ways his book remains the best, most rigorous and most complete development of the yaw-plane model equations of motion. The point is raised to illustrate the fact that even in the most rigorous relevant work, the slip angle notion is muddled.

In “Race Car Vehicle Dynamics,” Bill and Doug Milliken accept the SAE axis definition with some clear reservation. They defer to an aerodynamic term yaw angle, where the difference between the velocity of the tire and its plane is because of the steering input, and not the slip of the tire because of lateral force. The Millikens admit that “of the two ways of creating an out-of-plane velocity component, the use of yaw angle has considerable logic for presenting data from tire tests. . . A positive yaw angle would line up with a positive rotation. . . it would be compatible with the definition of positive steer angle. . . In a RH turn the yaw angles at the wheels would normally be positive as well as the lateral tire forces. The cornering curves would plot in the first quadrant.” However, in the end, the Millikens chose to abide by SAE convention in their work [6].

Taken together, it is impossible to find more respected authorities in the vehicle dynamics field than Gillespie, Karnopp, Ellis, and the Millikens, and all use the SAE slip angle convention. Other sources are mixed in the use of the SAE slip angle.

The Millikens later annotated the notes of Maurice Olley, who began thinking about vehicle dynamic concepts in the first half of the 20th century. It is significant that perhaps the first person that thought deeply about the yaw-plane model used yaw angles rather than slip angles. “With Olley’s notion

of the slip angle as yaw angle, [the result is] positive vehicle yaw rate, positive vehicle attitude, positive lateral acceleration, and positive tire lateral forces. This contrasts with the SAE convention in which negative slip angles exist in right hand turns, spoiling the uniformity of positive values. . . . Unfortunately, since the Olley slip angle convention is not the SAE convention, it differs from the bulk of literature published in the present day.” [7]

Wong uses the opposite of the SAE slip angle in his text, as contemplated by the Millikens. [8]¹ Pacejka similarly chose the “sign of the slip angle” to be “opposite with respect to the SAE definition.” (All the above-mentioned works consider lateral velocity to be a degree of freedom. Pacejka uniquely scales lateral velocity by the assumed constant longitudinal velocity, forming an angle of the velocity vector of the vehicle, a practice that will be adopted in this work [9].) More recently, Rajamani refers to slip angle in his text, but mathematically uses the opposite yaw angle [10]. Similar to Rajamani, Maywerk refers to slip angle but actually uses yaw angle [11]. This listing of vehicle dynamic texts is not intended to be exclusive, rather to illustrate that the literature differs on its slip angle convention, but many well-regarded texts use the standard convention. To summarize the literature, there is no consensus on the sign of the difference between the plane of the steered tire and the velocity vector, and the relationship between this difference and the lateral force produced by the tire, but most authoritative works use the slip angle convention.

In contrast, all the above-referenced classic texts locate the front and rear axles by the absolute distance between the respective axles and the center of mass of the vehicle. Axle locations are consistently specified in a manner appropriate for two-axle vehicles, but inappropriate when the convention is extrapolated to vehicles with three or more axles.

Axles in this work will be located with a signed location relative to the center of gravity. This was done in the [Chapter 5](#) on the multiaxle pitch plane to allow compact modeling equations. In the following chapters on handling, it will allow algebraic simplification to provide multiaxle characterizations consistent with two-axle experience. Attack angles (yaw angles) will be used to generate positive lateral forces on the tires through positive cornering coefficients. As will be shown in later chapters, such changes will be appreciated when taking a control theoretic approach to vehicle dynamics, and when analyzing more complex vehicles. The new convention does not limit the analysis of the common two-axle vehicle that existing convention treats acceptably, in fact the two-axle vehicle is shown to be a special case of a more general theory.

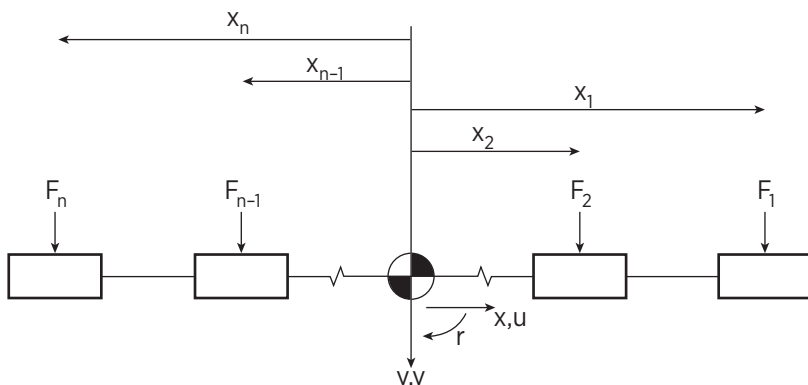
¹ It is quite likely that a motivation for the author’s opinion lies in the fact that his first exposure to vehicle dynamics was in a class where the lecture notes reflected the Ellis text which had just gone out of print, and the text specified for the class was Wong.

9.3 New Axle Location Convention

The first convention change from the standard yaw-plane model is to use signed distances to measure the location of axles relative to the vehicle center of mass. Recall we have fixed our translating and rotating axis to the vehicle center of mass, with the x -axis pointing out the front of the vehicle along its centerline. Consistent with the assumptions of the single-track bicycle model, each axle is located by its signed x -coordinate. This convention was already used in the ride section, but is presented in more detail here as the yaw plane or bicycle model is more commonly accepted as a standard.

As shown in [Figure 9.1](#), axles located forward of the center of mass are located by a positive x_i . Axles behind the center of mass would be located by a negative x_i . Note that for a two-axle vehicle, by definition the center of mass must be between the axles. Therefore, when summing the moments of the lateral tire forces, in the conventional two-axle vehicle model the absolute distance between the rear axle and the center of mass is multiplied by the lateral force on that rear axle, and subtracted from the moment produced by the front axle. In other words, the sign of negative moment arm of the rear axle was embedded in the equation summing yaw moments rather than being captured by a signed axle location as seen in Eq. 7.37 and in Eq. 7.54 of the previous chapter.

FIGURE 9.1 Signed Axle location.



Reprinted with permission from © SAE International.

9.4 New Attack Angle Convention

Recall the original logic in the slip angle concept from the conventional model. Based on the centrifugal force experienced by the vehicle in the turn, a lateral velocity perpendicular to the plane of the rolling wheel is created. The vector

result of that lateral velocity and the longitudinal velocity is the instantaneous velocity vector of the vehicle. Yaw rate acting on the lever arm of axle location adds to or subtracts from the vehicle velocity to yield an instantaneous axle velocity. If the axle is steered the steer angle is subtracted from the instantaneous axle velocity to yield conventionally defined slip angle. The slip angle is thus defined as this instantaneous velocity angle at an axle, minus the axle's steering input, if present.

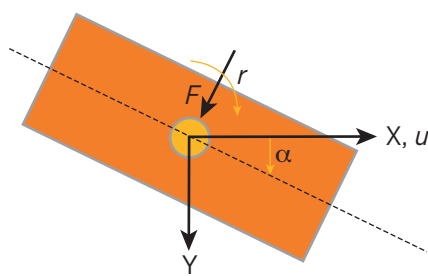
In practice, the angular steering input must be significantly larger than the velocity vector of the wheel. The conventional slip angle becomes negative when generating positive lateral forces on the vehicle and turning in a positive direction. In rigorous vehicle modeling we are concerned with the external forces on the vehicle, in this case the force the road exerts on the tires of the vehicle, the relationship between this conventionally defined slip angle the lateral force on the tires is negative, requiring a negative cornering stiffness, and yielding the irregular block diagram shown in the previous chapter.

This work uses a more straightforward and intuitive, if less common, convention. Just as with the more conventional case, a positive steering input produces a positive lateral force on the tire, and creates at the front a positive yaw moment. Using control systems intuition, the steering input is seen as a command to the dynamic system, and the velocity vector of the wheel is seen as its response. The attack angle of the tire is seen as the difference between the command and the system response, and the cornering stiffness is seen as the closed loop error gain.

Intuitively the attack angle convention is easier to visualize. Imagine a tire fixed directly below the center of mass of a vehicle, and inclined at a positive angle β to the direction of travel u .

It is quite easy to conceptualize how a tire so inclined to the direction of travel will experience a positive force from the road perpendicular to the plane of the tire, as shown in [Figure 9.2](#).

FIGURE 9.2 A tire inclined to the direction of vehicle travel along x-axis.



Now consider if there was also a small lateral component of velocity, v , of the overall vehicle. Now the velocity component of the vehicle is the vector sum of u and v . As before, the imaginary tire is located directly below the center of gravity of the vehicle and is inclined to the vehicle's direction of travel.

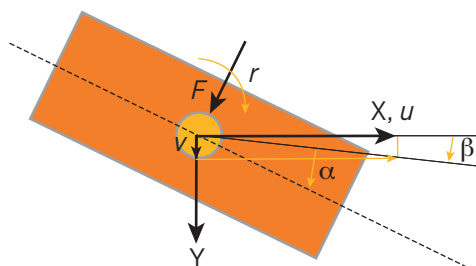
From [Figure 9.3](#), it is evident that the presence of a positive lateral velocity serves to reduce the angle α between the direction the tire is moving, and the direction it is pointed. The angle of this velocity vector is shown as β . Formally stated, the attack angle is the angular inclination of the steered wheel relative to the X-axis coincident with the centerline of the vehicle, minus the angular displacement of the velocity vector again referenced to the X-axis.

Next a positive angular displacement δ of the tire relative to the center line of the vehicle is assigned, as shown in [Figure 9.4](#).

The attack angle can now be written as a function of the steer angle displacement and the velocities of the vehicle,

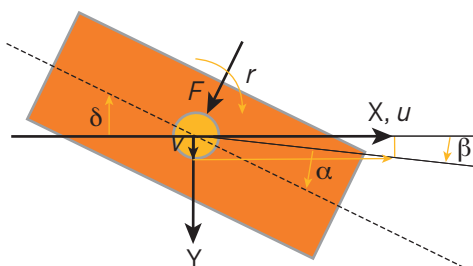
$$\alpha = \delta - \beta \quad (9.1)$$

FIGURE 9.3 A tire inclined to the direction of travel with x and y components.



© SAE International.

FIGURE 9.4 Inclined with steering input identified.



© SAE International.

and the angle of the velocity vector can be calculated.

$$\alpha = \delta - \tan^{-1} \left(\frac{v}{u} \right). \quad (9.2)$$

Equation 9.2 shows the attack angle for a steered wheel located directly below the center of gravity of a vehicle with both a longitudinal velocity and a lateral velocity. Next, we consider the steered wheel at an axle location defined by x_i , the signed convention previously introduced.

When the axle is located by a positive x_i , the lateral velocity of the tire is increased because of the yaw rate r acting through the lever arm x_i . Equation 9.2 is modified to include this effect.

$$\alpha_i = \delta_i - \tan^{-1} \left(\frac{v + x_i r}{u} \right). \quad (9.3)$$

The attack angles of tires are generally small. Therefore, it is appropriate to use a small-angle approximation to linearize Eq. 9.3.

$$\alpha_i = \delta_i - \frac{v + x_i r}{u}. \quad (9.4)$$

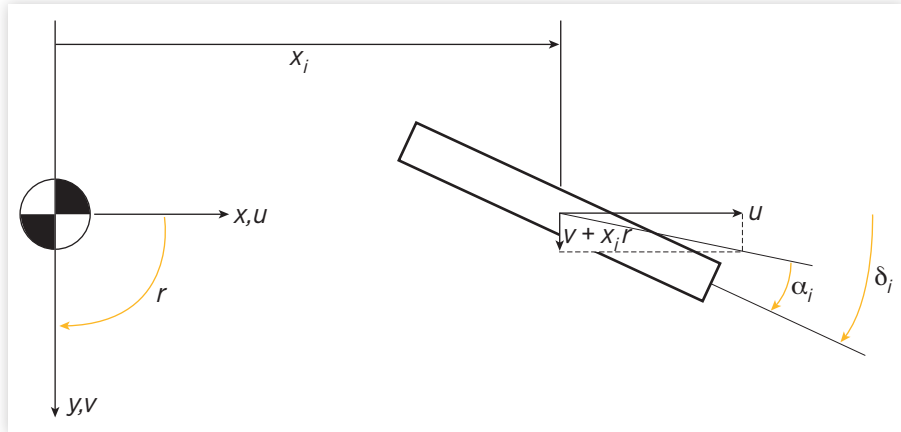
Note in Eq. 9.4 the consistency in sign relative to the reference frame at the center of mass. All positive angles are a clockwise rotation from the centerline of the vehicle which is the x -axis. Equation 9.4 is intuitively pleasant to the control theorist. The steering input δ_i is a command or reference signal, and the angular displacement of the velocity vector is the system response or feedback. Thus, Eq. 9.4 is recognized as an error term.

Equation 9.4 was derived to describe a steered front axle. It easily accommodates a typical unsteered rear passenger car axle by simply assuming a zero steering input. Note that this generality is provided by the signed axle location being negative for a rear axle. In this way, Eq. 9.4 can be seen applicable to any arbitrary axle location, whether it is steered or unsteered.

A positive attack angle described by Eq. 9.4 produces a positive lateral force on the tire through a positive cornering coefficient.

$$F_i = C_i \left(\delta_i - \frac{v + x_i r}{u} \right). \quad (9.5)$$

Equation 9.5 thus described the lateral force generated by tires on the i th axle located by x_i with respect to the vehicle center of mass, with a steering input on that axle of δ_i and a cornering coefficient of C_i . In Eq. 9.5, C_i can be interpreted in two ways. First, C_i is a proportional error gain in a control

FIGURE 9.5 Steered wheel at offset axle location.

Reprinted with permission from © SAE International.

systems perspective. This interpretation will lead to a more conventional block diagram of the yaw-plane model. Second, C_i can be interpreted as a spring constant, where δ_i is the input displacement of the spring and the angular velocity is the output side. This interpretation intuitively justifies referring to C_i as a “cornering stiffness.”

The cornering stiffness C_i is a tire property, varying with tire construction, inflation, and so on. This linear approximation between side force and attack angle is only good for small angles of input. At high angles it saturates, and there is a nonlinear transition region in between. In very round numbers, the tire stiffness is approximately 100 lbs/deg. (the metric conversion is not quite so round.)

Equation 9.5, a direct result of the two key assumptions suggested in this chapter, will be used throughout the rest of this work to generate the external forces that act on the vehicle in the reference frame rotating and translating with it.

9.5 Summary

The thoughts presented in this chapter were recently published in a paper that includes more detail than is possible in this chapter. The interested reader is referred to this paper [12].

Two small departures from accepted convention are made in this work: attack angle/side force coefficient, and a signed axle location. These two changes in convention seem almost too insignificant to justify an incongruence with the existing body of literature for the two-axle model. However, the reader will soon see that as multiple axles are considered, these small changes in convention are

justified by a surprising reduction in complexity. With these two assumptions, a generalized expression for lateral force of a steered or unsteered axle at an arbitrary location is developed.

Taking a step back from vehicle dynamics it is interesting to consider the nature and origin of conventions. Slip angles make sense only in a steady-state turn when centrifugal force is erroneously considered the input to the vehicle dynamic system. Absolute axle locations make perfect sense for a two-axle passenger car. Taken together, it is easy to understand how these conventions were established as passenger cars were first studied on the skid pad. These choices, however, have limited the progress of vehicle dynamics.

References

- [1] Kuhn, Thomas, *The Structure of Scientific Revolutions*, 3rd Edition, University of Chicago Press, Chicago IL, 1996.
- [2] Gillespie, Thomas, *Fundamentals of Vehicle Dynamics*, Society of Automotive Engineers, Warrendale PA, 1992.
- [3] Karopp, Dean, *Vehicle Dynamics, Stability and Control*, 2nd Edition, CRC Press, New York, 2013.
- [4] Reimpell, J., and Stoll, H., *The Automotive Chassis: Engineering Principles*, Society of Automotive Engineers, Warrendale, PA, 1996.
- [5] Ellis, J.R., *Vehicle Dynamics*, Business Books, London, 1969.
- [6] Milliken, William F. and Douglas L., *Race Car Vehicle Dynamics*, Society of Automotive Engineers, Warrendale, PA, 1995.
- [7] Milliken, W.F. and D.L. Milliken, *Chassis Design*. SAE International, Warrendale, PA, 2002.
- [8] Wong, J.Y., *Theory of Ground Vehicles*, John Wiley and Sons, New York, 1978.
- [9] Pacejka, Hans B., *Tire and Vehicle Dynamics*, Society of Automotive Engineers, Warrendale PA, 2002.
- [10] Rajamani, Rajesh, *Vehicle Dynamics and Control*, Springer, New York, 2012.
- [11] Maywerk, Martin, *Vehicle Dynamics*, Wiley, 2015.
- [12] Williams, D., and Margolis, D., “Rationale for New Vehicle Dynamic Convention,” *Journal of Vibration and Control*, 27(11–12), 2020. DOI:[10.1177/1077546320939831](https://doi.org/10.1177/1077546320939831).

Two-Axle Yaw-Plane Model

“ . . . a new approach to automotive stability and control based on a transfer of technology from the aircraft field. . . the modern vehicle dynamics era began right there.

—Bill Milliken

10.1 Introduction

When Bill Milliken and his colleagues set out to write the equations of motion of passenger cars, they borrowed from techniques developed for aeronautical dynamics and control. Unfortunate conventions were already established in the gestation of vehicle dynamics, and carried forward. This chapter will illustrate how the changes in convention discussed in the previous chapter allow a more intuitive application of controls techniques to vehicle dynamics.

This handling section was opened with a chapter that developed low-speed kinematics of driving, as well as a basic model of steering compliance and the common yaw-plane model developed with slip angles. The yaw-plane model was developed somewhat hastily, similar to what is commonly found in the literature. This first chapter on handling was presented as a quick summary of state-of-the-art vehicle dynamics.

The second chapter took a step backward, and more rigorously developed the accelerations of a rigid body that experienced complex translation and rotation. Clearly stated assumptions transformed the general rigid body accelerations to the accelerations found in state-of-the-art yaw-plane models. Specifically, these assumptions amounted to no longitudinal acceleration, no heave or pitch displacement, no roll displacement, and symmetry associated with the reference frame moving with the car and aligned with the principle

axis of inertia of the vehicle. Of these assumptions, roll was perhaps the most dubious, as yaw-plane motion will produce centripetal accelerations resulting in suspension deflection and body roll. Therefore, a vehicle without roll in the yaw plane cannot have a suspended sprung mass, at least in the practical sense (i.e. passive or nonactive).

Finally, in the immediately preceding chapter, two changes in convention allowed the formation of a general lateral force developed by a tire. First, axles are located by a signed value, and second attack angles rather than slip angles are used to generate lateral forces.

In the present chapter, the formally derived accelerations will be joined with the generalized lateral forces to form a yaw-plane model. The result will be a yaw-plane model for a passenger car that is completely analogous to those commonly found in the literature. The conventions assumed in this present work will allow convenient application to more complicated vehicles, in addition to providing the valuable and expected passenger car result. Using these new conventions, the two-axle yaw-plane model is derived in this chapter. In future chapters, these conventions will allow straightforward derivations of a three-axle yaw-plane model, and finally a generalized multiaxle yaw-plane model.

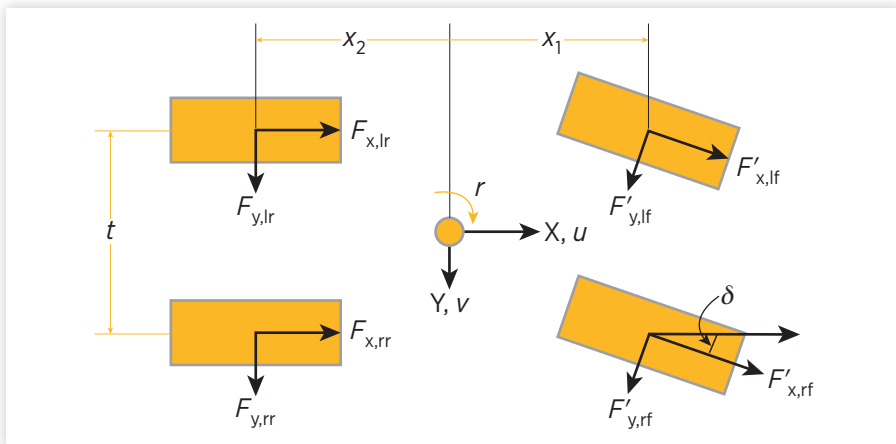
10.2 The Two-Axle Vehicle Model

Characterization of vehicle handling was first performed on two-axle passenger cars. It has long been appreciated that for vehicles travelling at a relatively constant forward speed with lateral accelerations so limited to correspond to the linear range of the tires, a simple model including yaw and lateral velocity degrees of freedom can be used to predict vehicle performance. This simple and yet illuminating vehicle model can be constructed by assuming that side forces generated by either tire on a given axle combine to act equivalently at a point where the axle intersects the centerline of the vehicle as shown earlier. This “axle” can be an abstraction when discussing independently suspended vehicles, but it remains a convenient abstraction to describe any combination of tires located by the same longitudinal displacement from the center of mass. Geometry errors because of steering linkage and dual tires [1] are considered negligible. Longitudinal dynamics are likewise neglected so a constant forward speed is assumed. Because such a model neglects sprung mass roll, and the action of tires on a common axle are combined, the result is referred to for obvious reasons as the “bicycle model,” and its parsimonious combination of simplicity and ability to characterize well-known vehicle properties has resulted in wide use [2–4].

All of the significant external forces on a car in vehicle handling occur at the contact patch of the tire and can be resolved into longitudinal forces in the plane of the tire and forces perpendicular to the tire plane. The only significant

FIGURE 10.1 Tire forces on a steered passenger car.

© Dan E. Williams.



force on the vehicle not transmitted by the tires is generated by aerodynamics. Typically at highway speed aero forces roughly equal the rolling resistance of the tires. Therefore, below highway speed aero forces are less significant; above highway speeds they are more significant.

As shown in [Figure 10.1](#), the lateral and longitudinal forces on the rear tires align with the rotating axis fixed to the center of mass of the vehicle. At the front, the steered tire is displaced relative to the X-axis on the centerline of the vehicle. The longitudinal and lateral forces on the steered tire can be resolved into lateral and longitudinal forces relative to the vehicle as shown in [Figure 10.2](#).

$$F_{x,rf} = F'_{x,rf} \cos \delta - F'_{y,rf} \sin \delta, \quad (10.1)$$

$$F_{y,rf} = F'_{y,rf} \cos \delta + F'_{x,rf} \sin \delta \quad (10.2)$$

FIGURE 10.2 Forces on the steered tire.

© Dan E. Williams.

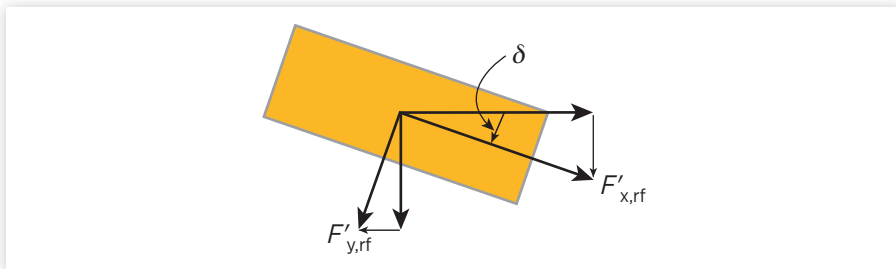
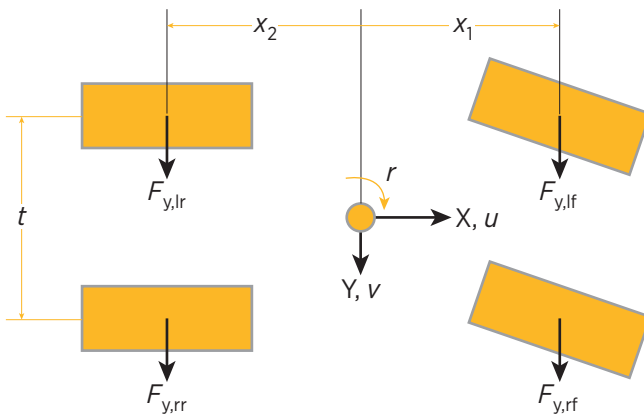


FIGURE 10.3 Lateral tire forces on a two-axle vehicle.

© Dan E. Williams.

Equation 10.1 is not important in the present development. Longitudinal tire forces serve to accelerate and decelerate the vehicle, and in the derivation of the accelerations it was assumed that there was no longitudinal acceleration, therefore these tire forces will only need to overcome rolling resistance and aero drag. If the axle is nondriven, there will be no longitudinal force on the tire. Therefore, assuming the longitudinal force on the steered tire is negligible, and using small steering angle approximations as shown in [Figure 10.2](#), the tire force lateral to the tire's steered centerline is considered to be the lateral force parallel to the vehicle's Y-axis as shown in [Figure 10.3](#).

$$F_{y,rf} \equiv F'_{y,rf}. \quad (10.3)$$

Lateral forces are shown to act on the tires of a typical two-axle vehicle, as shown in [Figure 10.3](#). The lateral forces can be summed in the Y-direction,

$$\sum F_y = F_{y,lr} + F_{y,rr} + F_{y,lf} + F_{y,rf}, \quad (10.4)$$

and similarly yaw moments can be summed.

$$\sum M_z = x_1 F_{y,lf} + x_1 F_{y,rf} + x_2 F_{y,lr} + x_2 F_{y,rr}. \quad (10.5)$$

Recall the generalized tire force expression derived as Eq. 9.5.

$$F_i = C_i \left(\delta_i - \frac{v + x_i r}{u} \right). \quad (10.6)$$

To review, Eq. 10.6 describes the lateral force generated by a tire with cornering stiffness C_i , located a longitudinal position x_i relative to the center of mass of a vehicle with longitudinal, lateral, and yaw velocities u , v , and r , respectively, and

steered with displacement δ_i relative to that vehicle's center line. If we assume that both sides of the axle have the same steering input, we can observe that both sides of the axle have the same location along the X-axis relative to the center of mass, Eqs 10.4 and 10.5 can include Eq. 10.6.

$$\sum F_y = (C_{y,lr} + C_{y,rr}) \left(\delta_1 - \frac{v + x_1 r}{u} \right) + (C_{y,lf} + C_{y,rf}) \left(\delta_2 - \frac{v + x_2 r}{u} \right), \quad (10.7)$$

$$\sum M_z = x_1 (C_{y,lr} + C_{y,rr}) \left(\delta_1 - \frac{v + x_1 r}{u} \right) + x_2 (C_{y,lf} + C_{y,rf}) \left(\delta_2 - \frac{v + x_2 r}{u} \right). \quad (10.8)$$

Finally, these yaw-plane force equations are simplified by defining the cornering stiffness of an axle as the sum of the cornering stiffness of the tires on either side (In fact, if the axle has dual tires, they all add.)

$$C_1 = (C_{y,lf} + C_{y,rf}), \quad (10.9)$$

$$C_2 = (C_{y,lr} + C_{y,rr}), \quad (10.10)$$

where C_1 is the combined tire stiffness of the front axle, and similarly C_2 for the rear.

Given Eqs 10.9 and 10.10 and the previously stated assumptions, it is possible to use Eq. 10.6 to express the lateral force generated by each axle i

$$F_i = C_i \left(\delta_i - \frac{v + x_i r}{u} \right), \quad (10.11)$$

where F_i is the resulting lateral force generated by the axle.

Although Eqs 10.6 and 10.11 are written identically, they apply a slightly differently index. In Eq. 10.6, the index was the individual wheel or tire denoted by its position (i.e., front or rear, right or left); in Eq. 10.11, the index is the axle numbered sequentially from front to rear. Intuitively, it can be viewed that the vehicle experiences external lateral forces acting on an imaginary tire located at the intersection of the centerline of the vehicle and the axle and that this imaginary tire has the combined cornering stiffness of its constituent tires of the given axle.

The generalized side force expressed in Eq. 10.11 can be used to produce the classic passenger car bicycle model, by a steered front axle 1 producing a side force F_1 a distance x_1 ahead of the vehicle center of gravity, and a fixed rear axle 2 producing a side force F_2 a distance x_2 behind the center of gravity of the vehicle, as shown in [Figure 10.4](#). Because of the positively defined x -axis is projected forward from the center of gravity on the centerline of the vehicle, the value of x_2 is negatively signed as it is behind the center of gravity. Lateral forces can be summed and equated to lateral acceleration in a reference frame moving with the vehicle given the assumptions previously stated.

The translational equation of lateral motion with respect to a coordinate frame fixed to the vehicle is the sum of the lateral axle forces equated to the lateral acceleration of Eq. 8.48,

$$m(\dot{v} + ur) = F_1 + F_2, \quad (10.12)$$

where m is the total mass of the vehicle. These lateral forces also produce yawing moments about the vehicle center of gravity that can be summed and equated with the yaw acceleration of Eq. 8.49, giving the yaw or rotational equation of motion,

$$I_z \dot{r} = x_1 F_1 + x_2 F_2, \quad (10.13)$$

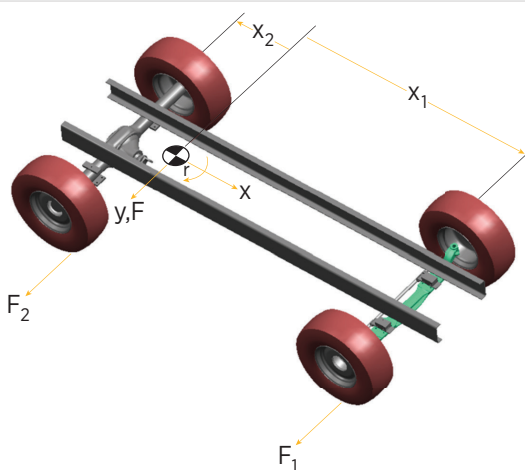
where I_z is the yaw moment of rotational inertia of the vehicle. Together, Eqs 10.12 and 10.13 describe the dynamic behavior of a vehicle with a constant longitudinal velocity u . Equation 10.11 for the front and rear axles can be inserted into the lateral force Eq. 10.12,

$$m(\dot{v} + ur) = C_1 \left(\delta_1 - \frac{v + x_1 r}{u} \right) + C_2 \left(0 - \frac{v + x_2 r}{u} \right) \quad (10.14)$$

and similarly for the yaw moment Eq. 10.13.

$$I_z \dot{r} = x_1 C_1 \left(\delta_1 - \frac{v + x_1 r}{u} \right) + x_2 C_2 \left(0 - \frac{v + x_2 r}{u} \right). \quad (10.15)$$

FIGURE 10.4 The two-axle vehicle.



Taken together Eqs 10.14 and 10.15 are seen to be coupled first-order differential equations in yaw rate r and lateral acceleration v . As such, these equations can be solved for the highest-order derivatives, in terms of states r and v , and steering input δ_1 .

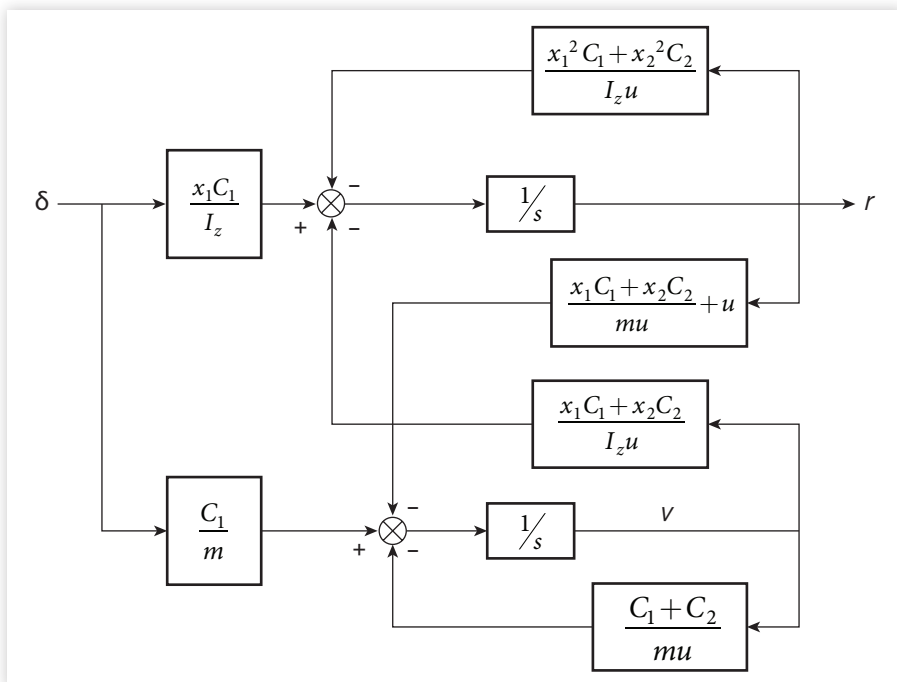
$$\dot{v} = \left(\frac{-C_1 - C_2}{mu} \right) v + \left(\frac{-x_1 C_1 - x_2 C_2}{mu} - u \right) r + \left(\frac{C_1}{m} \right) \delta_1, \quad (10.16)$$

$$\dot{r} = \left(\frac{-x_1 C_1 - x_2 C_2}{I_z u} \right) v + \left(\frac{-x_1^2 C_1 - x_2^2 C_2}{I_z u} \right) r + \left(\frac{x_1 C_1}{I_z} \right) \delta_1. \quad (10.17)$$

Equations 10.16 and 10.17 can be put in block diagram form.

The block diagram of the yaw-plane model with new conventions, shown in [Figure 10.5](#), can be compared with the conventional yaw-plane diagram shown as [Figure 7.13](#) in the first chapter of this section. To a control system theorist, [Figure 10.5](#) is much more comfortable. Feedback is subtracted from the command, and there are no negative signs on the gains.

FIGURE 10.5 Block diagram with new conventions.



Slight modification can be made to Eqs 10.16 and 10.17,

$$\dot{v} = \left(\frac{C_1}{m} \right) \left[-\left(\frac{C_1 + C_2}{C_1 u} \right) v - \left(\frac{x_1 C_1 + x_2 C_2}{C_1 u} + \frac{mu}{C_1} \right) r + \delta_1 \right], \quad (10.18)$$

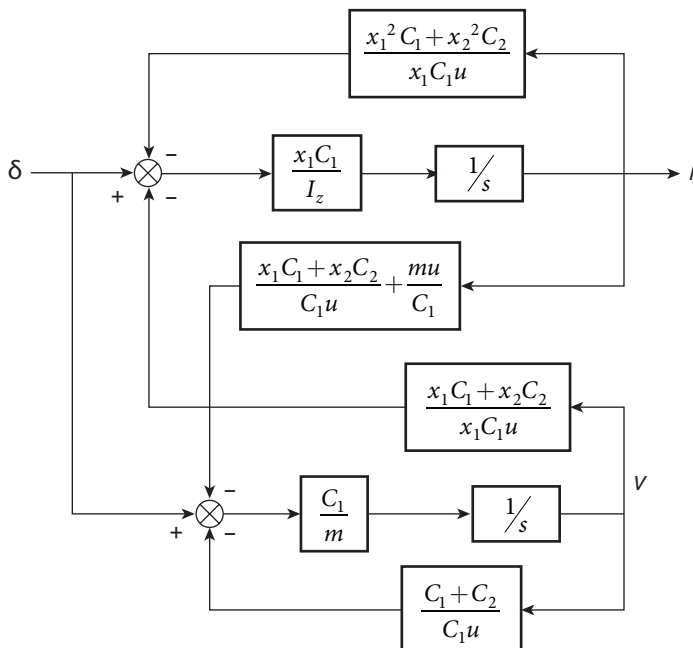
$$\dot{r} = \left(\frac{x_1 C_1}{I_z} \right) \left[-\left(\frac{x_1 C_1 + x_2 C_2}{ux_1 C_1} \right) v - \left(\frac{x_1^2 C_1 + x_2^2 C_2}{ux_1 C_1} \right) r + \delta_1 \right]. \quad (10.19)$$

The block diagram of [Figure 10.5](#) can be further simplified and expressed in a standard feedback form using Eqs 10.18 and 10.19.

[Figure 10.6](#) is perhaps the most intuitively revealing block diagram describing the yaw-plane model. Feedback and coupling terms are all subtracted from the steering command. All gain terms are positive. When $x_1 C_1 + x_2 C_2 = 0$ yaw rate is decoupled from lateral acceleration, (but lateral acceleration remains coupled to yaw rate through the centripetal acceleration term) and weakly coupled when this condition is approximated.

[Figure 10.6](#) provides a clear conception of the closed loop error gain. For both yaw rate and lateral velocity, the closed loop stiffness is increased with front axle stiffness and decreased by the relative inertia of the model. In terms

FIGURE 10.6 Block diagram with pure steering input.



of the analogous displaced mechanical spring, the input displacement is the command, the output “displacement” is the feedback, and the closed loop error gain is the stiffness. This is a most compelling reason to adopt the proposed change in convention.

From these block diagrams it is evident that slip angles used in the conventional yaw-plane model are completely analogous to Hooke’s misleading stiffness convention seen in [Chapter 2](#). Attack angles are analogous to the vertical stiffness convention used in [Chapter 2](#), that more appropriately consider inputs.

Perhaps most importantly, it is intuitively clear in this block diagram that the input to the dynamic system is a steering command, and the result is a scaled yaw rate. [Figure 10.6](#) (along with Eqs 10.18 and 10.19 from which it is constructed) also makes various control systems properties obvious by inspection such as time constants, steady-state error constants, and so on.

10.3 Drift Angle and Yaw Rate Transfer Functions

A vehicle drift angle β can be formed by scaling the time-varying lateral velocity v by the constant longitudinal velocity u .

$$\beta = \frac{v}{u}. \quad (10.20)$$

This scaling is occasionally found in the literature [6], and β can be physically interpreted as the angle of the velocity vector of the center of mass of the vehicle, consistent with the notation in [Chapter 9](#). From Eq. 9.1 of that chapter, with zero axle displacement corresponding to the center of mass,

$$\alpha = \delta - \beta, \quad (10.21)$$

where α is the angle of attack, and δ is the steering input. As we are considering the velocity of the vehicle center of mass there is no steering input and no lateral velocity generated by the yaw motion, so one can think of the drift angle of the center of mass as opposite of its angle of attack. If the vehicle drifts it has a negative angle of attack, and vice versa.

With this modification, Eqs 10.12 and 10.13 are combined using Eq. 10.11 in matrix form for a typical vehicle where only the front axle is steered.

$$\begin{bmatrix} \dot{\beta} \\ \dot{r} \end{bmatrix} = \begin{bmatrix} \frac{-C_1 - C_2}{mu} & \left(\frac{-x_1 C_1 - x_2 C_2}{mu^2} - 1 \right) \\ \frac{-x_1 C_1 - x_2 C_2}{I_z} & \frac{-x_1^2 C_1 - x_2^2 C_2}{I_z u} \end{bmatrix} \begin{bmatrix} \beta \\ r \end{bmatrix} + \begin{bmatrix} \frac{C_1}{mu} \\ \frac{x_1 C_1}{I_z} \end{bmatrix} \begin{bmatrix} \delta_1 \end{bmatrix} \quad (10.22)$$

If the vehicle is neutral steering as initially defined by Eq.7.5, Eq. 10.22 is upper triangular and the Laplace transform of the yaw rate equation can be written.

$$sr(s) = \left(\frac{-x_1^2 C_1 - x_2^2 C_2}{I_z u} \right) r(s) + \left(\frac{x_1 C_1}{I_z} \right) \delta_i(s). \quad (10.23)$$

Equation 10.23 can be solved for the transfer function between yaw rate and steering input,

$$\frac{r(s)}{\delta_i(s)} = \frac{\frac{x_1 C_1}{I_z}}{s + \left(\frac{-x_1^2 C_1 - x_2^2 C_2}{I_z u} \right)}. \quad (10.24)$$

Equation 10.24 is recognized as a first-order lag as discussed in the first chapter. In such first-order lag systems, the pole defines a frequency where the phase lag is 45°, and can be considered indicative of the dynamics of the system. So the decoupled yaw rate frequency can be written.

$$\omega_r = \left(\frac{x_1^2 C_1 + x_2^2 C_2}{I_z u} \right)^{1/2}. \quad (10.25)$$

If Eq. 10.22 is upper diagonal (neutral steer) another natural frequency can be written, this one connected with the drift angle.

$$\omega_\beta = \left(\frac{C_1 + C_2}{m u} \right)^{1/2}. \quad (10.26)$$

Equations 10.25 and 10.26 can be found as the feedback terms of [Figure 10.5](#) (and also loop gain of [Figure 10.6](#)). Therefore, we can characterize the yaw plane dynamics of a vehicle as having first-order frequencies described by Eqs 10.25 and 10.26, which can both be around 4 Hz, and as seen in the block diagrams coupled by a term relating to the understeer: $x_1 C_1 + x_2 C_2$. It is important to note that although this neutral steering condition decouples yaw rate from drift angle, it does not strictly decouple drift angle from yaw rate. Equation 10.25 determines the dynamic yaw rate response of a neutrally steering vehicle, but the drift angle response will have both frequencies from Eqs 10.25 and 10.26—which can be close to each other. This coupling remains and is because of the centripetal acceleration term. To summarize one of the properties of a neutral steering vehicle is that Eq. 10.25 defines the first-order yaw rate response dynamics.

In general the steer angle δ_i can be a variable control input, or in the case of a nonsteered or rigid axle it becomes zero. The steer angle δ_i is measured at

the tire, and therefore does not include the effect of steering system nonlinearities, ratio and compliance, and the self-aligning torque of the tire as discussed in [Chapter 7](#). These effects will be considered later. The normalized dynamic response per unit δ of the two-axle system described by Eq. 10.22 can be expressed using a process described by Maciejowski [7] and introduced in the first chapter.

$$\begin{bmatrix} \frac{\beta(s)}{\delta_1(s)} \\ \frac{r(s)}{\delta_1(s)} \end{bmatrix} = \begin{bmatrix} s + \frac{C_1 + C_2}{mu} & \left(\frac{x_1 C_1 + x_2 C_2}{mu^2} + 1 \right) \\ \frac{x_1 C_1 + x_2 C_2}{I_z} & s + \frac{x_1^2 C_1 + x_2^2 C_2}{I_z u} \end{bmatrix}^{-1} \begin{bmatrix} \frac{C_1}{mu} \\ \frac{x_1 C_1}{I_z} \end{bmatrix}. \quad (10.27)$$

The Laplace transform solution of the two-axle front steered vehicle can be written, where $s = \sigma + jw$ is the Laplace variable.

$$\begin{bmatrix} \frac{\beta(s)}{\delta_1(s)} \\ \frac{r(s)}{\delta_1(s)} \end{bmatrix} = \frac{\begin{bmatrix} mu(sIu + x_1^2 C_1 + x_2^2 C_2) & -(x_1 C_1 + x_2 C_2 + mu^2) I_z \\ -mu^2(x_1 C_1 + x_2 C_2) & (smu + C_1 + C_2) I_z u \end{bmatrix} \begin{bmatrix} \frac{C_1}{mu} \\ \frac{x_1 C_1}{I_z} \end{bmatrix}}{s^2 mu^2 I_z + s(mu(x_1^2 C_1 + x_2^2 C_2) + I_z u(C_1 + C_2)) + C_1 C_2 (x_1^2 - 2x_1 x_2 + x_2^2) - mu^2(x_1 C_1 + x_2 C_2)}. \quad (10.28)$$

The transfer function from steering input to drift angle is

$$\frac{\beta(s)}{\delta_1(s)} = \frac{s C_1 Iu - C_1 C_2 x_2 (x_1 - x_2) - x_1 C_1 mu^2}{s^2 mu^2 I_z + s(mu(x_1^2 C_1 + x_2^2 C_2) + I_z u(C_1 + C_2)) + C_1 C_2 (x_1^2 - 2x_1 x_2 + x_2^2) - mu^2(x_1 C_1 + x_2 C_2)}. \quad (10.29)$$

and the transfer function from steering input to yaw rate likewise can be written.

$$\frac{r(s)}{\delta_1(s)} = \frac{s C_1 x_1 mu^2 + C_1 C_2 u(x_1 - x_2)}{s^2 mu^2 I_z + s(mu(x_1^2 C_1 + x_2^2 C_2) + I_z u(C_1 + C_2)) + C_1 C_2 (x_1^2 - 2x_1 x_2 + x_2^2) - mu^2(x_1 C_1 + x_2 C_2)}. \quad (10.30)$$

The distance between the front and rear axles of the two-axle vehicle is commonly recognized as the wheelbase and can be expressed as a difference of the signed convention of axle locations.

$$l_2 = x_1 - x_2. \quad (10.31)$$

In this work, the two-axle understeer coefficient K_2 is defined using Eq. 10.31.

$$K_2 = \frac{-m(x_1 C_1 + x_2 C_2)}{C_1 C_2 l_2}. \quad (10.32)$$

This definition of understeer differs from that commonly found in the literature [8] by a factor of g as well as the change in convention. Using the definition of K_2 and l_2 , state variable responses to steering input are considerably simplified.

$$\frac{\beta(s)}{\delta_1(s)} = \frac{s \frac{I_z u}{l_2 C_2} - x_2 - \frac{x_1 m u^2}{l_2 C_2}}{s^2 \frac{m u^2 I_z}{l_2 C_1 C_2} + s \frac{u}{l_2} \left(\frac{m x_1^2 + I_z}{C_2} \right) \left(\frac{m x_2^2 + I_z}{C_1} \right) + l_2 + u^2 K_2}, \quad (10.33)$$

$$\frac{r(s)}{\delta_1(s)} = \frac{s \frac{x_1 m u^2}{l_2 C_2} + u}{s^2 \frac{m u^2 I_z}{l_2 C_1 C_2} + s \frac{u}{l_2} \left(\frac{m x_1^2 + I_z}{C_2} \right) \left(\frac{m x_2^2 + I_z}{C_1} \right) + l_2 + u^2 K_2}. \quad (10.34)$$

Equations 10.33 and 10.34 describe the general dynamic relationship between the steering input and both the drift angle and yaw rate outputs. Both have the general form of a zero over two poles. A simplified vehicle model will be used to gain insight into these transfer functions. Then a different kind of simplification is made with a steady-state analysis. Finally, transient properties of the transfer functions will be evaluated.

10.4 Ideal Two-Axle Model

To gain intuition about what the block diagram of [Figure 10.6](#) and Eqs 10.33 and 10.34 reveal, it is useful to consider an idealized two-axle vehicle. John Bardeen, the only two-time Nobel prize winner in physics, often tried to understand a simpler problem that contained the basic physics and work his way into more complicated problems. The inventor of the transistor and discoverer of superconductivity said “You reduce a problem to its bare essentials, so that it contains just as much of the physics as necessary” [5]. The same process will occasionally be used in this work. This simplified vehicle has the same cornering stiffness on the front and rear axles,

$$C = C_1 = C_2 \quad (10.35)$$

and the center of mass between the two axles,

$$x = x_1 = -x_2 \quad (10.36)$$

with half the mass over each axle.

$$I_z = mx^2. \quad (10.37)$$

Equations 10.35, 10.36, and 10.37 are inserted into Eq. 10.19.

$$\dot{r} = \left(\frac{C}{mx} \right) \left[\delta_1 - (0)v - \left(\frac{2x}{u} \right) r \right]. \quad (10.38)$$

The first-order yaw rate differential Eq. 10.38 of the ideal car is immediately seen to be decoupled from lateral velocity. A steady-state relationship between steering input and yaw rate can be written.

$$\frac{r}{\delta_1} = \frac{u}{2x}. \quad (10.39)$$

Equation 10.39 is evident in the yaw rate feedback term of the ideal two-axle vehicle control in [Figure 10.6](#). The ideal car is thus recognized to have the ideal Ackermann relationship between yaw rate and steering input as previously described in the kinematic analysis of [Chapter 7](#). The pole of first-order yaw rate response of the ideal car can be written.

$$\sigma = -\frac{2C}{mu}. \quad (10.40)$$

If the approximate cornering stiffness of 100 lbs/deg is used, and the mass of the ideal car is 2000 lbs, and the car is traveling at 60 mi/hr, the first-order pole is about 4 Hz. This is faster than a typical handwheel input. This vehicle responds well to a driver's steering input. It is clear that there is a fundamental relationship between the steering input and yaw rate. From Eq. 10.39, it is evident that the steady-state yaw rate response increases with vehicle speed and decreases with wheelbase. As the pole of the system of Eq. 10.40 moves to the left in the complex plane, the first-order exponential response becomes faster. Increased cornering stiffness on the tires speeds up the vehicle yaw rate response, and increased mass and speed decrease it. Thus, Prof. Bardeen would conclude that a responsive car would have stiff tires, low mass and short wheelbase.

Steering is also an input in the lateral acceleration term when the ideal vehicle assumptions of Eqs 10.35, 10.36, and 10.37 are inserted into Eq. 10.18.

$$\dot{v} = \left(\frac{C}{m} \right) \left[\delta_1 - \left(\frac{2}{u} \right) v - \left(\frac{mu}{C} \right) r \right]. \quad (10.41)$$

In the ideal vehicle, the lateral acceleration equation remains coupled to yaw rate. The steady-state value for yaw rate from Eq. 10.39 can be used in Eq. 10.41.

$$\dot{v} = 0 = \left(\frac{C}{m} \right) \left[\delta_1 - \left(\frac{2}{u} \right) v - \left(\frac{mu}{C} \right) \left(\frac{u}{2x} \right) \delta_1 \right]. \quad (10.42)$$

And solved for the steady-state “lateral velocity response.”

$$\frac{v}{\delta_1} = \frac{1 - \frac{mu^2}{2Cx}}{\frac{2}{u}}. \quad (10.43)$$

Equation 10.43 is difficult to interpret. At low speeds there is a positive lateral velocity associated with a positive steering input. There is a speed where there is zero lateral velocity. At this speed, the car’s velocity vector is aligned with its centerline which defines the x -axis. The driver would have a difficult task indeed if it were really important to control lateral velocity. Comparing Eqs 10.43 and 10.39 it is evident that yaw rate is the relevant response to a steering input.

Moving back to the dynamic response of the ideal vehicle, the parameters of the highly symmetric vehicle of Eqs 10.20, 10.21, and 10.22 can be inserted in the general yaw rate response of Eq. 10.39,

$$\frac{r(s)}{\delta_1(s)} = \frac{Cxu(sm u + 2C)}{x^2(s^2 u^2 m^2 + s(4muC) + C^2(4))} \quad (10.44)$$

and simplified.

$$\frac{r(s)}{\delta_1(s)} = \frac{Cxu(sm u + 2C)}{x^2(sm u + 2C)^2}. \quad (10.45)$$

Equation 10.45 is quite interesting—and revealing. In it you can see that the term within the parentheses appears once as a zero in the numerator, and is repeated in the denominator, forming the characteristic polynomial of the system. With the assumptions of the symmetric vehicle, the zero can cancel one pole.

$$\frac{r(s)}{\delta_1(s)} = \frac{\frac{C}{m}}{x\left(s + \frac{2C}{mu}\right)}. \quad (10.46)$$

The symmetric vehicle has a simple first-order yaw rate response. This first-order response can be seen in [Figure 10.6](#) as the symmetric assumption eliminates the coupling between lateral velocity (scaled drift angle) and yaw rate, and further in Eq. 10.22 where the state matrix becomes upper triangular. The idealized yaw rate response of Eq. 10.42 can be compared with the actual yaw rate response Eq. 10.34. Yaw rate response sensitivity to broadly defined parameters is more visible in Eq. 10.42. Furthermore, Eq. 10.46 can be solved for steady state,

$$\left. \frac{r(s)}{\delta_1(s)} \right|_{ss} = \frac{u}{2x}, \quad (10.47)$$

which is again the ideal Ackerman relationship of Eq. 10.39.

Similarly, the parameters of the highly symmetric vehicle of Eqs 10.35, 10.36, and 10.37 can be inserted in the general drift angle response of Eq. 10.29,

$$\frac{\beta(s)}{\delta(s)} = \frac{Cx(smxu + C2x - mu^2)}{x^2(s^2m^2u^2 + s(4muC) + C^2(4))} \quad (10.48)$$

and simplified.

$$\frac{\beta(s)}{\delta(s)} = \frac{C\left(smu + 2C - \frac{mu^2}{x}\right)}{(smu + 2C)^2}. \quad (10.49)$$

It is notable that the denominator of Eq. 10.49 has roots that agree with Eq. 10.40. Furthermore, it can be seen that the pole/zero cancellation apparent in the ideal vehicle yaw rate response cannot occur in the ideal vehicle drift angle response of Eq. 10.49.

As expected, when the assumptions of the symmetric vehicle are applied to Eq. 10.25, Eq. 10.40 is recovered. What is somewhat surprising, when the same assumptions of the symmetric vehicle are applied to the drift angle response of Eq. 10.26, the same Eq. 10.40 results.

Looking at yaw plane frequencies for the ideal vehicle and the neutrally steered vehicle provides a simple analysis that can build intuition and is reasonably valuable as many vehicles only slightly understeer. These idealizations are no substitute for a general derivation of the two-axle yaw plane transfer functions that follows.

Summarizing this work with the symmetric vehicle, it has been shown that the yaw rate response is a simple first-order lag, and the steady-state response is the ideal Ackermann relationship. The drift angle response is more complicated with a zero over two poles. It is precisely the centripetal acceleration term that prevents decoupling of lateral velocity from yaw rate in [Figure 10.6](#) that similarly prevents the pole-zero cancellation and resulting simplification. However at sufficiently low speeds there is approximate pole/zero cancellation. At speeds such that approximate cancellation does not occur, the drift angle response will be a bit slower than the yaw angle response, as the drift angle has repeated poles.

10.5 Steady-State Analysis

The steady-state values of the transfer functions of the “nonideal” vehicle shown in Eqs 10.33 and 10.34 can be found by evaluating them at $s = 0$. It is important to recall that steady-state for a given constant input is achieved when the time derivatives of the state variables are zero, implying the states are unchanging. Therefore this section describes how a vehicle at constant forward speed will respond to a constant steering input. In general the vehicle is tracing out a circle on a vehicle dynamics skid pad.

Equation 10.33 can be solved for the steady-state drift angle response,

$$\frac{\beta_{ss}}{\delta_{1,ss}} = \frac{-x_2 - \frac{x_1 mu^2}{l_2 C_2}}{l_2 + u^2 K_2} \quad (10.50)$$

and similarly Eq. 10.34 can be solved for the steady-state yaw rate response.

$$\frac{r_{ss}}{\delta_{1,ss}} = \frac{u}{l_2 + u^2 K_2} \quad (10.51)$$

Equation 10.51 is a well-known steady-state vehicle yaw rate response and has been derived in the literature in a variety of ways. In this work the steady-state response is found as a special case of the general dynamic yaw rate response.

It is possible to find a speed where the drift angle response of Eq. 10.50 is zero, and therefore the vehicle is pointed in the direction of its velocity.

$$u_{\beta=0} = \sqrt{\frac{-l_2 C_2 x_2}{m x_1}}. \quad (10.52)$$

Using reasonable vehicle parameters, it is evident that the vehicle will have a zero drift angle at a certain plausible speed, and positive or negative drift angles away from it. By itself drift angle is unimportant. Vehicles could have

a drift angle because of a misalignment and can be easily driven. In fact the driver will not notice as the sign of the drift angle changes as the vehicle goes through this transition velocity. The direction the vehicle is moving is much more important to the driver than the direction it is pointing. For example, the driver will naturally look out the side window of a severely oversteering car with no regard to the actual centerline of the vehicle. Even at less extreme operating conditions, it can be shown that the drift angle changes sign. The reader is asked to consider if this phenomena has been noticed.

Two important conclusions can be drawn from this line of reasoning. First, this discussion supports the notion that the velocity vector is more important than the vehicle centerline as a reference to the driver, and therefore the notion allowed by attack angles that the velocity vector is a response to the steering input makes physical sense. Second, the drift angle (i.e., the scaled lateral velocity) is not a relevant vehicle property to the driver.

Far more relevant to the driver is the steady-state yaw rate response of Eq. 10.51. Several interesting and informative vehicle results can be obtained from Eq. 10.51 that expresses the yaw velocity gain. When K_2 is positive, the vehicle requires a larger steering input δ_1 as the forward speed u increases to achieve the same steady-state yaw rate r . This condition is known as understeer and was introduced as a result of steering compliance in [Chapter 7](#). Conversely, the vehicle is said to be oversteering if K_2 is negative, and the vehicle requires a smaller steering input as speed increases to achieve a given yaw rate. When K_2 is negative and the vehicle is therefore oversteering there is a critical forward speed u_{crit} where the denominator of Eq. 10.51 goes to zero, and therefore the yaw rate response becomes infinite. Below this critical speed a steering input produces the same sign of yaw rate, but as the critical speed is approached from below the steering becomes more sensitive. At the critical speed the yaw rate is theoretically infinite for small steering input, which can be recognized practically as extremely sensitive steering, and the steering input actually changes polarity when a critical speed is exceeded. Somewhat counterintuitively (at least to someone not having seen sprint cars running on dirt) at speeds above the critical speed a positive steering input will result in a negative yaw rate. As Doc Hudson in the movie Cars explains, “I’ll put it simple, If you’re going hard enough left, you’ll find yourself turning right”

$$u_{\text{crit}} = \sqrt{\frac{l_2}{-K_2}}. \quad (10.53)$$

Oversteer implies that large yaw rates are generated from very small control inputs. Practically speaking, this oversteering vehicle would be very hard for the average driver to control at this critical speed. Consequently, it is desirable that production vehicles have some degree of understeer.

It is interesting to look at the derivative of the yaw rate response of Eq. 10.51 with respect to forward speed u .

$$\frac{\partial}{\partial u} \left[\frac{r_{ss}}{\delta_1} \right] = \frac{(l_2 - K_2 u^2)}{(l_2 + K_2 u^2)^2}. \quad (10.54)$$

An understeering characteristic speed can be defined where the derivative of the yaw rate response with respect to vehicle speed is zero, indicating the maximum yaw rate that is achievable at any speed for a given steering input. This characteristic speed u_{char} has an obvious relationship to the oversteering critical speed of Eq. 10.53 [9].

$$u_{char} = \sqrt{\frac{l_2}{K_2}} \quad (10.55)$$

At the characteristic speed, the yaw rate response of Eq. 10.51 becomes

$$\left(\frac{r_{ss}}{\delta_1} \right)_{char} = \frac{\sqrt{\frac{l_2}{K_2}}}{2l_2} = \frac{1}{2\sqrt{l_2 K_2}}. \quad (10.56)$$

At this characteristic speed defined by Eq. 10.55 for an understeering vehicle the yaw rate response of another neutrally handling vehicle would be:

$$\left(\frac{r_{ss}}{\delta_1} \right)_{char} = \frac{\sqrt{\frac{l_2}{K_2}}}{l_2} = \frac{1}{\sqrt{l_2 K_2}}. \quad (10.57)$$

The characteristic speed of an understeering vehicle has two interpretations: first, it is the speed at which the maximum yaw rate response is achievable for any given steering input, and second, it is the speed at which the vehicle requires twice the steering input of a neutrally steering vehicle to achieve a given yaw rate. Both the oversteering critical speed and the understeering characteristic speed are similar functions of the vehicle wheelbase and understeering coefficient only.

Lateral acceleration in the vehicle-fixed frame can be omitted in steady-state. Therefore steady-state lateral acceleration is due only to the vehicle yawing with a constant forward velocity.

$$a_{ss} = ur. \quad (10.58)$$

Multiplying both sides of Eq. 10.51 by the forward velocity u , the lateral acceleration response for a given steering input is obtained.

$$\frac{a_{ss}}{\delta_1} = \frac{u^2}{l_2 + u^2 K_2}. \quad (10.59)$$

The understeering coefficient K_2 as defined in this work can be physically interpreted as the reciprocal of the lateral acceleration response at high speed. This in fact is the essence of the SAE definition of the understeer/oversteer gradient [8].

The steady-state yaw rate can be related to the longitudinal velocity and radius of curvature R .

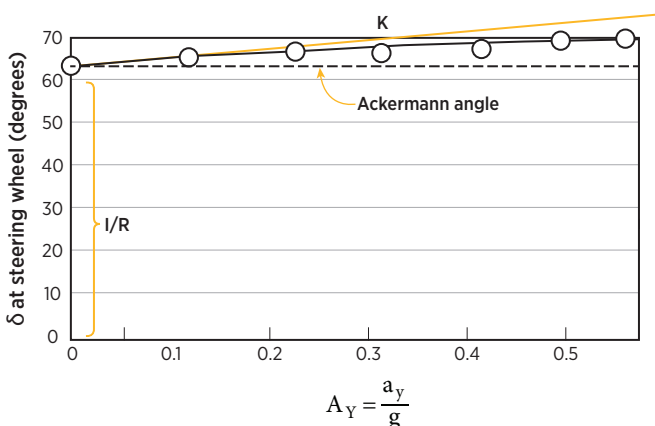
$$r = \frac{u}{R}. \quad (10.60)$$

Equation 10.60 is inserted into Eq. 10.51 and solved for the steering input.

$$\delta_1 = \frac{l_2}{R} + urK_2. \quad (10.61)$$

Equation 10.61 reveals much about a vehicle's steady-state handling behavior, and has well-known implications for vehicle testing. The steering angle input is comprised of a constant geometric component determined by the so-called Ackermann angle l/R introduced as Eq. 7.4 and a dynamic component that is proportional to the centripetal acceleration term ur . At very low speeds and therefore negligible lateral accelerations the steering input is defined by the Ackermann ratio of wheelbase to radius of curvature. As seen in [Figure 10.6](#) for low speed and using small angle approximations the steering input determines the radius of curvature of the trajectory as the intersection between perpendiculars from the wheel planes of tires on the front and rear axles. In this condition no lateral force is required from the tires and therefore no attack angles are generated. At higher speeds, the neutrally steering vehicle dynamically requires this same kinematically defined steering input. For the neutral steering condition Eq. 10.47 is zero and the required steering input defined by Eq. 10.61 is independent of centripetal acceleration.

Depending on the sign of K_2 as determined by $x_1 C_1 + x_2 C_2$ via Eq. 10.32, the nominal Ackermann steering input is modified by a term dependent upon centripetal acceleration. If the sign is positive the vehicle is understeering and more steering input is required for a given geometrical turn with higher lateral acceleration. If the sign is negative the vehicle is oversteering and steering input is reduced with lateral acceleration. So this is yet another physical interpretation of the understeer coefficient K_2 . The steady-state interpretation of the understeer coefficient of Eqs 10.47 and 10.61 is well known in the literature, in no small measure because of the ease in which it is established by vehicle tests using readily controlled speeds and turning radii.

FIGURE 10.7 Experimentally determined understeer.

© Dan E. Williams.

A real advantage of Eq. 10.61 is how understeer can be found experimentally. A test vehicle can be driven around a known constant radius turn at increasing speeds and lateral acceleration can be measured. In a steady-state turn there is no $\dot{\nu}$ so a lateral accelerometer will measure ur . Steering input can be measured at the handwheel and as we have seen knowing the steering ratio can be converted to a steering input at the road wheel.

As seen in [Figure 10.7](#), when the steering input required to maintain the constant radius is plotted against increasing measured lateral acceleration, the understeer is apparent from the slope. Although trivial for a two axle vehicle, we will see the concept of wheelbase is more ambiguous for vehicles with multiple axles, but the effective wheelbase of a multi-axle vehicle can be determined from [Figure 10.7](#) because of the radius of the circle is known and steering angle is measured.

Steady-state handling properties of the two-axle vehicle are completely determined by its wheelbase and understeer as long as the assumptions of the bicycle model are valid. The theoretical effect of K_2 on the dynamic system can be observed from the state matrix of Eq. 10.22, which becomes upper-triangular when K_2 in Eq. 10.32 becomes zero. When this occurs, the yaw rate response is independent of vehicle drift angle and lateral acceleration. Not surprisingly, in the following it will be seen that the wheelbase and understeer have a role in characterizing the dynamic response of the two-axle vehicle.

10.6 Pole Locations

It is interesting to factor the characteristic polynomial or denominator of Eqs 10.29 and 10.30. As is common in control systems, the roots of characteristic

polynomial can be used to determine overall stability and how fast the system can respond to inputs.

$$p(s) = s^2 mu^2 I_z + s(mu(x_1^2 C_1 + x_2^2 C_2) + I_z u(C_1 + C_2)) + C_1 C_2 l^2 - mu^2 (x_1 C_1 + x_2 C_2). \quad (10.62)$$

Equation 10.62 has physical significance as the denominator of the various transfer functions describing state variable behavior in response to steering input. When Eq. 10.62 is zero, the state variable response is infinite. This occurs at frequencies of the Laplace variable corresponding to the roots of this equation.

Ellis used notation to simplify the terms of Eq. 10.27. That concept will be modified to account for the new axle location convention in this work. The change in axle location convention allows uniform signs to be used which greatly enhances the subsequent utility of the notation. For the two-axle vehicle, the difference is only convenience. However, in future chapters, this notational change will be quite powerful.

$$C_a = C_1 + C_2, \quad (10.63a)$$

$$C_b = x_1 C_1 + x_2 C_2, \quad (10.63b)$$

$$C_c = x_1^2 C_1 + x_2^2 C_2. \quad (10.63c)$$

Equation 10.62 can be rewritten.

$$p(s) = s^2 mu^2 I_z + s(mu C_c + I_z u C_a) + (C_1 C_2 l^2 - mu^2 C_b). \quad (10.64)$$

Using a convenient relationship that is easily demonstrated by multiplying out terms defined in Eq. 10.63

$$C_a C_c - C_b^2 = C_1 C_2 l^2 \quad (10.65)$$

the characteristic polynomial Eq. 10.62 becomes

$$p(s) = s^2 mu^2 I_z + s(mu C_c + I_z u C_a) + (C_a C_c - C_b^2 - mu^2 C_b), \quad (10.66)$$

whose roots can be found using the quadratic equation,

$$s_{1,2} = \frac{-(\mu C_c + I_z u C_a) + / - \sqrt{(\mu C_c + I_z u C_a)^2 - 4\mu u^2 I_z (C_a C_c - C_b^2 - \mu u^2 C_b)}}{2\mu u^2 I_z} \quad (10.67)$$

and using Eqs 10.31, 10.32, and 10.65 it can be shown that

$$C_a C_c - C_b^2 - mu^2 C_b = C_1 C_2 l_2 (l_2 + K_2 u^2) \quad (10.68)$$

so that Eq. 10.67 becomes

$$s_{l_1, l_2} = \frac{-(mC_c + I_z C_a) + / - \sqrt{(mC_c + I_z C_a)^2 - 4muI_z C_1 C_2 l_2 (l_2 + K_2 u^2)}}{2muI_z}. \quad (10.69)$$

Recall from Eq. 10.53 of the previous section that a speed can be found at which an oversteering vehicle will produce very large yaw rates for very small steering inputs. At this critical speed defined by

$$l_2 + K_2 u^2 = 0, \quad (10.70)$$

where the negative term within the square root radical of Eq. 10.69 that is subtracted from a squared term vanishes. The radical is subtracted from the term that is squared to form one root of the polynomial, so the only way the real part of the root can be positive (and thus unstable) is if the condition described by the critical speed is exceeded. At the critical speed the characteristic polynomial Eq. 10.66 can be easily factored

$$p(s) = s \left(s + \frac{mC_c + I_z C_a}{mI_z \sqrt{\frac{l_2}{-K_2}}} \right) \quad (10.71)$$

and written in terms of the original cornering coefficients.

$$p(s) = s \left(s + \frac{m(x_1^2 C_1 + x_2^2 C_2) + I_z (C_1 + C_2)}{muI_z} \right). \quad (10.72)$$

With a real root on the origin of the complex plane, it is evident that the critical speed condition signifies marginal dynamic stability. As this condition is approached, small changes in steering input will result in large changes in yaw rate as the denominator of the transfer function approaches zero, consistent with the previous steady-state finding.

In the oversteering condition K_2 is negative, and when the critical speed is exceeded it is evident in Eq. 10.69 that a pole moves to the right half

plane indicating instability. The oversteering condition appears to the driver as the rear of the vehicle sliding out, and it is popularly termed “loose.” Thus we can see the control theoretic point of mythical NASCAR crew chief Harry Hoag in “Days of Thunder,” who said “loose is fast, but on the edge of out of control.”

Another interesting special condition occurs when $C_b = 0$. Using Eq. 10.47, it is evident that this is equivalent to neutral steering and the characteristic polynomial can be simplified. As earlier mentioned, when this special case occurs the state matrix of Eq. 10.31 is upper-triangular (all zero elements below the main diagonal), and the yaw rate response is de-coupled from the vehicle attack angle. As before, the roots of the neutral steering characteristic polynomial can be factored using the quadratic equation as found in Eq. 10.67 when $C_b = 0$,

$$s_{1,2} = \frac{-(muC_c + I_zuC_a) + / - \sqrt{(muC_c + I_zuC_a)^2 - 4mu^2I_z(C_aC_c)}}{2mI_zu^2} \quad (10.73)$$

and simplified.

$$s_{1,2} = \frac{-(mC_c + I_zC_a) + / -(mC_c - I_zC_a)}{2mI_zu}. \quad (10.74)$$

The neutral steering characteristic polynomial can be factored,

$$p(s) = \left(s + \frac{C_a}{mu} \right) \left(s + \frac{C_c}{I_zu} \right) \quad (10.75)$$

and written in terms of the original cornering coefficients.

$$p(s) = \left(s + \frac{(C_1 + C_2)}{mu} \right) \left(s + \frac{(x_1^2C_1 + x_2^2C_2)}{I_zu} \right). \quad (10.76)$$

It is interesting to observe that when the parametric values of the highly symmetric vehicle are inserted into Eq. 10.76 the expected repeated roots are observed.

It was shown earlier that wheelbase and understeer combine to completely determine the steady-state handling characteristics of a vehicle. It has just been shown that the steady-state handling parameters of wheelbase and understeer determine pole locations of the dynamic equation and combine to define the critical speed that determines marginal stability. Wheelbase and understeer are

therefore important in characterizing both steady-state and dynamic vehicle response.

10.7 Summary

In this chapter the formally defined accelerations were joined with the generalized lateral force to result in Newton's second law for a two-axle passenger car. The two resulting first-order differential equations were put in block diagram form, and found to be much more pleasing to the control theorist. Feedback is subtracted from a positive command to form an error signal and most gains in the various blocks are positive. Therefore, it is easy to see stiffness, scaling and time constants of the coupled first-order differential equations.

The two first-order differential equations in yaw rate and drift angle (a scaled version of lateral acceleration) were found to be decoupled in a condition known as neutral steering. When this condition holds, yaw rate is completely decoupled from drift angle—but drift angle remains coupled to yaw rate. In this neutral steer condition, the yaw rate response is seen to be a simple first-order lag, whose steady-state value is the ideal Ackermann relationship.

The concept of a symmetric vehicle was introduced to form an even simpler model to gain intuition of vehicle behavior. The yaw-plane model is perhaps less intuitive than previously analyzed ride models that feature second-order dynamics. Masses bouncing on springs are relatively easy to conceptualize, but coupled first-order differential equations are a bit less intuitive.

Vehicle behavior was examined in the steady state, where all time derivatives of the state variables are zero. Steady-state yaw rate response was found to be completely characterized by the wheelbase and understeer parameters. Key transition speeds were identified.

The characteristic polynomial was derived, and roots found for several interesting vehicle conditions including neutral steer and an oversteering vehicle at the critical speed. It is very interesting that the wheelbase and understeer parameters that completely define steady-state behavior are important in understanding the characteristic polynomial and therefore the dynamic response as well.

New conventions have been applied to the well-known bicycle or yaw-plane model resulting in a formulation more familiar to control theorists. The new conventions allowed a notation innovation that produced more compact mathematical expressions, particularly in expressing the eigenvalues of the model. But in essence, these innovations merely simplify a familiar problem that was not overly complex. In future chapters these innovations are essential to addressing new vehicle dynamics problems. Specifically, the new conventions will allow direct computation of these important equivalent wheelbase and understeer quantities for arbitrarily complex vehicles.

References

- [1] Fancher, Paul S., Static stability of articulated commercial vehicles, Vehicle System Dynamics, Vol 14, No 4, 1985, p. 201–227.
- [2] Wong, J.Y., Theory of Ground Vehicles, Wiley, New York, 1978.
- [3] Gillespie, Thomas D., Fundamentals of Vehicle Dynamics, Society of Automotive Engineers, 1992.
- [4] Milliken, William F., and Douglas L. Milliken, Race car vehicle dynamics, Society of Automotive Engineers, 1995.
- [5] Hoddeson, Lillian, and Vicki Daitch, True genius: The life and science of John Bardeen, Joseph Henry Press, 2002, Washington, DC.
- [6] Pacejka, Hans B., Tire and Vehicle Dynamics, Society of Automotive Engineers, Warrendale PA, 2002.
- [7] Maciejowski, J.M. Multivariable feedback design, Addison-Wesley, 1989.
- [8] Vehicle Dynamics Terminology, Society of Automotive Engineers, Warrendale, PA.
- [9] Bundorf, R.T., The Effect of Vehicle Design Parameters on Characteristic Speed and Understeer, SAE paper 670078, 1967.

Rear Axle Steering and Lanekeeping

“The miracle of the appropriateness of the language of mathematics for the formulation of the laws of physics is a wonderful gift which we neither understand nor deserve.

—Eugene Wigner

11.1 Introduction

The previous chapter developed the two-axle yaw plane model based on rigorous treatment of accelerations in rotating reference frames, and a generalized lateral force developed by an axle arbitrarily located with respect to the vehicle center of gravity, and possibly steered. Although the derived equations were general, the ensuing discussion and analysis in the preceding chapter assumed a conventional two-axle vehicle, with the front axle steered. This present chapter will demonstrate further usefulness of the yaw-plane model.

This chapter combines relatively simple concepts from vehicle dynamics, control theory, and human modeling to derive a new result that is recognized to have practical utility. The “bicycle” or yaw-plane vehicle dynamic model is well known and control theoretic notions of single-input-single-output systems such as stability margin and steady-state error constants are very familiar. These concepts are combined with perhaps the simplest accepted model of the driver and vehicle combination. The resulting system suggests a rear axle steer and corresponding control law that provides positive-real stability characteristics at high speed by eliminating imaginary zeros. Somewhat surprisingly, this control law derived from high-speed stability considerations exhibits the low-speed steady-state behavior appreciated in existing vehicle applications.

Steering an auxiliary axle in addition to the primary steered front axle adds an additional control input that has been appreciated by practical vehicle designers for some time. Early efforts at steering the rear axle included a mechanical gearbox connecting the front and rear wheels such that for small inputs the rear wheels steered with angular displacement in the same direction as the driver controlled front wheels (crab-steer), and at larger steering inputs the rear axle steered in the opposite direction (counter-steer).^[1] Indirectly this system allowed for crab-steer at high vehicle speeds as the magnitude of steering inputs is practically limited, and counter-steer at lower speeds where larger steering inputs can be achieved. A similar control strategy was used by the electronically controlled Delphi Quadrasteer system, where high-speed crab-steer was featured to improve stability and towing characteristics and counter-steer at low speeds to improve maneuverability ^[2]. More recently, electronically controlled rear axle steering systems are offered on European production commercial vehicles that fully counter-steer at low speeds, and remain at their nominal center positions at higher vehicle speeds ^[3]. Thus, a number of practically achievable rear axle steering concepts make use of low-speed counter-steer and transition to either crab-steer or a fixed axle at high speeds. This work will develop a theoretical understanding of the functionality of these systems that are available in practice.

There is a great deal of literature devoted to different theoretical rear axle steering strategies. For an overview, Furukawa et al. ^[4] provides an excellent summary of early efforts at passenger car four-wheel steer; You and Jeong ^[5] provide a more theoretical study of the lateral control opportunities of passenger car rear axle steer. Gohring et al. ^[6] report all-wheel-steer vehicle results for a two-axle medium duty commercial vehicle. More recently Bayar and Unlusoy ^[7] describe theoretical opportunities to improve the handling of three-axle vehicles. Steering the third axle of a three-axle commercial vehicle at low speeds is known to improve vehicle maneuverability ^[8] and reduce tire wear ^[9]. Qu and Zu ^[10] consider the driver in their work on steering the third axle of a commercial vehicle to insure that a reference model is followed in the presence of unknown road inputs and uncertain vehicle parameters.

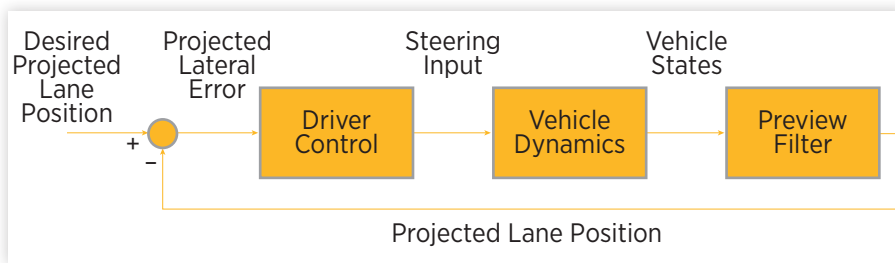
The ability of a vehicle to maintain a lane is dependent upon the driver. MacAdam ^[11] gives an excellent review of prior work in driver modeling, in addition to providing a state-of-the-art literature review. MacAdam cites prior work ^[12] that measured “driver ‘sight-point’ ahead of the vehicle and developed a steering model based on deviations between the sight point and the desired course. . . . Preview allows the driver to directly observe the time-advanced path input requirement and to then project into the future a predicted vehicle response based upon the estimated control response needed to achieve a certain goal (path error minimization . . . , etc.).”

Erseus et al. [13] generated a driver model that captured varying degrees of driving skill. The model included several types of preview, and they found in general highly skilled drivers exhibit a greater preview window than less skilled drivers.

Driver modeling is a fascinating field that has borrowed much from pilot modeling in aircraft control. Fundamental contributions in this area come from R.A. Hess [14–17] recently retired from UC Davis, and Systems Technology, Inc. [18,19]. Driver dynamics and vehicle dynamics combine to form a closed loop. In its simplest embodiment, the driver senses a lane position—perhaps previewed as just discussed—and determines the appropriate handwheel input, thus closing a loop on lane position. Embedded within this closed loop are driver dynamics in series with vehicle dynamics. The simplest model assumes that driver control dynamics are sufficient to provide a well-compensated driver–vehicle open-loop, characterized by a 90° phase margin. This “crossover” model has appeal for vehicle dynamic work because it requires minimal characterization of the driver. MacAdam [11] notes the crossover model is “specifically related to the task of straight-line automobile regulation.” The open-loop crossover frequency is a fundamental property of human control and can be assumed to be approximately in the range of 2 rad/sec [14] to 4 rad/sec [11], while a previous source suggests this frequency is “commensurate with task demands” [15].

Control theory provides techniques to evaluate the performance of closed-loop systems, where output from a system is fed back and compared with a desired input, and the system of interest is driven by this error, with the result that the error is reduced. The transfer function of the open-loop system (without feedback) determines the performance and stability of the closed-loop system (with feedback). It is well known that if the phase lag between the output and input signals of the open-loop system is greater than 180°, closed-loop stability will limit achievable system performance. Also, it is known that if the open-loop transfer function includes a free integrator, the closed loop will track a nonzero steady-state input signal without error. If the system possesses more free integrators, it can track more complex inputs without errors [20] but stability is sacrificed.

The crossover model belongs in a class of dynamic systems termed “positive-real” [21]. Positive-real systems or dissipative systems are characterized by a 90° open-loop phase margin. We have already experienced such a system with the inertial damping of the ride section. If driver dynamics couple with vehicle dynamics and preview in such a way as to form a positive-real system consistent with the crossover model, the man-machine system will be very stable and robust and will perform well in a closed loop. In fact the underlying assumption of the crossover model is that the driver will develop a control compensating the vehicle dynamics to result in the desirable positive-real man–machine system. Thus, the closer the vehicle dynamics approach a positive-real system, the simpler the compensating driver dynamics can be.

FIGURE 11.1 Driver-vehicle closed-loop.

Reprinted with permission from © SAE International.

This work will combine well-known concepts from the literature to form the man-machine closed-loop shown in [Figure 11.1](#). The driver control is assumed to convert a projected lane position error to a steering input. Preview will be applied so that the lane position error will be projected in front of the moving vehicle, and steering input occurs if the vehicle is not projected to achieve its desired lane position. Starting with the yaw-plane model developed in the previous chapter, inertially referenced states and a rear axle steer control input are appended. A rear axle steer control strategy is suggested that insures generally complex zeros of the open-loop transfer function between steering input and projected lane position are real and repeated. The driver and vehicle models are combined and analyzed using concepts from linear system theory, so the effect of various nonlinearities that might be present in the vehicle are beyond the scope of this work.

Given conditions easily realizable on practical vehicles, this condition is shown to insure approximate positive-real behavior at relevant frequencies. Using an idealized vehicle, the derived rear axle steer control law is shown to minimize the compensatory dynamics required of the driver by crossover model requirements, while simultaneously enhancing the lane tracking properties of the driver/vehicle combination and improving low-speed maneuverability. The proposed control strategy is generally familiar to practical vehicle designers: counter-steering at low vehicle speed and crab-steering at high speed. The main contribution of this chapter is therefore a classical control theoretic analysis of the man-machine system providing insight into the theoretical functional performance enhancement achieved by a practically applied speed dependent rear-axle steering strategy.

11.2 Vehicle Model with Rear Axle Steering

As derived in [Chapter 9](#), Eq. 9.5 expresses the side force F of displaced tires on axle i ,

$$F_i = C_i \left(\delta_i - \frac{v + x_i r}{u} \right), \quad (11.1)$$

where C_i is the combined linear cornering coefficient of tires on the i th axle, δ_i is the angular displacement input, x_i is the longitudinal location of the tire forward of the vehicle center of gravity, v is the lateral velocity, r the yaw rate, and u the constant longitudinal velocity. Using this generalized tire side force model, it is important to keep in mind that an axle located behind the vehicle center of gravity is located by a negatively signed distance x_i . The steer angle δ_i can be a variable control input, or in the case of a nonsteered or rigid axle it becomes zero. In this chapter steering is allowed on the rear axle, as shown in [Figure 11.2](#).

As derived in [Chapter 10](#), a vehicle model can be constructed by summing the forces and moments produced by the combined tires on each axle.

$$m(\dot{v} + ur) = F_1 + F_2, \quad (11.2)$$

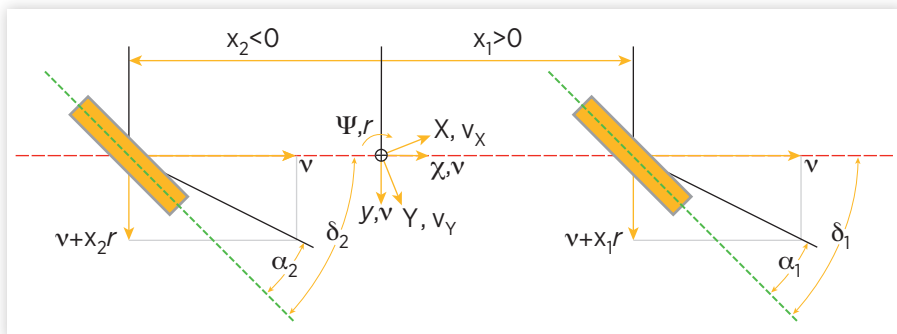
$$I_z \dot{r} = x_1 F_1 + x_2 F_2, \quad (11.3)$$

where m is the vehicle mass and I is the moment of yaw inertia.

Together, Eqs 11.2 and 11.3 describe the dynamic behavior of a vehicle with a constant longitudinal velocity u . A vehicle sideslip angle β can be formed by scaling the time-varying lateral velocity v by the constant longitudinal velocity u [24] and β can be physically interpreted as the “drift angle” of the vehicle with respect to a body-fixed coordinate frame.

Translational displacements are measured relative to the reference frame yawing with the vehicle. Lanekeeping displacements of interest are relative to an inertially fixed reference frame in which the lane markings are located. Therefore, a coordinate transformation is required. Relative to the inertial frame, the body-fixed coordinate system is rotated an angle ψ which is the integral of the yaw rate as shown in [Figure 11.2](#). Using ψ the body-fixed vehicle dynamic velocities can be transformed to velocities relative to the inertial frame where lane position is referenced.

FIGURE 11.2 Yaw-plane model.



Using the definition of the vehicle side-slip angle β , and if β and ψ are both small, a condition consistent with lane-keeping, velocities in the inertial frame can be written as linear functions of the state variables.

$$V_x = u, \quad (11.4)$$

$$V_y = u(\psi + \beta). \quad (11.5)$$

In the lane maintenance mode the longitudinal velocity is the same constant value in both the body-fixed and inertially fixed reference frames as seen in Eq. 11.4. Lateral velocity in the inertially fixed frame is a function of the constant forward velocity and state variables, and is the derivative of lateral displacement Y with respect to time.

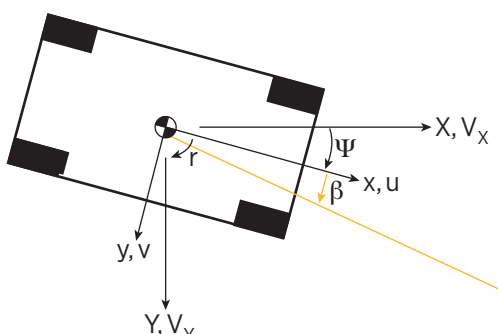
$$\dot{Y} = u\beta + u\psi. \quad (11.6)$$

Another dynamic state is apparent by noting that the time derivative of yaw angle is simply yaw rate.

$$\dot{\psi} = r. \quad (11.7)$$

Equations 11.2, 11.3, 11.6, and 11.7 can be written in state-space form [6,7], where the new states are easily appended to the state space model derived in [Chapter 10](#). The original vehicle dynamic states are decoupled from the newly appended states.

FIGURE 11.3 Transformation to inertially referenced velocities.



$$\begin{bmatrix} \dot{\beta} \\ \dot{r} \\ \dot{\psi} \\ \dot{Y} \end{bmatrix} = \begin{bmatrix} \frac{-C_1 - C_2}{mu} & \left(\frac{-x_1 C_1 - x_2 C_2}{mu^2} - 1 \right) & 0 & 0 \\ \frac{-x_1 C_1 - x_2 C_2}{I_z} & \frac{-x_1^2 C_1 - x_2^2 C_2}{I_z u} & 0 & 0 \\ 0 & 1 & 0 & 0 \\ u & 0 & u & 0 \end{bmatrix} \begin{bmatrix} \beta \\ r \\ \psi \\ Y \end{bmatrix} + \begin{bmatrix} \frac{C_1}{mu} & \frac{C_2}{mu} \\ \frac{x_1 C_1}{I_z} & \frac{x_2 C_2}{I_z} \\ 0 & 0 \\ 0 & 0 \end{bmatrix} \begin{bmatrix} \delta_1 \\ \delta_2 \end{bmatrix}. \quad (11.8)$$

Consistent with [Chapter 10](#), nomenclature is introduced for compactness.

$$C_a = C_1 + C_2, \quad (11.9)$$

$$C_b = x_1 C_1 + x_2 C_2, \quad (11.10)$$

$$C_c = x_1^2 C_1 + x_2^2 C_2. \quad (11.11)$$

A single-input system is formed if it is assumed that the rear steering input δ_2 is proportional to the front steering input δ_1 .

$$\delta_2 = \eta \delta_1. \quad (11.12)$$

When $\eta = 1$, the front and rear axles are steered with the same steering angle in crab steer, and when $\eta = -1$, they oppose each other in counter steer. The dynamic response of the augmented two-axle system can be expressed using methods generally described in Eq. 11.13 [[25](#)].

$$\begin{bmatrix} \beta(s) \\ \delta_1(s) \\ r(s) \\ \dot{\delta}_1(s) \\ \psi(s) \\ \dot{\delta}_1(s) \\ Y(s) \\ \dot{\delta}_1(s) \end{bmatrix} = \frac{\begin{bmatrix} \frac{s^2(sIu + C_c)}{I_z u} & \frac{-s^2(C_b + mu^2)}{mu^2} & 0 & 0 \\ \frac{-s^2C_b}{I_z} & \frac{s^2(smu + C_a)}{mu} & 0 & 0 \\ \frac{-sC_b}{I_z} & \frac{s(smu + C_a)}{mu} & \frac{\Delta}{s} & 0 \\ \frac{(s^2I_z u + sC_c - uC_b)}{I_z} & \frac{(-sC_b + uC_a)}{mu} & \frac{u\Delta}{s^2} & \frac{\Delta}{s} \end{bmatrix}}{\Delta} \begin{bmatrix} \frac{C_1}{mu} + \frac{C_2}{mu}\eta \\ \frac{x_1 C_1}{I_z} + \frac{x_2 C_2}{I_z}\eta \\ 0 \\ 0 \end{bmatrix}, \quad (11.13)$$

where

$$\Delta = \frac{s^2(s^2mu^2I_z + su(mC_c + I_z C_a) + C_a C_c - C_b^2 - C_b mu^2)}{mu^2 I_z}. \quad (11.14)$$

Thus, the transfer functions from the single control input to the various state variables can be written when the rear axle is steered using the simple proportional relationship of Eq. 11.12.

$$\frac{\beta(s)}{\delta_1(s)} = \frac{(sI_z u + C_c)(C_1 + C_2 \eta) - (C_b + mu^2)(x_1 C_1 + x_2 C_2 \eta)}{s^2 mu^2 I_z + su(mC_c + I_z C_a) + C_a C_c - C_b^2 - C_b mu^2}, \quad (11.15)$$

$$\frac{r(s)}{\delta_1(s)} = \frac{u(smu + C_a)(x_1 C_1 + x_2 C_2 \eta) - C_b u(C_1 + C_2 \eta)}{s^2 mu^2 I_z + su(mC_c + I_z C_a) + C_a C_c - C_b^2 - C_b mu^2}, \quad (11.16)$$

$$\frac{\psi(s)}{\delta_1(s)} = \frac{u(smu + C_a)(x_1 C_1 + x_2 C_2 \eta) - u C_b (C_1 + C_2 \eta)}{s(s^2 mu^2 I_z + su(mC_c + I_z C_a) + C_a C_c - C_b^2 - C_b mu^2)}, \quad (11.17)$$

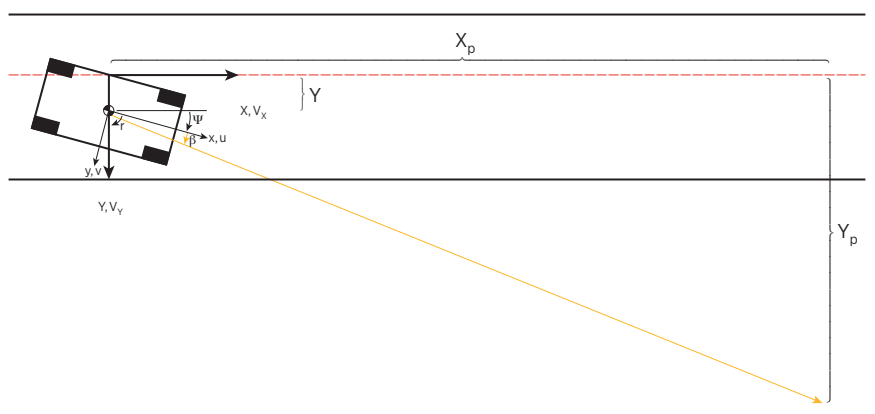
$$\frac{Y(s)}{\delta_1(s)} = \frac{u(uC_a - sC_b)(x_1 C_1 + x_2 C_2 \eta) + u(s^2 I_z u + sC_c -uC_b)(C_1 + C_2 \eta)}{s^2(s^2 mu^2 I_z + su(mC_c + I_z C_a) + C_a C_c - C_b^2 - C_b mu^2)}. \quad (11.18)$$

When there is no rear steering and $\eta = 0$, Eqs 11.15–11.18 describe the behavior of a conventionally steered vehicle in a lanekeeping mode where small angle approximations apply derived in [Chapter 10](#). If in fact $\eta = 0$, Eqs 11.15 and 11.16, revert to the familiar results of [Chapter 10](#). Equation 11.17 is interesting as ψ , the integral of yaw rate, results in a free integrator multiplying the familiar characteristic polynomial. In Eq. 11.18, the transfer function from steering into to lane position is the familiar yaw rate characteristic polynomial multiplied by a double integrator. Therefore, we can immediately suspect that a simple loop closed on lane position will have low frequency stability issues with the 180° phase lag produced by the double integrator. This double integrator will soon become important.

As shown in [Figure 11.4](#), the lateral position Y_p of a point located on the projected velocity vector of the vehicle a distance x_p from the center of mass can be expressed in terms of the state variables. This can be interpreted as the vehicle's lateral position error that would occur at some future time if the vehicle continues along its current velocity vector.

FIGURE 11.4 | Projected lateral lane position.

Reprinted with permission from © SAE International.



$$Y_p = Y + (\beta + \psi)x_p. \quad (11.19)$$

The lateral position Y_p can be expressed relative to the steering input δ_1 using Eqs 11.15, 11.17, and 11.18.

$$\frac{Y_p(s)}{\delta_1(s)} = \left(\frac{s x_p + u}{s^2} \right) \left(\frac{C_1 \left(s^2 I_z u + s(C_c - x_1 C_b) + u(x_1 C_a - C_b) \right) + \eta C_2 \left(s^2 I_z u + s(C_c - x_2 C_b) + u(x_2 C_a - C_b) \right)}{s^2 m u^2 I_z + su(m C_c + I_z C_a) + C_a C_c - C_b^2 - C_b m u^2} \right). \quad (11.20)$$

Equation 11.20 is the general expression for the inertially referenced lateral position Y_p of a point displaced x_p from the center of mass of the vehicle as a function of steering input δ_1 with a proportional rear steering input η . There are two components of Eq. 11.20. The numerator of the first term is a zero determined by the preview distance x_p and forward speed u . The denominator of the first term includes two free integrators. The final term is a second-order compensator based on vehicle dynamic properties.

11.3 Determination of Rear Axle Steer Control

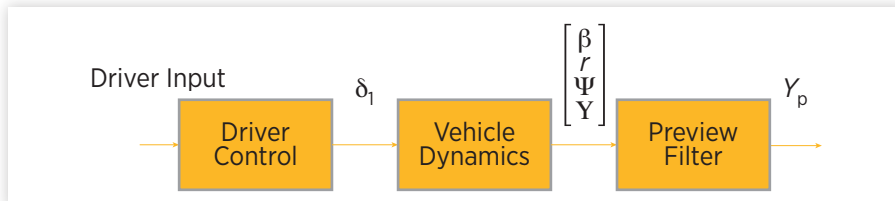
Key elements of the man-machine closed-loop described in [Figure 11.1](#) can now be identified. The vehicle dynamics are described by transfer functions Eqs 11.15–11.18 that report state variables as a function of steering input. The

preview filter is described by Eq. 11.19 that is a linear transformation of vehicle states to a projected lateral lane position. The vehicle dynamics and preview are combined together in Eq. 11.20. Recall the fundamental notion of the crossover model is that the open-loop transfer function of the driver and vehicle in series is well compensated because of unspecified driver dynamics. A rear axle steer control law will be developed that results in a very simple driver control required to satisfy the crossover model. In effect we are shaping the open loop response of the vehicle so that the man-machine system can be more simply controlled. Consider a simple case of a driver controlling lane position of a point projected some distance ahead of the vehicle center of mass with a simple proportional gain K . In view of [Figures 11.1](#) and [11.3](#), the driver control would be a front axle steering input δ_1 determined by the gain K multiplied by the error in projected lane position as shown in [Figure 11.5](#).

It is interesting to observe that if the controlled position is behind the vehicle center of gravity a non-minimum phase system [26] is formed with the preview zero in the right half-plane. Such vehicles are not typical, but they are not unknown. A minimum phase system is characterized by a unique relationship between the minimum number of poles and zeros and phase of the open loop transfer function. If all poles and zeros occur in the left half plane, the system will be minimum phase, and will also be stable, so such systems are common. A system with a pole in the right half plane can be stabilized through feedback. Zeros in the right half plane are more mysterious. The output of such systems has the counter-intuitive effect of initially opposing an input before tracking the input.

When I first met nonminimum phase systems as a student in control theory, I thought they were some arcane mathematical construct that did not occur in practice. It was hard to imagine a system that initially reacted opposite to the final reaction. Then I considered an experience growing up on a farm, driving a tractor with a rigid rear mounted tillage implement that dragged pieces of iron in between rows of crops to cut out weeds. Such a configuration was hard to control. When I was getting too close to a row on the right, if I would turn to the left the rear hanging implement would initially get even

FIGURE 11.5 Driver-vehicle open-loop forming the crossover model.



Reprinted with permission from © SAE International.

FIGURE 11.6 A paintstripner.

Reprinted with permission from © SAE International.



closer, perhaps even cutting out the row crop. Such a configuration required precise control on center, and if there was significant deviation from center, the operator had a choice of an extreme maneuver to return to center quickly, with a higher likelihood of cutting out the crop for a shorter period of time, or a more gentle maneuver that would be less likely to cut out the crop, but if it did, would cut it out for a longer period of time. Making this connection, I realized that nonminimum phase systems were in fact quite real. Zeros of the transfer function “depend on the physical placement of the sensors and actuators relative to the underlying dynamics. The concept of a zero distinguishes control theory from dynamical systems theory” [27].

Figure 11.6 shows such a specialty vehicle designed to apply a painted stripe with the boom hanging behind the rear axles. There is the opportunity for the vehicle to be controlled from the rear. Imagine being the driver, trying to lay down a straight line, and you are drifting a bit to the right. You would naturally steer back to the left. But in steering to the left the boom you are trying to control initially moves even more to the right because of the vehicle yawing before the boom follows the center of gravity to the left.

The double integrator provides a 180° phase lag in the open-loop transfer function of the vehicle shown in Eq. 11.20. At frequencies beyond u/x_p rad/sec, the preview zero adds 90° of phase lead. Thus the combination of the double integrator and preview zero—the first parenthetical component of Eq. 11.20—results in 90° of phase lag at frequencies beyond the preview zero. The driver has discretion to determine the preview distance x_p to ensure this condition. Given sufficient preview, the driver control effectively can compensate many second order pole/zero combinations of the vehicle dynamics to result in a well-compensated open-loop system at crossover. Recall that Erseus [20] showed that a more highly skilled driver can be characterized by a longer preview window that serves to better compensate the open loop. If the zeros are real and lower frequency than real poles of the vehicle dynamics, the driving task is easy as the system is already positive-real at sufficiently high frequencies. If the transfer function has imaginary (oscillatory) zeros, or if the poles are lower frequency than the zeros, the open-loop transfer function of Eq. 11.20 will have a phase lag of greater than 180° and therefore driver dynamics will be required for compensation to stabilize the loop closed on a projected lateral lane displacement. Thus steering the rear axle can have an effect on the vehicle dynamic pole/zero combination for which the driver's control task compensates.

It is possible to find a η that allows a location of the general vehicle dynamic zeroes of Eq. 11.20 that will simplify the driving task defined by the cross-over driving model and improve the closed-loop lane tracking behavior of the vehicle/driver system. To ensure that the open-loop phase lag does not fall below 180° a value for the rear steer coefficient η is selected that insures two zeros from the second order term in the numerator of Eq. 11.20 are real, repeated and lower frequency than the centroid of the poles of the second order term of the denominator.

The roots of the second-order term of the numerator of Eq. 11.20 can be found.

$$s_{1,2} = \frac{-C_1(C_c - x_1 C_b) - \eta C_2(C_c - x_2 C_b) \pm \sqrt{\begin{aligned} & \left(C_1(C_c - x_1 C_b) + \eta C_2(C_c - x_2 C_b) \right)^2 \\ & - 4I_z u^2 (C_1 + \eta C_2)(C_1(x_1 C_a - C_b)) \\ & + \eta C_2(x_2 C_a - C_b) \end{aligned}}}{I_z u (C_1 + \eta C_2)}. \quad (11.21)$$

The discriminant of Eq. 11.21 is itself a second order function of η , and its roots can be similarly obtained.

$$\eta_{1,2} = \frac{x_1 x_2 C_1 C_2 (x_1 - x_2) + 2I_z u^2 (C_2 - C_1) \pm 2u \sqrt{I_z (-C_b^3 + I_z u^2 C_a^2 + C_a C_b C_c)}}{C_1 C_2 x_1^2 (x_1 - x_2) + 4I_z u^2 C_2}. \quad (11.22)$$

Thus, when the rear axle is steered in proportion to the front with the constant η given by Eq. 11.22, the open-loop transfer function of Eq. 11.20 has real, repeated zeros. The rear axle steer control law of Eq. 11.22 is a function of tire properties, axle locations, inertia, and a nonlinear function of vehicle speed. Hereafter, this strategy is referred to as “real repeated zero (RRZ)” control.

At speeds approaching $u = 0$, the rear axle steering defined by Eq. 11.22 is a counter-steering function of axle locations (recall x_2 is necessarily negative).

$$\eta_{1,2} \Big|_{u=0} = \frac{x_2}{x_1}. \quad (11.23)$$

It is quite interesting that the control law of Eq. 11.22, designed from dynamic compensation considerations, yields the steady-state low-speed result now valued in the marketplace to enhance maneuverability [8,9]. Low-speed maneuverability enhancement is not the objective of RRZ control, but is nonetheless an important practical benefit. To paraphrase Wigner, this is “a wonderful gift which we neither understand nor deserve.”

When Eq. 11.22 is used to select a control law resulting in repeated real zeros, the location of those repeated zeros can be determined relative to the centroid of the poles of Eq. 11.20. From Eq. 11.21, the real zeros can be located.

$$\Re_{\text{zeros}} = -\frac{C_1(C_c - x_1 C_b) + \eta C_2(C_c - x_2 C_b)}{I_z u(C_1 + \eta C_2)}. \quad (11.24)$$

The real centroid of the poles of Eq. 11.20 can be written consistent with Eq. 10.69 from [Chapter 10](#).

$$\Re_{\text{poles}} = -\frac{(mC_c + I_z C_a)}{muI}. \quad (11.25)$$

Comparing Eqs 11.24 and 11.25, a condition can be specified for the zeros to be at a lower frequency than the poles to insure an addition of phase to the open-loop transfer function thereby increasing the stability margin.

$$\frac{-C_1}{C_2} \leq \eta. \quad (11.26)$$

Equation 11.26 limits the magnitude of counter-steer ($\eta < 0$) that insures stability at any given speed. If front and rear cornering coefficients are equal, the limit corresponds to the rear axle mirroring the front axle steering input. In most anticipated vehicle configurations the inequality of Eq. 11.26 will hold, and the zeros will therefore be real and at a lower frequency than the poles, ensuring a stable closed-loop with simple preview proportional control when the rear axle steer gain η is determined by Eq. 11.22 to provide RRZ.

11.4 Open-Loop Response of Ideal Vehicle

The basic properties of the derived transfer functions can be demonstrated on an idealized vehicle that has the same cornering coefficient on the front and rear axles, and has half its mass at a point on either axle. This highly symmetric vehicle was introduced in [Chapter 10](#). By making these simplifications the response of the idealized vehicle is more readily conceptually appreciated. The vehicle dynamic parameters of such an ideal vehicle are simplified,

$$\begin{aligned} C &= C_1 = C_2 \\ x &= x_1 = -x_2 \\ mx^2 &= I_z \end{aligned} \quad (11.27)$$

and used in turn to simplify Eqs 11.9, 11.10, and 11.11.

$$\begin{aligned} C_a &= C_1 + C_2 = 2C \\ C_b &= x_1 C_1 + x_2 C_2 = 0 \\ C_c &= x_1^2 C_1 + x_2^2 C_2 = 2Cx^2 \end{aligned} \quad (11.28)$$

The transfer functions of the ideal vehicle are considerably simplified, making the fundamental effect of varying η more obvious. Inserting Eqs 11.27 and 11.28 into Eq. 11.16, the relationship between the steering input δ_1 and yaw rate r can be written for the ideal vehicle with rear axle steering.

$$\frac{r(s)}{\delta_1(s)} = \frac{\frac{C}{xm}(1-\eta)}{\left(s + \frac{2C}{mu} \right)}. \quad (11.29)$$

It is interesting to look at the steady-state yaw rate of Eq. 11.29 without a rear steering input ($\eta = 0$).

$$\left. \frac{r_{ss}}{\delta_{1ss}} \right|_{\eta=0} = \frac{u}{2x}. \quad (11.30)$$

Equation 11.30 represents the familiar Ackermann relationship for yaw rate gain when it is observed that the wheelbase is $2x$. When the rear axle is fully counter-steering ($\eta = -1$), the steady-state yaw rate gain of Eq. 11.29 is twice the unsteered value, or equivalently the effective wheelbase is cut in half serving

to improve steady-state handling. When the rear axle is fully crab-steering ($\eta = 1$), the vehicle cannot generate a yaw rate.

The lateral position y_p of a point displaced from the center of gravity by x_p can be expressed for an ideal vehicle using Eqs 11.27 and 11.28 substituted into Eq. 11.20.

$$\frac{Y_p(s)}{\delta_1(s)} = \frac{\frac{Cx_p}{mu} \left(s + \frac{u}{x_p} \right) \left(\frac{2C}{mx} (1-\eta) + s \left(s + \frac{2C}{mu} \right) (1+\eta) \right)}{s^2 \left(s + \frac{2C}{mu} \right)^2}. \quad (11.31)$$

If $x_p = 0$, Eq. 11.31 describes lateral displacement at the center of mass of the ideal vehicle. At the extremes, Eq. 11.31 can again be characterized by full crab-steer when $\eta = 1$:

$$\left. \frac{Y_p(s)}{\delta_1(s)} \right|_{\eta=1} = \frac{(x_p s + u) \frac{2C}{mu}}{s \left(s + \frac{2C}{mu} \right)}, \quad (11.32)$$

and full counter-steer when $\eta = -1$.

$$\left. \frac{Y_p(s)}{\delta_1(s)} \right|_{\eta=-1} = \frac{(x_p s + u) \frac{4C^2}{m^2 ux}}{s^2 \left(s + \frac{2C}{mu} \right)}. \quad (11.33)$$

11.5 Specified Preview

In both the crab-steer of Eq. 11.32 and the counter-steer of Eq. 11.33, there is a zero because of the preview distance x_p . In both cases (and indeed in the conventionally steered case), free integrators in the denominator insure that there will be zero steady-state tracking error; however, the counter-steer condition will be more robust in tracking a time-varying input with the additional free integrator in the denominator [20]. As long as the zero of Eq. 11.32 at u/x_p is lower frequency than the pole at $2C/mu$, Eq. 11.32 will exhibit positive-real characteristics.

$$x_p \geq \frac{mu^2}{2C}. \quad (11.34)$$

The inequality expressed in Eq. 11.34 can provide insight to driver behavior. Part of the dynamic driver behavior postulated by the crossover model is to compensate the vehicle dynamic transfer function to result in positive-real behavior. The driver is able to select the look-ahead or preview distance x_p , to vary the amount of phase lead. This preview distance needs to increase with the mass of the vehicle and the square of vehicle speed (i.e., energy). The driver of a heavily loaded commercial vehicle on a highway needs to look farther ahead when determining lane position error than would the driver of a smaller car in an urban environment. If the driver would look farther ahead than suggested by the quality of Eq. 11.34 more positive phase lead would be added to the open-loop transfer function of Eq. 11.31 making the closed-loop system more stable. Of course, there is a practical limit of visibility/eyesight.

Equation 11.34 is inserted as an equality into Eq. 11.31. This allows convenient pole-zero cancellation to occur in the idealized ideal vehicle, but it should be appreciated that in general the driver can select the preview distance to satisfy phase requirements of the crossover driver model without specific pole-zero cancellation. The specific pole-zero cancellation does allow for simplified vehicle response functions that are useful in developing an intuitive appreciation for rear axle steer functionality. Equation 11.31 is thus simplified to report the projected lateral lane position response for a given rear axle steer coefficient η .

$$\frac{Y_p(s)}{\delta_1(s)} = \frac{\frac{u}{2}(1+\eta) \left(s^2 + s \frac{2C}{mu} + \frac{2C(1-\eta)}{mx(1+\eta)} \right)}{s^2 \left(s + \frac{2C}{mu} \right)}. \quad (11.35)$$

And the expression for crab-steer from Eq. 11.32 becomes

$$\left. \frac{Y_p(s)}{\delta_1(s)} \right|_{\eta=1} = \frac{u}{s}. \quad (11.36)$$

The free integrator in Eq. 11.36 insures zero steady-state tracking error of a constant input. As shown in [Figure 11.1](#) when the driver produces a steering input δ_1 in response to an error between a point extended along its current velocity vector and the constant desired trajectory—keeping an idealized lane—the long-term error approaches zero. Such a loop would be extremely stable, as the phase margin of a closed-loop around a free integrator is 90°. In practice, the value of the simple proportional driver control K could be quite high, limited by actuator dynamics not considered in this work. If the input signal—the lateral

position of the road—varied as a linear function of time, the steady-state error between the desired trajectory and actual trajectory of y_p can be expressed as u/K . This steady-state error is the result of the crab-steering vehicle having no ability to generate a yaw rate. The crab-steering vehicle with preview determined by Eq. 11.34 will have an increasing error when trying to track an input signal with a constant curvature. The crab-steering system can track a constant lane very well, and is very stable. It cannot track a dynamically changing lane.

Using the preview condition of Eq. 11.34 inserted into Eq. 11.33 the expression for counter-steer becomes

$$\left. \frac{Y_p(s)}{\delta_1(s)} \right|_{\eta=-1} = \frac{\frac{2Cu}{mx}}{s^2 \left(s + \frac{2C}{mu} \right)}. \quad (11.37)$$

If a loop could be closed around the projected lateral position y_p in a counter-steering vehicle, it would have better tracking properties. As Eq. 11.37 shows, it would have two free-integrators in the open loop. As such, with simple preview control, it would track steady-state inputs and linearly changing inputs without steady-state error [20]. If the proportional driver control gain K could be large enough, the counter-steering vehicle would be able to track a curved road very well. Unfortunately, K cannot be very large at all; in fact, a simple loop cannot be closed around the open-loop man-machine transfer function of Eq. 11.37 as the phase lag is always greater than 180° and thus unstable for any reasonable gain. Such a vehicle can no doubt be driven in practice but, similar to an oversteering vehicle above its critical speed, the driver will be dynamically compensating the vehicle, not merely selecting the appropriate preview distance and proportional gain.

So it appears that the two extremes of crab-steer and counter-steer are not practical strategies for lanekeeping if the road has curvature, although each extreme exhibits its own advantages: counter-steering is more effective at tracking a time-varying trajectory (e.g., a ramp or input with constant curvature) and crab-steering is more stable.

11.6 Determination of Rear Axle Control of Ideal Vehicle

As before with the general model of Eq. 11.20 the zeros of Eq. 11.35 can be expressed.

$$s_{1,2} = \frac{-C}{mu} \pm \sqrt{\left(\frac{C}{mu} \right)^2 - \frac{-2C}{mx} \left(\frac{1-\eta}{1+\eta} \right)}. \quad (11.38)$$

A condition for η can be stated that insures two repeated real zeros as the discriminant of Eq. 11.38 vanishes. This condition is a special case of the more general Eq. 11.22 for RRZ control.

$$\eta = \frac{2mu^2 - Cx}{2mu^2 + Cx}. \quad (11.39)$$

The remaining real part of Eq. 11.38 results in two zeros at $-C/mu$ rad/sec, at precisely half the frequency of the real pole of Eq. 11.35, insuring the desired positive-real system properties.

Equation 11.39 provides the theoretically interesting and yet practically familiar behavior of counter-steering at low speed ($\eta < 0$) and as speed increases the vehicle moves toward crab-steer ($\eta > 0$). At speeds approaching zero ($u \approx 0$), the vehicle is fully counter-steering and therefore more maneuverable and conversely at high speeds the vehicle becomes counter-steering. When the rear axle steer control law of Eq. 11.39 is inserted into the driver-vehicle open-loop transfer function of Eq. 11.35, the result is simplified with obvious potential of pole/zero phase compensation as the real zeros must be at a lower frequency than the real pole.

$$\frac{Y_p(s)}{\delta_1(s)} = \frac{\left(\frac{2mu^3}{2mu^2 + Cx} \right) \left(s + \frac{C}{mu} \right)^2}{s^2 \left(s + \frac{2C}{mu} \right)}. \quad (11.40)$$

Equation 11.40 describes the open-loop transfer function of front axle steer input to projected lateral lane position when the rear axle is controlled using Eq. 11.39.

11.7 Numerical Results

The open-loop frequency response of a specific ideal vehicle can be predicted using Eq. 11.35. Typical parameter values are arbitrarily selected to represent a two-axle commercial vehicle.

$$\begin{aligned} m &= 9070 \text{ kg}, \\ C &= 1110 \text{ N/deg} = 63,600 \text{ N/rad}, \\ x &= 1.27 \text{ m}. \end{aligned}$$

For this vehicle traveling at 26.8 m/sec the pole(s) is at 0.52/sec and imaginary zeros at $0.26 \pm 2.35i/\text{sec}$. If instead the speed was halved to 13.4 m/sec, the pole becomes 1.04/sec. As long as the zero and pole are roughly relatively located, there is little practical consequence in the absolute location. The preview zero

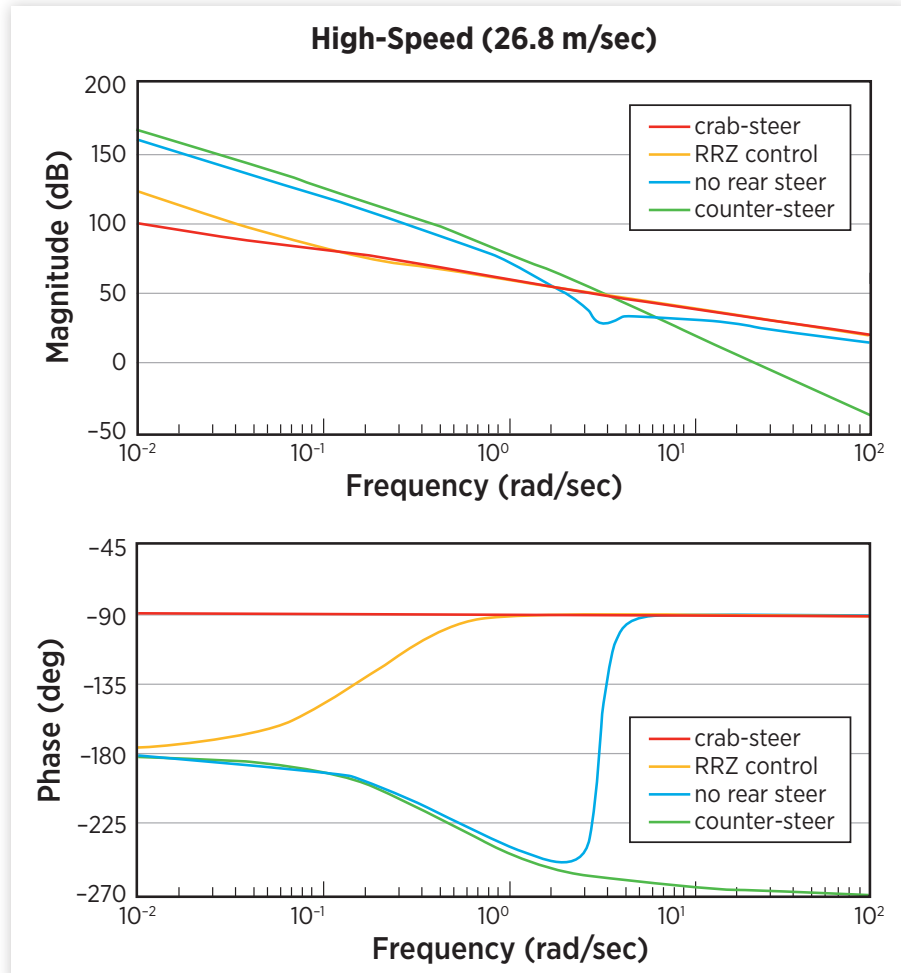
will keep the phase of the open-loop crab-steer transfer function of Eq. 11.32 from approaching 180° phase lag, and the counter-steer open-loop transfer function of Eq. 11.33 will fall below 180° by virtue of the two free integrators. Recall the preview distance is assumed to be determined by Eq. 11.34 satisfied as an equality. This means the preview distance is the minimum required to insure a positive-real crossover model. Using the parameters of the ideal vehicle, at 13.4 m/sec the preview window is just less than 1 sec, and at 26.8 m/sec it is less than two seconds. Odhams and Cole [22] found most drivers use a 2-sec preview window, and Erseus et al. [13] found that more highly skilled drivers use a larger preview window.

The open-loop frequency response of a projected lateral lane position from rear steer input as shown in Eq. 11.35 for various values of η is shown for high and low vehicle speeds in [Figures 11.7](#) and [11.8](#), respectively. Clearly in both the low- and high-speed conditions, the crab-steering vehicle with preview results in the strictly positive-real system of Eq. 11.36 characterized by a constant phase lag of 90° . At the other extreme is the counter-steering vehicle with preview described by Eq. 11.37. In this case, the two free integrators provide a low-frequency phase lag of 180° that goes toward 270° with the effect of the remaining real pole.

When there is no rear steering input the vehicle response is described by Eq. 11.35 where $\eta = 0$. Here, the phase contribution of the poles is greater than the zeros of the second order vehicle dynamics, and the overall phase lag exceeds 180° before the influence of the zeros returns it to the 90° of lag at high frequencies. As seen in [Figures 11.7](#) and [11.8](#), the unsteered vehicle's phase lag is asymptotically approaching the positive-real value of 90° around 5 rad/sec—slightly above the expected driver crossover frequency. Between roughly 0.1 and 3 rad/sec the vehicle without rear axle steer exhibits a phase lag of greater than 180° , and would therefore require compensatory driver dynamics to fulfill the requirements of the crossover model.

It is interesting that MacAdam [11] notes a shortcoming of the basic crossover model is that while experiments show that “the linear regime describing function of actual driver-vehicle systems exhibits crossover model behavior, it does so only in the immediate vicinity of the crossover frequency. In fact, at lower frequencies where much of our driving actually occurs, driver vehicle-measurements show a significant increase in slope gain that transitions towards -60 db/decade and a corresponding phase shift of -270° at steady state.”

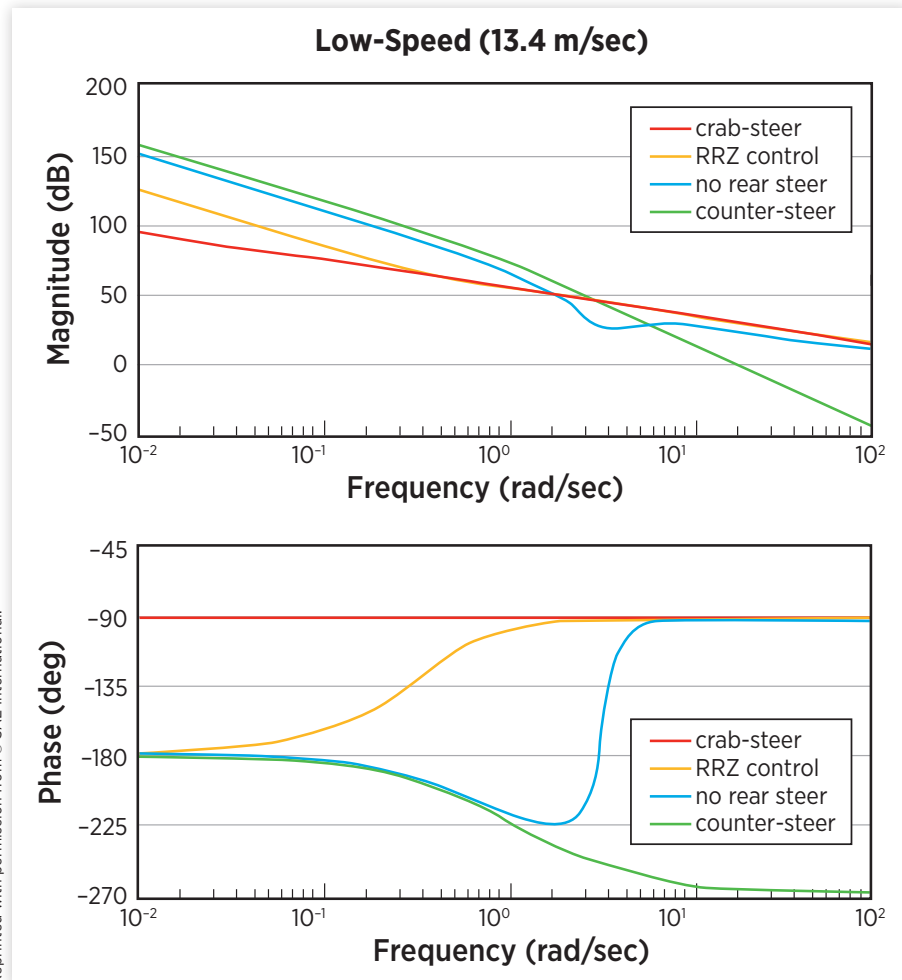
The unsteered vehicle at high-speed approaches this condition, as shown in [Figure 11.4](#). MacAdam goes on to note that a valid model exhibits “increased gain and phase shifts at low frequencies and accompanying crossover model behavior in the mid-frequency range.” Therefore, the open-loop driver-vehicle transfer function of Eq. 11.31 with a preview distance described by Eq. 11.34 provides the generally anticipated response without rear axle steering as shown in [Figures 11.4](#) and [11.5](#).

FIGURE 11.7 High-speed open-loop frequency response.

Reprinted with permission from © SAE International.

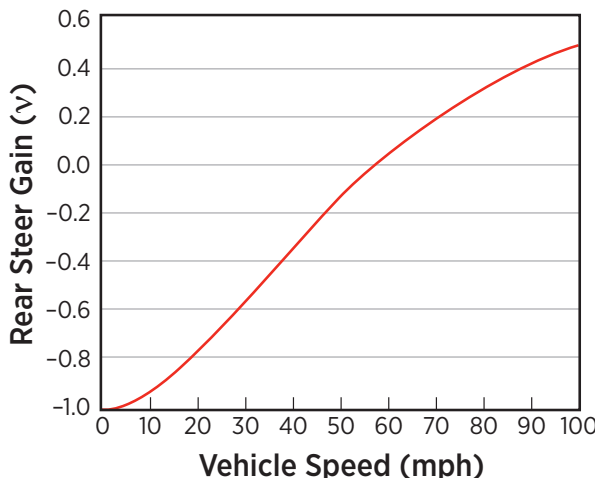
Without rear axle steer the driver would have to provide some other compensatory task beyond selecting the minimum preview distance to cancel a vehicle dynamic pole as anticipated by the crossover model. It is possible that selecting a preview distance greater than the minimum required by Eq. 11.34 would result in a stable closed-loop, but more complicated driver dynamics may be required. Without the proposed RRZ rear axle steering the driver control task is more complicated than simple preview.

When the rear axle steer is controlled on the ideal vehicle in accordance with Eq. 11.39, it can be seen that the phase lag never exceeds 180° and is

FIGURE 11.8 Low-speed open-loop frequency response.

Reprinted with permission from © SAE International.

moving toward a stable 90° phase lag at low frequencies. It is interesting to observe that at 2 rads/sec, a frequency thought by some to be critical to the lane maintenance driver dynamics [14] the rear axle steer control of Eq. 11.39 coupled with a simple driver preview selection of Eq. 11.34 produces an open-loop consistent with the crossover driver model with a simple phase lag of 90°. Intuitively, one might expect the faster vehicle to be less stable and indeed the open-loop response of the faster vehicle exhibits greater phase lag, but recall the rear axle control strategy tends to a stabilizing crab-steer at higher speeds as shown in [Figure 11.9](#), and therefore the open-loop vehicle frequency response is relatively independent of speed when using Eq. 11.39.

FIGURE 11.9 Variation of RRZ rear steer gain with vehicle speed.

Reprinted with permission from © SAE International.

The ideal vehicle has shown that a control law of Eq. 11.39 that insures real repeated zeros in the open-loop transfer function from steering input to projected lane position both decreases the closed-loop error when tracking a lane of constant curvature, and reduces the driver task required to stabilize the vehicle dynamics relative to a nonsteered ideal vehicle. Because of these effects are defined by the relative locations of poles and zeros, the effect of the general rear axle steer control law of Eq. 11.22 will be similar given the easily satisfied condition of Eq. 11.26.

11.8 Theoretical Interpretation of Practical Systems

As the proposed control law is similar to what has been used in practice, it is possible to use the preceding development to gain understanding of the theoretical advantages of rear axle steer in lanekeeping. The proposed rear axle steer control strategy reduces steady-state tracking errors. Furthermore, the strategy insures the open-loop transfer function has phase lag less than the 180° required for instability, and has a 90° phase lag in the neighborhood of the driver “crossover frequency” allowing highly stable “positive-real” characteristics. Recall a fundamental premise of the “crossover” model is that the driver will add sufficient dynamics to compensate the open loop in the neighborhood of the crossover frequency. When the proposed rear axle steer control law is used, the open loop is well behaved without requiring compensatory dynamics

from the driver. The driver control task is simply moving the steering wheel in proportion to the adequately projected lane deviation. From the standpoint of directly predicting the stabilizing effect of rear axle steer the presented model is consistent with the literature and clearly demonstrates how speed-dependent rear axle steering improves both low-speed trajectory tracking and high-speed stability while minimizing the driver control task. In fact commercially available rear axle steer systems that counter-steer at low speed and tend toward crab-steering at highway speed provides the same general functionality as the RRZ control derived in this work for the ideal vehicle, as shown in [Figure 11.6](#).

11.9 Summary

The well-known yaw-plane or “bicycle” model was augmented by a coordinate transformation to get a fourth order model of a vehicle including an inertially defined trajectory. Rear axle steer was added as a second control input. A simple driver model was used where the driver selects a forward distance where lane displacement is observed and generates a steering input based on the projected lateral lane deviation. It was shown that with a proper selection of preview distance and a rear axle control law that insured repeated real zeros at a lower frequency than poles of the open-loop transfer function, the man-machine system is “positive-real” and consistent with notions of the “crossover” driver model found in the literature.

The crossover model has been used extensively in the theoretical development of the rear axle steer control law. The literature indicates that the crossover model is likely appropriate for a particular frequency range while the vehicle is lanekeeping. The results presented should not be considered as a control law dependent upon the validity of the crossover model. Rather, the results should be interpreted that the derived control will allow very simple driver control to perform well when incorporated into the man-machine system.

The effect of the proposed rear axle steer control law was compared with the extremes of full crab-steer and full counter-steer as well as no rear axle steer for a generic two-axle commercial vehicle. With the driver model in place, the idealized vehicle was seen to be very stable when the rear axle is crab-steered (in-phase with the front axle), and a loop can be closed on previewed lane position with a very high gain; however, the closed-loop vehicle cannot track a curved road. When the rear axle is counter-steered (out-of-phase with the front axle) it might be possible to better track a curved road; however, the simple preview driver model will not allow a stable closed-loop and therefore the driving task will be more complex.

It is both intellectually interesting and practically satisfying that the proposed control law results in a fully counter-steering rear axle at low speeds. A control law developed to compensate the open-loop dynamics of the man-machine system also provides the desired steady-state behavior although this was not a criterion in the development of the control law. High-speed lane-keeping and low-speed maneuvering are principle components of vehicle duty cycles. In practice steady-state maneuverability is considered the prime benefit of commercially available rear axle steering systems.

The proposed control law counter-steers at low vehicle speeds and crab-steers at high speeds. As such, it is consistent with strategies used in practice. Ad hoc rear axle steer control strategies resemble a theoretical effort to eliminate imaginary zeroes in the driver-vehicle open-loop transfer function. By using such a control law, the vehicle will be more maneuverable at low speeds, it will be able to track complex trajectories with lower error, and it will demand less complicated control action from the driver than not steering the rear axle, or steering the rear axle entirely in-phase or out-of-phase with the driver input.

This chapter extends the two-axle yaw plane model developed in [Chapter 10](#) in two important ways. First, it allows steering of the rear axle making use of the generalized lateral force equation of [Chapter 9](#). It also allows two more dynamic states so that maintaining a lane defined in an inertial reference frame can be modeled. This chapter also augmented the vehicle with a driver model that closed a loop on a projected lateral lane position. This chapter is an example of the value of the basic yaw-plane model in its extension to cover practicalities like driver dynamics, rear axle steer, and inertially defined trajectories.

At a higher level of abstraction, this chapter demonstrates the advantage of combining vehicle dynamics with control theory. It was possible to develop a nonlinear speed varying control law that ensures that zeros are real and repeated, and of higher frequency than the vehicle dynamic poles. Therefore, closed-loop stability is not only insured, but when the man machine open loop is considered, control approaches what is recognized in the literature as a crossover control. What is particularly intriguing about this exercise is that the nonlinear speed-dependent control law designed for high-speed stability provides the correct counter-steering action at low speed that improves vehicle maneuverability. This theoretical study therefore illuminates the ad hoc control that has been practically used for many early rear axle steer projects.

References

- [1] Sano, S., Furukawa, Y., Nihei, T., Abe, M. et al., "Handling Characteristics Of Steer Angle Dependent Four Wheel Steering System," SAE Technical Paper 885034, 1988, <https://doi.org/10.4271/885034>.

- [2] http://www.ece.mtu.edu/labs/EElabs/EE3306/Revisions_2008/str_quadra.pdf
- [3] http://trucksteering.trw.com/sites/trucksteering.trw.com/files/pdf/product_sheet/EMAS_08.pdf
- [4] Furukawa, Y., Yuhara, N., Sano, S., Takeda, H., and Matsushita, Y., "A review of four-wheel steering studies from the viewpoint of vehicle dynamics and control," *Vehicle System Dynamics*, 18 (1989), pp. 151–186.
- [5] You, S.S., and S.K. Jeong, "Vehicle dynamics and control synthesis for four-wheel steering passenger cars," *Journal of Automobile Engineering*, 212 (1998), pp. 449–461.
- [6] Gohring, E., E.-C. Von Glasner, H.-C. Pflug, and R. Povel, "Optimization of maneuverability and directional stability of commercial vehicles by an electronically controlled all-wheel steering system," *Society of Automotive Engineers*, 945090 (1994).
- [7] Bayar, Kerem and Y. Samim Unlusoy, "Steering strategies for multi-axle vehicles," *International Journal of Heavy Vehicle Systems*, 15, No. 2–4 (2008), pp. 208–236.
- [8] Williams, D.E. Handling benefits of steering a third axle. *Proc. IMechE, Part D: J. Automobile Engineering*, 2010, 224(D12), 1501–1511. DOI:[10.1243/09544070JAUTO1528](https://doi.org/10.1243/09544070JAUTO1528).
- [9] Williams, D.E. and Sherwin, K.A., "Vehicle performance improvement by steering the third axle," *SAE paper 2010-01-1890*, October 2010.
- [10] Qu, Quizhen, and Jean W. Zu, On steering control of commercial three-axle vehicle, *Journal of Dynamic Systems, Measurement and Control, American Society of Mechanical Engineers*, 130 (2008), 021010-1-10.
- [11] MacAdam, Charles C., "Understanding and modeling the human driver," *Vehicle System Dynamics*, 2003, 40, Nos 1–3, pp 101–134.
- [12] Kondo, Masaichi, and Akio Ajimine. *Driver's sight point and dynamics of the driver-vehicle-system related to it*. Society of Automotive Engineers, 1968.
- [13] Erseus, Andreas, Lars Drugge, and Annika Stensson Trigell, "A path tracking driver model with representation of driving skill," *International Journal of Vehicle Systems Modelling and Testing*, Vol 6, No. 2, 2011.
- [14] Hess, R.A., "A unified theory for aircraft handling qualities and adverse aircraft-pilot coupling," *Journal of Guidance, Control and Dynamics*, 20, No.6, 1997, pp. 1141–1148.
- [15] Modjtahedzadeh, A., and R.A. Hess, "A model of driver steering control behavior for use in assessing vehicle handling qualities," *Journal of Dynamic System, Measurement and Control*, September, 1993.
- [16] Hess, R.A. and Modjtahedzadeh, A., "A control theoretic model of driver steering behavior," *IEEE Control Systems Magazine*, August, 1990.
- [17] Hess, R.A., "Analyzing manipulator and feel systems effects in aircraft flight control," *IEEE Trans. Of Sys., Man., and Cybernetics*, July/August, 1990.
- [18] McRuer, D., *Lectures on theory on Theory on Manual Control*, 1972.
- [19] Allen, R.W., "Stability and Performance Analysis of Automobile Driver Steering Control," *SAE paper 820303*, 1982.
- [20] Ogata, Katsuhiko, *System Dynamics*, Prentice-Hall, Englewood Cliffs, NJ, 1978.
- [21] Haddad, W.M., and V. Chellebonia, *Nonlinear Dynamical Systems and Control: A Lyapunov-Based Approach*, Princeton University Press, Princeton, NJ, 2008.
- [22] Keen, Steven D., and David J. Cole, "Steering Control Using Model Predictive Control and Multiple Internal Models." *Proceedings of AVEC '06, The 8th International Symposium on Advanced Vehicle Control*, August 20–14, Taipei, Taiwan, AVEC 060095.

258 Generalized Vehicle Dynamics

- [23] Odhams A.M.C., and D.J. Cole, "Identification of a Driver's Preview Steering Control Behaviour Using Data from a Driving Simulator and a Randomly Curved Road," AVEC '10.
- [24] Pacejka, Hans B., Tire and Vehicle Dynamics, Society of Automotive Engineers, 2002.
- [25] Maciejowski, J.M., Multivariable Feedback Design, Addison-Wesley, 1989.
- [26] Hag, J.B. and Daniel Bernstein, "Non-minimum phase zeroes—much ado about nothing—classical control revisited—part II," IEEE Control Systems Magazine, Volume 27, Issue 3, June 2007.
- [27] Hoagg and Bernstein, "Non-minimum phase zeroes—much ado about nothing—classical control revisited Part II," IEEE Control Systems Magazine, June 2007.

Two-Axle Vehicles that Roll

“

A very complicated interplay of factors decides whether, ultimately, a car has been well designed or not.

—Niki Lauda

”

12.1 Introduction

Chapter 11 explored additions to the two-axle yaw-plane model developed in Chapter 10, such as rear axle steer, inertial state augmentation, and a look at a simple driver model for lanekeeping. The present chapter refers back to Chapter 10 and further develops the two-axle yaw-plane model in a different direction, to allow vehicle roll.

The overall purpose of this chapter will be to introduce a differential equation of motion allowing the sprung mass to roll on the vehicle, restrained by the suspension. The reference frame derivation of Chapter 8 will be essential, and key simplifying assumptions will be made allowing a simple set of equations to describe a yawing and rolling vehicle.

The ride aspect of vehicle roll was presented in Chapter 5. There, the sprung mass was allowed to roll on the suspension, but the input was from road irregularities. In this chapter, the road is assumed smooth, but rather than going straight the vehicle is allowed to turn, presenting a centripetal acceleration to sprung mass. Because of the coupling present in the equations, the roll mode is affected by yaw. We will see that based on suspension design, the roll displacement can in turn affect yaw. In Chapter 5, more generally in the first part of the book on vehicle ride, the effect of suspension parameters on vehicle ride was developed. In the present chapter, the effect of vehicle suspension on handling is developed. As such, consideration of roll is quite interesting in the trade-offs it motivates between ride and handling.

It is unfortunate that many otherwise good vehicle dynamic texts have not considered roll. Consideration of roll requires a rigorous development of reference frames and the yaw-plane model. This chapter draws on material from R.A. Ellis, as presented in his Vehicle Dynamics book [1]. Ellis presents detail not included in this work, and the interested reader will enjoy his book—if you can find it. Ellis' concepts were streamlined and benefit from notation developed by L.D. Metz and presented in his vehicle dynamics notes at the University of Illinois. Between them, they provide a useful method of allowing the fundamental mechanisms of vehicle roll to be conceptualized.

Models are derived for particular purposes and not suited for others. The model presented here is not intended to predict vehicle performance, there are many multibody simulation packages that are better suited for this task. This model is intended to allow conceptualization of roll dynamics, and how roll mode displacement affects vehicle yaw behavior. The assumptions made will provide for a suitable generalization, without supporting prediction of a specific circumstance. This chapter will provide the reader with a general conception of how roll influences yaw-plane dynamics. The engineer's task at different times requires analysis and synthesis. Multibody analysis packages have come a long way since Ellis simulated his equations on an analog computer. But in the synthesis role, it is valuable to have such a general intuition of how roll affects vehicle dynamics.

12.2 Roll Axis Definitions

This chapter starts with the general accelerations derived in [Chapter 8](#). Of particular interest is the roll equation, which was not used in the development of the two-axle yaw-plane model that assumed a rigid body, and more specifically a rigid suspension connection between the sprung and unsprung masses. We start with restating Eq. 8.45.

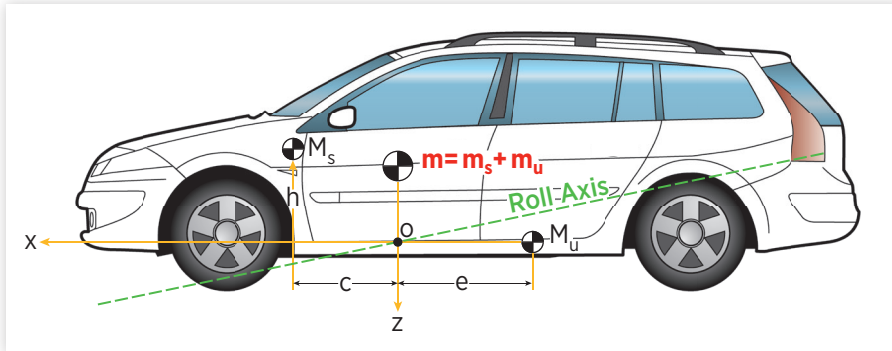
$$\sum M_x = I_x \ddot{p} + (I_z - I_y)qr + P_{yz}(r^2 - q^2) - P_{xz}(pq + \dot{r}) + P_{xy}(pr - \dot{q}). \quad (12.1)$$

Equation 12.1 describes the accelerations and velocities resulting from the summation of moments about the x -axis, or roll moments. Recall the resulting roll acceleration \ddot{p} is assumed to be about the x -axis, which is further assumed to be a principle axis of the rigid body vehicle.

Unfortunately, not the entire vehicle rolls together. The mass supported by the suspension, referred to as the sprung mass, rolls significantly, and the unsprung mass does not. Furthermore, the sprung mass is much more massive than the unsprung mass. One might be tempted to just say all the mass rolls with the sprung mass and just neglect the problem of unsprung mass in roll (an assumption made in [Chapter 5](#)). Unsprung mass is considered separate from

FIGURE 12.1 Roll axis and centers of mass.

© SAE International.



sprung mass because the relative displacement between sprung and unsprung masses can affect vehicle dynamics, and the kinematics of this motion constrain sprung mass motion. While all the vehicle mass yaws and moves laterally, only the sprung mass portion rolls ([Figure 12.1](#)). Furthermore, based on kinematic constraints, the sprung mass does not roll about its own principle axis. Rather, the sprung mass rolls about an axis defined at the front and rear axles by the front and rear suspension kinematics.

Assuming left and right suspension symmetry, the sprung mass of the vehicle rolls about an axis lying within the x - z plane. A kinematic analysis of the front suspension defines a point in the x - z plane about which the sprung mass rolls. A similar analysis produces a point at the rear, and the line connecting these two points forms the roll axis. In real world application it is possible to have an, albeit small, plan view angle of the roll axis due to production variability or by design (e.g. circle track cars).

The rotating axis fixed to the vehicle is carefully placed to simplify the subsequent equations. This rotating axis is placed directly below the overall vehicle center gravity, where the z -axis intersects the roll axis, as shown in [Figure 12.1](#). Instead of a single center of mass for the entire vehicle, we now define two centers of mass. One for the unsprung mass that does not roll, the other for the sprung mass that does. For most front-engined cars, the center of unsprung mass is ahead of the overall vehicle center of mass. Therefore the center of sprung mass m_s is located along the x -axis by a positive value c . If the center of sprung mass is ahead of the overall center of mass, the center of unsprung mass m_u is necessarily behind. Therefore, the unsprung mass center is located by a negative value e along the x -axis. The center of sprung mass is above the origin of the rotating axis, and therefore is located along the z -axis by a negative value h —an important fact to remember in subsequent equations. Furthermore, we assume that the roll axis is sufficiently flat that it can be approximated by a horizontal line along the x -axis that passes through the unsprung mass center, so that the sprung mass rolls with a constant vertical moment arm h about the horizontal roll axis.

All of these assumptions are by themselves plausible, but taken together result in an idealized vehicle. We know not only is the roll axis typically inclined, as shown in [Figure 12.1](#), but that the roll axis and the moment arm move with suspension deflection. The best we can say is that these assumptions result in a model that will allow evaluation of directional tendencies. As we begin to develop the relevant differential equations of motion, the reader should appreciate the simplifying effect of this axis placement, originally attributable to Ellis.

12.3 Acceleration Equations

From Eq. 8.46, the lateral acceleration of a point in a rotating reference frame is described.

$$\dot{v} = \dot{V} - pW + rU - (p^2 + r^2)y + (rq - \dot{p})z + (pq + \dot{r})x. \quad (12.2)$$

Equation 12.2 will be written separately for lateral accelerations of the sprung and unsprung masses. Certain simplifications can be made for both the acceleration of the sprung mass and the unsprung mass.

- In both cases, the masses are on the x - z plane so $y = 0$.
- In both cases, there is no vertical velocity so $W = 0$.
- In both cases, there is no pitch, so $q = 0$.

With these conditions, Eq. 12.2 can be generally simplified for both the lateral velocities of the sprung and unsprung masses.

$$\dot{v} = \dot{V} + rU - \dot{p}z + \dot{r}x. \quad (12.3)$$

The combined sum of the lateral forces on the vehicle creates lateral accelerations of the sprung and unsprung masses.

$$\sum F_y = m_s \dot{v}_s + m_u \dot{v}_u. \quad (12.4)$$

Writing Eq. 12.3, specifically for both masses inserting into Eq. 12.4,

$$\sum F_y = m_s (\dot{V}_s + r_s U_s - \dot{p}_s z_s + \dot{r}_s x_s) + m_u (\dot{V}_u + r_u U_u - \dot{p}_u z_u + \dot{r}_u x_u), \quad (12.5)$$

observing that the only motion of the sprung mass relative to the unsprung mass is roll, and recognizing that the vertical location of the sprung mass is h

(negative), the longitudinal location of the sprung mass is c (positive), and the longitudinal location of the unsprung mass is e (negative).

$$\sum F_y = m_s (\dot{V} + rU - \dot{p}h + \dot{r}c) + m_u (\dot{V} + rU + \dot{r}e). \quad (12.6)$$

Terms are collected in Eq. 12.6.

$$\sum F_y = (m_s + m_u)(\dot{V} + rU) + m_s(-\dot{p}h) + (m_s c + m_u e)\dot{r}. \quad (12.7)$$

Remembering that e is negative, and using the definition of center of mass,

$$m_s c + m_u e = 0 \quad (12.8)$$

and recalling the total vehicle mass is comprised of the sprung and unsprung masses, Eq. 12.7 can be simplified.

$$\sum F_y = m(\dot{V} + rU) + m_s(-\dot{p}h). \quad (12.9)$$

Equation 12.9 makes intuitive sense, and the sum of the lateral forces creates conventional accelerations in the combination of sprung and unsprung masses, plus a term relating to the roll acceleration of the sprung mass relative to the unsprung mass, which is motion in the newly allowed roll degree of freedom.

The general yaw acceleration equation was written in Eq. 8.47.

$$\sum M_z = I_z \dot{r} + (I_y - I_x)qp + P_{xy}(q^2 - p^2) - P_{yz}(rp + \dot{q}) + P_{xz}(rq - \dot{p}). \quad (12.10)$$

Because of the judicious choice of axis location, P_{xy} and P_{yz} are both zero. However, P_{xz} is defined for the point that is the sprung mass using the general Eq. 8.41,

$$P_{xz} = \sum \delta m xz, \quad (12.11)$$

and the x and z coordinates defined by the unpsrunng mass location are used.

$$P_{xz} = m_s hc. \quad (12.12)$$

So accounting for symmetry in axis placement, lack of pitch motion, and using Eq. 12.12, Eq. 12.10 can be simplified.

$$\sum M_z = I_z \dot{r} - m_s hcp. \quad (12.13)$$

The roll degree of freedom has just been added to the lateral acceleration and yaw equations, resulting in relatively minor changes owing to the judicious axis placement and associated assumptions. Now, we can turn to the roll mode itself. Because we are considering roll of particles displaced from the axis, we start with restating Eq. 8.30

$$\sum M_x = \sum \delta m (y\dot{w} - z\dot{v}). \quad (12.14)$$

Using Eq. 8.11 written for the sprung mass,

$$\dot{v}_s = \dot{V} + rU - \dot{p}h + \dot{r}c \quad (12.15)$$

and with no vertical acceleration Eq. 12.14 is simplified for the sprung mass.

$$\sum M_x = -m_s h (\dot{V} + rU - \dot{p}h + \dot{r}c). \quad (12.16)$$

Equation 12.16 describes the acceleration of the point sprung mass in response to the sum of rolling moments. As the actual sprung mass is distributed about the center of sprung mass, and will roll about its own principle axis as the center of mass rolls, an additional term is added to Eq. 12.16,

$$\sum M_x = I'_x \dot{p} + m_s h^2 \dot{p} - m_s h(\dot{V} - rU) - m_s h c \dot{r}, \quad (12.17)$$

where I'_x is the roll moment of inertia of the sprung mass about its principle axis. Eq. 12.17 is quite interesting and worth considering in parts. The first part can be thought of as the basic roll motion of the sprung mass.

$$I'_x \dot{p} + m_s h^2 \dot{p}.$$

This is essentially the parallel axis theorem. If the only degree of freedom of motion was the sprung mass rolling about the roll axis, this term would describe the roll acceleration in response to a moment about the x-axis. The next term is familiar.

$$-m_s h(\dot{V} - rU).$$

This includes our old friend—the centripetal acceleration term. It acts on the sprung mass through its lever arm h relative to the roll axis. It is always important to keep track of the signs of the various parameters used, and particularly so in this discussion. We have encountered the general term $m u r$ before, and considered it to be the “centrifugal force.” Between the negative sign in front of this term, the negative sign on $r u$, and the fact that h is negative in our axis system, this overall term is negative.

The final term is vaguely familiar.

$$-m_s h c \dot{r}.$$

This term actually contains the product of inertia term P_{xz} already shown in Eq. 12.12. In Eq. 12.13, it multiplies the roll acceleration term in the yaw moment summation; here, it multiplies the yaw acceleration in the roll moment summation.

Taken together, Eqs 12.9, 12.13, and 12.17 describe the acceleration response to external lateral forces, yaw moments, and roll moments.

12.4 External Roll Forces on Sprung Mass

As attention is now shifted to the external forces on the “left side” of Newton’s second law, our examination starts with the sprung mass. There are two reasons for initially looking at roll moments on the sprung mass. First, roll is a new degree of freedom, and therefore the external forces associated with this mode are introduced for the first time. Second, although the lateral forces on the tires have already been introduced, they are modified by effects from the roll mode displacement. Therefore the roll mode displacement is both created by and modifies lateral tire forces.

The external moment generated on the sprung mass comes from the roll stiffness and damping effect of the suspension. As such, it is not really an external force to the vehicle, only to the sprung mass. Ultimately, the force the suspension exerts on the sprung mass is reacted through the contact patch of the tire as a normal force on the road. To the extent lateral tire forces are dependent upon normal forces, these reaction forces affect vehicle handling in a nonlinear way. This effect was exploited in [Chapter 6](#) to affect vehicle handling through active roll moment distribution.

The front and rear axles are allowed to have different roll stiffness and roll damping values. These terms are effectively added in parallel as the torsional compliance of the sprung mass is assumed negligible, a reasonable assumption for two-axle unibody vehicles. By allowing a difference between front and rear roll stiffness and damping, roll motion can be resisted more at the front or rear. Similar to the roll bar effect we saw previously in [Chapter 5](#), more roll resistance on the front axle induces understeer, and more on the rear causes an oversteering tendency. Damper properties are easily varied in jounce and rebound, changing the roll moment distribution as the vehicle rolls away from its normal position and then back to center. Therefore, handling properties can be altered specifically in the entry and exit of turns. Because this book relies on linear analysis techniques, these effects are largely neglected, but they are important second-order handling effects.

The sprung mass sees a roll resisting moment $L_{x,\dot{\phi}}$ because of the roll stiffness provided by the front and rear suspension.

$$L_{x,\phi} = -\left(\frac{\partial L}{\partial \phi}\Big|_f + \frac{\partial L}{\partial \phi}\Big|_r\right)\dot{\phi}. \quad (12.18)$$

The sprung mass also sees a roll resisting damping moment $L_{x,\ddot{\phi}}$ at the front and rear because of the suspension.

$$L_{x,\ddot{\phi}} = -\left(\frac{\partial L}{\partial \dot{\phi}}\Big|_f + \frac{\partial L}{\partial \dot{\phi}}\Big|_r\right)\ddot{\phi}. \quad (12.19)$$

There is another external moment on the sprung mass because of the overturning moment of gravity when there is a roll displacement.

$$L_{x,\phi} = -m_s g h \sin \phi \sim -m_s g h \phi. \quad (12.20)$$

Again, note that with the negative value of h , a positive displacement creates a positive moment tending to overturn the sprung mass.

Using the roll mode acceleration of Eq. 12.17 and the external forces of Eqs 12.18, 12.19, and 12.20, a roll mode differential equation of motion can be written.

$$\begin{aligned} I'_x \ddot{p} + m_s h^2 \ddot{p} - m_s h (\dot{V} - rU) - m_s h c \dot{r} \\ = -\left(\frac{\partial L}{\partial \phi}\Big|_f + \frac{\partial L}{\partial \phi}\Big|_r\right)\dot{\phi} - \left(\frac{\partial L}{\partial \dot{\phi}}\Big|_f + \frac{\partial L}{\partial \dot{\phi}}\Big|_r\right)\ddot{\phi} - m_s g h \phi. \end{aligned} \quad (12.21)$$

A bit of nomenclature is introduced that will simplify Eq. 12.21,

$$I_{x,\phi} = I'_x + m_s h^2, \quad (12.22)$$

where $I_{x,\phi}$ is the combined roll moment of inertia about the roll axis parallel to the principle axis of the sprung mass,

$$K_\phi = \left(\frac{\partial L}{\partial \phi}\Big|_f + \frac{\partial L}{\partial \phi}\Big|_r + m_s g h \right), \quad (12.23)$$

the effective roll stiffness is K_ϕ , and the effective roll damping is D_ϕ .

$$D_\phi = \left(\frac{\partial L}{\partial \dot{\phi}}\Big|_f + \frac{\partial L}{\partial \dot{\phi}}\Big|_r \right) \quad (12.24)$$

Translational velocities are the same in the rotating reference frame so going forward all translational velocities are lower case. Similarly, the roll rate \dot{p} can also be written as $\dot{\theta}$, and using Eqs 12.22, 12.23, and 12.24, Eq. 12.21 can be re-written more compactly.

$$I_{x,\theta} \ddot{\theta} - m_s h(\dot{v} - u\dot{r}) - m_s h c \dot{r} = -K_\theta \theta - D_\theta \dot{\theta}. \quad (12.25)$$

An interesting transfer function between yaw rate and roll angle can be written.

$$\frac{\theta(s)}{r(s)} = \frac{m_s h c s + m_s h u}{I_{x,\theta} s^2 + D_\theta s + K_\theta}. \quad (12.26)$$

Recall that yaw rate is the fundamental response to a steering input. With that in mind, Eq. 12.26 can relate roll angle to steering input. The roll mode is seen to have a second-order denominator in the transfer function, and therefore is said to have second-order dynamics. Because the roll mode has such second-order dynamics, we can speak of roll mode natural frequencies and damping with clear physical significance, unlike the coupled first-order yaw and lateral velocity modes. Equation 12.26 also provides the steady-state relationship between centripetal acceleration and roll angle.

The roll-mode natural frequency is typically between a 0.5 and 3 Hz. Thus, the roll mode can be excited by the first-order yaw rate response to steering. Unfortunately, it is possible that the roll mode can be underdamped and can overshoot. It would be nice in some ways if the roll natural frequency was high, with high stiffness and critically damped. Such a vehicle could result in vertical suspension stiffnesses inconsistent with a good ride, so unless the vehicle is actively suspended a roll displacement is inevitable. But this roll displacement gives the vehicle designer more freedom to affect handling.

12.5 Camber Effects

Tire camber is the angle the plane of the tire makes with a plane perpendicular to the road. Occasionally this angle is referred as inclination in the literature. Tire camber can be thought of as a tire's rotational displacement about the x -axis, and in this sense it is similar to the roll of the sprung mass, just as the steer angle of a tire is similar to yaw as rotations about the z -axis. In the yaw-plane model we have seen how the difference between the steer angle and velocity vector produces a lateral force on the vehicle from the road. A lateral force can also be generated by the tire rotated relative to the x -axis.

FIGURE 12.2 Experimental car steered by camber effect.

Reprinted with permission from © SAE International.

This is how a bicycle can be turned without a steer angle input from the rider. The more the cycle is banked, the greater the side force generated by the tire. Motorcycle tires are designed and specifically constructed to generate lateral force from camber, but conventional passenger car tires can also generate side force through camber. Bill Milliken built an experimental vehicle that varied camber to steer ([Figure 12.2](#)).

A linear relationship can express the change in lateral force for a given camber angle of the tire.

$$\Delta Y_i = \frac{\partial Y_i}{\partial \phi_i} \phi_i \quad (12.27)$$

Equation 12.27 suggests that the camber angle of the i th tire ϕ_i creates a change in lateral force that adds to the side force created by the steer angle. This relationship is based on a linearization and is a function of the tire.

As the sprung mass rolls, it creates a corresponding roll or camber angle in the individual tires through the suspension kinematics that locate the wheel relative to the sprung mass. In fact, the same suspension kinematics that define the vertical velocity ratio seen in the ride section also define the roll axis position, and define the camber angle of the tire. In practice this relationship can be nonlinear, but in this work we assume a linear relationship between tire camber and sprung mass roll.

$$\phi_t = \left. \frac{\partial \phi_t}{\partial \phi} \right|_{f,r} \phi. \quad (12.28)$$

The relationship between tire camber and roll can vary from the front to the rear.

Equation 9.5 describes the lateral force developed by the attack angle and tire cornering stiffness. Equations 12.27 and 12.28 are used to describe the additional effect of how a change in camber generates a lateral force.

$$Y_i = C_i \left(\delta - \frac{v + x_i r}{u} \right) + \left. \frac{\partial Y_i}{\partial \phi_t} \frac{\partial \phi_t}{\partial \phi} \right|_{f,r} \phi. \quad (12.29)$$

As a review, the first term of Eq. 12.29 reveals that positive attack angle combined with a positive cornering stiffness results in a positive lateral force. Similarly, in the second term, a positive roll angle combined with a positive gradient between tire camber and roll, and another positive gradient between lateral force and tire camber, results in another positive contribution to the lateral force generated by the tire.

In round numbers the gradient between roll angle and camber is less than one and the gradient between lateral force and camber is 500–1000 lbs/rad, or less than around 10 lbs/deg for typical passenger car tires. This is roughly an order of magnitude less than the cornering stiffness, so for passenger car tires camber changes are important as secondary effects.

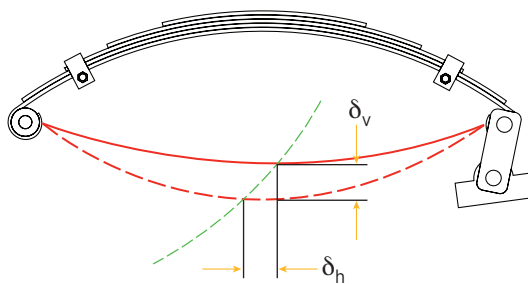
12.6 Roll Steer Effects

Some suspensions, particularly solid axles with leaf springs, exhibit the property that body roll causes a change in attack angle. This can be thought of as a modified steering control input as a function of sprung mass roll.

[Figure 12.3](#) shows how the position of the axle attachment on a leaf spring moves as the spring is compressed and effectively pivots about a pin joint. As the sprung mass experiences a positive roll angle, the right side of the axle moves rearward by an amount δ_h as the spring is compressed by δ_v . On the opposite left side, the spring is extended vertically by δ_v and thereby the axle attachment point is moved forward by δ_h . As the spring deflects there is a positive change in attack angle because of a positive roll.

The change in attack angle can be written as a function of horizontal spring deflection and track,

$$\Delta \alpha = \frac{2\delta_h}{t} \quad (12.30)$$

FIGURE 12.3 Leaf spring kinematics.

Reprinted with permission from © SAE International.

and similarly the roll angle can be expressed as function of vertical spring deflection and track.

$$\phi = \frac{2\delta_v}{t}. \quad (12.31)$$

Equations 12.30 and 12.31 are combined to express the change in attack angle because of roll.

$$\Delta\alpha = \frac{\delta_h}{\delta_v} \phi = \varepsilon_{f,r} \phi. \quad (12.32)$$

Equation 12.32 shows a general linear relationship between roll angle and a change in attack angle, with a constant of proportionality ε . In the case of a leaf spring, as has just been shown, this roll steer coefficient is the ratio of horizontal deflection to vertical deflection. Other wheel suspensions can have more complicated roll steer functions, but all can yield a linearized roll steer parameter. A positively defined roll steer coefficient means that a positively defined roll results in a positively defined change in attack angle. Front and rear axles can have different roll steer coefficients. Thus, a positively defined roll steer coefficient at the front results in a vehicle that is more oversteering, and a positively defined roll steer coefficient at the rear results in a more understeering vehicle. Typical values of the roll steer coefficient are between -0.05 and 0.05 .

The roll steer effects of Eq. 12.32 and the camber steer effect of Eq. 12.29 are combined with the generalized side force equation of Eq. 9.5,

$$Y_i = C_i \left(\delta - \frac{v + x_i r}{u} + \varepsilon_{f,r} \phi \right) + \left. \frac{\partial Y_i}{\partial \phi_t} \frac{\partial \phi_t}{\partial \phi} \right|_{f,r} \phi \quad (12.33)$$

and written in terms of state variables.

$$Y_i = -C_i \left(\frac{v}{u} \right) - \left(\frac{C_i x_i}{u} \right) r + \left(C_i \varepsilon_i + \frac{\partial Y_i}{\partial \phi_t} \frac{\partial \phi_t}{\partial \phi} \Big|_i \right) \phi + C_i \delta_i \quad (12.34)$$

Equation 12.34 can be written for each tire, but in this work it is written for the i th axle.

12.7 Differential Equations of Motion with Roll

The acceleration response of the vehicle to lateral forces was previously derived in Eq. 12.9. (Recall the roll rate p is the time derivative of the roll angle ϕ .) The summation of forces is supplied by Eq. 12.34 applied to the front and rear axles, so that the differential equation of lateral motion can be written.

$$\begin{aligned} \sum F_y &= m(\dot{V} + rU) + m_s(-\ddot{\phi}h) \\ &= (-C_1 - C_2) \left(\frac{v}{u} \right) + \left(\frac{-C_1 x_1 - C_2 x_2}{u} \right) r \\ &\quad + \left(C_1 \varepsilon_1 + \frac{\partial Y_1}{\partial \phi_t} \frac{\partial \phi_t}{\partial \phi} \Big|_1 + C_2 \varepsilon_2 + \frac{\partial Y_2}{\partial \phi_t} \frac{\partial \phi_t}{\partial \phi} \Big|_2 \right) \phi + C_1 \delta_1 + C_2 \delta_2. \end{aligned} \quad (12.35)$$

Similarly, the summation of yaw moments from Eq. 12.13 can be equated with the moments produced by the generalized forces described by Eq. 12.34 acting on the front and rear axles.

$$\begin{aligned} \sum M_z &= I_z \dot{r} - m_s h c \ddot{\phi} \\ &= (-x_1 C_1 - x_2 C_2) \left(\frac{v}{u} \right) + \left(\frac{-C_1 x_1^2 - C_2 x_2^2}{u} \right) r \\ &\quad + \left(x_1 \left(C_1 \varepsilon_1 + \frac{\partial Y_1}{\partial \phi_t} \frac{\partial \phi_t}{\partial \phi} \Big|_1 \right) + x_2 \left(C_2 \varepsilon_2 + \frac{\partial Y_2}{\partial \phi_t} \frac{\partial \phi_t}{\partial \phi} \Big|_2 \right) \right) \phi + x_1 C_1 \delta_1 \\ &\quad + x_2 C_2 \delta_2. \end{aligned} \quad (12.36)$$

Thus, Eqs 12.35 and 12.36 are two of the differential equations of motion for the yaw-plane model with roll. The third differential Eq. 12.25 is added to describe the roll mode. Again, we use nomenclature to make these equations more concise. First, we recall Eqs 10.63a, 10.63b, and 10.63c.

$$\begin{aligned} C_a &= C_1 + C_2, \\ C_b &= x_1 C_1 + x_2 C_2, \\ C_c &= x_1^2 C^1 + x_2^2 C_2. \end{aligned}$$

Two new nomenclature terms are defined.

$$C_{\emptyset,1} = C_1 \varepsilon_1 + \left. \frac{\partial Y_i}{\partial \emptyset_t} \frac{\partial \emptyset_t}{\partial \emptyset} \right|_1, \quad (12.37)$$

$$C_{\emptyset,2} = C_2 \varepsilon_2 + \left. \frac{\partial Y_i}{\partial \emptyset_t} \frac{\partial \emptyset_t}{\partial \emptyset} \right|_2. \quad (12.38)$$

Using this nomenclature, Eqs 12.35, 12.36, and 12.25 are written and solved for the highest time derivatives on the left-hand side.

$$m\dot{v} + m_s(-\ddot{\emptyset}h) = \left(\frac{-C_a}{u} \right) v + \left(\frac{-C_b}{u} - mu \right) r + (C_{\emptyset,1} + C_{\emptyset,2})\emptyset + C_1 \delta_1 + C_2 \delta_2, \quad (12.39)$$

$$I\dot{r} - m_s h c \ddot{\emptyset} = \left(\frac{-C_b}{u} \right) v + \left(\frac{-C_c}{u} \right) r + [x_1 C_{\emptyset,1} + x_2 C_{\emptyset,2}] \emptyset + x_1 C_1 \delta_1 + x_2 C_2 \delta_2, \quad (12.40)$$

$$I_{x,\emptyset} \ddot{\emptyset} - m_s h \dot{v} - m_s h c \dot{r} = m_s h u r - D_{\emptyset} \dot{\emptyset} - K_{\emptyset} \emptyset. \quad (12.41)$$

Equations 12.39, 12.40, and 12.41 can be written in matrix form.

$$\begin{bmatrix} m & 0 & -m_s h \\ 0 & I_z & -m_s h c \\ -m_s h & -m_s h c & I_{x,\emptyset} \end{bmatrix} \begin{bmatrix} \dot{v} \\ \dot{r} \\ \ddot{\emptyset} \end{bmatrix} = \begin{bmatrix} \frac{-C_a}{u} & \frac{-C_b}{u} - mu & 0 & C_{\emptyset,1} + C_{\emptyset,2} & C_1 & C_2 \\ \frac{-C_b}{u} & \frac{-C_c}{u} & 0 & x_1 C_{\emptyset,1} + x_2 C_{\emptyset,2} & x_1 C_1 & x_2 C_2 \\ 0 & m_s h u & -D_{\emptyset} & -K_{\emptyset} & 0 & 0 \end{bmatrix} \begin{bmatrix} v \\ r \\ \dot{\emptyset} \\ \emptyset \\ \delta_1 \\ \delta_2 \end{bmatrix}. \quad (12.42)$$

The inertia matrix of Eq. 12.42 is invertible, so that Eq. 12.42 can be solved for the highest-order state derivatives.

$$\begin{bmatrix} \dot{v} \\ \dot{r} \\ \ddot{\emptyset} \end{bmatrix} = \begin{bmatrix} m & 0 & -m_s h \\ 0 & I_z & -m_s h c \\ -m_s h & -m_s h c & I_{x,\emptyset} \end{bmatrix}^{-1} \begin{bmatrix} \frac{-C_a}{u} & \frac{-C_b}{u} - mu & 0 & C_{\emptyset,1} + C_{\emptyset,2} & C_1 & C_2 \\ \frac{-C_b}{u} & \frac{-C_c}{u} & 0 & x_1 C_{\emptyset,1} + x_2 C_{\emptyset,2} & x_1 C_1 & x_2 C_2 \\ 0 & m_s h u & -D_{\emptyset} & -K_{\emptyset} & 0 & 0 \end{bmatrix} \begin{bmatrix} v \\ r \\ \dot{\emptyset} \\ \emptyset \\ \delta_1 \\ \delta_2 \end{bmatrix}. \quad (12.43)$$

Equations 12.39, 12.40, and 12.41 are written in terms of the lateral velocity state variable. These equations can be rewritten in terms of the drift angle state.

$$mu\dot{\beta} + m_s(-\ddot{\phi}h) = -C_a\beta + \left(\frac{-C_b}{u} - mu\right)r + (C_{\phi,1} + C_{\phi,2})\phi + C_1\delta_1 + C_2\delta_2, \quad (12.44)$$

$$I_r - m_s h c \ddot{\phi} = -C_b \beta + \left(\frac{-C_c}{u}\right)r + (x_1 C_{\phi,1} + x_2 C_{\phi,2})\phi + x_1 C_1 \delta_1 + x_2 C_2 \delta_2, \quad (12.45)$$

$$I_{x,\phi} \ddot{\phi} - m_s h u \dot{\beta} - m_s h c \dot{r} = m_s h u r - D_\phi \dot{\phi} - K_\phi \phi. \quad (12.46)$$

These equations can be written for steady state and no rear axle steering input, respectively.

$$0 = -C_a\beta + \left(\frac{-C_b}{u} - mu\right)r + (C_{\phi,1} + C_{\phi,2})\phi + C_1\delta_1, \quad (12.47)$$

$$0 = -C_b \beta + \left(\frac{-C_c}{u}\right)r + (x_1 C_{\phi,1} + x_2 C_{\phi,2})\phi + x_1 C_1 \delta_1, \quad (12.48)$$

$$0 = m_s h u r - K_\phi \phi. \quad (12.49)$$

Equation 12.49 can be used to define the steady-state relationship between roll angle and yaw rate.

$$\frac{m_s h u}{K_\phi} r = \phi. \quad (12.50)$$

Because h is negative (above the roll axis), there is a negative relationship between yaw rate and roll angle. A positive yaw rate produces a negative roll angle. It is worth noting that the steady-state decoupled roll mode transfer function of Eq. 12.26 agrees with Eq. 12.50.

Equation 12.50 can be inserted into the generalized side force with roll Eq. 12.33 to result in a steady-state side force expression that includes roll effects, but no explicit roll angle.

$$Y_i = C_i \left(\delta - \frac{v + x_i r}{u} + \varepsilon_i \frac{m_s h u}{K_\phi} r \right) + \left. \frac{\partial Y_i}{\partial \phi_t} \frac{\partial \phi_t}{\partial \phi} \right|_{f,r} \frac{m_s h u}{K_\phi} r. \quad (12.51)$$

Because of the negative value of h , if the roll steer coefficient is positive a positive yaw rate will reduce the attack angle. Recall the actual roll steer coefficient can be negative. For similar reasons camber effects usually reduce the lateral force produced by an axle as the partial derivatives are generally positive. When these roll effects reduce an axle's ability to generate a lateral force, its attack angle must grow to generate the lateral force required. Thus a positive roll steer coefficient and typical camber effects in the front produce understeering tendencies, and conversely if on the rear axle they cause oversteer.

Equation 12.49 can likewise be used in Eqs 12.47 and 12.48 to result in steady-state equations in terms of drift angle and yaw rate, having eliminated roll.

$$0 = -C_a \beta + \left(\frac{-C_b}{u} - mu \right) r + (C_{\emptyset,1} + C_{\emptyset,2}) \frac{m_s h u}{K_\emptyset} r + C_1 \delta_1, \quad (12.52)$$

$$0 = -C_b \beta + \left(\frac{-C_c}{u} \right) r + (x_1 C_{\emptyset,1} + x_2 C_{\emptyset,2}) \frac{m_s h u}{K_\emptyset} r + x_1 C_1 \delta_1. \quad (12.53)$$

To eliminate the drift angle to result in a single equation relating steer angle to yaw rate, Eq. 12.52 is solved for drift angle,

$$\beta = \left(\frac{-C_b}{C_a u} - \frac{mu}{C_a} + (C_{\emptyset,1} + C_{\emptyset,2}) \frac{m_s h u}{C_a K_\emptyset} \right) r + \frac{C_1}{C_a} \delta_1 \quad (12.54)$$

substituted into Eq. 12.53,

$$0 = -C_b \left(\left(\frac{-C_b}{C_a u} - \frac{mu}{C_a} + (C_{\emptyset,1} + C_{\emptyset,2}) \frac{m_s h u}{C_a K_\emptyset} \right) r + \frac{C_1}{C_a} \delta_1 \right) + \left(\frac{-C_c}{u} + (x_1 C_{\emptyset,1} + x_2 C_{\emptyset,2}) \frac{m_s h u}{K_\emptyset} \right) r + x_1 C_1 \delta_1 \quad (12.55)$$

written in terms of steering input and yaw rate.

$$\left(\frac{C_b C_1}{C_a} - x_1 C_1 \right) \delta_1 = \left(\left(\frac{C_b^2}{C_a u} - \frac{C_c}{u} + \frac{C_b}{C_a} mu + \left(x_1 C_{\emptyset,1} + x_2 C_{\emptyset,2} - (C_{\emptyset,1} + C_{\emptyset,2}) \frac{C_b}{C_a} \right) \frac{m_s h u}{K_\emptyset} \right) r \right) \quad (12.56)$$

and finally solved for the yaw rate response.

$$\frac{r}{\delta_1} = \frac{u C_1 (C_b - x_1 C_a)}{C_b^2 - C_a C_c + C_b m u^2 + (x_1 C_a C_{\emptyset,1} + x_2 C_a C_{\emptyset,2} - (C_{\emptyset,1} + C_{\emptyset,2}) C_b) \frac{m_s h u^2}{K_\emptyset}}. \quad (12.57)$$

Using a familiar identity,

$$C_b^2 - C_a C_c = -C_1 C_2 (x_1 - x_2)^2,$$

the yaw rate response can be simplified.

$$\frac{r}{\delta_1} = - \frac{\frac{u}{(x_1 - x_2) + u^2}}{\left(-C_b m + (C_b (C_{\emptyset,1} + C_{\emptyset,2}) - C_a (x_1 C_{\emptyset,1} + x_2 C_{\emptyset,2})) \frac{m_s h}{K_\emptyset} \right)} \cdot \frac{C_1 C_2 (x_1 - x_2)}{C_1 C_2 (x_1 - x_2)} \quad (12.58)$$

So we can write the understeer coefficient of a vehicle with roll.

$$K_{2,\emptyset} = \frac{-C_b m + (C_b (C_{\emptyset,1} + C_{\emptyset,2}) - C_a (x_1 C_{\emptyset,1} + x_2 C_{\emptyset,2})) \frac{m_s h}{K_\emptyset}}{C_1 C_2 (x_1 - x_2)} \quad (12.59)$$

Equation 12.59 is recognized as the traditional understeer coefficient plus a term dependent upon the roll properties of the vehicle's suspension.

$$K_{2,\emptyset} = K_2 + \frac{(C_b (C_{\emptyset,1} + C_{\emptyset,2}) - C_a (x_1 C_{\emptyset,1} + x_2 C_{\emptyset,2})) \frac{m_s h}{K_\emptyset}}{C_1 C_2 (x_1 - x_2)} \quad (12.60)$$

Thus, the effect of the roll mode on directional stability of the vehicle is shown to be additive to the simple understeer term of Eq. 10.32. Through this new term, the suspension affects understeer and thereby allows many more options for the vehicle designer to influence handling. As previously mentioned, suspension kinematics and roll stiffness also determine ride. Eq. 12.60 therefore provides both opportunities and constraints for the vehicle designer.

12.8 Roll Steer Compensation

If the numerator in Eq. 12.59 is zero, the vehicle is neutral steering.

$$(C_b (C_{\emptyset,1} + C_{\emptyset,2}) - C_a (x_1 C_{\emptyset,1} + x_2 C_{\emptyset,2})) \frac{m_s h}{K_\emptyset} = C_b m \quad (12.61)$$

Recall in the simple yaw-plane model of [Chapter 10](#), neutral steer was equivalent to $C_b = 0$. This condition is essentially a balance between cornering stiffness of the tires and weight distribution. Thus, it is possible that roll steer effects can compensate for the understeer inherent in a vehicle because of its tires and weight distribution. As an example, Eq. 12.61 can be compensated with only rear roll steer. Previously presented Eqs 12.37 and 12.38 are thus defined.

$$C_{\emptyset,1} = 0.$$

$$C_{\emptyset,2} = C_2 \varepsilon_2.$$

In this case Eq. 12.61 is simplified,

$$C_2 \varepsilon_2 (C_b - C_a x_2) \frac{m_s h}{K_\emptyset} = C_b m, \quad (12.62)$$

and solved for the rear roll steer coefficient

$$\varepsilon_2 = \frac{K_\emptyset C_b m}{m_s h C_2 (C_b - C_a x_2)}. \quad (12.63)$$

In a similar manner camber effects, or a combination of camber and roll steer effects can modify the understeer properties of a vehicle. Many vehicles have a solid rear axle with leaf spring suspension and can therefore use this method to affect vehicle handling.

It is significant that Eq. 12.63 contains roll stiffness. Roll stiffness is dependent upon single-wheel stiffness, and we have seen in the ride section that single-wheel stiffness determines ride. Higher roll stiffness (and single-wheel stiffnesses) results in lower roll displacement, therefore the roll steer coefficient must be higher to achieve the desired neutral steer result. The less roll for a given yaw rate, the more the reaction must be for the same desired change in attack angle. It is through consideration of the roll mode that fundamental compromises between ride and handling can be appreciated. Going the other direction, if the roll steer coefficient is large enough, road inputs can create objectionable yaw moments.

The roll steer compensation of Eq. 12.63 depends only upon the composite roll stiffness K_\emptyset , and not the individual front and rear axle stiffness. Therefore the effect is independent of stabilizer placement front and rear of [Chapter 5](#), allowing valuable design freedom.

12.9 Including Steering Compliance in Understeer

The development of Eq. 12.58 led to the interesting and valuable result that roll steer affects the handling balance of a vehicle similar to the traditional cornering stiffness balance. With a bit of updating the steering compliance developed in [Chapter 7](#) can likewise be considered.

Recall Eq. 7.64,

$$\frac{r}{\delta_{hw}} = \frac{u}{\frac{d\eta}{p}l + \left(\frac{2pt_m b}{d\eta \varepsilon K_{steer} l} + \frac{d\eta(aC_f - bC_r)}{pC_f C_r l} \right) mu^2},$$

and revised with more recent nomenclature.

$$\frac{r}{\delta_{hw}} = \frac{p}{d\eta} \left(\frac{u}{(x_1 - x_2) + u^2 \left(\frac{2p^2 t_m x_2 m}{d^2 \eta^2 \varepsilon K_{steer} (x_1 - x_2)} + K_2 \right)} \right). \quad (12.64)$$

The conventional roll steer coefficient is replaced by the revised roll steer coefficient including roll effects of Eq. 12.60. With a bit of algebraic manipulation similar to that shown in Eqs 12.54–12.58, Eq. 12.64 can be combined with Eq. 12.58, with the result reporting yaw rate for a given handwheel control input.

$$\frac{r}{\delta_{hw}} = \frac{p}{d\eta} \left(\frac{u}{(x_1 - x_2) + u^2 \left(K_2 + \frac{m_s h (C_b (C_{\emptyset,1} + C_{\emptyset,2}) - C_a (x_1 C_{\emptyset,1} + x_2 C_{\emptyset,2}))}{K_{\emptyset} C_1 C_2 (x_1 - x_2)} \right)} \right. \\ \left. + 2 \left(\frac{p^2}{d^2 \eta^2 \varepsilon} \right) \left(\frac{t_m}{K_{steer}} \right) \left(\frac{x_2 m}{(x_1 - x_2)} \right) \right). \quad (12.65)$$

Equation 12.65 shows the additive effect of the three sources of understeer: (1) the traditional understeer because of weight distribution and tire cornering stiffness, (2) understeer because of roll effects, and (3) understeer because of steering compliance. The understeer term from steering compliance has been partitioned into mechanical properties of the steering gearbox, properties determining steering feel, and properties of the mass distribution of the vehicle.

12.10 Inclusion of Nonlinear Tires

In Eq. 12.65, the effects of cornering stiffness balance, roll steer, and steering compliance are shown to combine to yield a composite understeer term. An additional term that affects the handling balance of a vehicle was introduced in [Chapter 6](#): the nonlinear effect of roll moment distribution. The cornering stiffness of a tire is known to be a function of normal force through the contact patch of the tire. The more load the tire is supporting, the less compliant it is in the lateral direction, making it stiffer. A linear approximation of this property does not affect handling, as the cornering stiffness gained on one side by the added normal force is lost from the other side of the axle which loses the transferred weight. The relationship between normal force and cornering stiffness is nonlinear, however, and the tire receiving the weight transfer gains less cornering stiffness than is lost by the other tire on the axle. Therefore, whether it is through a change in suspension stiffness or a stabilizer bar, when one axle supports more of the roll moment than the other, it loses net cornering stiffness. For that axle to generate the lateral force required by the driver, the attack angle must be larger, creating understeer if the roll moment is biased to the front, and oversteer if biased to the rear. Using Eqs 12.23 and 12.24, the suspension reaction forces can be calculated at each corner knowing the roll angle and roll velocity. Given that knowledge, the nonlinear effect on cornering stiffness can be included in simulation. If there is a specific lateral acceleration of interest, a linearized model could be used in the neighborhood of interest, but linearization around zero, the most common operating condition of most vehicles, will result in no weight transfer effect. Therefore this second-order effect, shown to have authority to influence vehicle handling in aggressive maneuvers in [Chapter 6](#), is not considered in this linear analysis.

12.11 Summary

This chapter developed a rolling sprung mass mode of motion with certain assumptions attributed to Professors J.R. Ellis and L.D. Metz that allow a parsimonious rolling yaw-plane model. Roll mode dynamics are important in their

own right as developed in the first section of this book on ride. There, roll dynamics were considered to be excited by road irregularities and a source of driver discomfort. In this chapter, the roll mode is excited by accelerations produced by a translating and yawing vehicle. The most interesting thing about the inclusion of roll in the yaw-plane model, however, is that roll can influence vehicle handling.

Two mechanisms were developed for roll to affect handling. First, as the sprung mass rolls, the tire rolls based on suspension kinematics. Roll displacement of a tire, referred to as camber, produces a side force. Second, as the suspension is displaced in roll, again depending upon suspension kinematics, the wheels on an axle can be deflected similar to a steering input. If these suspension properties are chosen judiciously, the vehicle can have a desirable slight understeer, and if they are ignored the vehicle could handle poorly.

The understeer coefficient from the common yaw-plane model is seen to be modified by roll effects and steering compliance to result in an overall vehicle understeer. As roll effects are produced by suspension kinematics and stiffness, they also are considered and thus constrained by ride. Steering effects can be similarly functionally compromised or constrained. Therefore, these additional ways to influence the vehicle handling balance are confounded by other vehicle functions, allowing an appreciation for the opening chapter quote from Nikki Lauda.

The simplified roll mode introduced in this chapter is possible because of a judicious axis placement and various simplifying assumptions. As throughout this work, the linear analysis techniques require linear dynamic models, and some significant nonlinear effects are omitted. The resulting model might not be applicable for predicting actual vehicle performance, but this chapter hopefully allows the reader to develop some intuition about the handling effect of roll, and an appreciation of the compromises it presents in ride and handling.

Reference

- [1] Ellis, J.R., *Vehicle Dynamics*, Business Books, London, 1969.

Three-Axle Vehicle Dynamics



All truths are easy to understand once they are discovered.

—Galileo



13.1 Introduction

The framework of this book has been a standard presentation of vehicle dynamics, with the quarter-car and pitch-plane ride models, and the two-axle yaw-plane handling model. This represents the standard body of knowledge received by most students of vehicle dynamics. The roll mode was included in the ride section, and the effect of roll on a two-axle vehicle was included in the handling section, making an uncommon, but not unprecedented addition to the standard presentation. Two other chapters more relating to vehicle control systems have likewise been added to the standard presentation, one on active suspension, and the other on rear axle steer. These have been natural extensions of the standard presentation relevant to two-axle vehicles.

The next two chapters will extend standard vehicle dynamics in a different direction. The body of vehicle dynamics knowledge has been developed by and large to describe and analyze behavior of two-axle passenger cars. This is quite understandable and appropriate, as this type of vehicle is responsible for most of the motor vehicle production. Certain conventions were adopted in the conventional two-axle development that were not inappropriate for these vehicles of primary focus, but greatly hampered the application of vehicle dynamics concepts and methods to the minority of vehicles with more than two axles. These conventions were addressed in [Chapter 9](#) and had an immediate positive aesthetic influence on the equations of motion of the two-axle vehicle, at least to a control systems engineer.

The primary motivation for these new conventions, however, was not to produce block diagrams consistent with control theory convention, nor to eliminate unnecessary negations in the differential equations, nor even the simplifications of the equations from the nomenclature allowed by these conventions. These are merely positive side effects. The primary motivation for these new conventions was to extend the standard vehicle dynamics presentation to vehicles with more than two axles.

The most common type of multiaxle vehicles are commercial vehicles that haul freight. Multiaxle vehicles have other applications, such as military and specialized machinery. An interesting, if largely forgotten application of multiaxle vehicle dynamics is racing. The year 1976 is remembered by most Formula 1 racing fans for the historic duel between Niki Lauda and James Hunt. Lauda, driving for Ferrari, was the defending series champion, and an “engineer’s” driver. (Lauda would author a book addressing race car design the following year [1].) James Hunt, driving for McLaren, was popular for his brash driving style and good looks. As told in the movie “Rush,” Lauda had an early lead in points, but was badly burned in a horrific mid-season accident. Hunt evened the points total as Lauda willed an amazing medical recovery with the season point’s championship coming down to the final race in the rain. Lost in this drama, is that Tyrell drivers Jody Schekter and Patrick Depailler finished third and fourth in the points that year—and finished one and two in the Swedish Grand Prix—driving a car with six wheels arranged on three “axles.” These vehicles were so successful that the March and Williams teams started multiaxle development programs. The Tyrell cars were less successful in 1977, becoming heavier and wider, thereby losing the initial aerodynamic advantage of smaller front wheels.

This chapter generally extends the prior work derived for the common two-axle vehicle configuration to a three-axle vehicle. In some cases, intermediate development steps are truncated, with the hope that the reader understands they follow in lockstep from the two-axle case, indeed owing to the conventions previously established. This chapter is thus a combination of Chapters 10 and 11 as they are applied to three-axle vehicles.

13.2 Peculiarities of the Three-Axle Vehicle

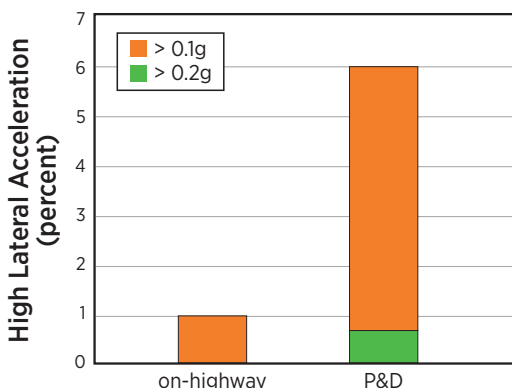
Multiaxle commercial vehicle handling is of great interest as roadway congestion and energy costs drive increased vehicle utilization, and the most common vehicle configuration with more than two axles is a single front steer axle and a rear tandem of two closely spaced axles. Concern for roadway damage demands longer wheelbases and multiple axles on larger vehicles that must be

driven safely on existing roadways by operators with varying experience. Such massive and long multiaxle vehicles can be made more maneuverable with the use of auxiliary steering axles (i.e., steerable wheels on axles other than the front). A methodology for the prediction of handling properties of such vehicles over the wide range of commercial vehicle configurations is valuable. Ellis recommended a method of equating the action of a tandem axle “bogie” to a single-equivalent axle acting between the tandem spread [1]. If it is assumed that the load is equally shared between the tandem axles and all tires have the same cornering coefficients this method results in a simple augmentation of existing two-axle models. Winkler and Gillespie developed a more general steady-state handling model for a three-axle vehicle [3]. Although articulated vehicles are not addressed in this work directly it is appreciated that stability of tractor-trailer combinations depends on the tractor [4]. Winkler has developed a comprehensive statement of steady-state multiaxle vehicle handling [5] through extensive use of Pacejka’s handling diagrams [6]. As in Winkler, the present work is restricted to a rigid vehicle. Winkler’s appeal to geometry and Ellis’ equivalent axle and moment method both generate an equivalent wheelbase of a three-axle vehicle consistent with the handling characteristics of the steady-state solution of the dynamic equations of motion. The results derived in this present chapter have been shown to agree with these other two independent methods of Winkler and Ellis to express the equivalent wheelbase of three-axle vehicles [7].

Commercial vehicles have fundamental vehicle dynamic differences relative to two-axle passenger cars. Commercial vehicles are not only much larger, but in most cases they are designed to carry a payload. Therefore, the most obvious difference is that vehicle mass is much greater and more variable.

Perhaps, the most significant difference, however, is that the increased vehicle mass is typically placed at a higher vertical location. At first glance this may seem immaterial to the yaw-plane (bicycle) model formulation as developed in the [Chapter 10](#) for a two-axle vehicle, but the higher center of gravity places important limitations on the operation that makes the bicycle model even more applicable to commercial vehicles.

Commercial vehicles can have a slightly larger track width than two-axle passenger cars, but not nearly enough to compensate for the higher center of mass. This taller aspect ratio gives rise to the most important difference between commercial vehicle and passenger car dynamics. The achievable steady-state lateral acceleration of commercial vehicles is limited by rollover, and not the friction characteristics of the tire/road interface as in typical passenger cars. Commercial vehicles rollover before they spin out. This property of commercial vehicles is actually an evolutionary attribute of a vocational duty cycle that does not typically require high lateral accelerations. Most commercial vehicles haul payload from point-to-point, therefore their duty cycle is dominated

FIGURE 13.1 Lateral accelerations of typical commercial vehicle duty cycles.

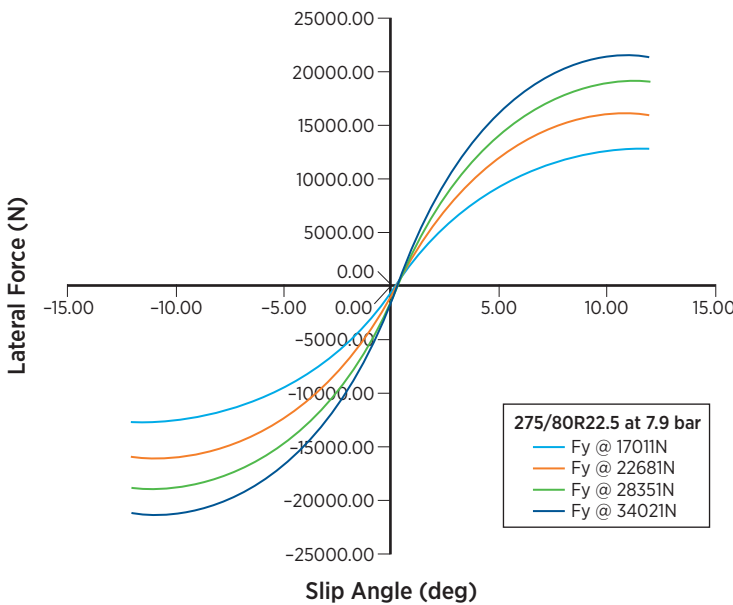
Reprinted with permission from © SAE International.

by lanekeeping. As seen in [Figure 13.1](#), the representative over-the-road duty cycle exceeds 0.1g lateral acceleration only 1% of the time. The more aggressive pickup-and-delivery duty cycle exceeds 0.1g lateral acceleration 6% of the time, and exceeds 0.2g lateral acceleration roughly 0.75% of the time. The rollover threshold of commercial vehicles is variable, and load dynamics are important although uncertain, so experienced drivers will remain well below 0.3g lateral acceleration. This limit does not typically constrain commercial vehicle operation, as the dominant lane-keeping portion of the duty cycle inherently demands low steering inputs, and the remaining portion is mostly maneuvering the load in a dock yard, which can require large steering inputs but at low speed, so again characterized by low lateral accelerations.

Another particular property of commercial vehicles is also consistent with bicycle model assumptions. Passenger car tires exhibit a nonlinear relationship between side force and normal load. Because of the sign of this curvature, passenger car tires always lose more side force with the loss of a unit of normal load than they gain with an addition of a unit of normal load. As weight is transferred across an axle from one tire to the opposite tire, the passenger car “axle” loses its ability to generate a side force. Therefore, if the passenger car suspension provides different roll stiffness at the front than the rear, the stiffer axle will lose ability to generate side force for a given attack angle. This is an example of the “secondary effects,” Olley built into his bicycle model analysis. If roll is resisted at the front axle, the passenger car tends toward understeer, if it is resisted at the rear, it tends increasingly toward oversteer. In the same manner, roll damping as determined by the shock absorbers on an axle have a dynamic effect on tire side force. This effect was used in [Chapter 6](#) to modify passenger car handling properties.

FIGURE 13.2 Lateral force produced by commercial vehicle tire.

Reprinted with permission from © SAE International.



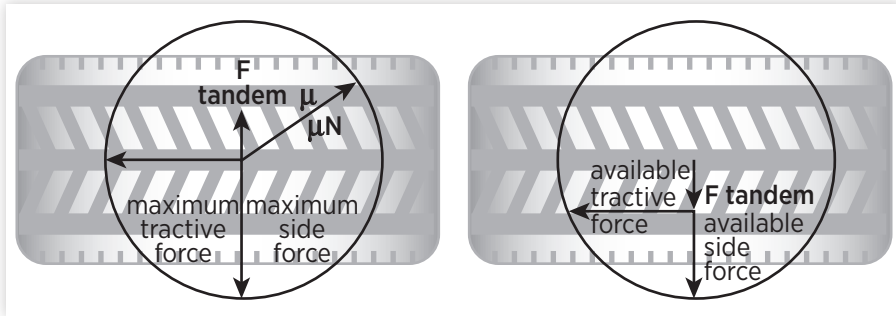
The payload of commercial vehicles varies causing changes in the normal load through the contact patch of the tire. Furthermore even moderate lateral accelerations act on a relatively high center of gravity to produce variations in tire loading. Happily, the bicycle model remains applicable for commercial vehicles because of the differences in tire construction. Commercial vehicle tires are more linear in their relationship between side force and normal load than passenger car tires as shown in [Figure 13.2](#). The relatively long and torsionally compliant ladder frames allow less transfer of roll moment between axles. Taken together, the combination of lower lateral acceleration, more linear tires, and less torsional rigidity makes the bicycle model assumption of neglecting suspension roll dynamics for handling even more appropriate for some commercial vehicles than passenger cars. At the same time, rollover dynamics, particularly for articulated commercial vehicles, are even more important.

Often commercial vehicles are distinguished by multiple rear axles. If rear tires are not steered, vehicle maneuverability and tire wear are compromised by the spread distance between tandem axles. The bridge formulas that determine axle weight allow an exception for closely placed tandem axles. Therefore to reduce tire wear tandem rear axles are closely spaced to form a common three-axle vehicle configuration, in either a straight truck or semi-tractor.

FIGURE 13.3 Deflected tandem axles.

Reprinted with permission from © SAE International.

When a vehicle with rigid rear tandem axles yaws, the axles work together to generate a moment opposing the yawing motion as shown by the tire sidewall deformation in [Figure 13.3](#). This moment results from opposing lateral forces generated at the contact patches of tires on the two rear axles. The total vector sum of lateral and longitudinal forces at the contact patch of the tire is limited by the normal force on the contact patch multiplied by the coefficient of friction between the tire and road surface as illustrated in [Figure 13.4](#). The kinematically overdetermined case of a yawing vehicle with more than two axles is another significant difference between the two-axle model derived and discussed in [Chapter 10](#) and the three-axle model that is the subject of this chapter. As will be discussed in the following section, this kinematic effect gives rise to the longer effective wheelbase of the three-axle vehicle with an adverse effect on vehicle maneuverability.

FIGURE 13.4 Friction circles of tandem axles.

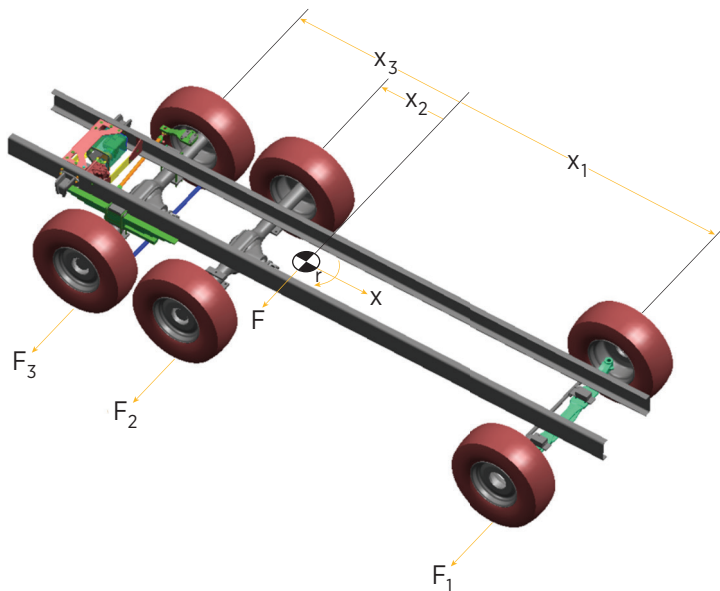
Reprinted with permission from © SAE International.

13.3 The Three-Axle Model

The development of handling equations for the three-axle vehicle will be similar to the previous, perhaps more familiar, two-axle vehicle of [Chapter 10](#). Important vehicle characteristics such as wheelbase and understeer will be shown to emerge from the three-axle vehicle model as more complicated expressions with the same physical significance. As shown in [Figure 13.5](#), a fixed third axle can be added a distance x_3 behind the center of gravity to the classic bicycle model described in [Chapter 10](#) using the generalized side force model of Eq. 9.5 without a steering input. In some vehicles, the tandem axle forces are reacted to the sprung mass in complicated ways; however many times, including most on-highway air suspensions, lateral forces are reacted primarily through a “torque-rod” running more or less along the centerline of the axle in a plan view. As before in the two-axle development of Eq. 10.31, lateral forces and yaw moments are summed to result in expressions for drift angle (scaled lateral velocity) and yaw rate, and written in matrix form.

$$\begin{bmatrix} \dot{\beta} \\ \dot{r} \end{bmatrix} = \begin{bmatrix} \frac{-C_1 - C_2 - C_3}{mu} & \left(\frac{-x_1 C_1 - x_2 C_2 - x_3 C_3}{mu^2} - 1 \right) \\ \frac{-x_1 C_1 - x_2 C_2 - x_3 C_3}{I_z} & \frac{-x_1^2 C_1 - x_2^2 C_2 - x_3^2 C_3}{I_z u} \end{bmatrix} \begin{bmatrix} \beta \\ r \end{bmatrix} + \begin{bmatrix} \frac{C_1}{mu} \\ \frac{x_1 C_1}{I_z} \end{bmatrix} \begin{bmatrix} \delta_1 \end{bmatrix}. \quad (13.1)$$

Using the method of [Chapter 2](#), the dynamic response of the three-axle system described by Eq. 13.1 can be written.

FIGURE 13.5 The three-axle vehicle.

Reprinted with permission from © SAE International.

$$\begin{bmatrix} \beta(s) \\ \delta_1(s) \\ r(s) \\ \dot{\delta}_1(s) \end{bmatrix} = \begin{bmatrix} s + \frac{C_1 + C_2 + C_3}{mu} & \left(\frac{x_1 C_1 + x_2 C_2 + x_3 C_3}{mu^2} + 1 \right) \\ \frac{x_1 C_1 + x_2 C_2 + x_3 C_3}{I_z} & s + \frac{x_1^2 C_1 + x_2^2 C_2 + x_3^2 C_3}{I_z u} \end{bmatrix}^{-1} \begin{bmatrix} \frac{C_1}{mu} \\ \frac{x_1 C_1}{I_z} \end{bmatrix}. \quad (13.2)$$

The characteristic equation becomes visible in the denominator when the state matrix is inverted.

$$\begin{bmatrix} \beta(s) \\ \delta_1(s) \\ r(s) \\ \dot{\delta}_1(s) \end{bmatrix} = \frac{\begin{bmatrix} mu(sI_z u + x_1^2 C_1 + x_2^2 C_2 + x_3^2 C_3) & -I_z(x_1 C_1 + x_2 C_2 + x_3 C_3 + mu^2) \\ -mu^2(x_1 C_1 + x_2 C_2 + x_3 C_3) & I_z u(smu + C_1 + C_2 + C_3) \end{bmatrix} \begin{bmatrix} \frac{C_1}{mu} \\ \frac{x_1 C_1}{I_z} \end{bmatrix}}{s^2(mu^2 I_z) + s(I_z u(C_1 + C_2 + C_3) + mu(x_1^2 C_1 + x_2^2 C_2 + x_3^2 C_3)) + (C_1 C_2 (x_1 - x_2)^2 + C_1 C_3 (x_1 - x_3)^2 + C_2 C_3 (x_2 - x_3)^2 - mu^2(x_1 C_1 + x_2 C_2 + x_3 C_3))}. \quad (13.3)$$

The transfer function from steering input to drift angle for the three-axle vehicle can be written from Eq. 13.3.

$$\frac{\beta(s)}{\delta_1(s)} = \frac{s(C_1 I_z u) - x_2 C_1 C_2 (x_1 - x_2) - x_3 C_1 C_3 (x_1 - x_3) - x_1 C_1 m u^2}{s^2 (m u^2 I_z) + s(I_z u (C_1 + C_2 + C_3) + m u (x_1^2 C_1 + x_2^2 C_2 + x_3^2 C_3)) + (C_1 C_2 (x_1 - x_2)^2 + C_1 C_3 (x_1 - x_3)^2 + C_2 C_3 (x_2 - x_3)^2 - m u^2 (x_1 C_1 + x_2 C_2 + x_3 C_3))} \quad (13.4)$$

and likewise the transfer function from steering input to yaw rate for the three-axle vehicle can be written.

$$\frac{r(s)}{\delta_1(s)} = \frac{s(C_1 x_1 m u^2) + C_1 C_2 u (x_1 - x_2) + C_1 C_3 u (x_1 - x_3)}{s^2 (m u^2 I_z) + s(I_z u (C_1 + C_2 + C_3) + m u (x_1^2 C_1 + x_2^2 C_2 + x_3^2 C_3)) + (C_1 C_2 (x_1 - x_2)^2 + C_1 C_3 (x_1 - x_3)^2 + C_2 C_3 (x_2 - x_3)^2 - m u^2 (x_1 C_1 + x_2 C_2 + x_3 C_3))} \quad (13.5)$$

Displacement expressions similar to the two-axle wheelbase used in Eq. 10.31 are used to simplify the three-axle system,

$$\begin{aligned} l &= x_1 - x_3 \\ t &= x_2 - x_3 \\ l - t &= x_1 - x_2 \end{aligned} \quad (13.6)$$

where l is the distance between the front and rear axles, and t is the tandem spread or the distance between the rear tandem axle bogies. Equation 13.5 is seen to be of the form of the two-axle yaw rate response of Eq. 10.30. Recall in this equation the steady-state handling properties of the two-axle vehicle were captured by the wheelbase and understeer parameters to yield the simplified Eq. 10.33. Expressions for an equivalent wheelbase l_3 and equivalent understeer coefficient K_3 can be developed to similarly simplify Eq. 13.5.

$$l_3 = \frac{C_1 C_2 (l - t)^2 + C_1 C_3 l^2 + C_2 C_3 t^2}{(C_1 C_2 (l - t) + C_1 C_3 l)}, \quad (13.7)$$

$$K_3 = \frac{-m(x_1 C_1 + x_2 C_2 + x_3 C_3)}{(C_1 C_2 (l - t) + C_1 C_3 l)}. \quad (13.8)$$

It should be appreciated that the three-axle wheelbase of Eq. 13.7 and understeer of Eq. 13.8 are completely analogous to their more familiar two-axle counterparts and simplify the characteristic polynomial of Eqs 13.4 and 13.5 in a similar manner. Equation 13.7 can be factored to provide physical significance.

$$l_3 = (l-t) + t \frac{C_1 C_3 l + C_2 C_3 t}{(C_1 C_2(l-t) + C_1 C_3 l)}. \quad (13.9)$$

Equation 13.9 is a very revealing relationship. The effective wheelbase of the three-axle vehicle is the distance between axles one and two, plus a term that is dependent upon the square of the tandem spread, as well as the three cornering coefficients and wheelbase. The first geometric term states that the vehicle basically wants to turn about the forward tandem axle similar to the familiar Ackermann relationship of the two-axle vehicle. The second term is a function of the vehicle configuration and cornering coefficients only, and serves to increase the effective wheelbase as calculated from the geometric term. As this second term is not dependent upon velocity—it is kinematic rather than dynamic—it always adds to the steering requirement for a given maneuver independent of vehicle speed so it is appropriate to consider as an augmentation to the simple wheelbase. This term is not found in the two-axle equation, because it is derived from the tandem axles opposing one another in yaw. Equations 13.6a, 13.6b, 13.6c, and 13.8 can be used with Eq. 13.9 to simplify the transfer functions of Eqs 13.4 and 13.5.

$$\frac{\beta(s)}{\delta_1(s)} = \frac{s \left(\frac{C_1 I_z u}{C_1 C_2(l-t) + C_1 C_3 l} \right) + \left(\frac{-x_2 C_1 C_2(l-t) - x_3 C_1 C_3 l - x_1 C_1 mu^2}{C_1 C_2(l-t) + C_1 C_3 l} \right)}{s^2 \left(\frac{mu^2 I_z}{C_1 C_2(l-t) + C_1 C_3 l} \right) + s \left(\frac{I_z u(C_1 + C_2 + C_3) + mu(x_1^2 C_1 + x_2^2 C_2 + x_3^2 C_3)}{C_1 C_2(l-t) + C_1 C_3 l} \right) + (l_3 + u^2 K_3)}, \quad (13.10)$$

$$\frac{r(s)}{\delta_1(s)} = \frac{s \left(\frac{mx_1 C_1 u^2}{C_1 C_2(l-t) + C_1 C_3 l} \right) + u}{s^2 \left(\frac{mu^2 I_z}{C_1 C_2(l-t) + C_1 C_3 l} \right) + s \left(\frac{I_z u(C_1 + C_2 + C_3) + mu(x_1^2 C_1 + x_2^2 C_2 + x_3^2 C_3)}{C_1 C_2(l-t) + C_1 C_3 l} \right) + (l_3 + u^2 K_3)}. \quad (13.11)$$

The steady-state values of the transfer functions Eqs 13.10 and 13.11 can be found by evaluating them at $s = 0$.

$$\frac{\beta_{ss}}{\delta_{1,ss}} = \frac{-x_2 C_1 C_2(l-t) - x_3 C_1 C_3 l - x_1 C_1 mu^2}{C_1 C_2(l-t) + C_1 C_3 l}, \quad (13.12)$$

$$\frac{r_{ss}}{\delta_{1,ss}} = \frac{u}{l_3 + u^2 K_3}. \quad (13.13)$$

The lateral acceleration response can again be found from Eq. 13.13.

$$\frac{a_{ss}}{\delta_1} = \frac{u^2}{l_3 + u^2 K_3}. \quad (13.14)$$

It is seen that the three-axle K_3 has the same physical significance of the two-axle K_2 , namely, it is the inverse lateral acceleration response at high speeds. Similarly, a three-axle expression for required steady-state steering input can be written similar to [Chapter 2](#).

$$\delta_1 = \frac{l_3}{R} + urK_3. \quad (13.15)$$

Again, the three-axle understeer coefficient K_3 has the same physical significance of the two-axle K_2 . It is the coefficient of the lateral acceleration based steering correction. Furthermore, the equivalent wheelbase l_3 has the same physical significance as the two-axle l_2 . In both cases, the wheelbase divided by the turning radius forms the kinematic relationship that characterizes neutral steering at both high and low speeds. Thus, the more complicated three-axle understeer and wheelbase expressions have the same physical steady-state significance as their simpler two-axle counterparts. These values can be found with the same experimental and graphical means suggested in [Chapter 10](#).

An important feature of Eq. 13.9 is that equivalent wheelbase can be expressed as a function of individual rear axle cornering coefficients. Previous literature [2,3,5] assumed the rear tandem axle is equipped with the same tires on each axle, and the load is equally shared. In that case,

$$C_r = C_2 = C_3, \quad (13.16)$$

and Eq. 13.9 becomes

$$l_3 = (l - t) + \frac{t^2}{2l - t} \left(\frac{l}{t} + \frac{C_r}{C_1} \right). \quad (13.17)$$

It has been shown that Eq. 13.17 is consistent with the literature [7]. Partial derivatives of Eq. 13.17 can be found with respect to both front and rear cornering coefficients.

$$\left. \frac{\partial l_3}{\partial C_r} \right|_{C_1=C_0} = \frac{t^2}{C_1(2l-t)}, \quad (13.18)$$

$$\left. \frac{\partial l_3}{\partial C_1} \right|_{Cr=C_0} = \frac{t^2}{(2l-t)} \left(-\frac{C_r}{C_1^2} \right). \quad (13.19)$$

Equation 13.18 states that as the rear cornering coefficient increases, so does the effective wheelbase of the three-axle vehicle. The nonsteered rear tandem creates a yaw resisting moment that must be overcome by the front axle. Equation 13.19 shows as the front cornering coefficient increases, it is better able to overcome the yaw resisting moment of the rear tandem and the effective wheelbase decreases. Equation 13.19 also points out a potential problem with vehicle handling when the front tires begin to saturate and no longer produce a side force proportional to attack angle. In this case, the effective front cornering coefficient is decreased, and the effective vehicle wheelbase increases.

It is evident that the equivalent wheelbase l_3 and understeer coefficient K_3 serve an identical role in the three-axle steady-state responses shown above in Eqs 13.12 and 13.13 as their two-axle counterparts l_2 and K_2 in [Chapter 10](#). To extend the equivalence to the dynamic case the two-axle notation suggested by Ellis [8], modified in this work, and consistent with [Chapter 10](#) is again used with changes in convention. The modified Ellis notation of Eq. 10.63a, 10.63b, and 10.63c is augmented to include the third axle.

$$C_a = C_1 + C_2 + C_3,$$

$$C_b = x_1 C_1 + x_2 C_2 + x_3 C_3, \quad (13.20)$$

$$C_c = x_1^2 C_1 + x_2^2 C_2 + x_3^2 C_3,$$

The signed axle convention allows uniformity not present in Ellis' original nomenclature and essential for the next steps. Fortunately, an identity can be found for the three-axle vehicle having a similar usefulness as Ellis' expression for the two-axle vehicle used in [Chapter 10](#) to simplify the three-axle model.

$$C_a C_c - C_b^2 = C_1 C_2 (l - t)^2 + C_1 C_3 l^2 + C_2 C_3 t^2, \quad (13.21)$$

So the characteristic polynomial can again be written.

$$p(s) = s^2 (mu^2 I_z) + s (I_z u C_a + mu C_c) + (C_a C_c - C_b^2 - mu^2 C_b) \quad (13.22)$$

Equation 13.22 is identical to its two-axle equivalent of Eq. 10.66, only the values of C_a , C_b , and C_c have become more complicated with the added axle. This reasonable result is possible because of the choice of convention used in this work and discussed in [Chapter 9](#). Just as for the two-axle vehicle, the quadratic equation can be used to express the roots of Eq. 13.22.

$$s_{1,2} = \frac{-(mu C_c + I_z u C_a) + / - \sqrt{(mu C_c + I_z u C_a)^2 - 4mu^2 I_z (C_a C_c - C_b^2 - mu^2 C_b)}}{2mu^2 I_z} \quad (13.23)$$

Using Eqs 13.7, 13.8, and 13.21, it can be shown that

$$C_a C_c - C_b^2 - mu^2 C_b = (l_3 + K_3 u^2)(C_1 C_2 (l-t) + C_1 C_2 l) \quad (13.24)$$

so that Eq. 13.23 becomes,

$$s_{1,2} = \frac{-(mu C_c + I_z u C_a) + / - \sqrt{(mu C_c + I_z u C_a)^2 - 4mu^2 I_z (C_1 C_2 (l-t) + C_1 C_2 l)(l_3 + K_3 u^2)}}{2mu^2 I_z}. \quad (13.25)$$

Just as with the two-axle vehicle previously developed, at the critical speed defined by,

$$l_3 + K_3 u^2 = 0, \quad (13.26)$$

the characteristic polynomial Eq. 13.22 of the three-axle vehicle can be easily factored,

$$p(s) = s \left(s + \frac{m C_c + I_z C_a}{mu I_z} \right) \quad (13.27)$$

and expressed in terms of the original cornering coefficients used in the three-axle notation of Eqs 13.20a, 13.20b, and 13.20c.

$$p(s) = s \left(s + \frac{m(x_1^2 C_1 + x_2^2 C_2 + x_3^2 C_3) + I_z (C_1 + C_2 + C_3)}{mu I_z} \right) \quad (13.28)$$

When $C_b = 0$, the three-axle vehicle is neutral steering and the characteristic polynomial can be simplified similar to the two-axle vehicle. The quadratic equation is used to find the real roots of the neutral steering three-axle vehicle.

$$s_{1,2} = \frac{-(m C_c + I_z C_a) \pm (m C_c - I_z C_a)}{2mu I_z}. \quad (13.29)$$

The factored characteristic polynomial can be written,

$$p(s) = \left(s + \frac{C_a}{mu} \right) \left(s + \frac{C_c}{I_z u} \right) \quad (13.30)$$

and the three-axle cornering coefficients substituted.

$$p(s) = \left(s + \frac{(C_1 + C_2 + C_3)}{mu} \right) \left(s + \frac{(x_1^2 C_1 + x_2^2 C_2 + x_3^2 C_3)}{I_z u} \right). \quad (13.31)$$

Using a generalized tire force model based on the attack angle convention, locating axles with a signed distance from the vehicle center of gravity, Ellis' modified notation that simplifies two-axle dynamic handling equations is extended to the three-axle vehicle. In doing so, more complex three-axle notions of wheelbase and understeer are useful. It is important to appreciate that these notions of wheelbase and understeer have similar utility in the two-axle and three-axle models, both for steady-state and dynamic analysis.

13.4 Third Axle Steering

In [Chapter 11](#), it was suggested that steering the rear of a two-axle vehicle can allow both improved low-speed trajectory tracking and high-speed stability [9]. Steering the third axle has been shown to improve low speed vehicle handling properties [10] as well as tire wear [11]. Steering the third axle of a three-axle vehicle has perhaps more economic utility than steering the second axle of a two-axle vehicle. Now, electronically controlled rear axle steering systems are offered on European production commercial vehicles that fully counter-steer at low speeds, and remain at their nominal center positions at higher vehicle speeds [12]. Qu and Zu [13] describe theoretical opportunities to improve the handling of three-axle vehicles. Bayar and Unlusoy likewise describe improvements in three-axle vehicle handling [14].

The third axle included in the system of [Figure 13.5](#) can be allowed to steer with an input δ_3 using the generalized side force model of Eq. 9.5 with a steer angle of δ_3 .

$$\begin{bmatrix} \dot{\beta} \\ \dot{r} \end{bmatrix} = \begin{bmatrix} \frac{-C_1 - C_2 - C_3}{mu} & \left(\frac{-x_1 C_1 - x_2 C_2 - x_3 C_3}{mu^2} - 1 \right) \\ \frac{-x_1 C_1 - x_2 C_2 - x_3 C_3}{I_z} & \frac{-x_1^2 C_1 - x_2^2 C_2 - x_3^2 C_3}{I_z u} \end{bmatrix} \begin{bmatrix} \beta \\ r \end{bmatrix} + \begin{bmatrix} \frac{C_1}{mu} & \frac{C_3}{mu} \\ \frac{x_1 C_1}{I_z} & \frac{x_3 C_3}{I_z} \end{bmatrix} \begin{bmatrix} \delta_1 \\ \delta_3 \end{bmatrix}. \quad (13.32)$$

A simple proportional relationship between the front and rear steered wheels is used to determine the steering input of the third axle similar to the two-axle Eq. 11.12 as shown in [Figure 13.6](#).

$$\delta_3 = \eta_3 \delta_1. \quad (13.33)$$

So that Eq. 13.32 becomes

$$\begin{bmatrix} \dot{\beta} \\ \dot{r} \end{bmatrix} = \begin{bmatrix} \frac{-C_1 - C_2 - C_3}{mu} & \left(\frac{-x_1 C_1 - x_2 C_2 - x_3 C_3}{mu^2} - 1 \right) \\ \frac{-x_1 C_1 - x_2 C_2 - x_3 C_3}{I_z} & \frac{-x_1^2 C_1 - x_2^2 C_2 - x_3^2 C_3}{I_z u} \end{bmatrix} \begin{bmatrix} \beta \\ r \end{bmatrix} + \begin{bmatrix} \frac{C_1}{mu} + \frac{C_3}{mu} \eta_3 \\ \frac{x_1 C_1}{I_z} + \frac{x_3 C_3}{I_z} \eta_3 \end{bmatrix} \begin{bmatrix} \delta_1 \\ \delta_3 \end{bmatrix}. \quad (13.34)$$

As in the three-axle vehicle with a rigid (non-steered) rear axle, in steady-state the time derivatives are zero and the steady-state variables can be solved in terms of the control input.

$$\begin{bmatrix} \beta_{ss} \\ r_{ss} \end{bmatrix} = - \begin{bmatrix} \frac{-C_1 - C_2 - C_3}{mu} & \left(\frac{-x_1 C_1 - x_2 C_2 - x_3 C_3}{mu^2} - 1 \right) \\ \frac{-x_1 C_1 - x_2 C_2 - x_3 C_3}{I_z} & \frac{-x_1^2 C_1 - x_2^2 C_2 - x_3^2 C_3}{I_z u} \end{bmatrix}^{-1} \begin{bmatrix} \frac{C_1}{mu} + \frac{C_3}{mu} \eta_3 \\ \frac{x_1 C_1}{I_z} + \frac{x_3 C_3}{I_z} \eta_3 \end{bmatrix} \begin{bmatrix} \delta_1 \\ \delta_3 \end{bmatrix}. \quad (13.35)$$

FIGURE 13.6 First and last axles steered.



The steady-state response ratios are

$$\frac{\beta_{ss}}{\delta_1} = \frac{C_1 C_2 x_2 (x_1 - x_2) + C_1 C_3 x_3 (x_1 - x_3) + mu^2 x_1 C_1 - \eta_3 (C_1 C_3 x_1 (x_1 - x_3) + C_2 C_3 (x_2 - x_3) - mu^2 x_3 C_3)}{-C_1 C_2 (x_1^2 - 2x_1 x_2 + x_2^2) - C_1 C_3 (x_1^2 - 2x_1 x_3 + x_3^2) - C_2 C_3 (x_2^2 - 2x_2 x_3 + x_3^2) + mu^2 (x_1 C_1 + x_2 C_2 + x_3 C_3)} \quad (13.36)$$

and

$$\frac{r_{ss}}{\delta_1} = \frac{u(-x_1 C_1 C_2 - x_1 C_1 C_3 + x_2 C_1 C_2 + x_3 C_1 C_3 + \eta_3 (x_1 C_1 C_3 + x_2 C_2 C_3 - x_3 C_1 C_3 - x_3 C_2 C_3))}{-C_1 C_2 (x_1^2 - 2x_1 x_2 + x_2^2) - C_1 C_3 (x_1^2 - 2x_1 x_3 + x_3^2) - C_2 C_3 (x_2^2 - 2x_2 x_3 + x_3^2) + mu^2 (x_1 C_1 + x_2 C_2 + x_3 C_3)}. \quad (13.37)$$

Using Eq. 13.6, defining wheelbase and tandem spread, Eqs 13.36 and 13.37 are simplified.

$$\frac{\beta_{ss}}{\delta_1} = \frac{C_1 C_2 x_2 (l-t) + C_1 C_3 x_3 l + mu^2 x_1 C_1 - \eta_3 (C_1 C_3 x_1 l + C_2 C_3 (l-t) - mu^2 x_3 C_3)}{-C_1 C_2 (l-t)^2 - C_1 C_3 l^2 - C_2 C_3 t^2 + mu^2 (x_1 C_1 + x_2 C_2 + x_3 C_3)} \quad (13.38)$$

$$\frac{r_{ss}}{\delta_1} = \frac{-u(C_1 C_2 (l-t) + C_1 C_3 l - \eta_3 (C_1 C_3 l + C_2 C_3 t))}{-C_1 C_2 (l-t)^2 - C_1 C_3 l^2 - C_2 C_3 t^2 + mu^2 (x_1 C_1 + x_2 C_2 + x_3 C_3)}. \quad (13.39)$$

The yaw rate response ratio is written in the standard form of Eq. 13.13.

$$\frac{r_{ss}}{\delta_1} = \frac{u}{\frac{C_1 C_2 (l-t)^2 + C_1 C_3 l^2 + C_2 C_3 t^2}{C_1 C_2 (l-t) + C_1 C_3 l - \eta_3 (C_1 C_3 l + C_2 C_3 t)} + u^2 \frac{-m(x_1 C_1 + x_2 C_2 + x_3 C_3)}{(C_1 C_2 (l-t) + C_1 C_3 l - \eta_3 (C_1 C_3 l + C_2 C_3 t))}}. \quad (13.40)$$

so the equivalent wheelbase of the rear steering vehicle is

$$l_3 = \frac{C_1 C_2 (l-t)^2 + C_1 C_3 l^2 + C_2 C_3 t^2}{C_1 C_2 (l-t) + C_1 C_3 l - \eta_3 (C_1 C_3 l + C_2 C_3 t)}. \quad (13.41)$$

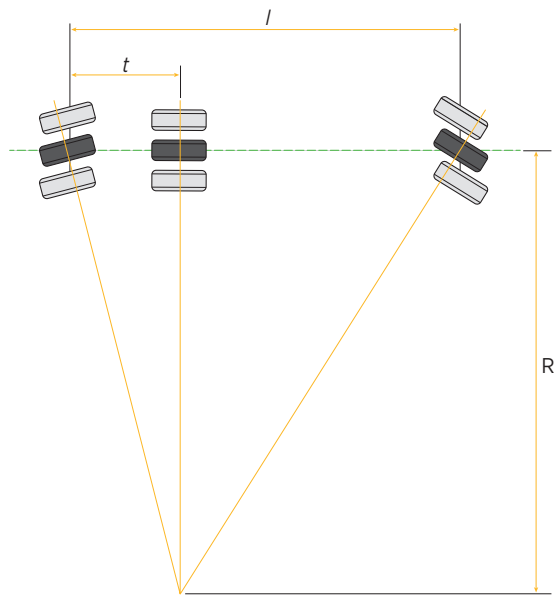
An interesting relationship between the front and rear wheel steering inputs is formed if the rear wheels are turned to steer around the geometric center defined by the front and second axle, as shown in [Figure 13.7](#). This relationship can be expressed simply as a ratio of wheelbases,

$$\delta_3 = -\left(\frac{x_2 - x_3}{x_1 - x_2}\right)\delta_1 \quad (13.42)$$

and in terms of vehicle geometry, [Figure 13.7](#) defines the ratio of front-to-rear steering inputs as

FIGURE 13.7 Steering front and rear axles perpendicular to radii.

Reprinted with permission from © SAE International.



$$\eta_3 = -\frac{t}{l-t}. \quad (13.43)$$

When the rear axle is steered in this manner a line extending from the unsteered second-axle intersects the instantaneous center of the turn, and at low speeds all axles have negligible slip. The entire frictional capability of the tires can be used to accelerate or brake the vehicle, an important consideration on low friction surfaces or off-road terrain. At these low speeds the vehicle essentially yaws about the second axle. If all three axles were steered the vehicle could yaw about any specified location. The proposed configuration is used in practice as it more economically provides minimal low speed tire scrub with steering only two axles rather than three, saving the considerable expense of another electronically controlled steerable axle and retaining much of the vehicle performance benefit. Equation 41 becomes

$$l_3 = \frac{C_1 C_2 (l-t)^3 + C_1 C_3 l^2 (l-t) + C_2 C_3 t^2 (l-t)}{C_1 C_2 (l-t)^2 + C_1 C_3 l (l-t) + t (C_1 C_3 l + C_2 C_3 t)}. \quad (13.44)$$

TABLE 1. Comparison of derived handling parameters.

	Effective wheelbase, l_3	Understeer coeff., K_3
Non-steered rear axle	$\frac{C_1 C_2 (l-t)^2 + C_1 C_3 l^2 + C_2 C_3 t^2}{(C_1 C_2 (l-t) + C_1 C_3 l)}$	$\frac{-m(x_1 C_1 + x_2 C_2 + x_3 C_3)}{(C_1 C_2 (l-t) + C_1 C_3 l)}$
Steered rear axle	$(l-t)$	$\frac{-m(x_1 C_1 + x_2 C_2 + x_3 C_3)}{C_1 C_2 (l-t) + C_1 C_3 \frac{l^2}{l-t} + C_2 C_3 \frac{t^2}{l-t}}$

And with algebraic manipulation reduces to

$$l_3 = (l-t). \quad (13.45)$$

The vehicle will effectively turn about the second axle, as intuitively expected. The difference Δl_e between the effective wheelbase with an unsteered third axle of Eq. 13.9 and the simply steered effective wheelbase of Eq. 13.45 indicates one source of improvement in the steady-state handling properties of a rear axle steered vehicle.

The improvement in effective wheelbase when simply steering the third axle is a function of cornering coefficients, wheelbase and tandem spread.

$$\Delta l_e = t \frac{C_1 C_3 l + C_2 C_3 t}{(C_1 C_2 (l-t) + C_1 C_3 l)}. \quad (13.46)$$

A second source of handling modification through steering the third axle is apparent in the 3-axle understeer coefficient required to reduce Eq. 13.40 to standard form.

$$K_3 = \frac{-m(x_1 C_1 + x_2 C_2 + x_3 C_3)}{(C_1 C_2 (l-t) + C_1 C_3 l - \eta_3 (C_1 C_3 l + C_2 C_3 t))}. \quad (13.47)$$

Equation 13.43 can be inserted.

$$K_3 = \frac{-m(x_1 C_1 + x_2 C_2 + x_3 C_3)}{C_1 C_2 (l-t) + C_1 C_3 \frac{l^2}{l-t} + C_2 C_3 \frac{t^2}{l-t}}. \quad (13.48)$$

The magnitude of the understeering coefficient is reduced when steering the rear axle, as this effect always increases the denominator relative to the unsteered denominator of Eq. 13.8.

Dividing Eq. 13.48 by Eq. 13.8, it is evident that the ratio of

$$\frac{K_{3,\text{steered}}}{K_{3,\text{unsteered}}} = \frac{C_1 C_2 (l-t) + C_1 C_3 l}{C_1 C_2 (l-t) + C_1 C_3 \frac{l^2}{l-t} + C_2 C_3 \frac{t^2}{l-t}} \quad (13.49)$$

is always less than one. Steering the third axle decreases the magnitude of the understeer coefficient as a function of the tire cornering coefficients, wheelbase and tandem spread. The ratio of steered to understeer is the same as the ratio of steered to unsteered equivalent wheelbase. These results can be compared with the nonsteered rear tandem.

13.5 Trajectory Tracking

Inertially defined dynamic states of Eqs 11.6 and 11.7 were added to the two-axle state-space bicycle model of Eq. 10.22 to produce the augmented two-axle bicycle model including inertially defined states of Eq. 11.8. Similarly, these inertially defined states can be augmented to the three-axle state-space model of Eq. 13.1.

$$\begin{bmatrix} \dot{\beta} \\ \dot{r} \\ \dot{\psi} \\ \dot{Y} \end{bmatrix} = \begin{bmatrix} \frac{-C_1 - C_2 - C_3}{mu} & \left(\frac{-x_1 C_1 - x_2 C_2 - x_3 C_3}{mu^2} - 1 \right) & 0 & 0 \\ \frac{-x_1 C_1 - x_2 C_2 - x_3 C_3}{I_z} & \frac{-x_1^2 C_1 - x_2^2 C_2 - x_3^2 C_3}{I_z u} & 0 & 0 \\ 0 & 1 & 0 & 0 \\ u & 0 & u & 0 \end{bmatrix} \begin{bmatrix} \beta \\ r \\ \psi \\ Y \end{bmatrix} + \begin{bmatrix} \frac{C_1}{mu} \\ \frac{x_1 C_1}{I_z} \\ 0 \\ 0 \end{bmatrix} \begin{bmatrix} \delta_1 \\ \delta_3 \end{bmatrix}. \quad (13.50)$$

In a three-axle vehicle, the third axle is more commonly steered than the second as previously discussed. The appropriate additional control input is added to Eq. 13.50.

$$\begin{bmatrix} \dot{\beta} \\ \dot{r} \\ \dot{\psi} \\ \dot{Y} \end{bmatrix} = \begin{bmatrix} \frac{-C_1 - C_2 - C_3}{mu} & \left(\frac{-x_1 C_1 - x_2 C_2 - x_3 C_3}{mu^2} - 1 \right) & 0 & 0 \\ \frac{-x_1 C_1 - x_2 C_2 - x_3 C_3}{I_z} & \frac{-x_1^2 C_1 - x_2^2 C_2 - x_3^2 C_3}{I_z u} & 0 & 0 \\ 0 & 1 & 0 & 0 \\ u & 0 & u & 0 \end{bmatrix} \begin{bmatrix} \beta \\ r \\ \psi \\ Y \end{bmatrix} + \begin{bmatrix} \frac{C_1}{mu} & \frac{C_3}{mu} \\ \frac{x_1 C_1}{I_z} & \frac{x_3 C_3}{I_z} \\ 0 & 0 \\ 0 & 0 \end{bmatrix} \begin{bmatrix} \delta_1 \\ \delta_3 \end{bmatrix} \quad (13.51)$$

If the third axle is steered as a fixed proportion of the front steering input, as in Eq. 13.33, the two-input system of Eq. 13.51 can be written as a single-input system.

$$\begin{bmatrix} \dot{\beta} \\ \dot{r} \\ \dot{\psi} \\ \dot{Y} \end{bmatrix} = \begin{bmatrix} \frac{-C_1 - C_2 - C_3}{mu} & \left(\frac{-x_1 C_1 - x_2 C_2 - x_3 C_3}{mu^2} - 1 \right) & 0 & 0 \\ \frac{-x_1 C_1 - x_2 C_2 - x_3 C_3}{I_z} & \frac{-x_1^2 C_1 - x_2^2 C_2 - x_3^2 C_3}{I_z u} & 0 & 0 \\ 0 & 1 & 0 & 0 \\ u & 0 & u & 0 \end{bmatrix} \begin{bmatrix} \beta \\ r \\ \psi \\ Y \end{bmatrix} + \begin{bmatrix} \frac{C_1}{mu} + \eta_3 \frac{C_3}{mu} \\ \frac{x_1 C_1}{I_z} + \eta_3 \frac{x_3 C_3}{I_z} \\ 0 \\ 0 \end{bmatrix} \begin{bmatrix} \delta_1 \end{bmatrix}. \quad (13.52)$$

And again using the process described in [Chapter 2](#), the state variable transfer functions can be written as before using Eqs 13.20a, 13.20b, and 13.20c.

$$\frac{\beta(s)}{\delta_1(s)} = \frac{(sI_z u + C_c)(C_1 + C_3 \eta_3) - (C_b + mu^2)(x_1 C_1 + x_3 C_3 \eta_3)}{s^2 mu^2 I_z + su(mC_c + I_z C_a) + C_a C_c - C_b^2 - C_b mu^2}, \quad (13.53)$$

$$\frac{r(s)}{\delta_1(s)} = \frac{u(smu + C_a)(x_1 C_1 + x_3 C_3 \eta_3) - C_b u(C_1 + C_3 \eta_3)}{s^2 mu^2 I_z + su(mC_c + I_z C_a) + C_a C_c - C_b^2 - C_b mu^2}, \quad (13.54)$$

$$\frac{\psi(s)}{\delta_1(s)} = \frac{u(smu + C_a)(x_1 C_1 + x_3 C_3 \eta_3) - u C_b (C_1 + C_3 \eta_3)}{s(s^2 mu^2 I_z + su(mC_c + I_z C_a) + C_a C_c - C_b^2 - C_b mu^2)}, \quad (13.55)$$

$$\frac{Y(s)}{\delta_1(s)} = \frac{u(u C_a - s C_b)(x_1 C_1 + x_3 C_3 \eta_3) + u(s^2 Iu + s C_c - u C_b)(C_1 + C_3 \eta_3)}{s^2(s^2 mu^2 I_z + su(mC_c + I_z C_a) + C_a C_c - C_b^2 - C_b mu^2)}. \quad (13.56)$$

Equations 13.54–13.56 represent vehicle and trajectory states of a three-axle vehicle that allow the third axle to be steered proportionally to the primary front axle steering control input. Of course the transfer function for an unsteered vehicle is returned by assigning $\eta_3 = 0$. These equations appear to be quite similar to their two-axle counterparts of Eqs 15–18 of [Chapter 11](#), with the only immediately noticeable difference between the third axle location and cornering coefficient substituted for the second in the numerators. Such a preliminary conclusion fails to appreciate the usefulness of the nomenclature suggested in this work. Comparing the two-axle expressions of Eqs 10.63a, 10.63b, 10.63c with the three-axle expressions of Eqs 13.20a, 13.20b, and 13.20c, it is evident that when the products of terms are formed in the denominators of the transfer functions, the three-axle equations are significantly more complex when written in terms of the original cornering coefficients and axle locations.

The three-axle expressions would be even more complicated if written in terms of unsigned axle locations.

The previously presented driver model can be combined with the inertially referenced vehicle model with rear steer, as with the two-axle model. The practical utility of this combination is not as great as in the two-axle case, however. At high speed the two-axle rear steer control was seen to crab to improve vehicle stability. This is certainly a functional possibility for the three-axle application; however, this functionality will come at the expense of greatly increased tire wear for most commercial vehicle duty cycles if the second axle remains unsteered. Therefore, in practice most three-axle vehicles counter-steer at low speed to improve maneuverability and tire wear, and the third axle is fixed in its nominal straight-ahead position at high speed to preserve desirable understeer. All axles of a multiaxle vehicle must be steered to allow the high-speed stability benefits of crab-steer without increasing tire wear.

13.6 Summary

Using the conventions and ensuing nomenclature suggested in this work, the development of three-axle vehicle dynamics has been shown to be a simple extension of the two-axle case. The characteristic polynomial has been shown to be similar, so the transient vehicle dynamic cases developed in [Chapter 10](#) apply to vehicles with three axles.

As developed in [Chapter 10](#) for vehicles with two axles, the yaw plane dynamics for a three-axle vehicle can be solved in steady state, yielding the familiar yaw rate response equation. In this yaw rate response, terms corresponding to the two-axle development can be identified for wheelbase and understeer. These terms have the same physical significance in either application. The three-axle wheelbase term is shown to be the distance between the first and second axles, plus a complicated term dependent upon other vehicle parameters. This method of deriving the equivalent wheelbase of a three-axle vehicle is more general than other attempts, but shown in the literature to agree with the special cases treated by the others.

Rear axle steering was seen to be a slightly different application than previously presented for two-axle vehicles. In the two axle case the rear steering strategy was shown to transition from crab steer to counter steer. For the three axle case, at low speeds the third axle counter steers to allow the vehicle to turn about the second axle, eliminating tire scrub to both reduce turning radius and tire wear.

When using the nomenclature and conventions developed in this work, the two-axle and three-axle bicycle models are seen to be similar. Concepts of wheelbase and understeer have equivalent meaning in the two-axle and

three-axle vehicles. Using the conventions described in this work the trajectory tracking model is similar for two and three axles, with only defined nomenclature functions of cornering coefficients becoming more complex. In the following section it will be shown that this is no coincidence, and the two-axle model and the three-axle model are in fact special cases of a general model.

References

- [1] Lauda, N, "The Art and Science of Grand Prix Driving," Motorbooks International, Osceola Wisconsin, 1977.
- [2] Ellis, John R., "Steering of Multiple Axle Bogie Systems," *Vehicle System Dynamics*, Vol. 5, Issue 4, 1976, p. 221–238.
- [3] Winkler, Chris B., and Thomas D. Gillespie, "On the Directional Response Characteristics of Heavy Trucks," *Vehicle System Dynamics*, Vol. 6, No. 2–3, 1977, p. 120.
- [4] Fancher, Paul S., Static Stability of Articulated Commercial Vehicles, *Vehicle System Dynamics*, Vol 14, No 4, 1985, p. 201–227.
- [5] Winkler, Christopher B., "Simplified Analysis of the Steady-State Turning of Complex Vehicles," *Vehicle System Dynamics*, 29 (1998), pp. 141–180.
- [6] Pacejka, H.B., *Tire and Vehicle Dynamics*, Society of Automotive Engineers, Warrendale, PA, 2002.
- [7] Williams, Daniel E., "On the Equivalent Wheelbase of a Three-Axle Vehicle," *Vehicle System Dynamics*, DOI: [10.1080/00423114.2010.530670](https://doi.org/10.1080/00423114.2010.530670).
- [8] Ellis, John R., *Vehicle Dynamics*, Business Books, London, 1969.
- [9] Williams, D.E., Using Rear Axle Steer to Improve Driver-Vehicle Performance, *Vehicle System Dynamics*, Volume 52, Issue 4, 2014. DOI:[10.1080/00423114.2013.854397](https://doi.org/10.1080/00423114.2013.854397).
- [10] Williams, Daniel E., "Handling Benefits of Steering a Third Axle." Proceedings of IMechE, Part D: *Journal of Automobile Engineering*, 2010, 224(D12), 1501–1511. DOI [10.1243/09544070AUT01528](https://doi.org/10.1243/09544070AUT01528).
- [11] Williams, D., "Tire Wear Improvement by Steering a Third Axle," *SAE International Journal of Commercial Vehicle* 4(1):1–12, 2011, DOI:[10.4271/2011-01-2148](https://doi.org/10.4271/2011-01-2148).
- [12] TRW Commercial Steering Systems, EMAS Product Literature, Lafayette, Indiana, 2010.
- [13] Qu, Quizhen, and Jean W. Zu, On Steering Control of Commercial Three-Axle Vehicle, *Journal of Dynamic Systems, Measurement and Control*, American Society of Mechanical Engineers, 130 (2008), pp. 1–10.
- [14] Bayar, Kerem and Y. Samim Unlusoy, "Steering Strategies for Multi-Axle Vehicles," *International Journal of Heavy Vehicle Systems*, Volume 15, No. 2–4 (2008), pp. 208–236.

Generalized Multiaxle Vehicle Dynamics

“ Do not laugh at notations; invent them, they are powerful. In fact, mathematics is, to a large extent, inventions of better notations.

—Richard Feynman

”

14.1 Introduction

We began this section on handling by introducing the concept of understeer in terms of kinematic steering compliance. We rederived the standard yaw-plane passenger car handling model [1–3] using new conventions that did not harm the passenger car application and allowed block diagrams more aligned with control theorists expectations. Owing to these new conventions, the two-axle yaw-plane model was easily extended to vehicles with three axles. We formally derived Newton’s second law accelerations in rotating reference frames and made plausible assumptions to justify the standard passenger car yaw-plane model. Using this formal derivation, we were able to make convenient yet plausible assumptions that allowed freedom of the sprung mass to roll [4]. We also described the functionality of steering the rear axle of both conventional two-axle passenger cars and three-axle vehicles.

The three-axle handling analysis made use of the new conventions and nomenclature. (The astute reader could detect common themes that are generalized in this chapter.) Adoption of these conventions and nomenclature will be clearly justified in the present chapter. These innovations will allow the development of a general multiaxle state space model. Derivations of the two-axle and three-axle vehicle models can be generalized so that the two degrees of freedom handling properties of any multiaxle vehicle, including multiple steerable axles, are immediately available for computation using simple vehicle parameters

without having to resort to Newton's second law and summing forces and moments for a specific vehicle [5]. In the two-axle chapter, we saw how the concepts of wheelbase and understeer completely characterized steady-state vehicle response and were significant in the transient response. We have long been able to directly express these characterizations for two-axle vehicles, and in [Chapter 13](#) it has been shown how they can be written for three-axle vehicles [6]. In the present chapter, the concepts of equivalent wheelbase and understeer will be expressed in a way not possible with other generalized multiaxle models thanks to the conventions adopted and nomenclature used [7,8]. The previously derived two- and three-axle models are seen as special cases of this general model, and likewise vehicle handling parameters such as wheelbase and understeer that have a direct physical interpretation for a two-axle vehicle are shown to be generally obtainable for all multiaxle vehicles. Compared with a previously suggested generalized model [7,8], the presented model is very compact and parsimonious in form, owing to nonstandard choices of convention. Furthermore, the proposed model effectively accommodates any arbitrary axle configuration, such as a twin-steer vehicle. It is remarkable that when these conventions are combined with a simplifying identity similar to that used by Ellis [4] for the two-axle model, a generalized vehicle model results that describes the yaw plane motion of a vehicle with an arbitrary number of steered and nonsteered axles as well as direct computation of the equivalent wheelbase and understeer.

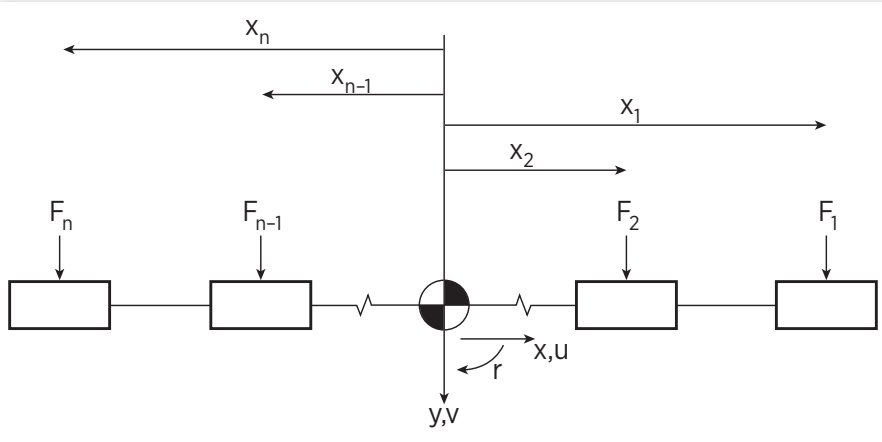
This present work combines the n -axle model developed by the author [5,9] with the roll plane degree of freedom developed by Ellis and Metz. The algebraic manipulation in this chapter is tedious. One option would be to step the reader through the algebra, but it was decided to move more directly to results, and the reader that has followed the journey thus far and wants more detail is invited to consult the referenced literature [10].

14.2 General Model

Given the obvious similarities in the development of the two-axle and three-axle handling analysis, concepts will now be extended to account for any number of steered and nonsteered axles on an arbitrarily complex multiaxle vehicle. The x - y axis in [Figure 9.1](#) of [Chapter 9](#) is fixed to the center of mass of the vehicle with the x -axis corresponding to the vehicle's longitudinal center line and the vehicle yaws about the center of gravity. All the simplifying assumptions taking the general rigid body accelerations derived in [Chapter 8](#) to form the simple yaw plane accelerations of [Chapter 10](#) are made and not repeated here, thus similarly limiting these results. The summation of lateral forces from an arbitrary number of axles shown in [Figure 14.1](#) is equal to the lateral acceleration in the coordinate axis fixed to the vehicle plus the centripetal acceleration of that axis.

FIGURE 14.1 Generalized multiaxle vehicle.

Reprinted with permission from © SAE International.



$$\sum_{i=1}^n F_i = m(\dot{v} + ur) = F_1 + F_2 + \dots + F_{n-1} + F_n. \quad (14.1)$$

Similarly moments produced by an arbitrary number of axles can be summed about the center of mass.

$$\sum_{i=1}^n M_i = I_z \dot{r} = x_1 F_1 + x_2 F_2 + \dots + x_{n-1} F_{n-1} + x_n F_n. \quad (14.2)$$

The generalized side force expression of Eq. 9.5 can be inserted into Eqs 14.1 and 14.2, and the results solved for the highest-order derivatives.

$$\dot{v} = \frac{-\sum_{i=1}^n C_i}{mu} v + \left(\frac{-\sum_{i=1}^n x_i C_i}{mu} - u \right) r + \sum_{i=1}^n \frac{C_i}{m} \delta_i, \quad (14.3)$$

$$\dot{r} = \frac{-\sum_{i=1}^n x_i C_i}{I_z u} v + \frac{-\sum_{i=1}^n x_i^2 C_i}{I_z u} r + \sum_{i=1}^n \frac{x_i C_i}{I_z} \delta_i. \quad (14.4)$$

The lateral velocity v in Eqs 14.3 and 14.4 can be scaled by the longitudinal velocity u that is constant by assumption. The resulting product is again defined as the vehicle drift angle β . Using this notation, Eqs 14.3 and 14.4 can be rewritten in matrix form.

$$\begin{bmatrix} \dot{\beta} \\ \dot{r} \end{bmatrix} = \begin{bmatrix} -\sum_{i=1}^n C_i & \left(\frac{-\sum_{i=1}^n x_i C_i}{mu} - 1 \right) \\ \frac{-\sum_{i=1}^n x_i C_i}{I_z} & \frac{-\sum_{i=1}^n x_i^2 C_i}{I_z u} \end{bmatrix} \begin{bmatrix} \beta \\ r \end{bmatrix} + \begin{bmatrix} \frac{C_1}{mu} & \dots & \frac{C_n}{mu} \\ \frac{x_1 C_1}{I_z} & \dots & \frac{x_n C_n}{I_z} \end{bmatrix} \begin{bmatrix} \delta_1 \\ \vdots \\ \delta_n \end{bmatrix}. \quad (14.5)$$

Equation 14.5 is a fundamental generalized result that can be used to describe the handling dynamics of various vehicle configurations, and can be compared with the two-axle system of Eq. 10.22,

$$\begin{bmatrix} \dot{\beta} \\ \dot{r} \end{bmatrix} = \begin{bmatrix} \frac{-C_1 - C_2}{mu} & \left(\frac{-x_1 C_1 - x_2 C_2}{mu^2} - 1 \right) \\ \frac{-x_1 C_1 - x_2 C_2}{I_z} & \frac{-x_1^2 C_1 - x_2^2 C_2}{I_z u} \end{bmatrix} \begin{bmatrix} \beta \\ r \end{bmatrix} + \begin{bmatrix} \frac{C_1}{mu} \\ \frac{x_1 C_1}{I_z} \end{bmatrix} \begin{bmatrix} \delta_1 \end{bmatrix}$$

and the three-axle system of Eq. 13.1.

$$\begin{bmatrix} \dot{\beta} \\ \dot{r} \end{bmatrix} = \begin{bmatrix} \frac{-C_1 - C_2 - C_3}{mu} & \left(\frac{-x_1 C_1 - x_2 C_2 - x_3 C_3}{mu^2} - 1 \right) \\ \frac{-x_1 C_1 - x_2 C_2 - x_3 C_3}{I_z} & \frac{-x_1^2 C_1 - x_2^2 C_2 - x_3^2 C_3}{I_z u} \end{bmatrix} \begin{bmatrix} \beta \\ r \end{bmatrix} + \begin{bmatrix} \frac{C_1}{mu} \\ \frac{x_1 C_1}{I_z} \end{bmatrix} \begin{bmatrix} \delta_1 \end{bmatrix}.$$

Both of the two above equations are special cases of this generalization. At this point some general observations can be made.

The system of Eq. 14.5 can be simplified if the following neutral condition occurs.

$$\sum_{i=1}^n x_i C_i = 0. \quad (14.6)$$

Recall x_i is the distance from the vehicle center of gravity to the i th axle, and for axles behind the center of gravity this quantity is negative. Therefore, it is possible to choose axle locations and tire side force coefficients so that Eq. 14.6 is satisfied. When this occurs, the state transition matrix of Eq. 14.5 becomes upper-triangular, and the yaw rate r is completely independent of the vehicle drift angle β , and the vehicle is said to be neutral steering, as in previous chapters.

It is interesting to compare the structure of Eq. 14.5 and the state equation of the generalized pitch-plane model of Eq. 4.68. In the yaw-plane model, lateral forces act at the axle locations and vertical forces at the same axle locations in the pitch plane. The coupling terms of both models found in the off-diagonal

locations are similar sums of stiffnesses and axle locations. The diagonal terms are likewise similar. There are two main differences in these generalized models. First is the centripetal acceleration term in the yaw-plane model. Second, is that Eq. 14.5 is two coupled first-order differential equations, and Eq. 4.68 is two coupled second-order differential equations. In Eq. 4.68, the coefficients are traditional stiffness terms, creating an accelerating force based on relative displacement. In Eq. 14.5, the attack angle is the instantaneous velocity vector subtracted from the steering input. Because of Eq. 14.5 produces accelerating forces based on velocities, the resulting differential equations are first order.

In general, the dynamic states of the multiaxle vehicle can be expressed using the format introduced in [Chapter 1](#),

$$\begin{bmatrix} \beta \\ r \end{bmatrix} = \begin{bmatrix} s + \frac{\sum_{i=1}^n C_i}{mu} & \left(\frac{\sum_{i=1}^n x_i C_i}{mu^2} + 1 \right) \\ \frac{\sum_{i=1}^n x_i C_i}{I_z} & s + \frac{\sum_{i=1}^n x_i^2 C_i}{I_z u} \end{bmatrix}^{-1} \begin{bmatrix} \frac{C_1}{mu} & \dots & \frac{C_n}{mu} \\ \frac{x_1 C_1}{I_z} & \dots & \frac{x_n C_n}{I_z} \end{bmatrix} \begin{bmatrix} \delta_1 \\ \vdots \\ \delta_n \end{bmatrix} \quad (14.7)$$

and rewritten.

$$\begin{bmatrix} \beta(s) \\ r(s) \end{bmatrix} = \frac{\begin{bmatrix} mu(sIu + \sum_{i=1}^n x_i^2 C_i) & -I_z(\sum_{i=1}^n x_i C_i + mu^2) \\ -mu^2 \sum_{i=1}^n x_i C_i & I_z u(smu + \sum_{i=1}^n C_i) \end{bmatrix} \begin{bmatrix} \frac{C_1}{mu} & \dots & \frac{C_n}{mu} \\ \frac{x_1 C_1}{I_z} & \dots & \frac{x_n C_n}{I_z} \end{bmatrix} \begin{bmatrix} \delta_1(s) \\ \vdots \\ \delta_n(s) \end{bmatrix}}{s^2 mu^2 I_z + s(mu \sum_{i=1}^n x_i^2 C_i + I_z u \sum_{i=1}^n C_i)} \quad (14.8)$$

The transfer function of a vehicle with n axles relating the drift angle to the primary steering input can be expressed.

$$\frac{\beta(s)}{\delta_1(s)} = \frac{s C_1 I_z u + C_1 \sum_{i=1}^n x_i^2 C_i - x_1 C_1 (\sum_{i=1}^n x_i C_i + mu^2)}{s^2 mu^2 I_z + s(mu \sum_{i=1}^n x_i^2 C_i + I_z u \sum_{i=1}^n C_i) + \left((\sum_{i=1}^n C_i) (\sum_{i=1}^n x_i^2 C_i) - (\sum_{i=1}^n x_i C_i)^2 - mu^2 \sum_{i=1}^n x_i C_i \right)} \quad (14.9)$$

And similarly the transfer function of a vehicle with n axles relating the yaw rate to the primary steering input can be expressed.

$$\frac{r(s)}{\delta_1(s)} = \frac{s\mu^2 x_1 C_1 + C_1 u \left(x_1 \sum_{i=1}^n C_i - \sum_{i=1}^n x_i C_i \right)}{s^2 m u^2 I_z + s \left(m u \sum_{i=1}^n x_i^2 C_i + I_z u \sum_{i=1}^n C_i \right) + \left(\left(\sum_{i=1}^n C_i \right) \left(\sum_{i=1}^n x_i^2 C_i \right) - \left(\sum_{i=1}^n x_i C_i \right)^2 - m u^2 \sum_{i=1}^n x_i C_i \right)}. \quad (14.10)$$

The steady-state expressions can be found by assigning a zero value to the Laplace variable in Eq. 14.8.

$$\begin{bmatrix} r_{ss} \\ \beta_{ss} \end{bmatrix} = \frac{\begin{bmatrix} m u \sum_{i=1}^n x_i^2 C_i & -I_z \left(\sum_{i=1}^n x_i C_i + m u^2 \right) \\ -m u^2 \sum_{i=1}^n x_i C_i & I_z u \sum_{i=1}^n C_i \end{bmatrix} \begin{bmatrix} \frac{C_1}{m u} & \dots & \frac{C_n}{m u} \\ \frac{x_1 C_1}{I_z} & \dots & \frac{x_n C_n}{I_z} \end{bmatrix}}{\left(\sum_{i=1}^n C_i \right) \left(\sum_{i=1}^n x_i^2 C_i \right) - \left(\sum_{i=1}^n x_i C_i \right)^2 - m u^2 \sum_{i=1}^n x_i C_i} \begin{bmatrix} \delta_1 \\ \vdots \\ \delta_n \end{bmatrix}. \quad (14.11)$$

If only the front axle is steered, the steady-state yaw rate response becomes:

$$\frac{r_{ss}}{\delta_{1ss}} = \frac{u C_1 \sum_{i=1}^n C_i (x_1 - x_i)}{\left(\sum_{i=1}^n C_i \right) \left(\sum_{i=1}^n x_i^2 C_i \right) - \left(\sum_{i=1}^n x_i C_i \right)^2 - m u^2 \sum_{i=1}^n x_i C_i} \quad (14.12)$$

and is manipulated to a familiar form.

$$\frac{r_{ss}}{\delta_{1ss}} = \frac{u}{\frac{\left(\sum_{i=1}^n C_i \right) \left(\sum_{i=1}^n x_i^2 C_i \right) - \left(\sum_{i=1}^n x_i C_i \right)^2}{C_1 \sum_{i=1}^n C_i (x_1 - x_i)} - u^2 \frac{m \sum_{i=1}^n x_i C_i}{C_1 \sum_{i=1}^n C_i (x_1 - x_i)}}. \quad (14.13)$$

The generalized understeer coefficient for a multiaxle vehicle with one steered front axle is

$$K_n = \frac{-m \sum_{i=1}^n x_i C_i}{C_1 \sum_{i=1}^n C_i (x_1 - x_i)} \quad (14.14)$$

and the generalized effective wheelbase is

$$l_n = \frac{\left(\sum_{i=1}^n C_i \right) \left(\sum_{i=1}^n x_i^2 C_i \right) - \left(\sum_{i=1}^n x_i C_i \right)^2}{C_1 \sum_{i=1}^n C_i (x_1 - x_i)} \quad (14.15)$$

so that

$$\frac{r_{ss}}{\delta_{1ss}} = \frac{u}{l_n + u^2 K_n} \quad (14.16)$$

and l_n and K_n retain their usefulness in describing the steady-state handling properties of the generalized vehicle.

The roots of the characteristic polynomial of transfer functions Eqs 14.9 and 14.10 can be found using the quadratic formula.

$$s_{1,2} = \frac{-\left(m \sum_{i=1}^n x_i^2 C_i + I_z \sum_{i=1}^n C_i\right) + / - \sqrt{4mI_z \left(\left(\sum_{i=1}^n C_i\right) \left(\sum_{i=1}^n x_i^2 C_i\right) - \left(\sum_{i=1}^n x_i C_i\right)^2 - mu^2 \sum_{i=1}^n x_i C_i \right)}}{2muI_z}. \quad (14.17)$$

Using the expressions defined in Eqs 14.14 and 14.15, Eq. 14.8 becomes

$$\begin{bmatrix} \beta(s) \\ r(s) \end{bmatrix} = \frac{\begin{bmatrix} mu \left(sI_z u + \sum_{i=1}^n x_i^2 C_i \right) & -I_z \left(\sum_{i=1}^n x_i C_i + mu^2 \right) \\ -mu^2 \sum_{i=1}^n x_i C_i & I_z u \left(smu + \sum_{i=1}^n C_i \right) \end{bmatrix} \begin{bmatrix} \frac{C_1}{mu} & \dots & \frac{C_n}{mu} \\ \frac{x_1 C_1}{I_z} & \dots & \frac{x_n C_n}{I_z} \end{bmatrix} \begin{bmatrix} \delta_1(s) \\ \vdots \\ \delta_n(s) \end{bmatrix}}{s^2 mu^2 I_z + s \left(mu \sum_{i=1}^n x_i^2 C_i + I_z u \sum_{i=1}^n C_i \right) + \left(l_n + u^2 K_n \right)}, \quad (14.18)$$

and the roots of the characteristic polynomial expressed in Eq. 14.17 become

$$s_{1,2} = \frac{-\left(m \sum_{i=1}^n x_i^2 C_i + I_z \sum_{i=1}^n C_i\right) + / - \sqrt{\left(m \sum_{i=1}^n x_i^2 C_i + I_z \sum_{i=1}^n C_i\right)^2 - 4mI_z \left(l_n + u^2 K_n\right)}}{2muI_z}. \quad (14.19)$$

Again, it is interesting to examine the roots of the characteristic polynomial when the special condition of marginal stability at the critical speed,

$$l_n + u^2 K_n = 0 \quad (14.20)$$

is satisfied. The characteristic polynomial becomes

$$p(s) = s \left(s + \frac{m \sum_{i=1}^n x_i^2 C_i + I_z \sum_{i=1}^n C_i}{muI_z} \right). \quad (14.21)$$

In the special case of neutral steer described by Eq. 14.6, Eq. 14.17 becomes

$$s_{1,2} = \frac{-\left(m \sum_{i=1}^n x_i^2 C_i + I_z \sum_{i=1}^n C_i\right) + / - \left(m \sum_{i=1}^n x_i^2 C_i - I_z \sum_{i=1}^n C_i\right)}{2muI_z}. \quad (14.22)$$

So in this special case, the characteristic polynomial becomes

$$p(s) = \left(s + \frac{\sum_{i=1}^n x_i^2 C_i}{I_z u} \right) \left(s + \frac{\sum_{i=1}^n C_i}{mu} \right). \quad (14.23)$$

TABLE 1. Pole locations for various vehicle conditions and axle configurations.

Axes	Marginally Stable Oversteer	Neutral Steer
Two	$s \left(s + \frac{m(x_1^2 C_1 + x_2^2 C_2) + I_z(C_1 + C_2)}{muI_z} \right)$	$\left(s + \frac{(C_1 + C_2)}{mu} \right) \left(s + \frac{(x_1^2 C_1 + x_2^2 C_2)}{I_z u} \right)$
Three	$s \left(s + \frac{m(x_1^2 C_1 + x_2^2 C_2 + x_3^2 C_3) + I_z(C_1 + C_2 + C_3)}{muI_z} \right)$	$\left(s + \frac{(C_1 + C_2 + C_3)}{mu} \right) \left(s + \frac{(x_1^2 C_1 + x_2^2 C_2 + x_3^2 C_3)}{I_z u} \right)$
n	$s \left(s + \frac{m \sum_{i=1}^n x_i^2 C_i + I_z \sum_{i=1}^n C_i}{muI_z} \right)$	$\left(s + \frac{\sum_{i=1}^n x_i^2 C_i}{I_z u} \right) \left(s + \frac{\sum_{i=1}^n C_i}{mu} \right)$

14.3 An Arbitrarily Steered Axle

In general, the effect of steering an arbitrary axle can be described by considering a control input from only a specific axle k in Eq. 14.5.

$$\begin{bmatrix} \dot{\beta} \\ \dot{r} \end{bmatrix} = \begin{bmatrix} -\sum_{i=1}^n C_i & \left(-\sum_{i=1}^n x_i C_i \over mu^2 - 1 \right) \\ -\sum_{i=1}^n x_i C_i & -\sum_{i=1}^n x_i^2 C_i \over I_z u \end{bmatrix} \begin{bmatrix} \beta \\ r \end{bmatrix} + \begin{bmatrix} C_k \\ mu \\ x_k C_k \over I_z \end{bmatrix} \delta_k. \quad (14.24)$$

As before the transfer function of a vehicle with n axles relating the drift angle to a steering input of the k th axle can be expressed.

$$\frac{\beta(s)}{\delta_k(s)} = \frac{sC_k I_z u + C_k \sum_{i=1}^n x_i^2 C_i - x_k C_k \sum_{i=1}^n x_i C_i + mu^2}{s^2 mu^2 I_z + s \left(mu \sum_{i=1}^n x_i^2 C_i + I_z u \sum_{i=1}^n C_i \right) + \left(\left(\sum_{i=1}^n C_i \right) \left(\sum_{i=1}^n x_i^2 C_i \right) - \left(\sum_{i=1}^n x_i C_i \right)^2 - mu^2 \sum_{i=1}^n x_i C_i \right)}. \quad (14.25)$$

And similarly the transfer function of a vehicle with n axles relating the yaw rate to the steering input of the k th axle can be expressed.

$$\frac{r(s)}{\delta_k(s)} = \frac{s\mu^2 x_k C_k - C_k u \left(\sum_{i=1}^n x_i C_i + u \sum_{i=1}^n C_i \right)}{s^2 \mu u^2 I_z + s \left(\mu u \sum_{i=1}^n x_i^2 C_i + I_z u \sum_{i=1}^n C_i \right) + \left(\left(\sum_{i=1}^n C_i \right) \left(\sum_{i=1}^n x_i^2 C_i \right) - \left(\sum_{i=1}^n x_i C_i \right)^2 - \mu u^2 \sum_{i=1}^n x_i C_i \right)}. \quad (14.26)$$

A practical condition is described when the k th axle of Eqs 14.25 and 14.26 is the rearmost, or n th axle, and it is driven proportionally to the front, similar to the three-axle control law of Eq. 13.33.

$$\delta_n = \eta_n \delta_1. \quad (14.27)$$

The control law of Eq. 14.27 is used to combine via superposition the drift angle of the vehicle in response to the primary steered first axle of Eq. 14.9 added to the drift angle response because of the n th axle steered proportionally from Eq. 14.25 using Eq. 14.27.

$$\frac{\beta(s)}{\delta_1(s)} = \frac{sIu(C_1 + \eta_n C_n) + (C_1 + \eta_n C_n) \sum_{i=1}^n x_i^2 C_i - (x_1 C_1 + \eta_n x_n C_n)}{s^2 \mu u^2 I_z + s \left(\mu u \sum_{i=1}^n x_i^2 C_i + I_z u \sum_{i=1}^n C_i \right) + \left(\left(\sum_{i=1}^n C_i \right) \left(\sum_{i=1}^n x_i^2 C_i \right) - \left(\sum_{i=1}^n x_i C_i \right)^2 - \mu u^2 \sum_{i=1}^n x_i C_i \right)}. \quad (14.28)$$

Through a similar operation, the yaw rate can be described in response to a rear steering input proportional to the primary input combining Eqs 14.10, 14.26, and 14.27.

$$\frac{r(s)}{\delta_1(s)} = \frac{s\mu u^2 (x_1 C_1 + \eta_n x_n C_n) - u(C_1 + \eta_n C_n) \left(\sum_{i=1}^n x_i C_i + u \sum_{i=1}^n C_i \right)}{s^2 \mu u^2 I_z + s \left(\mu u \sum_{i=1}^n x_i^2 C_i + I_z u \sum_{i=1}^n C_i \right) + \left(\left(\sum_{i=1}^n C_i \right) \left(\sum_{i=1}^n x_i^2 C_i \right) - \left(\sum_{i=1}^n x_i C_i \right)^2 - \mu u^2 \sum_{i=1}^n x_i C_i \right)}. \quad (14.29)$$

Equation 14.29 can be expressed in steady state.

$$\frac{r_{ss}(s)}{\delta_1(s)} = \frac{-u(C_1 + \eta_n C_n) \left(\sum_{i=1}^n x_i C_i + u \sum_{i=1}^n C_i \right)}{\left(\left(\sum_{i=1}^n C_i \right) \left(\sum_{i=1}^n x_i^2 C_i \right) - \left(\sum_{i=1}^n x_i C_i \right)^2 - \mu u^2 \sum_{i=1}^n x_i C_i \right)}. \quad (14.30)$$

Equation 14.30 is seen to be a super position of the generalized primary steered steady-state yaw rate response of Eq. 14.9 for a vehicle with n axles with the same response for a vehicle with an arbitrarily steered axle of Eq. 14.26 where $k = n$. Because both the primary steered axle and the n th steered axle jointly determine the vehicle yaw rate response, a single-input-single-output (SISO) steady-state expression such as Eq. 14.16 is only possible when the n th input is a linear function of the primary input. It is only in this condition (known in control systems as “SISO”) that it makes sense to speak of equivalent wheelbase and understeer.

When the rear axle of an n -axle vehicle is steered proportionally to the front, its wheelbase can be expressed.

$$l_{n,s} = \frac{\left(\sum_{i=1}^n C_i\right)\left(\sum_{i=1}^n x_i^2 C_i\right) - \left(\sum_{i=1}^n x_i C_i\right)^2}{(C_1 + \eta_n C_n) \sum_{i=1}^n C_i (x_1 - x_i)}. \quad (14.31)$$

A similar expression for the understeer of an n -axle vehicle with the rear steered proportionally to the front can be written.

$$K_{n,s} = \frac{-m \sum_{i=1}^n x_i C_i}{(C_1 + \eta_n C_n) \sum_{i=1}^n C_i (x_1 - x_i)}. \quad (14.32)$$

The development of this special case has been presented for the rearmost axle and can be easily repeated for any other axle. As we have seen, many of the ways vehicle handling is characterized and tested are derived from Eq. 14.16, so in general multiple steered axles become more of a control problem and less of a vehicle dynamics problem as introduced in the two-axle discussion of a driver/vehicle system maintaining a lane.

14.4 All Arbitrary Axles Steered Proportionally

A gain vector can be defined that relates the steering input displacement of the i th axle δ_i with the primary steering input.

$$\begin{bmatrix} \delta_1 \\ \delta_2 \\ \vdots \\ \delta_n \end{bmatrix} = \begin{bmatrix} \eta_1 \\ \eta_2 \\ \vdots \\ \eta_n \end{bmatrix} \delta. \quad (14.33)$$

For vehicles with mechanical connections between the handwheel and primary front steered axles η_1 can be considered 1 and then all other η_i are simply ratios of the i th axle steering input to the front. It should be noted that Eq. 14.33 can describe proportional steering of arbitrary subsets of axles as η_i can be zero for rigid or non-steered axles. Through definition of η_i the vehicle can be made to steer about many arbitrary points. Eq. 14.33 can be inserted into the general model of Eq. 14.8.

$$\begin{bmatrix} \beta(s) \\ r(s) \end{bmatrix} = \frac{\begin{bmatrix} mu\left(sIu + \sum_{i=1}^n x_i^2 C_i\right) & -I_z\left(\sum_{i=1}^n x_i C_i + mu^2\right) \\ -mu^2 \sum_{i=1}^n x_i C_i & I_z u\left(smu + \sum_{i=1}^n C_i\right) \end{bmatrix} \begin{bmatrix} \frac{C_1}{mu} & \dots & \frac{C_n}{mu} \\ \frac{x_1 C_1}{I_z} & \dots & \frac{x_n C_n}{I_z} \\ \vdots \\ \eta_n \end{bmatrix} \delta}{s^2 mu^2 I_z + s\left(mu \sum_{i=1}^n x_i^2 C_i + I_z u \sum_{i=1}^n C_i\right) + \left(\left(\sum_{i=1}^n C_i\right)\left(\sum_{i=1}^n x_i^2 C_i\right) - \left(\sum_{i=1}^n x_i C_i\right)^2 - mu^2 \sum_{i=1}^n x_i C_i\right)}. \quad (14.34)$$

In steady state, the general model of Eq. 14.34 can be expressed,

$$\begin{bmatrix} \beta_{ss}(s) \\ r_{ss}(s) \end{bmatrix} = \frac{\begin{bmatrix} mu\left(\sum_{i=1}^n x_i^2 C_i\right) & -I_z\left(\sum_{i=1}^n x_i C_i + mu^2\right) \\ -mu^2 \sum_{i=1}^n x_i C_i & I_z u\left(\sum_{i=1}^n C_i\right) \end{bmatrix} \begin{bmatrix} \frac{C_1}{mu} & \dots & \frac{C_n}{mu} \\ \frac{x_1 C_1}{I_z} & \dots & \frac{x_n C_n}{I_z} \\ \vdots \\ \eta_n \end{bmatrix} \delta}{\left(\left(\sum_{i=1}^n C_i\right)\left(\sum_{i=1}^n x_i^2 C_i\right) - \left(\sum_{i=1}^n x_i C_i\right)^2 - mu^2 \sum_{i=1}^n x_i C_i\right)} \quad (14.35)$$

and the steady-state yaw rate response can be written as

$$\frac{r_{ss}}{\delta} = \frac{u \left[\sum_{i=1}^n C_i \eta_i \left(\sum_{j=1}^n C_j (x_i - x_j) \right) \right]}{\left(\left(\sum_{i=1}^n C_i \right) \left(\sum_{i=1}^n x_i^2 C_i \right) - \left(\sum_{i=1}^n x_i C_i \right)^2 - mu^2 \sum_{i=1}^n x_i C_i \right)}. \quad (14.36)$$

From Eq. 14.36, it is possible to write the general expression for the equivalent wheelbase of an arbitrary axle vehicle, any of which may be steered proportionally to the steering input.

$$l_n = \frac{\left(\sum_{i=1}^n C_i \right) \left(\sum_{i=1}^n x_i^2 C_i \right) - \left(\sum_{i=1}^n x_i C_i \right)^2}{\sum_{i=1}^n \eta_i C_i \left(\sum_{j=1}^n (x_i - x_j) \right)}. \quad (14.37)$$

Similarly, the generalized understeer coefficient can be written for this arbitrary vehicle.

$$K_n = \frac{-m \sum_{i=1}^n x_i C_i}{\sum_{i=1}^n \eta_i C_i \left(\sum_{j=1}^n C_j (x_i - x_j) \right)}. \quad (14.38)$$

Equations 14.37 and 14.38 reflect the key handling parameters for arbitrary axles steered proportionally to the primary steering input. As derived in [Chapter 11](#), there is value in these relationships varying with vehicle speed.

14.5 The Multiaxle Vehicle with Roll

Earlier in this section of the book, the two-axle yaw-plane model was derived with new conventions and nomenclature. Then, development occurred in three seemingly independent directions: rear axle steer, roll, and three-axle handling. In the first part of this chapter, the three-axle model was generalized to form a multiaxle model, and steering was appended. Now, roll will be added so that the three “independent” developments are combined into a single, general model.

Equations 12.9, 12.13, and 12.17 are acceleration responses to summations of forces and moments, where the sprung mass is allowed to roll relative to the unsprung mass, and as such remain valid as accelerations in response to external forces in the multiaxle case. Rather than front and rear axles, for the multiaxle case axles are numerated 1 through n . The roll mode stiffness and damping expressions are simply modified for the multiaxle condition by observing that all axle’s suspensions resist roll in parallel.

$$K_\phi = \left(\frac{\partial L}{\partial \dot{\phi}} \Big|_1 + \frac{\partial L}{\partial \dot{\phi}} \Big|_2 + \dots + \frac{\partial L}{\partial \dot{\phi}} \Big|_n \right) + m_s g h, \quad (14.39)$$

$$D_\phi = \left(\frac{\partial L}{\partial \ddot{\phi}} \Big|_1 + \frac{\partial L}{\partial \ddot{\phi}} \Big|_2 + \dots + \frac{\partial L}{\partial \ddot{\phi}} \Big|_n \right). \quad (14.40)$$

Equations 14.39 and 14.40 are now inserted into the roll acceleration response of Eq. 12.17.

$$I_{x,a} \ddot{\phi} - m_s h \dot{v} - m_s h c \dot{r} = m_s h u_r - K_\phi \phi - D_\phi \dot{\phi}. \quad (14.41)$$

The more interesting multiaxle generalizations come from the yaw and lateral velocity equations. Newton’s second law for lateral velocity and yaw degrees of freedom, Eqs 12.9 and 12.13 can be written to allow side force from any number of axles.

$$m(\dot{v} + ru) - m_s h \dot{p} = \sum F_i, \quad (14.42)$$

$$I_z \dot{r} - m_s c h \dot{p} = \sum F_i x_i. \quad (14.43)$$

The generalized tire force expressions of Eq. 12.29 can be written for each axle and inserted into Eq. 14.42 and expanded,

$$\begin{aligned} m(\dot{v} + ru) - m_s h \ddot{\phi} &= -C_1 \left(\frac{v}{u} \right) - \left(\frac{C_1 x_1}{u} \right) r + \left(C_1 \epsilon_1 + \frac{\partial Y_1}{\partial \phi_1} \frac{\partial \phi_1}{\partial \phi} \right) \phi + C_1 \delta_1 \\ &- C_2 \left(\frac{v}{u} \right) - \left(\frac{C_2 x_2}{u} \right) r + \left(C_2 \epsilon_2 + \frac{\partial Y_2}{\partial \phi_2} \frac{\partial \phi_2}{\partial \phi} \right) \phi + C_2 \delta_2 \\ &\dots \\ &- C_n \left(\frac{v}{u} \right) - \left(\frac{C_n x_n}{u} \right) r + \left(C_n \epsilon_n + \frac{\partial Y_n}{\partial \phi_n} \frac{\partial \phi_n}{\partial \phi} \right) \phi + C_n \delta_n \end{aligned} \quad (14.44)$$

and terms can be collected by state variables.

$$m(\dot{v} + ru) - m_s h \dot{p} = - \left(\frac{\sum C_i}{u} \right) v - \left(\frac{\sum C_i x_i}{u} \right) r + \sum \left(C_i \epsilon_i + \frac{\partial Y_f}{\partial \phi_f} \frac{\partial \phi_f}{\partial \phi} \right) \phi + \sum C_i \delta_i. \quad (14.45)$$

Similarly, the moments created by lateral forces at the axles can be summed and equated to yaw-rate acceleration from Eq. 14.43,

$$\begin{aligned} I_z \dot{r} - m_s c h \ddot{\phi} &= -x_1 C_f \left(\frac{v}{u} \right) - \left(\frac{C_1 x_1^2}{u} \right) r + x_1 \left(C_1 \epsilon_1 + \frac{\partial Y_1}{\partial \phi_1} \frac{\partial \phi_1}{\partial \phi} \right) \phi + x_1 C_1 \delta_1 \\ &- x_2 C_2 \left(\frac{v}{u} \right) - \left(\frac{C_2 x_2^2}{u} \right) r + x_2 \left(C_2 \epsilon_2 + \frac{\partial Y_2}{\partial \phi_2} \frac{\partial \phi_2}{\partial \phi} \right) \phi + x_2 C_2 \delta_2 \\ &\dots \\ &- x_n C_n \left(\frac{v}{u} \right) - \left(\frac{C_n x_n^2}{u} \right) r + x_n \left(C_n \epsilon_n + \frac{\partial Y_n}{\partial \phi_n} \frac{\partial \phi_n}{\partial \phi} \right) \phi + x_n C_n \delta_n \end{aligned} \quad (14.46)$$

and as before terms can be collected by state and control variables.

$$I_z \dot{r} - m_s c h \ddot{\phi} = - \left(\frac{\sum x_i C_i}{u} \right) v - \left(\frac{\sum C_i x_i^2}{u} \right) r + \sum \left(x_i C_i \epsilon_i + x_i \frac{\partial Y_i}{\partial \phi_i} \frac{\partial \phi_i}{\partial \phi} \right) \phi + \sum x_i C_i \delta_i. \quad (14.47)$$

For nomenclature purposes, the following terms are defined consistent with previous two-axle and three-axle development. Equations 10.63a, 10.63b, and 10.63c can be generated for multiple axles.

$$C_a = \sum C_i, \quad (14.48)$$

$$C_b = \sum x_i C_i, \quad (14.49)$$

$$C_c = \sum x_i^2 C_i. \quad (14.50)$$

Again, it is worth noting that this nomenclature is similar to that first suggested by Ellis, but the conventions adopted in this work allow the simple forms of Eqs 14.48–14.50. Without the change in axle location convention, Ellis' two-axle version of Eq. 14.49 would not be generalizable. A roll steer coefficient R_i is defined for each axle similar to Eqs 12.37 and 12.38 for the front and rear axles.

$$R_i = C_i \epsilon_i + \frac{\partial Y_i}{\partial \phi_i} \frac{\partial \phi_i}{\partial \phi}. \quad (14.51)$$

Using Eq. 14.51, expressions similar to Eqs 14.48 and 14.49 can be generated for multiple axles.

$$R_a = \sum R_i, \quad (14.52)$$

$$R_b = \sum x_i R_i. \quad (14.53)$$

Using the nomenclature of Eqs 14.48–14.53, Eqs 14.45 and 14.47 are recovered. The state variable coefficients are the same because of a judicious choice of nomenclature and convention. The control variables are many as steering any of the multiple axles is permitted in this general model of multiaxle vehicles with roll.

$$m(\dot{v} + ru) - m_s h \ddot{\phi} = -\left(\frac{C_a}{u}\right)v - \left(\frac{C_b}{u}\right)r + (R_a)\phi + \sum C_i \delta_i, \quad (14.54)$$

$$I_z \dot{r} - m_s ch \ddot{\phi} = -\left(\frac{C_b}{u}\right)v - \left(\frac{C_c}{u}\right)r + (R_b)\phi + \sum x_i C_i \delta_i, \quad (14.55)$$

Equations 14.54, 14.55, and 14.41 can be put in matrix form with terms including the highest-order derivatives of the left hand side, similar to Eq. 12.43.

$$\begin{bmatrix} \dot{v} \\ \dot{r} \\ \ddot{\phi} \\ \dot{\phi} \end{bmatrix} = \frac{\begin{bmatrix} m & 0 & -m_s h \\ 0 & I_z & -m_s ch \\ -m_s h & -m_s ch & I_{x,a} \end{bmatrix}^{-1} \begin{bmatrix} -C_a & -C_b - mu & 0 & R_a \\ -C_b & -C_c & 0 & R_b \\ 0 & 0 & -D_\phi & -K_\phi \end{bmatrix} \begin{bmatrix} v \\ r \\ \dot{\phi} \\ \phi \end{bmatrix}}{\begin{bmatrix} 0 & 0 & 1 & 0 \end{bmatrix}} \quad (14.56)$$

$$\begin{bmatrix} \ddot{\phi} \\ \dot{\phi} \end{bmatrix} = \frac{\begin{bmatrix} m & 0 & -m_s h \\ 0 & I_z & -m_s ch \\ -m_s h & -m_s ch & I_{x,a} \end{bmatrix}^{-1} \begin{bmatrix} C_1 & C_2 & \dots & C_n \\ x_1 C_1 & x_2 C_2 & \dots & x_n C_n \\ 0 & 0 & \dots & 0 \end{bmatrix} \begin{bmatrix} \delta_1 \\ \delta_2 \\ \dots \\ \delta_n \end{bmatrix}}{\begin{bmatrix} 0 & 0 & \dots & 0 \end{bmatrix}} +$$

Equation 14.56 is a full state dynamic model of a multiaxle vehicle with roll. Equation 14.56 also allows for steering of any particular axle, so it is a very general model of a multiaxle vehicle with roll and steering.

As before, these equations can be solved for steady state. Equations 14.54 and 14.55 become:

$$0 = -\left(\frac{C_a}{u}\right)v - \left(\frac{C_b}{u}\right)r + (R_a)\phi + \sum C_i \delta_i, \quad (14.57)$$

$$0 = -\left(\frac{C_b}{u}\right)v - \left(\frac{C_c}{u}\right)r + (R_b)\phi + \sum x_i C_i \delta_i. \quad (14.58)$$

As before, for a steady-state analysis, all time derivatives are zero so Eq. 14.41 becomes

$$\phi = \left(\frac{m_s h u}{K_\phi}\right)r. \quad (14.59)$$

At this point, it is assumed that all axles steer with a fixed ratio of the front, and a bit more nomenclature is introduced,

$$\sum C_i \delta_i = \sum C_i \eta_i \delta_1 = \Delta_a \delta_1, \quad (14.60)$$

$$\sum x_i C_i \delta_i = \sum x_i C_i \eta_i \delta_1 = \Delta_b \delta_1, \quad (14.61)$$

where Δ_a is the summation over each axle of the product of the side force coefficients and the proportion of the front axle steering input that is used. Similarly, Δ_b is the product expressed by Δ_a multiplied by the axle location. The assumption that each axle is steered as a proportion of the front is needed to transform the multiple control input model of Eq. 14.56 to a single-input model. Obviously, the steering proportion of an unsteered axle can be zero, allowing the special case of only the front axle steered (or only the first and last steered). Equations 14.59, 14.60, and 14.61 are inserted into Eqs 14.57 and 14.58.

$$0 = -\left(\frac{C_a}{u}\right)v - \left(\frac{C_b}{u} + mu - \frac{R_a m_s h u}{K_\emptyset}\right)r + \Delta_a \delta_1, \quad (14.62)$$

$$0 = -\left(\frac{C_b}{u}\right)v - \left(\frac{C_c}{u} - \frac{R_b m_s h u}{K_\emptyset}\right)r + \Delta_b \delta_1. \quad (14.63)$$

Through a series of algebraic steps Eqs 14.62 and 14.63 can be combined through elimination of the lateral velocity v . The result can then be used to form an expression for the ratio of the steady-state yaw rate to steering input.

$$\frac{r}{\delta_1} = \frac{u}{\frac{C_b^2 - C_a C_c}{(\Delta_a C_b - \Delta_b C_a)} + \frac{m \left(C_b + \frac{m_s h}{m K_\emptyset} (C_a R_b - C_b R_a) \right)}{(\Delta_a C_b - \Delta_b C_a)} u^2}. \quad (14.64)$$

As discussed in the literature, Eq. 14.64 is of the form of the two-axle steady-state yaw rate gain, and equivalent wheelbase and understeer can be identified, such that,

$$l_n = \frac{C_b^2 - C_a C_c}{(\Delta_a C_b - \Delta_b C_a)}, \quad (14.65)$$

and

$$K_n \frac{m \left(C_b + \frac{m_s h}{m K_\emptyset} (C_a R_b - C_b R_a) \right)}{(\Delta_a C_b - \Delta_b C_a)}. \quad (14.66)$$

Equations 14.65 and 14.66 describe the equivalent wheelbase and understeer of a multiaxle vehicle with roll, where any of the arbitrary number of axles is steerable with a fixed ratio of the front.

The simplicity of these equations is striking when one considers what they would look like when the vehicle states and parameters embedded in the nomenclature are multiplied out (particularly as products of those terms are expanded.). Richard Feynman's emphasis on notation is justified.

14.6 Summary

The bicycle model familiar for two-axle vehicle application and extended to three-axle vehicle application has been generalized to include an arbitrary number of axles, any of them potentially steerable. The useful vehicle characteristics of equivalent wheelbase and understeer are found to be readily generalizable and useful in describing steady state and transient behaviour of primary steered multiaxle vehicles and special cases of vehicles steering multiple axles. With new conventions slightly different from typical for the two-axle case, the n -axle model is significantly simplified, can include arbitrary axles steering proportionally to the front axle, and can provide expressions for equivalent wheelbase and understeer [5,9].

The two-axle roll mode dynamics developed by Ellis with Metz's nomenclature have been integrated into the multiaxle yaw-plane model that allows arbitrary steering of any axle. As such this is the most complete analytical yaw-plane model developed, incorporating the suspension effects on handling through the roll mode with a complex multiaxle vehicle, with any axle possibly steering.

A nomenclature, similar to the previous multiaxle yaw plane vehicle model, is used to compactly describe equivalent wheelbase and understeer of a rolling multiaxle vehicle with any axle steering.

Assumptions were made to allow a steady-state solution of this complex model. If a further assumption is made that all axles steer proportionally to the primary steering input from the driver, yaw rate can be expressed as a dynamic function of primary steering input. In this case, it is possible to speak of an equivalent wheelbase and understeer, as previously considered in the multiaxle vehicle model. It has been shown previously that these two handling parameters completely characterize steady-state vehicle response and are important in predicting transient vehicle response.

As the theoretical development of this work draws to a close it is worth taking a step back and recognizing Richard Feynman's opening quote. Without changes in nomenclature and convention, as articulated by Feynman and Kuhn, the wonderful simplicity of the closing equations of this chapter would not be possible.

References

- [1] Wong, J.Y., *Theory of Ground Vehicles*, Wiley, New York, 1978.
- [2] Gillespie, Thomas D., *Fundamentals of Vehicle Dynamics*, Society of Automotive Engineers, 1992.
- [3] Milliken, William F., and Douglas L. Milliken, *Race Car Vehicle Dynamics*, Society of Automotive Engineers, 1995.
- [4] Ellis, John R., *Vehicle Dynamics*, Business Books, London, 1969.
- [5] Williams, D.E., “Generalized Multi-Axle Vehicle Handling,” *Vehicle System Dynamics, Vehicle System Dynamics*, DOI:[10.1080/00423114.2011.577225](https://doi.org/10.1080/00423114.2011.577225).
- [6] Williams, Daniel E., “On the Equivalent Wheelbase of a Three-Axle Vehicle,” *Vehicle System Dynamics*, DOI:[10.1080/00423114.2010.530670](https://doi.org/10.1080/00423114.2010.530670).
- [7] Bayar, Kerem and Y. Samim Unlusoy, “Steering Strategies for Multi-Axle Vehicles,” *International Journal of Heavy Vehicle Systems*, Volume 15, No. 2–4 (2008), pp. 208–236.
- [8] Ding, Jinquan and Konghui Guo, “Development of a generalised equivalent estimation approach for multi-axle vehicle handling dynamics,” *Vehicle System Dynamics*, 54, No. 1, 2016.
- [9] Williams, D.E., *Multi-Axle Vehicle Dynamics*, SP-2337, Society of Automotive Engineers, 2012.
- [10] Williams, D.E., Multi-Axle Vehicles with Roll, *International Journal of Heavy Vehicle Systems*, IJHVS-176757, 26, No. 3/4, 2019. DOI:[10.1504/IJHVS.2019.10018564](https://doi.org/10.1504/IJHVS.2019.10018564).

Automated Vehicle Architecture from Vehicle Dynamics

“

Theories thus become instruments,
not answers to enigmas,
in which we can rest.

—Henry James

”

15.1 Introduction

This book contains two major sections. The first section on ride was closed with a real-world application of the presented concepts to active suspension. This second section focuses on handling, and the present chapter serves the same purpose of providing another actual practical application of concepts presented in this second section on handling as applied to autonomous vehicle design.

Automated—or driverless—vehicles will produce a quantum change in vehicle dynamics applications. Some might initially suppose that removing the driver from the vehicle will minimize the need for vehicle dynamic analysis as so much of our past effort has been to design vehicles that are subjectively pleasant for humans to control. The future could reveal the opposite.

Something approaching 20% of our driving population experiences some degree of motion sickness when they are not driving. Vehicle dynamics can address this through the computer controlled subsystems controlling ride and handling. Automated vehicles can be more fuel efficient on average than their human controlled counterparts, making better use of preview information regarding routes, grades, and traffic status. Automated vehicles can be safer with the autonomy continually updating a “minimum risk maneuver” that the vehicle will execute in the event of an emergency. Just as our modern computational power can execute more detailed chess scenarios farther into the

future and faster than humans, the autonomous vehicle controller can provide a better solution in the presence of a hazard [1]. A truly minimum risk scenario must accommodate the vehicle dynamics of the “ego” vehicle, as well as other potentially interacting vehicles.

Most accidents involve some types of human error, and autonomous vehicles hope to dramatically improve highway safety by eliminating this cause. For safe autonomous vehicle operation, the various electronically controlled chassis systems must be as reliable as the driver controlled mechanical systems they replace. The conventional hydromechanical steering system is quite reliable; in fact, more reliable than possible with current state of the art electronic systems that have more discrete components with more failure modes. Therefore, functional safety can be achieved through some form of redundancy. Current state-of-the-art steering assistance is computer controlled. It is safe because it is an “assistance” system. As long as a failure is benign, it is acceptable for the control system to gracefully shut itself off and the mechanical connection remains between the driver and the steered road wheel, albeit with a suboptimal steering feel.

Moderately autonomous vehicles (SAE L3) require a certain amount of time for a driver to reattach to the vehicle and its real-time operating environment upon any failure in the primary control systems. Such a failure could occur in the primary steering system, in which case a redundant steering system would have to provide means to directionally control the vehicle while the driver is reattaching to the driving task. In the event of failure in a primary control system in a moderately autonomous vehicle described in [Figure 14.1](#), such as lanekeeping, redundant control means could be required for the vehicle to continue autonomous operation until the driver could assume full responsibility. At the highest level of vehicle automation, the vehicle must react safely to a primary system failure without driver intervention for an even longer period of time in more complex and diverse operating environments. Steer-by-wire requires similar redundancy in the event of a failure in the primary steering control system.

Redundancy can be simply provided by duplicate sensors and actuators. This is an expensive and space consuming solution that adds no value to normal vehicle functionality. A more clever solution is to find means of redundancy that add value to everyday functionality of the vehicle. This chapter will suggest redundancy can be provided by steering the rear axle of a three-axle vehicle for both steer-by-wire and autonomy.

This chapter then uses previously derived vehicle dynamic models to suggest a novel three-axle vehicle configuration that reduces tire wear, improves maneuverability, increases payload capacity, and allows redundancy in lane-keeping for a failed primary axle steering system. The rear axle control strategy and the determination of improved functionality are direct applications of the

previously derived vehicle dynamic theory. The specific vehicle modifications and the improvements in functionality are particularly relevant to the three-axle commercial vehicle.

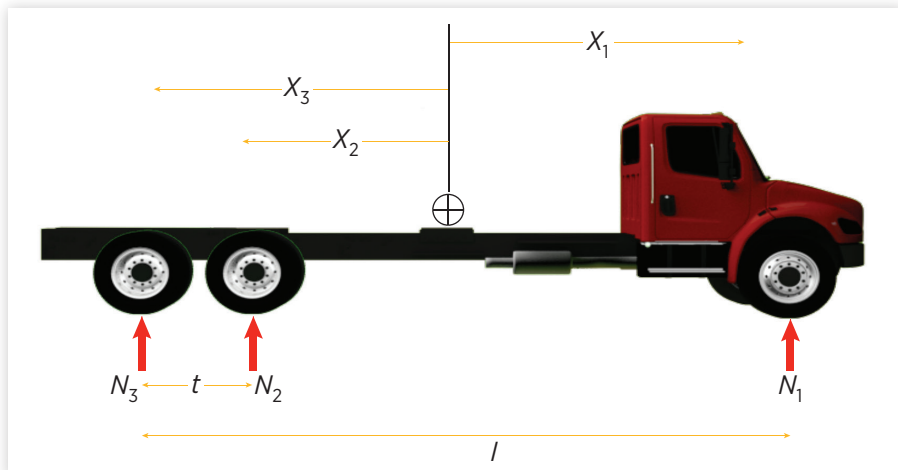
Rear axle steering in passenger cars can be used as redundancy for failure in the front axle steering system, but there are particular advantages for considering such a solution for multiaxle vehicles. The mechanical system could perhaps be less complex when steering the rear axle of a multiaxle vehicle. As seen in [Chapter 11](#), steering the rear axle of a passenger car can improve high-speed lanekeeping and low-speed maneuverability, but will not improve tire wear and longer wheelbase vehicles are more in need of maneuverability improvement. Furthermore, passenger cars will not value the improvement in payload capacity that different vehicle architectures allow. Therefore, while such a system is indeed feasible for passenger cars, the value proposition of using the rear axle for steering redundancy is perhaps more compelling for three-axle vehicles. This example could demonstrate the potential for significant changes in vehicle architecture relative to current vehicles. Many of the trade-offs, constraints, and compromises that to a large measure determine conventional vehicle architecture will change.

15.2 Properties of a Typical Three-Axle Commercial Vehicle

Commercial vehicles commonly have a three-axle configuration. The first axle steers the vehicle, and most commonly the second and third axles propel the vehicle, although occasionally only one of the rear axles is driven. Most commonly, the second and third axles are not steered. To minimize tire wear, the unsteered rear axles are usually placed as close as possible to each other as constrained by the rear suspension.

A vehicle with two nonsteering axles at the rear is kinematically over-determined, and the effective wheelbase of the three-axle vehicle is increased as seen in [Chapter 13](#). The increased effective wheelbase causes a decrease in maneuverability, as the turning radius for a given steering input is reduced. Therefore at the maximum steering input, the turning radius is larger than it would be for a two-axle vehicle that is not overdetermined [2]. As evident in [Figure 15.2](#), when the vehicle is yawing a moment is created by the nonsteered second and third axles that must be overcome by the primary steering front axle.

According to FMCSA regulation §658.17 the maximum amount of weight w in pounds carried by a combination of n axles separated by distance l feet can be calculated. Although the specific example used is from the United States, many governments adhere to the general principle that the more massive a vehicle the longer it needs to be.

FIGURE 15.1 A conventional three-axle truck.

Reprinted with permission from © Inderscience Enterprises Limited (UK).

FIGURE 15.2 Overdetermined three-axle vehicle in a turn.

Reprinted with permission from © Inderscience Enterprises Limited (UK).

$$w = 500 \left(\frac{\ell n}{n-1} + 12n + 36 \right) \quad (15.1)$$

Close coupled tandem rear axles are allowed to exceed the weight limit calculated in Eq. 15.1 by special exception, for a total allowable weight on the rear axle combination of 15,400 kg (34,000 lbs). A single axle at the front can support 9100 kg (20,000 lbs), so that the maximum amount of weight possible on such a conventional three-axle vehicle configuration shown in [Figure 15.1](#) is 24,500 kg (54,000 lbs) given sufficient length. Using Eq. 15.1, this overall length between the first and third axles is 7.3 m (24 ft).

Equation 13.9 calculated the effective wheelbase of a three-axle vehicle. It can be simplified significantly if all axles have the same cornering coefficient, $C_1 = C_2 = C_3$ and used to determine the effective wheelbase of such an idealized vehicle. This ends up being a good assumption, as the cornering coefficient of a commercial vehicle tire tends to be very load dependent, and axle loads reasonably close.

$$l_3 = \frac{2(l^2 + t^2 - lt)}{2l - t} \quad (15.2)$$

Using the distance between the first and third axles $l = 7.3$ m (24 ft) calculated using Eq. 15.1, and a tandem spread $t = 1.2$ m (4 ft), the equivalent wheelbase of the conventional three-axle vehicle shown in [Figure 15.1](#) is calculated using Eq. 15.2 to be 6.9 m (22.5 ft). Note that this is 0.15 m (0.5 ft) farther back than a simple assumption that the tandem combination yields an effective wheelbase midway between them.

The key feature of the conventional three-axle vehicle is the close coupled tandem rear axles. Weight regulations allow it to carry more weight than would be expected from the bridge formula of Eq. 15.1. This allows the vehicle to carry a large amount of weight while somewhat mitigating the maneuverability and tire wear disadvantages of the rear tandem combination. Even with the conventional close coupled tandem axle exception to the bridge formula, tire wear, and maneuverability are compromised with payload capacity. Next, the effect of steering the third axle will be examined.

15.3 Control of Rear Axle

Using the state matrices defined in Eq. 13.1, Laplace domain state variable responses as functions of the control inputs are written in Eqs 13.53–13.56. These equations are the Laplace domain expressions of the vehicle state variables' responses to steering control inputs at the front and rear axles.

The main purpose of this work is to determine a rear axle control input that provides similar vehicle dynamic behavior as the driver would expect if steering the front axle. Such a system would benefit a highly autonomous vehicle, so that the autonomous “virtual” driver would similarly rely on the same directional dynamics in a fail-operational mode. Throughout this work, the “driver” can be human or virtual.

As mentioned in the introduction, if this can be achieved rear axle steering can be used as a means of redundancy to provide robustness in the event of a failure in the front axle steering system. Such a control strategy could be useful in a moderately autonomous (SAE L3) commercial vehicle. Upon such a failure of the primary front axle steering system, the driver would assume control of a vehicle steered at the rear. It is assumed that the three-axle commercial vehicle is operating on the highway, in a lanekeeping mode, so that the small angle approximations used are valid. A more highly automated (SAE L4+) system would rely even more heavily on the redundant control means to put the vehicle in a safe state.

The goal is to construct a method to steer the rear axle so that the vehicle dynamics are as close as possible the vehicle dynamics when the front axle only is steered, assuming this is the normal operating mode. We assume a steering command δ_c such that it is the equivalent of the driver’s intention as seen by the front tire steering displacement. (It should be apparent to the reader that a more complicated “normal driving mode” could be used, and the method of determining the equivalent rear axle only control can still be applied.)

$$\delta_l = \delta_c. \quad (15.3)$$

So, when the rear is unsteered, and the front is steered, Eq. 15.3 is inserted in to Eqs 13.53–13.56 and $\delta_3(s) = 0$, the state variable transfer functions can be written that report vehicle dynamic behavior of a normally front axle steered vehicle in response to a driver control input $\delta_c(s)$.

$$\frac{r(s)}{\delta_c(s)} = \frac{C_1 u (s x_1 m u + x_1 C_a - C_b)}{s^2 m u^2 I_z + s u (m C_c + I_z C_a) + C_a C_c - C_b^2 - C_b m u^2}, \quad (15.4)$$

$$\frac{\varphi(s)}{\delta_c(s)} = \frac{C_1 u (s x_1 m u + x_1 C_a - C_b)}{s (s^2 m u^2 I_z + s u (m C_c + I_z C_a) + C_a C_c - C_b^2 - C_b m u^2)}, \quad (15.5)$$

$$\frac{\beta(s)}{\delta_c(s)} = \frac{C_1 (s I_z u + C_c - x_1 (C_b + m u^2))}{s^2 m u^2 I_z + s u (m C_c + I_z C_a) + C_a C_c - C_b^2 - C_b m u^2}, \quad (15.6)$$

$$\frac{Y(s)}{\delta_c(s)} = \frac{C_1 u (s^2 I_z u + s(C_c - x_1 C_b) + x_1 u C_a - u C_b)}{s^2 (s^2 m u^2 I_z + s u (m C_c + I_z C_a) + C_a C_c - C_b^2 - C_b m u^2)}. \quad (15.7)$$

Equations 15.4–15.7 are the state variable responses of the normally front steered three-axle vehicle. The only difference between Eqs 15.4 and 15.7 and the equations derived in [Chapter 13](#) is calling the control input $\delta_c(s)$ rather than $\delta_l(s)$.

Similarly, when the rear alone is steered and the front unsteered transfer functions can be written relating the vehicle state behavior to the third axle steering input again using Eqs 15.4–15.7.

$$\frac{r(s)}{\delta_3(s)} = \frac{C_3 u (s x_3 m u + x_3 C_a - C_b)}{s^2 m u^2 I_z + s u (m C_c + I_z C_a) + C_a C_c - C_b^2 - C_b m u^2}, \quad (15.8)$$

$$\frac{\varphi(s)}{\delta_3(s)} = \frac{C_3 u (s x_3 m u + x_3 C_a - C_b)}{s (s^2 m u^2 I_z + s u (m C_c + I_z C_a) + C_a C_c - C_b^2 - C_b m u^2)}, \quad (15.9)$$

$$\frac{\beta(s)}{\delta_3(s)} = \frac{C_3 (s I_z u + C_c - x_3 (C_b + m u^2))}{s^2 m u^2 I_z + s u (m C_c + I_z C_a) + C_a C_c - C_b^2 - C_b m u^2}, \quad (15.10)$$

$$\frac{Y(s)}{\delta_3(s)} = \frac{C_3 u (s^2 I_z u + s(C_c - x_3 C_b) + x_3 u C_a - u C_b)}{s^2 (s^2 m u^2 I_z + s u (m C_c + I_z C_a) + C_a C_c - C_b^2 - C_b m u^2)}. \quad (15.11)$$

15.4 Rear Axle Control for Yaw Rate Equivalence

The task at hand is to find the rear axle control input $\delta_3(s)$ that results in a vehicle dynamic response as similar as possible to what would have occurred had the driver been steering the front in normal operation. Because we have previously seen that the fundamental response of the steering input is a yaw rate, yaw rate response is used to determine the appropriate processing of the front steering input δ_l to form a steering input δ_3 equivalent in the sense of producing the same yaw rate response. The vehicle yaw rate response to a third axle steering input is described by Eq. 15.8. The goal is to find a transfer function relating the third axle steering input to the driver control input that, when multiplied by Eq. 15.8 results in the yaw rate response of the vehicle that the driver would expect if steering the front axle of Eq. 15.4.

$$\left(\frac{r(s)}{\delta_3(s)} \right) \left(\frac{\delta_3(s)}{\delta_c(s)} \right) = \frac{r(s)}{\delta_c(s)}. \quad (15.12)$$

Equation 15.12 can be explicitly solved for the desired transfer function relating the third axle control input to the driver control input.

$$\frac{\delta_3(s)}{\delta_c(s)} = \frac{r(s)}{\delta_c(s)} \left(\frac{r(s)}{\delta_3(s)} \right)^{-1}. \quad (15.13)$$

The desired transfer function of (Eq. 15.13) is seen to be a ratio of previously derived transfer functions Eqs 15.4 and 15.8. This ratio can be expressed quite simply as both Eqs 15.4 and 15.8 conveniently have the same denominator.

$$\frac{\delta_3(s)}{\delta_c(s)} = \frac{C_1 x_1 \left(smu + C_a - \frac{C_b}{x_1} \right)}{C_3 x_3 \left(smu + C_a - \frac{C_b}{x_3} \right)}. \quad (15.14)$$

Recall that $x_1 > 0$ and $x_3 < 0$ and C_b can be either positive or negative. Depending upon vehicle parameters, the relationship can be a first-order lead-lag filter, with possibly a right half plane pole or zero. For most reasonable parameters the relationship is negative, signifying that positive driver intent is achieved with a negative steering input at the rear.

$$\delta_3(s) = \frac{C_1 x_1 \left(smu + C_a - \frac{C_b}{x_1} \right)}{C_3 x_3 \left(smu + C_a - \frac{C_b}{x_3} \right)} \delta_c(s). \quad (15.15)$$

If the rear steer angle is formed by the driver steering command filtered as in Eq. 15.15, the yaw rate will be exactly what the driver would experience if directly steering the primary front axle. If the vehicle were neutrally steered, if the load were balanced so that $x_1 = -x_3$, and if tires on the front and rear axles had the same combined cornering force coefficients, the rear axle would be steered opposite of what the front would have been, which makes intuitive sense.

Because the yaw rate is identical, its integral, yaw angle, is likewise the same. A third state variable, drift angle is a bit different, however.

$$\beta_r(s) = \left(\frac{C_1 \frac{x_1}{x_3} (sI_z u + C_c - x_3(C_b + mu^2)) \left(smu + C_a - \frac{C_b}{x_1} \right)}{s^2 mu^2 I_z + su(mC_c + I_z C_a) + C_a C_c - C_b^2 - C_b mu^2} \right) \delta_c(s). \quad (15.16)$$

Because Eq. 15.16 is different from the target relationship of drift angle to control input of a normally steered front axle shown in Eq. 15.6, β_r is defined as the drift angle in response to a rear axle steering control input filtered by Eq. 15.15.

Ideally we would like the ratio of the drift angle when steered by the rear to the drift angle when normally steered by the front to be unity for vehicle dynamic equivalence.

$$\frac{\beta_r(s)}{\beta(s)} = \left(\frac{\frac{x_1}{x_3} (sI_z u + C_c - x_3(C_b + mu^2)) \left(smu + C_a - \frac{C_b}{x_1} \right)}{(sI_z u + C_c - x_1(C_b + mu^2)) \left(smu + C_a - \frac{C_b}{x_3} \right)} \right). \quad (15.17)$$

It is interesting to contemplate the ratio of drift angles for the normally steered and rear axle steered vehicle expressed in Eq. 15.17 when the vehicle neutrally steers ($C_b = 0$) and the center of mass is exactly in between the front and rear axles ($x_1 = -x_3$); Eq. 15.17 is significantly simplified.

$$\frac{\beta_r(s)}{\beta(s)} = \left(\frac{- (sI_z u + C_c + x_1 mu^2)}{(sI_z u + C_c - x_1 mu^2)} \right). \quad (15.18)$$

In a high-speed lanekeeping mode, Eq. 15.18 tends toward unity signifying that the drift angle response of the rear steered vehicle approaches the conventionally steered vehicle as speed increases. So while the drift angle responses are not identical, they are more consistent at higher speeds for the ideal balanced neutrally steering vehicle.

Similarly, using Eqs 15.7 and 15.11, it is evident lateral lane position Y_r (in the redundant mode) is a function of control input.

$$Y_r(s) = \left(\frac{C_3 u \left(s^2 I_z u + s(C_c - x_3 C_b) + x_3 u C_a - u C_b \right)}{s^2 \left(s^2 m u^2 I_z + su \left(m C_c + I_z C_a \right) + C_a C_c - C_b^2 - C_b m u^2 \right)} \right) \\ \left(\frac{C_1 x_1 \left(s m u + C_a - \frac{C_b}{x_1} \right)}{C_3 x_3 \left(s m u + C_a - \frac{C_b}{x_3} \right)} \right) \delta_c(s). \quad (15.19)$$

As above, we can form the ratio of lateral lane position when steered at the rear compared to steered at the front.

$$\frac{Y_r(s)}{Y(s)} = \left(\frac{\frac{x_1}{x_3} \left(s^2 I_z u + s(C_c - x_3 C_b) + x_3 u C_a - u C_b \right) \left(s m u + C_a - \frac{C_b}{x_1} \right)}{\left(s^2 I_z u + s(C_c - x_1 C_b) + x_1 u C_a - u C_b \right) \left(s m u + C_a - \frac{C_b}{x_3} \right)} \right). \quad (15.20)$$

Equation 15.20 likewise is simplified when the vehicle is neutral steering and the center of gravity is between the front and rear wheels.

$$\frac{Y_r(s)}{Y(s)} = \left(\frac{-\left(s^2 I_z u + s(C_c) - x_1 u C_a \right)}{\left(s^2 I_z u + s(C_c) + x_1 u C_a \right)} \right). \quad (15.21)$$

At high vehicle speeds and low-frequency steering inputs, Eq. 15.21 tends to unity, denoting consistency between the lateral position responses of the rear steered vehicle and conventionally steered vehicle.

To summarize, if the rear axle steering input is filtered steering command as defined by Eq. 15.15, the yaw rate response and yaw angle responses are equivalent for the conventionally steered and rear axle steered vehicles. While not identical, the drift angle responses and lateral lane position responses for a balanced and neutrally steering vehicle tend to converge to the expected response for high speed lanekeeping.

A rear axle steering control that assures the vehicle will have an equivalent yaw rate response to a similar vehicle conventionally steered at the front axle has been derived. The simplified control results in an equivalent yaw rate when the load is balanced and the vehicle neutrally steers. Both the simplified control and the equivalent yaw rate control result in drift angle responses that approach the conventionally steered vehicle for high speeds and slow steering inputs. The high degree of equivalence between vehicle dynamic responses of the front and rear steered vehicles is because of all responses having the same characteristic polynomial in the denominator of the various state variable responses.

Differences in the state variable responses are because of zeros of the respective transfer functions, not poles. This is an interesting validation of the quote from Hoagg and Bernstein of [Chapter 11](#). Poles related to the underlying vehicle dynamics cancel, and the difference is because of the zeroes that are a function of the different actuator locations.

Therefore, it seems plausible that steering the rear axle can maintain a lane as the driver reattaches or cautiously bring the vehicle safely to the shoulder in the event of an incapacitated driver. The rear axle steering control of Eq. 15.15 can be modified. It can be made simpler, and perhaps more significantly it can be modified to allow caster steering of the primary steered axle upon failure [3].

15.5 Vehicle Results

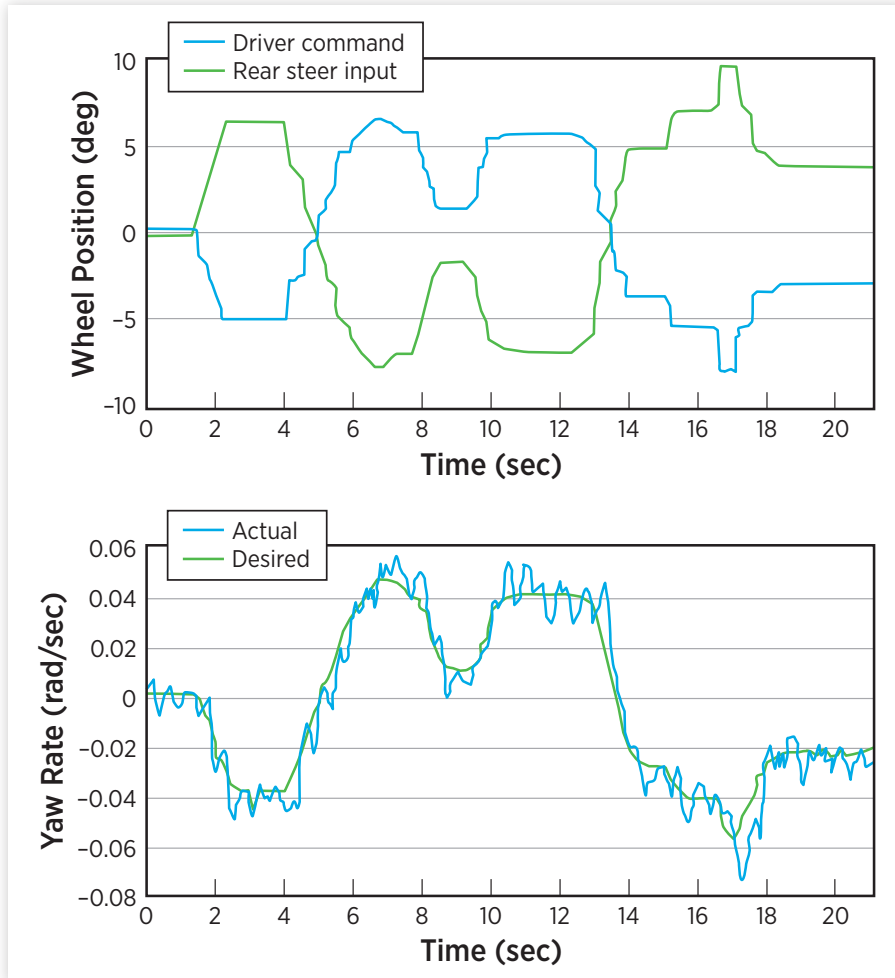
The proposed rear axle steer control of Eq. 15.15 was implemented by Amine Nhila on the actual vehicle shown in [Figure 15.3](#) [4]. The three-axle yaw plane model presented in this work was used to simulate the vehicle, and then parameters were optimized to correlate with actual vehicle performance.

This vehicle had a steer-by-wire system on both the front and rear axle that could be independently commanded. The front axle was commanded to a zero set point, locking it in a straight ahead position and the rear axle was steered according to Eq. 15.15. As shown in [Figure 15.4](#), in a double lane change steering maneuver, the control law of Eq. 15.15 provides the expected equivalent yaw rate result in an actual vehicle.

FIGURE 15.3 Test vehicle.



FIGURE 15.4 Steering command and yaw rate for equivalent rear-axle steering in a double-lane change maneuver.



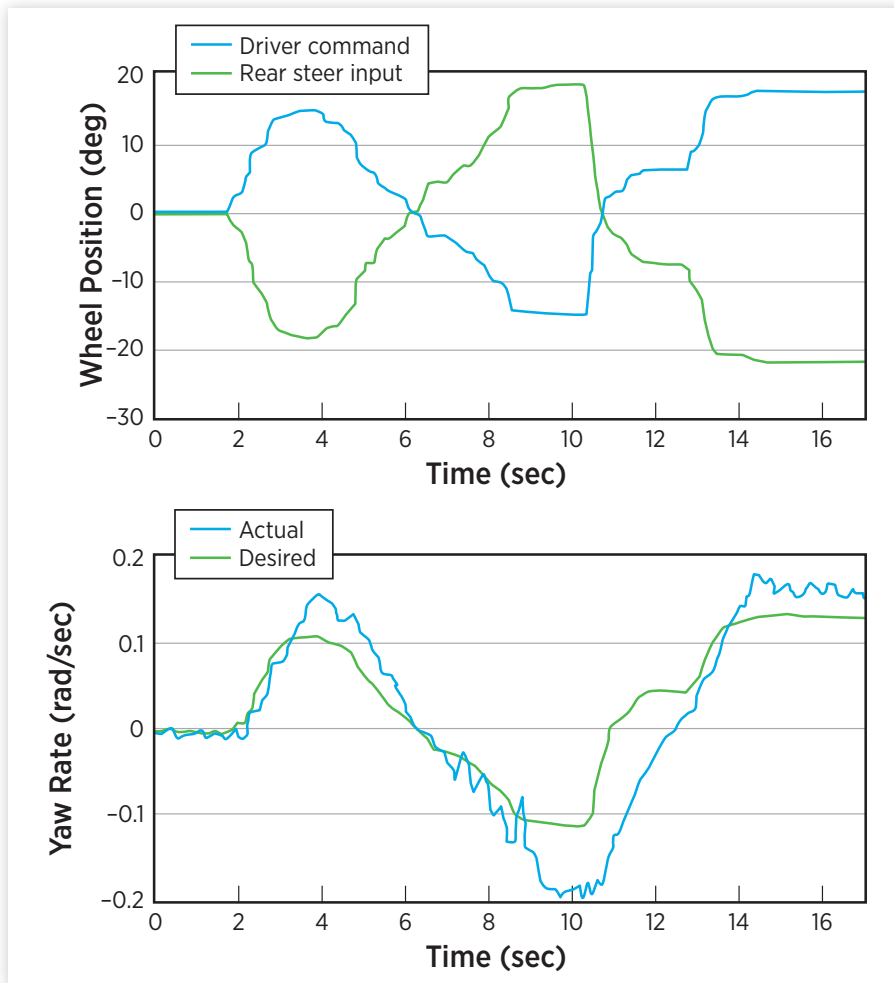
Reprinted with permission from © SAE International.

Based on the axle locations, vehicle loading, and other vehicle dynamic parameters the rear axle steers with slightly more amplitude to create an equivalent yaw rate. The measured vehicle yaw rate as a result of the rear axle steering generally tracks the desired yaw rate so that the driver, human or virtual, will be satisfied with the vehicle response to a steering command when the vehicle is in its failed-operational mode.

This process was repeated for larger inputs as shown in [Figure 15.5](#), with less favorable results evident in the yaw rate.

Before the rear wheel amplitude exceeds 10°, there is a significant deviation in the measured yaw rate response from the desired reference yaw rate. This

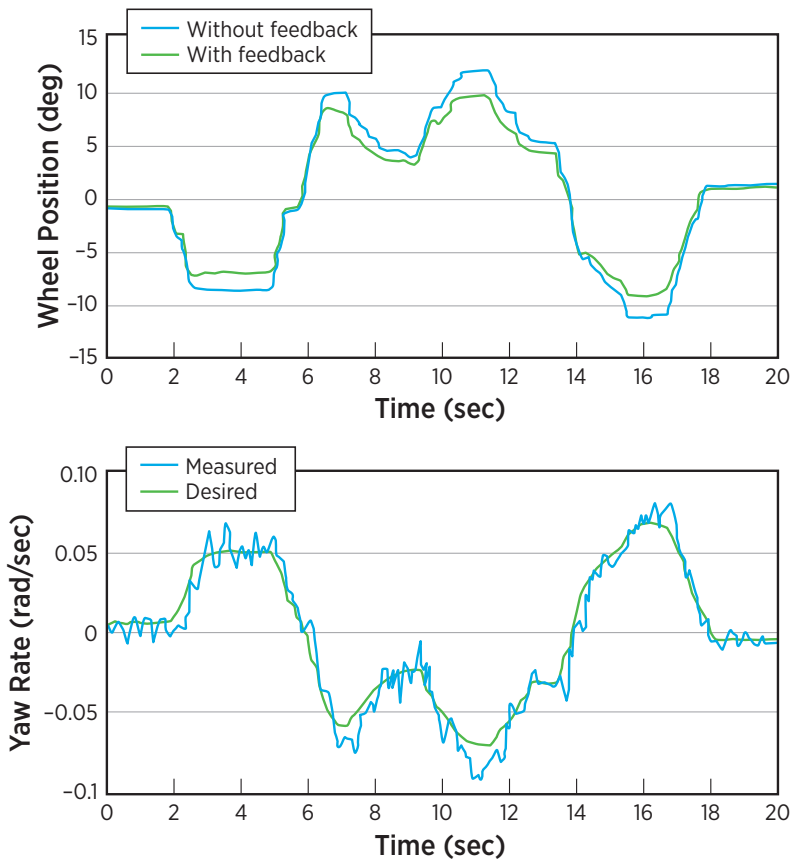
FIGURE 15.5 Steering command and yaw rate for equivalent rear-axle steering in a large amplitude maneuver.



Reprinted with permission from © SAE International.

deviation is because the tire cornering stiffness becomes nonlinear at higher attack angles.

This situation can be remedied using feedback control of a state variable—in this case, yaw rate. Equation 15.15 can be considered “open loop” in that it produces an actuator command based solely on the steering command and not any knowledge of the state variables affected by the actuation command. In this case, the actuation is desired to directly affect yaw rate. Equation 15.15 can be modified with a correction term, comparing the desired yaw rate with what is measured.

FIGURE 15.6 Large amplitude steering command with combined control.

Reprinted with permission from © SAE International.

$$\delta_3(s) = \frac{C_1 x_1 \left(s\mu u + C_a - \frac{C_b}{x_1} \right)}{C_3 x_3 \left(s\mu u + C_a - \frac{C_b}{x_3} \right)} \delta_c(s) + K_r (r_{des} - r). \quad (15.22)$$

The desired yaw rate r_{des} can be found from Eq. 13.13 knowing the three axle terms defined in Eqs 13.7 and 13.8. Equation 15.22 contains an open-loop part from Eq. 15.15 and a new closed-loop part. The open-loop part provides the ideal response, and the closed-loop part provides a correction to account for parameter deviation from the ideal. Using the closed-loop alone with a proportional error gain as shown would require a yaw rate error for a rear wheel steering actuator, therefore the ideal rear actuator displacement would not be achieved. Ideal rear steering actuator displacement could be more closely achieved by a

higher proportional gain or a more complicated controller, which would both encounter stability issues as the system is known to be nonlinear.

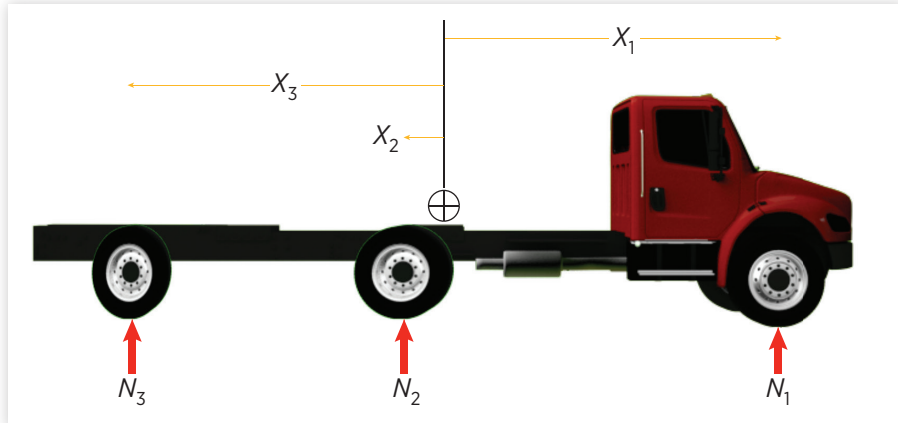
This notion of an ideal feedforward control augmented with a closed loop correction is a practical solution to many problems, and in fact has been used before in this work. In the active suspension chapter, ideal response of the suspension actuators to sprung mass lateral and longitudinal accelerations (feedforward) was augmented with pitch and roll inertial damping (feedback). The combined open-loop (feedforward) and closed-loop (feedback) controller shown in [Figure 15.6](#) is quite effective in improving the large amplitude yaw rate response of the simple open loop control shown in [Figure 15.5](#).

15.6 Proposed Three-Axle Vehicle

It has just been shown that steering the rear axle can provide transparent redundancy. It can also provide increased functionality by allowing a new three-axle vehicle configuration.

Axes are located relative to the center of gravity, and location of the center of gravity can be calculated for an optimally loaded vehicle. To load the rear combination at its maximum of 15,400 kg (34,000 lbs) and the front axle at 9,100 kg (20,000 lbs), the vehicle center of gravity must be roughly 4.3 m (14 ft) behind the front axle and 3 m (10 ft) front of the rear. The cornering coefficient of commercial vehicle tires tends to be proportional to load resulting in two relevant effects for this analysis. First, the effect of dual tires at the rear is largely mitigated, as the load is dispersed between the dual tires, but the cornering stiffnesses of all the tires add to provide axle stiffness. Second, assuming the same tires are on all the axles, cornering stiffness is dependent upon load. Thus, the front axle will have a higher cornering coefficient by the ratio of the axle weights. When the effect of axle locations and axle weights are considered for a neutrally steering vehicle in Eq. 15.15, the rear will need to be steered 60% more than the front for an equivalent vehicle dynamic result. In a lanekeeping driving mode, when inputs are small this is not problem, but if the vehicle is to be maneuvered at low speed or in complex duty cycles by steering the rear axle only and fixing the front, required rear wheel steering inputs may be unacceptably large to package.

Steering the rear axle of the conventionally configured three-axle vehicle shown in [Figure 15.1](#) has been seen to improve maneuverability and tire wear, and be able to directionally control the vehicle with relatively large rear steering inputs in the event of a failure in the primary axle steering system. With a change in vehicle configuration shown in [Figure 15.7](#) vehicle performance can be further improved. The nonsteered second axle is moved forward, equidistant from the first and third steered axles, and near the anticipated center of gravity of the loaded vehicle.

FIGURE 15.7 Proposed three-axle truck.

Reprinted with permission from © Inderscience Enterprises Limited (UK).

From Eq. 15.1, 27,200 kg (60,000 lbs) can be carried on three equally distant axles spanning 9.8 m (32 ft) between the first and third axles. By steering the third axle, from Equation 13.46 it is evident that the equivalent wheelbase is 4.9 m (16 ft). Therefore, the proposed vehicle configuration can potentially haul 2,700 kg (6,000 lbs) more payload with a reduction in equivalent wheelbase from 6.9 m (22.5 ft) to 4.9 m (16 ft).

Tire wear is expected to have a similar improvement to that of the conventional vehicle when the rear axle is steered. At low speeds, the rear will be steered at its kinematically correct position, eliminating the overdetermined axles fighting each other as the vehicle yaws.

Just as with the conventional three-axle vehicle, the proposed vehicle can be directionally controlled by fixing the front axle at its nominal straight ahead position and steering the rear. The steering input at the rear of the proposed vehicle configuration that results in an equivalent yaw rate response to a conventional steering input at the front is given by Eq. 15.15 when $x_1 = -x_3$ and x_2 is zero consistent with the vehicle shown in [Figure 15.7](#) [4]:

$$\delta_3(s) = -\frac{C_1(smu + C_2 + 2C_3)}{C_3(smu + 2C_1 + C_2)} \delta_c(s). \quad (15.23)$$

Equation 15.23 is a mild first order lead-lag filter. If all axles have the same cornering stiffness, Eq. 15.23 is greatly simplified.

$$\delta_3(s) = -\delta_c(s). \quad (15.24)$$

Equation 15.24 is valid for transient and steady state conditions. This is a very convenient result, stating that for the vehicle shown in [Figure 15.7](#), there is yaw rate equivalence between the vehicle steered at the front with the rear axle fixed, and the vehicle counter-steered at the rear with the front axle fixed. Most relevant, for this broad assumption, steering amplitudes are equal. Therefore, the front and rear axle can be similarly packaged with a similar space envelope allowing similar steering displacements.

The proposed vehicle is highly idealized. It is unlikely that all three axles can be optimally loaded. Some loads are more amenable to axle optimization than others. This situation is not unlike a conventional truck that many times has difficulty fully loading the front axle. It is quite possible that the effect of actual axle loadings on tire cornering stiffness will require the more complex Eq. 15.14 rather than the simplified Eq. 15.24. Given an ideally configurable load, the proposed three-axle vehicle can increase its payload. The improvement in maneuvering is more practically realized. The more the second and third axles are spread apart, the greater the maneuverability improvement possible by steering the third axle. It is a very convenient coincidence that when the second and third axles are spread out, in an effort to somewhat improve payload or dramatically improve maneuverability, the ability to use the steerable third axle as a means of control redundancy for a failed primary steered front axle is enhanced. This is the main message of this chapter: when the rear axle is steered, the tandem axles can be spread apart to improve maneuverability without sacrificing tire wear—and improving the ability of the steerable third axle to serve as redundancy for the front steering axle. Similar advantages can be calculated for vehicles with more than three axles.

Autonomous vehicles could look much different from our current vehicles that are built for human control as human control-related constraints are relaxed, and computer-controlled chassis systems are more easily networked. Each new system shares sensor information and perhaps actuation authority with other systems for new synergies. These new vehicle architectures will be guided and constrained by vehicle dynamics.

15.7 Summary

Highly autonomous vehicles and vehicles with advanced electronically controlled steering such as steer-by-wire require redundancy in the steering system for acceptable functional safety. Such redundancy can be simply achieved by parallel sensors and actuators. A more desirable solution is to use systems that enhance vehicle functionality in normal operation to directionally control the vehicle in the event of a primary steering system failure.

It has been shown that it is possible to directionally control a three-axle vehicle by steering the rear axle only. Therefore, it is possible to use rear axle steering as a means of redundancy for a failed front axle steering system. On conventional three-axle vehicles rear axle steer increases maneuverability and decreases tire wear. But if the rear axle steering is used for redundancy of primary steering, rear axle displacements will be larger than the conventional front axle displacements to produce the same yaw rate.

It has been seen that by steering only the rear axle, the vehicle produces the yaw rate expected by the driver for low amplitudes. At higher amplitudes the model based open-loop control can be improved by adding a closed loop on yaw rate. Adding a closed-loop term to an open-loop command improves both performance and robustness to parameter variation.

This chapter proposes a change in the conventional three-axle vehicle configuration. The conventional closely coupled second and third axles are spread apart, so that the second axle is at the midpoint of the vehicle. In this case, the load carrying capacity and steering displacements are the same at the front and rear axles, so they could be of the same design. A vehicle of this configuration could carry more payload, with greater maneuverability and with less tire wear than a comparable conventional vehicle, all the while providing steering redundancy. Therefore, the added cost of a redundant steering system for a highly automated vehicle could be at least partially offset by improvements in functionality.

The advantages of rear steering for a three-axle vehicle just described do not entirely apply to passenger cars. Passenger cars receive no tire wear benefit by steering the rear axle. Therefore, using rear axle steer for steering redundancy in a passenger car will provide less improvement in vehicle functionality and cost more.

This chapter demonstrates how the concepts developed in this book are applied to autonomous vehicle design. Much of the original vehicle is developed for a driver. As that constraint is relaxed, other functionality can be enhanced. Whether the autonomous vehicle of the future will look like the three-axle vehicle proposed, or some other architecture, the concepts presented in this book will help to predict its vehicle dynamic behavior. This closing chapter illustrates the possibility that as design constraints of autonomous vehicles differ, they might drive unforeseen changes in vehicle architecture.

References

- [1] Kasparov, Gary, *Deep Thinking*, John Murray, January 1, 2018.
- [2] Williams, D.E., "On the Equivalent Wheelbase of a Three-Axle Vehicle," *Vehicle System Dynamics*, Volume 49, Issue 9, 2011. doi:[10.1080/00423114.2010.530670](https://doi.org/10.1080/00423114.2010.530670).

- [3] Williams, D., and Nhila, A., "Directional Dynamics of Steering the Third Axle," *SAE International Journal of Commercial Vehicles* 8(2):323–331, 2015. doi:[10.4271/2015-01-2747](https://doi.org/10.4271/2015-01-2747).
- [4] Nhila, A., and Williams, D., "Directional Vehicle Control by Steering the Third Axle to Provide Redundancy for Steer-by-Wire Systems and Highly Autonomous Vehicles," Society of Automotive Engineers, CV-02-13-03-0015.

Afterword

To quote Dr. Metz from his foreword, “Control theory is a well-developed field but its application has been largely, though not completely, ignored by practicing vehicle dynamicists.” This probably stems from the fact that developing a vehicle for ride, steering and handling has historically been the task of someone with a mechanical engineering background, while control system design and analysis has been reserved for someone with education in electrical engineering.

This book takes readers by the hand and walks them into the land of dynamic system analysis, where ‘s’ can be frightening at first glance. Here, Dr. Williams rigorously and clearly develops the dynamic system equations in terms of practical design parameters and shows how they can be applied to analysis of steady state and transient vehicle behavior.

Along the way, Dr. Williams introduces convention and nomenclature that are slightly different than established conventions but nonetheless make development and application of the complex equations applicable to a broader array of vehicles. These new conventions and nomenclature also allow for the addition of the roll degree of freedom to the analysis. This is significant, as many previous papers and books have either neglected roll dynamics in handling analysis or lumped it in with ride analysis. Dr. Williams has developed the ‘and’ solution for ride and handling analysis inclusive of roll dynamics.

The capstone examples at the end of the ride and handling sections, respectively, do a great job of showing how the new formulation can be used in practice and give the reader some thought starters for their own application.

This book is a ‘Must Read’ for any engineer or researcher involved in vehicle dynamics, especially those involved in control systems for automated driving (autonomous) vehicles. For an engineer new to the field of vehicle dynamics, this book is a great follow-up to *The Fundamentals of Vehicle Dynamics, Revised Edition* by Thomas Gillespie or equivalent. For a seasoned vehicle dynamics engineer who is well versed in the fundamentals and steady state analysis, this

book is an excellent, non-intimidating and valuable foray into the development and application of control-theoretic models that can expand one's knowledge of the effect of changing parameters on transient vehicle response.

Tim Drotar
Vehicle Dynamicist

Index

A

- Accelerometer, 191
- Accidents
 - driver error, 5
 - human error, 322
- Ackermann relationship, 156, 161, 164
 - ideal relationship, 156, 164
 - three-axle vehicle
 - dynamics, 290
 - of two-axle vehicle, 290
- Ackermann steering, 150–157, 172
 - centrifugal forces, acting on tires, 161
 - conventional steering
 - linkage, with tie-rod, 154
 - error approximation, 156, 157
 - handwheel yaw rate, 164
 - ideal relationship, 156, 164
 - left wheel displacement, 154
 - mechanical trail, 163
 - radius of curvature, 152
 - right wheel displacement, 155
 - single-track
 - average, 160
 - comparison, 153
 - model, 152
 - relationship, 151, 152, 221
 - steered wheel geometry, 150
 - tie rod angle, 155
 - two-axle vehicle kinematic model, 151
 - yaw rate, 161
- Actuator displacements, 130

B

- Actuator dynamics, 124
- Aerodynamic forces, 181
- Ahmadian, Mehdi, 124
- Ahmadian's groundhook, 125
- Aircraft-handling expertise, 4
- Amplitude ratio, 21
- Angular steering, 201
- Angular torsion bar
 - displacement, 106
- Antiroll bars/stabilizer bars, 7, 96
- Aristotle's lead, 49
- Artificial intelligence, 2
- Attack angle convention, 200–204
- Automated vehicle architecture
 - autonomous vehicles, 322
 - driverless vehicle, 321
 - rear axle control, 325–327
 - rear axle steering, 323
 - redundancy, 322
 - three-axle vehicle
 - commercial vehicle, 323–325
 - proposed, 334–337
 - vehicle results, 331–334
 - yaw rate equivalence, 327–331
- Automated vehicles, 321
- Automatic controls, 3
- Axle locations, 162
 - convention, 200
 - vehicle dynamic parameters, 78
- Axes steered, first/last, 295
- Axle stiffnesses, 86, 87
 - generalized, 86, 89
 - individual, 88
 - matrix mapping, 87, 88
- B
- "Bicycle"/yaw-plane vehicle dynamic model, 2, 233
- Block diagram
 - algebra, 28–33
 - basic elements, 29
 - control systems, 30
 - conventional yaw plane, 174, 175
 - displaced mass, effect of, 30
 - double integrator, 29, 32
 - generic properties, 33
 - highest-order derivative, 32
 - Hooke's spring law, 31
 - Laplace domain, 32
 - new conventions, 213
 - Newton's Second Law (NSL), 31
 - pure steering input, 214
 - slip angles, 215
 - stiffness convention, 30
 - suspended mass
 - feedback, 33
 - Hooke's spring law, 31
 - Newton's Second Law (NSL), 31
 - temporary variable, 32
 - transfer functions
 - feedback, 30
 - series combination of, 29
 - vertical discomfort, filter, 136
 - yaw-plane model, 213, 214
- Bode plot, 21–23
- Boeing B17/B29, 3
- Box, George E. P., 39
- Bryan, George, 3

- Bump rubbers, 62
 Burns, Larry, 6
- C**
 Camber effect, experimental car steered, 268
 Centrifugal forces, 149 acting on rolling tire, 162 acting on tires, 161 on vehicle pushes, 167
 Chevrolet Corvair, 5
 Closed-loop stability properties, 123
 Commercial vehicle tires, 285
 Commercial vehicles duty cycles, 301 lateral accelerations of, 284 three-axle application, 301 two-axle passenger cars, 283 payload of, 285
 Control algorithm, 6
 Control theory, 235
 Conventional bicycle model, 170–175
 Conventional damping, quarter-car model, 120
 Conventional steering linkage, with tie-rod, 154 roll steer coefficient, 277
 Conventional three-axle truck, 324
 Conventional three-axle vehicle, 325
 Conventional yaw block diagram of, 174, 175 rate model, 170
 Copernican model, 196
 Cornell Aeronautical Laboratories, 4
 Coupled first-order differential equations, 307
 Cranfield Institute of Technology, 5
 Crashout stops, 62
 Crossover frequency, 254
- D**
 Damper design, second nonlinearity, 61
 Damping digressive, 61 ideal quarter-car model, 49
- inertial, 127
 pitch-plane model, 79, 81
 suspended mass, 19
 transmissibility, 54
 Deflected tandem axles, 286
 Delphi Quadrasteer system, 234
 Derived handling parameters, 298
 Differentiator's magnitude, 24
 Displacement expressions, 289
 Drift angle, 274, 329 angle transfer functions, 215–218 response, 222 steering input, 288
 Driver behavior, 248
 Driver discomfort, 139
 Driver modeling, 235
 Driver-vehicle open-loop crossover model, 242 forming, 242
 Dynamic filtering, 11
- E**
 Eigenfrequency/natural frequency, 47
 Einstein, Albert, 65
 Electric propulsion, 6
 Ellis' expression, 292
 Ellis, R. A., 4, 198, 260
 Ellis' two-axle version, 316
 Equivalent rear-axle steering, steering command/yaw rate, 332, 333
 Equivalent wheelbase, 9
 Euler angle transformation, 8
 Euler's identity, 16
 European production commercial vehicles, 294
- F**
 Feynman, Richard, 303
 Filter dynamics, 136
 First-order coupling, 118
 First-order lag, 25
 FMCSA regulation §658.17, 323
 Ford Explorer, 5
 Fore-and-aft vibrations human tolerance, 76 rocking motion, 65–66
 Front suspension deflection, 77
 Fuel economy/emissions, 6
 Full vehicle optimal control, 139–141
 Fundamentals of Vehicle Dynamics, 198
- G**
 Galileo, 281
 General Motors, 2, 4, 118
 GEP Box, 192
 Gillespie, Tom, 198
 Groundhook damping, 124
- H**
 Handwheel steer angle, 173
 Hard nonlinearity, 137
 Heave acceleration sensitivity, 76
 Heave-mode dynamics, 99
 Heave natural frequencies, 77
 Heave-only model, limitations of, 66
 High-speed open-loop frequency response, 252
 Honda, 234
 Hrovat, Davor, 125
- I**
 Ideal inertial damping open loop, 124
 Ideal rear steering actuator displacement, 334
 Ideal Two-Axle Model, 218–222
 Independent front suspension (IFS), 40 mechanical links, 40 quarter-car, 40
 Inertial damping, 119–126 closed loop, 123 isolation function, 123 open loop, with actuator, 125
 Isolation function amplitude, 122
- J**
 James, Henry, 321
- K**
 Kalman filter, 138
 Karnopp, Dean, 119
 Karnopp's skyhook, 125
 Koppen, Otto, 3
 Kuhn, Thomas, 195
- L**
 Lag transfer function, 27
 Lane position error, 248 projected lateral lane position, open-loop crab-steer transfer function, 251

- Laplace domain, 13
 Laplace transforms, 13, 17, 23, 28, 32, 34, 37, 46, 49, 50, 69, 82
 two-axle front steered vehicle, 217
 of yaw rate equation, 216
 Laplace variables, 18, 19, 24–26, 36, 70
 definition of, 83
 matrix multiplying, 70
 Lateral acceleration, 224
 Lateral lane position, 330
 Lateral motion, translational equation of, 212
 Lateral position, projected lateral lane position, 241
 Lauda, Niki, 259
 Lead-lag filter, 336
 Leaf spring kinematics, 270
 Linear dynamic systems analysis techniques, 12–18
 Linear quadratic regulator (LQR), 134, 138, 139 algorithms, 140–141 Kalman filter, 138, 139
 Linear time invariant, Laplace transform, 37
 Load supporting spring, 18
 Log transformation, 28
 Longitudinal dynamics, 208
 Loop gain, 30
 Lotus algorithm, 119
 Lotus modal control, 7, 126–127, 130
 Lotus suspension hardware, 127
 Low-speed open-loop frequency response, 253
- M**
 Magic carpet ride, 126
 Margolis, Don, 119
 Mass, axis fixed to vehicle center, 190
 MATLAB, 22
 Matrix form first-order differential equations, 36 Laplace variable, 36
 McPherson strut, 45, 102, 153
 Metz, L. Daniel, 5
 Milliken, Bill, 3–5, 11, 198, 207
 Milliken, Doug, 198
 Milliken, William, 4
- Minimum risk maneuver, 321
 Modal inertial damping, 127–131, 141, 145 handling, 142–144 matrix, 142
 Modal stiffness, 130
 Moderately autonomous vehicles (SAE L3), 322, 326
 Multiaxle commercial vehicle handling, 282
 Multiaxle vehicle dynamics, 282 arbitrarily steered axle, 310–312 proportionally, 312–314 dynamic states of, 307 general model, 304–310 multiaxle vehicle, with roll, 314–319 overview of, 303–304
- N**
 NASA ride index, 140, 141
 NASCAR crew, 229
 NASCAR vehicle modelers, 190
 Neutral steer, 310
 Newton, Isaac, 1
 Newton's first law, 122
 Newton's Second Law (NSL), 14, 31, 44, 46, 49, 67, 133, 185, 187, 304 accelerations, 303 block diagram, 31 equations, 191 junction feeding, 32
 Newton's third law, 50
 Nhila, Amine, 331
 Nonlinear damper behavior, 62
 Nonlinear damping, 61–62 behavior, 62 crashout stops, 62 functional dynamic characteristics, 62
- O**
 Olley, Maurice, 2–4, 7, 84, 149, 198
 Olley parameters, 86
 Olley ride criteria, 90, 97, 117, 181 heave and pitch step responses, 91 pitch FFT, 91
 On-center steering, 165
- Open-loop crab-steer transfer function, 251
 Optimal control, 141 optimal controller, full vehicle optimal control, 139–141 quarter-car model, 145 vehicle vibration isolation, 125
 Original equipment manufacturer (OEM), 7
 Overdetermined three-axle vehicle, in turn, 324
 Oversteering, 167
- P**
 Paintstriper, 243
 “Phantom” centrifugal force, 192
 Phase lag, 21
 Pitch acceleration, 68
 Pitch-plane model, 7, 75, 96, 99, 114, 119 analysis, 101 basic, 66–69 with damping, 78–81 free response, 69–72 generalized, 82 multiaxle, 81 natural frequencies, 90 Olley ride criteria, 76–78 Olley solution, 81–88 ride model, 141 ride quality, 76–78 road inputs, 72–76 schematic, 67 with damping, 79
 Plato's ideal quarter-car model, 49
 Poincare, Henri, 179
 Power steering systems, 165
 Projected lateral lane position, 241
 Proposed three-axle truck, 336
 Prototype passenger cars, 126
- Q**
 Quarter-car model, 12, 66, 72, 76, 77, 119, 145, 197 conventional, 48–55 conventional damping, 120 force actuator, 121 ideal inertial damping open loop, 124 independent suspension, 40 inertial damping, 121

as closed loop, 123
implications, 124
isolation function, 123
open loop with actuator,
 125
invariant points, 57
isolation function of, 57
multilink suspension
 forces/reaction forces,
 41
 schematic of, 41
 typical, 40
optimal control, 132–139
pitch-plane ride models, 281
problem, optimal control
 techniques, 138
relative damping isolation
 function, 122
ride model, 6
schematic model, 45
sprung/unsprung mass
 displacements, 42
suspension springs, 40
tire produces, vertical
 stiffness, 42
transmissibility of, 52
unsprung mass, 42

R

Race Car Vehicle Dynamics,
 198
Real repeated zero (RRZ) rear
 steer, 254
 axle steering, 252
 control, 250
 vehicle speed, 245
Rear axle steering
 control input, 327, 330
 control strategy, 245, 322,
 330, 331 (*See also*
 Rear axle steering
 strategies)
 in passenger cars, 323
Rear axle steering strategies
 axle locations, counter-
 steering function
 of, 245
 closed-loop stability, 235
 control theory, 235
 driver-vehicle closed-loop,
 236
 ideal vehicle
 determination, 249–250
 open-loop response of,
 246–247

lane maintaining, 234
numerical results, 250–254
open-loop transfer
 function, 245
practical systems,
 theoretical
 interpretation of,
 254–255
 preview distance, 247–249
 vehicle model, 236–241
Rear roll-plane models, 111
Rear steering input, 239
Rear wheel amplitude, 332
Recall prior kinematic analysis,
 161
Reference frames
 external forces/inertia,
 185–189
 in general, 180–181
 rotating reference frame,
 velocity/acceleration
 of, 183–185
 standard yaw-plane model,
 179
 translating with velocity,
 182–183
vehicle
 ride, 179
 as rigid body, 189–192
Regressive damping, nonlinear
 progressive, 62
REO Speedwagon, 96
Ride frequency, 52, 60
Ride natural frequencies, 77
Rigid body, 207
RMS actuation, cost of control,
 139
Road displacement, 51, 56
Road elevation, power
 spectrums of, 56
Road-induced vibrations, 179
Road irregularities, 131
Roll dynamics,
 conceptualization of, 260
Roll frequency, 78
Rolling moments, 101
Rolling tire, centrifugal forces,
 162
Roll mode dynamics, 9
Roll-mode natural frequency,
 267
Roll moment distribution, 132,
 143
 closed-loop, 144
 steering input, 143
Roll-plane model, 99, 100, 113
 closed-loop roll moment
 distribution, 144
generalized, 113
handling, 113–114
passenger car, 111–112
pitching motion, 95
second-order effect, 96
single axle, 100–103
single-wheel inputs, 109–111
stabilizer bar, 103–109
steering input, 143
two-axle, 96–100 (*See Two-
 axle vehicle model*)
Rolls-Royce, 3
Roll steer compensation, 276
Roll steer effects, 270
Roll stiffness, distribution of,
 113
Rotating reference frame, 262
 point translating, velocity,
 182
 velocity/acceleration, 183
Rough roads, 56
RWS system, 234

S

SAE slip angle, 199
Second-order dynamic
 behavior, 126
Self-reinforcing signal, 123
Signed axle location, 200
Single-input-single-output
 (SISO), 312
Single-track relationship, 151
Single-track steering,
 comparison of, 153
Single-wheel inputs, 109–111
Single-wheel stiffness, 276
Skid pad, 2
Skyhook damping, 7, 119, 120
 Lotus modal control, 119
 optimal controller, 138
Slip angle, 165
 front steering, 171
 of rear tires, 171
Slip angles, 165–168, 197
Sloan, Alfred, 117, 118
Soft nonlinearities, 137
Solid axle suspensions, 102
Spinning tire, 169
Sprung mass, 100, 263
 acceleration, 68
 acceleration feedforward,
 131–132

- displacements, 42, 67, 106
- dimensionless function, 44
- interest, two
 - fundamental frequencies, 46–48
- McPherson/leaf suspensions, 45
- Newton's second law, 43
- quarter-car schematic model, 45
- external roll forces, 265–267
- matrix multiplying, 70
- motion, 105
- natural frequency, 48, 71
- Newton's second law, 43
- resonance, 123
- road inputs, 97
- rolls, 114, 268
 - acceleration, 263
 - mode behavior, 111
 - resisting damping moment, 266
 - rigid, 111
- second-order dynamic behavior, 126
- vertical displacement of, 81
- Stabilizer bars
 - disadvantage of, 103
 - forces, 104
 - roll-plane suspension, 109
 - single-wheel equivalent, 110
 - input, 109
 - stiffness
 - effect of, 107, 110
 - roll, 108
 - single-wheel, 111
 - suspension schematic, 104
 - torsional stiffness, 106
- Stabilizer support mounts, 104
- State-of-the-art conventions, 196–199
- State space realization, 33–35
 - Laplace transform, 34
 - matrix equivalent, 35
 - second-order differential equation, 35
 - state variables, 33
- State variables
 - feedback control of, 333
 - linear combinations, 37
- Steady-state analysis, 222–226
- Steady-state centripetal force, 171
- Steady-state drift angle response, 222
- Steady-state expressions, 308
- Steady-state lateral acceleration, 224
- Steady-state response ratios, 296
- Steady-state side force expression, 273
- Steady-state vehicle testing, 2
- Steady-state yaw rate, 8, 308, 313
- Steer-by-wire system, 331
- Steered tire, forces, 209
- Steered wheel
 - geometry, 150
 - offset axle location, 204
- Steering
 - angle input, 225
 - auxiliary axle, 234
 - effect of, 310
 - front, rear axles
 - perpendicular to radii, 297
 - gearbox, 159
- Steering efforts
 - drag link force, 159
 - steered wheels, displacing, 158
- gearboxes, 159–160
- geometric relationship, 157
- pitman arm, 158
- Steering input, 226
 - critical speed, 228
 - identification, 202
 - multiaxle vehicle, 317
 - multiple control input model, 318
 - steady-state yaw rate, 318
- Steering systems, 165
 - on-center, 165
 - power steering, 165
- Stiffnesses, transmissibility, 55
- Suspended mass, 12–18, 47
 - block diagram
 - Hooke's spring law, 31
 - Newton's Second Law (NSL), 31
 - complete block diagram of, 33
 - with damping, 18–22
 - amplitude ratio, 21
 - Laplace transform, 19
 - load supporting spring, 18
- response mapped, to complex plane, 21
- sprung mass response, 20
- transmissibility, 19
- degrees of freedom, 66
- second-order dynamic behavior, 27
- Suspension, as linear dynamic system
 - displacement, 15
 - Euler's identity, 16
 - first-order matrix differential equations, 35–37
- frequency responses, basic functions
 - differentiator, 23–24
 - first-order lag, 25–26
 - gain, 22–23
 - integrator, 24–25
 - second-order dynamics, 26–28
- Laplace transform, 17, 18
- sinusoidal motion, 15
- sprung mass, 15
- suspended mass, 14, 17
 - (*See also* Suspended mass, with damping)
- system responses, 13
- transmissibility, 18
- vehicle ride, “seat of the pants” effect of, 11
- Suspension damping, 58
 - higher, 60
- isolation function, 59
- variation, 59, 60
- Suspensions. *See also* Suspended mass configuration, 128
- damping, 61
- deflection of, 42
- displacement, absolute value of, 61
- handling, determines, 142
- independent, 40
- isolate road acceleration, effect of, 55
- kinematics, 268
- linear dynamic system
 - (*See* Suspension, as linear dynamic system)

- Lotus suspension hardware, 127
- McPherson leaf, 45 strut, 102, 153
- multilink forces/reaction forces, 41 schematic of, 41 typical, 40
- spring force, 42, 47 sprung mass, 43 stiffnesses, 57, 66, 103 isolation function, 58 transmissibility, 53 variation of, 53
- Suspensions transmit forces, 117
- System ID, 22
- T**
- Tandem axles, friction circles, 287
- Test vehicle, 89
- The Structure of Scientific Revolutions, 196
- Third axle steering, 294–299
- Three-axle handling analysis, 303
- Three-axle vehicle dynamics, 288, 294
- Ackermann relationship, 290 characteristic equation, 288 displacement expressions, 289 equivalent wheelbase, 292 example, 88–91 handling equations, development of, 287 neutral steering three-axle vehicle, 293 overview of, 281–282 peculiarities of, 282–286 stiffnesses, 86 tandem axles, friction circles of, 287 third axle steering, 294–299 tire force model, 294 trajectory tracking, 299–301 vehicle and trajectory states of, 300 yield unique, 86
- Tires adhesions, 169 camber angle, 267, 268 centrifugal forces, 161
- commercial vehicle, 285 forces, 168–170 lateral on two-axle vehicle, 210 steered passenger car, 209 mechanical trail, 163 road interface, 8 rolling tire, centrifugal forces, 162 self-aligning torque of, 217
- Tire stiffness, isolation function, 60
- Tire wear, 336
- Torque-rod, 287
- Trade-off, 12
- Transfer functions double integrator combination, 29 of feedback, 30 series combination, 29 steady-state values, 290
- Translational displacements, 237
- Translational velocities, 267
- Transmissibility, 18, 52 filters road acceleration, 55 variation, 52
- Twin-steer vehicle, 304
- Two-axle commercial vehicle, 250
- Two-axle passenger cars, 208
- Two-axle state-space bicycle model, 299
- Two-axle vehicle model, 1, 197, 208–215 acceleration equations, 262–265 camber effects, 267–269 differential equation of motion, 259, 271–275 external roll forces, on sprung mass, 265–267 kinematic model, 151 nonlinear tires, inclusion, 278
- roll axis, definitions, 260–262
- roll steer compensation, 275–276 effects, 269–271 steady-state handling properties of, 226
- steering compliance, in understeer, 277–278 trade-offs, 259
- Two-axle yaw-plane model, 8, 207, 314
- drift angle transfer functions, 215–218 ideal two-axle model, 218–222 pole locations, 226–230 steady-state analysis, 222–226 vehicle model, 208–215 yaw rate transfer functions, 215–218
- Two-mass quarter-car model, 65
- U**
- UC Davis, and Systems Technology, Inc., 235
- Understeer, 164, 165 experimentally determined, 226 understeering coefficient, magnitude of, 299
- Unsprung mass, 263 displacements, 42, 105 dimensionless function, 44
- interest, two fundamental frequencies, 46–48
- McPherson/leaf suspensions, 45
- Newton's second law, 43
- quarter-car schematic model, 45
- isolation function, 58
- Newton's second law, 43 transmissibility, 54
- Unsteered vehicle at high-speed approaches, 251
- low-speed open-loop frequency response, 253
- V**
- Vehicle center of gravity, 306 driver's impression, 144
- Vehicle conditions drift angle, 311 pole locations, 310 transfer function of, 310

- Vehicle counter-steered, 337
 Vehicle design
 better handling car, 12
 better riding car, 12
 cheaper car, 12
 general public, 12
 inherent, 12
 Vehicle drift angle, 215
 Vehicle dynamic models,
 5, 198
 historical perspective, 2–6
 “nonlinear” functions, 13
 parameters, 246
 rear axle steering strategies,
 236–241
 Vehicle energy, 164
 Vehicle kinematics, 7
 Vehicle performance benefit,
 297
 Vehicle ride, effect of, 11
 Vehicle roll model, free body
 diagram of, 112
 Vehicle speed, RRZ rear steer,
 254
 Vehicle state behavior, 327
 Vehicle state variables, Laplace
 domain expressions
 of, 325
 Vehicle steering, 179
 Vehicle travel, direction of,
 201
 Vehicle wheelbase, 73
 front and rear axles, 172
 ratio of speed, 75
 Vehicle yaw rate response, 327
 Vertical suspension forces, 82
 Vertical vibration, human
 limits, 53
 Virtual driver, 5, 326
- W**
- Wheelbase
 filtering, 75, 76
 tandem spread, 296
- Wheel displacement
 drag link force
 steered wheels, 158
 steering system, 159
 left, 154
 right, 155
- Wheel-hop frequencies, 48, 117,
 122, 135, 137
 Wheel position, 335
 Wigner, Eugene, 233
- Y**
- Yaw moments, 271
 Yaw-plane model, 196, 237
 bicycle model, 195
 force equations, 211
 for passenger car, 208
 vehicle dynamic model, 233
- Yaw rate
 acceleration, 315
 Ackermann relationship, 246
 feedback, 219
 response, 161, 165, 274
 steady-state value, 220, 223,
 225
 transfer functions, 215–218
- Yields sprung mass
 acceleration, 57
- Z**
- Zero steady-state tracking
 error, 247

About the Author

Dan Williams has worked for over 30 years in engineering and planning positions of increasing responsibility in passenger car suspension and commercial vehicle steering business units. He began working for a joint venture between Moog and Lotus to develop passenger car active suspension systems. That business was purchased by TRW, and Dan has managed the development and launch of chassis control systems in North America and Europe. TRW was purchased by ZF, and Dan is currently Director of NA ADAS/AD Development for the ZF Truck business unit in Lafayette, IN. He has published over 90 papers and patents on various vehicle control systems and has served as a Visiting Assistant Professor at Purdue University teaching vehicle dynamics.



Dan received the B.S. (1985) and M.S. (1987) degrees in engineering from the University of Illinois; his thesis topic was optimal control of racing vehicles. He received the M.B.A. (1990) degree from the Florida Institute of Technology and then received his Ph.D. (1995) in Mechanical Engineering from Florida Tech. His dissertation compared practical and theoretically optimal active automotive suspension systems. He later completed his M.A. (2008) in History from Purdue University writing a thesis on the effect of the Morrill Act on Engineering.

He is a registered Professional Engineer and a member of Tau Beta Pi, Phi Kappa Phi, and FarmHouse Fraternity. Dan delivered the 2012 SAE Buckendale Lecture on “Multi-Axle Vehicle Dynamics,” and the 2016 ASME Milliken Lecture on “Active Suspension.” He is a Fellow of SAE, ASME, and IMechE.

Generalized Vehicle Dynamics

Daniel E. Williams

Author Daniel E. Williams, an industry professional with more 30 years of experience in chassis control systems from concept to launch, brings this experience and his unique approach to readers of **Generalized Vehicle Dynamics**.

This book makes use of nomenclature and conventions not used in other texts. This combination allows the derivation of complex vehicles that roll with multiple axles, any of which can be steered, to be directly predicted by manipulation of a generalized model. Similarly the ride characteristics of such a generalized vehicle are derived. This means the vehicle dynamic behavior of these vehicles can be directly written from the results derived in this work, and there is no need to start from Newton's Second Law to create such insight. Using new and non-standard conventions allows wider applicability to complex vehicles, including autonomous vehicles.

A fresh and more inclusive book that lays out much new material in vehicle dynamics.

L. Daniel Metz, Ph.D.

Generalized Vehicle Dynamics is divided into two main sections—ride and handling—with roll considered in both. Each section concludes with a case study that applies the concepts presented in the preceding chapters to actual vehicles.

Chapters include Simple Suspension as a Linear Dynamic System, The Quarter-Car Model, The Pitch Plane Model, The Roll Plane Model, Active Suspension to Optimize Ride, Handling Basics, Reference Frames, New Conventions, Two-Axle Yaw Plane Model, Rear Axle Steering and Lanekeeping, Two-Axle Vehicles that Roll, Three-Axle Vehicle Dynamics, Generalized Multi-Axle Vehicle Dynamics and Automated Vehicle Architecture from Vehicle Dynamics.

Cover image used under license Shutterstock.com

ISBN: 978-1-4686-0140-4



9 781468 601404